BLDSC no:- DX 182019

LOUGHBOROUGH
UNIVERSITY OF TECHNOLOGY
LIBRARY

AUTHOR/FILING TITLE

Goodwin, A.

ACCESSION/COPY NO.

04008204 4

VOL. NO. | CLASS MARK

LOAN COPY

20 FEB 1995

28 JUN 1996

27 JUN 1997

0400820447

BADMINTON PRESS
18 THE HALFCROFT
SYSTON
LEICESTER. LE7 8LD
ENGLAND
TEL: 0533 602917
FAX: 0533 696636

PHOTOCHEMISTRY OF LIGNOCELLULOSIC MATERIALS AND RELATED COMPOUNDS

By

Andrew Goodwin

B.Sc., C.Chem., M.R.S.C.

A Doctoral Thesis Submitted in Partial Fulfilment of the Requirements for the Award of

Doctor of Philosophy of Loughborough University of Technology

30th September 1993

(c) Andrew Goodwin 1993

Loughborough University
of Technology Library

Date Feb 94

Class

Acc. No. 04008204 4

0992383 5

To My Mother and Father, Ann and Albert Goodwin

With Love and Many Thanks

"Slow But Sure"

A tortoise and a hare started to dispute which of them was the swifter, and before separating they made an appointment for a certain time and place to settle the matter. The hare had such confidence in its natural fleetness that it did not trouble about the race but lay down by the wayside and went to sleep. The tortoise acutely conscious of its slow movements, padded along without ever stopping until it passed the sleeping hare and won the race.

"A naturally gifted man, through lack of application, is often beaten by a plodder"

From "Fables By Aesop", Translated By S.A. Handford
Penguin Books, (England), page 70, (1970)

Contents

Acknowledgements

I wish to express my sincere thanks to my supervisor, Professor Frank Wilkinson, for giving me the opportunity to do photochemistry research in his laboratory. His enthusiasm, guidance, and "open door" style of supervision were very much appreciated and will never be forgotten.

I would also like to thank the Pulp and Paper Research Institute of Canada (PAPRICAN) for providing financial support for the project. Many thanks are extended to Drs. Cyril Heitner and John Schmidt for many useful discussions during the term of our collaboration.

Throughout my academic career at Loughborough University, I have received nothing but encouragement from all my family and therefore wish to thank them at this time for all their help. A special heartfelt thank-you must go to my mother, father and sister, Ann, Albert and Jane Goodwin for their immense emotional and financial (Cheers Dad!) support over the last few years.

The photochemistry research group at Loughborough was always a great place to work. I made many great friends who, through their varied personalities, have always managed to keep me smiling and, at times, sane during my research period. Thanks are due to the following members of the group:- Dr. David "Bob" Worrall for the proof reading and valuable discussions during the production of this thesis, Dr. David "Taggart" McGarvey, Jon "Strange, Top Boy" Hobley, David "Shandy Man" Mandley, Garry "Spanner" Sturley and Darren "Derwood" Greenhill. A mention must also go to "honourymembers" of the Photochemistry Coffee Club, namely Alan "B.A." Davies, Dr. Andres "Red Hot Chilli Pepper" Olea, Dr. Simon "B.S." Cocks, Phil "Apples" Szekeres and Katrina "K.B" Bell who, with the above people, have provided many extra-curricula evenings in the local pubs and clubs of Loughborough. Thanks also go to Miss Claire Archer for the initial typing work on this thesis.

Many other people have made my stay in Loughborough a happy one and over the past three years none more than the staff of Rutherford Hall, namely Dr. Margaret Lucas, Ian and Agnes Jefferson, Pauline Bigham and Christine Cox who are all great friends and former colleagues. Thanks to you all.

Finally, and by no means least, a very special person in my life must get a mention at this time. My girlfriend, Dr. Liz Barrett, has provided me with love, encouragement, support and "much much more" throughout my postgraduate studies to which I will be eternally grateful. Thanks Liz!

Abstract

The primary photochemical processes of lignin rich high yield thermomechanical pulp (TMP) have been investigated with a view to understanding and ultimately preventing the yellowing (photoreversion) of such paper upon exposure to sunlight. This would enable their use in longer life paper products and therefore represent large raw material and cost savings to the pulp and paper manufacturer.

The technique of time resolved laser flash photolysis, in both transmission and diffuse reflectance mode, has been employed to study the photochemical behaviour of appropriate lignin model compounds, soluble milled wood lignin (MWL), and TMP itself.

The photochemistry of lignin model compounds possessing an α-carbonyl functionality which act as photosensitisers in the yellowing of TMP has been studied. Intersystem crossing quantum yield studies indicate that both singlet and triplet states contribute to the overall photodegradation processes of such compounds. Methoxyl substitution on the aromatic ring of such molecules and polar environments have the effect of bathochromically shifting the triplet-triplet absorption maximum and extending triplet excited state lifetimes due to the excited state possessing predominantly $^3(\pi,\pi^*)$ character. The efficient quenching of a lignin model compound triplet state with phenol (k_q = 6.3 x 10^9 l.mol.s.$^{-1}$) to form a phenoxy-ketyl radical pair has also been demonstrated.

The triplet state of MWL (in 1,4-dioxane solution) has been observed, and its absorption spectrum quantified, for the first time. Assignment of the first observed transient species was based upon its ability to sensitize singlet molecular oxygen ($^1\Delta_g(O_2)$). The triplet state is short lived due to it being quenched by other parts of the lignin macromolecule to form radical species, some of which may ultimately lead to permanent structural changes in the lignin macromolecule.

The transient absorption observed from TMP itself was assigned as the triplet state of α-carbonyl moieties on the grounds of its similarity to that observed for MWL and by oxygen quenching experiments. In agreement with previous preliminary studies, the removal of the phenolic moieties from the lignin structure was shown to increase the observed transient signal and reduced the extent to which the sample yellowed, both observations being consistent with the above assignment. The photochemical reaction of α-carbonyl triplets with phenolic hydroxyls via static quenching mechanisms on timescales faster than those available (< 200 ns) from our apparatus are implicated in the photoreversion processes, the observed photochemistry being that of relatively unreactive chromophoric moieties.

Chapter 1

Introduction

1 Introduction

1.1 Photochemical Principles

The Stark-Einstein Law states that "if a species absorbs radiation then one particle is excited for each quantum of radiation absorbed". Thus, when a molecule has absorbed a quantum of radiation (a photon), it is said to become "energy rich" or "excited" in the absorption process. The range of photon energies of interest to the photochemist are of sufficiently high energy to lead to electronic excitation of the absorbing species. Electronic transitions of this nature are quantised processes; that is to say, only a photon with a given energy will be absorbed by a molecule to produce an electronically excited state. This is illustrated in figure 1.1 for the absorption of a photon by a typical unsaturated hydrocarbon.

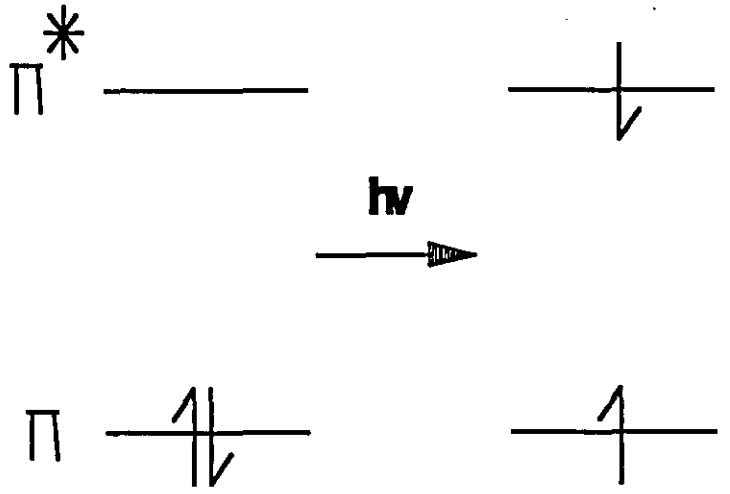

Figure 1.1:- Schematic Representation of the Absorption of a Photon by a Typical Unsaturated Hydrocarbon

The molar energy of the transition, ΔE, is defined according to equation 1.1:-

$$\Delta E = Nh\nu = \frac{Nhc}{\lambda} \qquad (1.1)$$

where h is Planck's constant (6.63×10^{-34} J.s.), ν is the frequency of radiation ($s.^{-1}$), c is the velocity of light in a vacuum (2.998×10^{8} m.$s.^{-1}$), λ is the wavelength (in metres) and N is Avogadro's number (6.022×10^{23} $mol.^{-1}$). The right hand side of equation 1.1 therefore gives an expression of molar excitation energy (in J.$mol.^{-1}$), a quantity frequently used to describe the excited state energy of a molecule relative to either its ground state or to a different excited state of the particular molecule.

A fundamental relationship between the fraction of light absorbed by a solution and the concentration of the absorbing species at a given wavelength is described according to the Beer-Lambert Law:-

$$A = \log_{10} \frac{I_0}{I_t} = \epsilon . c . l \qquad (1.2)$$

where I_0 and I_t are the intensities of the radiation entering and emerging from the sample respectively, A is known as absorbance, ϵ is the molar decadic absorption coefficient (also known as the extinction coefficient), c is the concentration of the absorbing species and l is the path length. Clearly, a linear relationship exists between absorbance and the concentration in solution of the absorbing species.

The quantum yield of a photochemical reaction (ϕ) can be defined in one of two ways:-

$$\phi = \frac{no.\,of\,molecules\,undergoing\,a\,process}{no.\,of\,quanta\,of\,light\,absorbed} \qquad (1.3)$$

$$\phi = \frac{rate\,of\,a\,process}{rate\,of\,absorption\,of\,quanta} \qquad (1.4)$$

A simple example to illustrate these equations is by considering the process of fluorescence (see section 1.1.3 for details). Equations 1.3 and 1.4 state that the quantum yield for a reaction can be defined in terms of a "ratio of numbers" (equation 1.3) or by a "ratio of rate constants" (equation 1.4) for a particular photochemical process. In the absence of any competing photochemical processes (such as internal conversion or intersystem crossing - see section 1.1.3), and assuming that the molecule does not react or decay none-radiatively from the excited state, the quantum yield of fluorescence (ϕ_f) will be unity. Competing processes have the effect of reducing ϕ_f. From equation 1.4, the extent to which this occurs is dependent upon the relative rates of the competing processes. In the case of fluorescence, favourable competing processes have the effect of increasing the radiative rate constant k_f (the reciprocal of the time taken for the concentration of excited states to decrease to 1/e, where e is the natural number, of its original value) since:-

$$k_f = k_f^0 + k_{IC} + k_{ISC} \qquad (1.5)$$

where k_f^0 is the fluorescent rate constant in the absence of all other competing processes (the natural radiative rate constant), k_{IC} and k_{ISC} being rate constant for internal conversion and intersystem crossing respectively (see section 1.1.3). From above and equation 1.5, it follows that:-

$$\tau_f = \frac{1}{k_f} \qquad (1.6)$$

and

$$\tau_f^0 = \frac{1}{k_f^0} \tag{1.6}$$

where τ_f^0 is the natural radiative lifetime for the fluorescence process. It can therefore be shown that:-

$$\phi_f = \frac{k_f^0}{k_f^0 + k_{IC} + k_{ISC}} \tag{1.7}$$

Clearly, the only condition which allows $\phi_f = 1$ is the situation where $(k_{IC} + k_{ISC}) = 0$.

1.1.1 The Nature of Electronic Energy Levels

The simplest approach to describe the position of the electrons in a molecule is that they occupy molecular orbitals formed by the combination of the atomic orbitals of the individual atoms. Such orbitals may be bonding, anti-bonding or non-bonding in character. Anti-bonding orbitals are distinguished from bonding orbitals by having the notation "*" superscripted above the orbital description (orbitals are described in terms of being σ, π, n or δ depending upon their wave function descriptions).

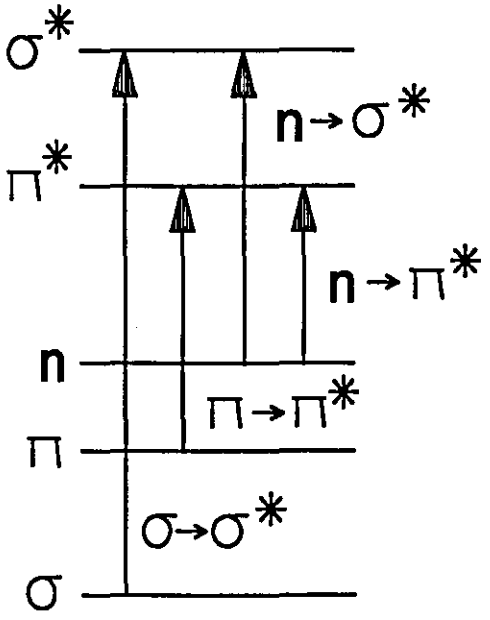

Figure 1.2:- Energy Level Diagram for the Aromatic Carbonyl Group Showing the Electronic Transitions of Most Interest to the Photochemist

Taking for example, the electronic transitions of a carbonyl moiety, an energy level diagram (figure 1.2) can be drawn to represent the electronic transitions occurring upon absorption of a quantum of radiation. The two transitions shown are the most widely studied by the photochemist, such transitions occurring in the near ultra-violet region of the electromagnetic spectrum. As can be seen from figure 1.2, the $\pi \rightarrow \pi^*$ (where the "*" represents an antibonding orbital) transition is of a higher energy than that of the $n \rightarrow \pi^*$ transition. Other high energy transitions are possible; eg. the $n \rightarrow \sigma^*$ and $\pi \rightarrow \sigma^*$ transitions occur at high energy (wavelengths less than 200 nm) and are therefore not easily studied.

Electronic states of molecules are known to possess certain properties which may directly affect their chemical behaviour. A fundamental property of the electronic states of molecules is a term known as the spin multiplicity, given the symbol M. This is calculated as $2S + 1$ where S is the vector sum of the spin angular momentum quantum numbers s describing the individual electrons in the molecule. The spin angular momentum quantum number for an electron has a unique value of 1/2, the quantised components of s along a particular direction having magnitude $m_s(h/2\pi)$ where m_s is known as the magnetic spin quantum number and h is Planck's constant. m_s can have the values $\pm 1/2$. When all the electrons in the molecule are spin paired, $S = 0$ and $2S + 1 = 1$, the state being termed a singlet state. If two electrons have parallel spins, $S = 1$ and therefore $2S + 1 = 3$, the state being described as a triplet state. As a direct result of Hund's Rule of maximum multiplicity which states that:-

(a) Electrons will occupy different orbitals wherever energetically possible and
(b) Two electrons occupying degenerate orbitals will have parallel spins in their lowest energy state,

it is predicted that triplet states will be lower in energy than their corresponding singlet states, an observation readily demonstrated by experiment. It must be noted that a triplet state may only occur if two unpaired electrons occupy *different* molecular orbitals since two electrons with the same spin in the same molecular orbital contradict Pauli's exclusion principle which states that no two electrons can possess precisely the same set of quantum numbers.

1.1.2 Electronic Transitions Between States

A frequently used pictorial description of the electronic absorption of a quanta of energy (a photon) uses potential energy/internuclear separation curves for the initial and final energy states involved in the transition. Such a diagram is shown in figure 1.3.

A direct result of the Boltzmann distribution is that the majority of molecules in the lower electronic energy state are located in the lowest vibrational energy level of that state ($\nu = 0$). Therefore electronic absorption occurs mostly from this lowest vibrational energy level. The Franck-Condon principle states[1] that "since electronic transitions are much faster than nuclear motion, electronic transitions occur most favourably when the nuclear structure

of the initial and final state are most similar". Thus, electronic transitions on diagrams such as figure 1.3, are drawn vertically upwards or downwards parallel to the potential energy axis.

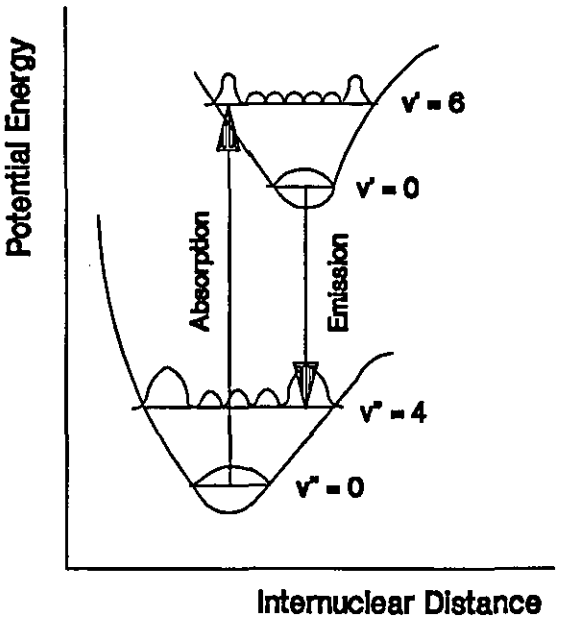

Figure 1.3:- Potential Energy/Internuclear Separation Curves for the Initial and Final Energy States Involved in an Electronic Transition Together with the Franck-Condon Factors for the Initial and Final States

The probability, and therefore the distribution of the intensity, of an electronic transition is determined by the amplitude of the Franck-Condon factors of the initial and final electronic states at a given internuclear separation (an easily remembered rule is that for a given vibrational energy level ν, there will be $\nu + 1$ maxima and ν nodes between the maxima for the vibrational wavefunction of the particular vibrational energy level). Absorption is assumed to take place from the position of highest Franck-Condon probability. Therefore, in figure 1.3, the $\nu'' = 0$ to $\nu' = 6$ transition represents an energy correspondence to the highest absorption probability/intensity. A similar argument can be presented when one considers the loss of electronic energy (eg. by the radiative loss of electronic energy). Again loss of energy will primarily occur from $\nu' = 0$ to a vibrational level of ν'' with maximum Franck-Condon amplitude. In the example shown in figure 1.3, the $\nu' = 0$ to $\nu'' = 4$ transition is the most likely and will manifest itself as the wavelength of maximum emission intensity. Clearly, absorption or emission will occur to a greater or lesser extent to many vibrational energy levels of the final electronic energy level of the molecule for the process in question. This, coupled with rotational quanta (which are present for each vibrational energy level) gives rise to the broad absorption bands typically observed for complex molecules.

The process of absorption of a photon of light to produce electronically excited states

can be described as the interaction between the electric field of the electromagnetic wave (the wave description of light can be considered as consisting of an electric and magnetic field sinusoidally oscillating in mutually perpendicular planes at right angles to the direction of propagation of the radiation) with the electrons of the molecule involved. There exists a series of selection rules for radiative (absorptive or emissive) transitions between states which can be summarised briefly below:-

(a) The radiative transition must take place with no change in total spin angular momentum; ie. $\Delta S = 0$ for allowed transitions. Thus, singlet-triplet absorptions are known as "forbidden" transitions.
(b) The orbitals involved must have good spatial overlap for the transition to occur. For example, the $\pi \rightarrow \pi^*$ transition in ketones is an allowed transition, whereas the $n \rightarrow \pi^*$ is not.

Such selection rules are, however, frequently broken and there exists many examples where forbidden transitions are observed. A frequently encountered mechanism whereby forbidden transitions are observed is known as spin-orbit coupling. Spin-orbit coupling can be envisaged as a mechanism whereby the electrons in molecular orbitals, being moving charges, can generate a magnetic field which can act locally on another electron. The magnetic torque is capable of flipping the spin of an electron resulting in a change in the total spin-angular momentum of the system. The jumping of the electron to another orbital is compensated for by a corresponding change in orbital angular momentum which serves to conserve the total angular momentum of the system. Such spin-orbit couplings make intersystem crossing between states of differing total spin multiplicity, singlet-triplet absorption and phosphorescence emission (see section 1.1.3) more possible.

1.1.3 The Jablonski Diagram

The Jablonski diagram (figure 1.4) can be used to adequately describe the electronic excited states and transitions between such states of all complex molecules.

From figure 1.4, a series of terms are introduced which are defined briefly below:-

(a) **Excited States** are defined in terms of the total spin angular momentum. That is to say, singlet states are termed S where S_0 is known as the ground state and S_1, S_2 etc. represent excited singlet states of increasing energy above the ground state. A similar numbering system for triplet states (T) is applied where the lowest lying triplet state is defined as T_1.
(b) **Internal conversion (IC):-** Internal conversion is the name given to the radiationless decay processes between states of the same spin multiplicity. The rate of internal conversion is dependent upon the energy separation between initial and final electronic states involved. For this reason, internal conversion from, for example, S_2 to S_1 or T_2 to T_1 will occur extremely rapidly whereas internal conversion between S_1 and S_0 is slow (due to a larger energy separation). This allows such processes as fluorescence or intersystem crossing to favourably compete. If absorption or emission are regarded as vertical transitions on the Jablonski diagram, then internal conversion can be described in terms of a horizontal transition.
(c) **Intersystem crossing (ISC):-** This is the term used to describe the radiationless transition

between electronic states of differing electron spin multiplicities. The two most important intersystem crossing processes are the S_1 to T_n (where n represents a higher triplet excited state) and the T_1 to S_0 transitions. For the former, the energy gap ($\Delta E_{S,T}$) is a determining factor as to the efficiency of the process. When $\Delta E_{S,T}$ is small, efficient intersystem crossing via a spin-orbit coupling mechanism may occur. For example, the quantum yield of intersystem crossing (S_1 (n,π^*) to T_2 (π,π^*)) for benzophenone (ϕ_T^{Bzp}) is unity in all solvents with a rate constant (k_{ISC}) of approximately 10^{11} s.$^{-1}$ due to $\Delta E_{S,T}$ being small for this molecule. The presence of heavy atoms may enhance intersystem crossing quantum yields due to enhancement of spin-orbit coupling mechanisms.

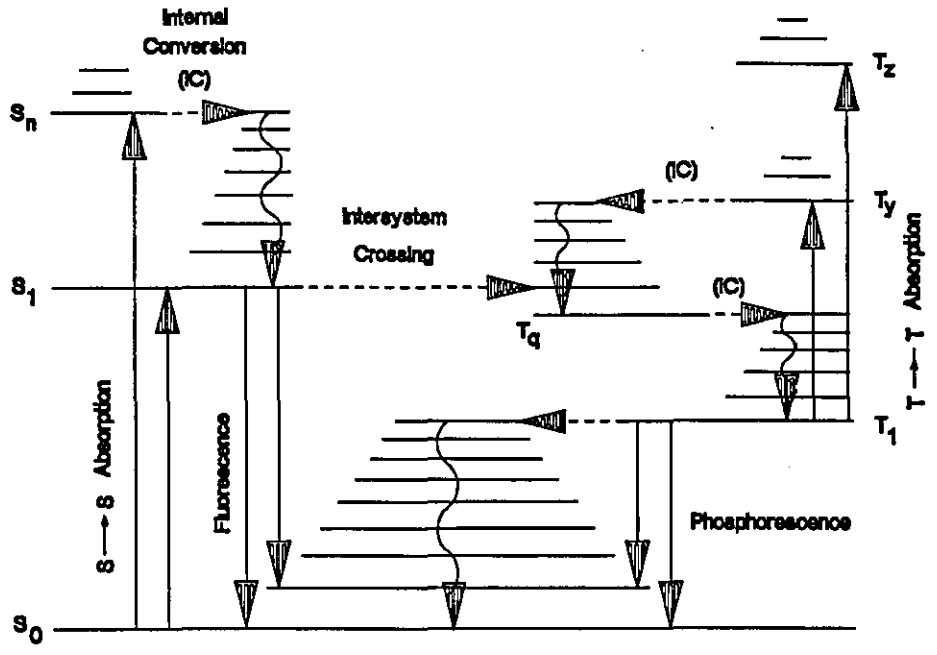

Figure 1.4:- Modified Jablonski Diagram For Complex Molecules

(d) Fluorescence:- Fluorescence is defined as a radiative transition between states of like multiplicity. Rate constants for fluorescence (k_{fl}) generally range between 10^6 s.$^{-1}$ and 10^9 s.$^{-1}$. The magnitude of such rate constants is frequently used to explain why fluorescence generally does not occur from higher excited states since internal conversion rate constants (k_{IC}) of the order of 10^{12} s.$^{-1}$ indicate that such processes will compete favourably as a deactivation mechanism for higher excited states. This observation forms the basis of Kasha's Rule[2] which states that "the emitting electronic energy level of a given spin multiplicity is the lowest excited energy level of that multiplicity". The notable exceptions to this rule are the fluorescence observed from azulene and some thioketones ($R_1R_2C=S$) which have both been demonstrated to be from the S_2 energy level to S_0. Fluorescence generally occurs from the lowest vibrational energy level of the excited state resulting in the quantum yield of fluorescence (ϕ_{fl}) being independent of excitation wavelength. Also, for many organic

molecules, Franck-Condon factors for both the excited state and ground state are often similar resulting in the well known "mirror image" relationship between absorption and fluorescence spectra.

(e) Phosphorescence:- The process of phosphorescence emission can be defined as radiative transitions between electronic states of differing spin multiplicities. In figure 1.4, this process is represented by the spin forbidden deactivation of the lowest lying triplet state T_1 to the ground state S_0. The forbidden nature of the transition ($\Delta S = 1$) results in the natural radiative lifetimes for such a process being long therefore allowing collisional electronic-vibrational energy transfer with solvent molecules to compete favourably with the radiative deactivation pathway of the excited triplet states. For this reason, phosphorescence emission is more readily observed when the emitting species is frozen in a rigid glass at liquid nitrogen temperature (77K) thereby reducing the rate of diffusional quenching of excited triplet states by solvent molecules. Although many phosphorescence studies have been confined to solution or solid phase (rigid glasses) media, gas phase phosphorescence has also been detected, the most common example of which being the phosphorescence emission observed from biacetyl vapour[3]. As a result of spin-orbit coupling, pure singlet and triplet states do not exist, triplet states therefore contain a certain degree of singlet state character. Spin-orbit perturbation is not allowed between states of the same configuration and thus, for example, a $^3(\pi,\pi^*)$ state borrows its singlet state character from the $^1(n,\pi^*)$ state or $^1(\sigma,\pi^*)$ state as opposed to the $^1(\pi,\pi^*)$ state. Radiative transitions from $^1(\pi,\pi^*)$ states are fully allowed transitions. It therefore follows that $^3(n,\pi^*) \rightarrow S_0$ transitions are more allowed than $^3(\pi,\pi^*) \rightarrow S_0$ transitions resulting in the natural phosphorescence radiative lifetimes (the phosphorescence lifetimes in the absence of any other deactivation pathway) of compounds containing lowest lying $^3(\pi,\pi^*)$ and $^3(n,\pi^*)$ states being of the order of 1 to 10 seconds and 10^{-2} to 10^{-1} seconds respectively.

1.1.4 Intermolecular Energy Transfer

The processes involved in the transfer of energy from an electronically excited donor molecule (designated D^*) to an acceptor (A) can be summarised according to equation 1.8 where A^* is the excited state of the acceptor and D is the ground state of the donor.

$$D^* + A \rightarrow D + A^* \qquad (1.8)$$

Energy transfer mechanisms are usually classified according to the initial spin multiplicity of D and the final spin multiplicity of A; for example the process shown in equation 1.9 is termed "triplet-triplet" energy transfer.

$$^3D^* + {}^1A \rightarrow {}^1D + {}^3A^* \qquad (1.9)$$

There exists several energy transfer mechanisms for differing photochemical systems, the salient points pertinent to each mechanism being briefly discussed below:-

(a) Radiative (Trivial) Mechanism:- The energy transfer mechanism involves the intermediate participation of a photon and can be represented according to equations 1.10 and 1.11:-

$$D^* \rightarrow D + h\nu \tag{1.10}$$

$$h\nu + A \rightarrow A^* \tag{1.11}$$

Clearly, an important requirement for such a process is that the absorption spectrum of the acceptor, A, and the emission spectrum of the donor, D^*, overlap, the efficiency of the reaction being dependent upon extent of such an overlap and also by the quantum yield of emission (ϕ_E^D) of the excited donor species D^*.

(b) Collisional (Exchange) Mechanism:- This mechanism can be envisaged as an exchange of electrons betwèen donor and acceptor molecules; an electron jumps from the donor molecule to the LUMO (Lowest Unoccupied Molecular Orbital) of the acceptor coupled with a simultaneous transfer of an electron from the HOMO (Highest Occupied Molecular Orbital) of the acceptor molecule into a corresponding orbital of the donor molecule. Such a mechanism is shown schematically in figure 1.5:-

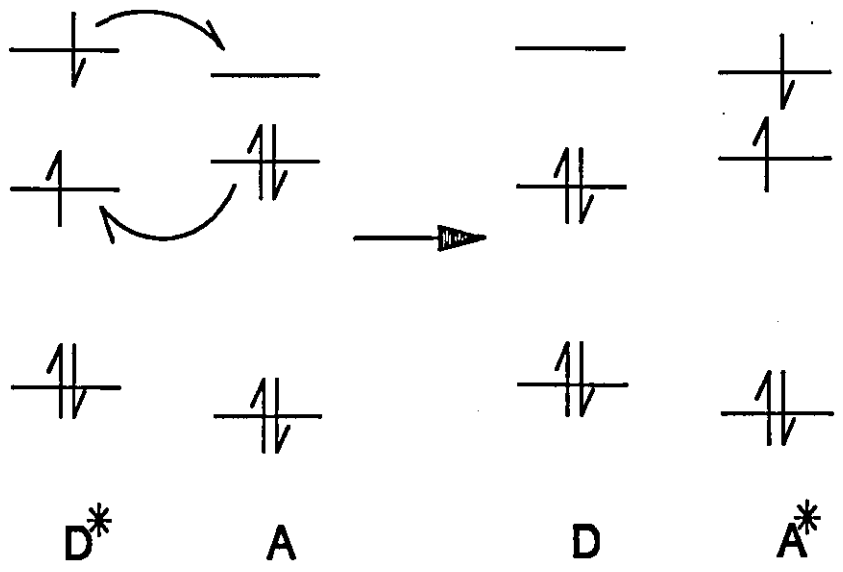

Figure 1.5:- Schematic Representation of Collisional Energy Transfer

Clearly, this mechanism requires the collision of donor and acceptor species in order for their respective electron clouds to interact so that electron exchange can take place.

The exchange mechanism of energy transfer was quantified by Dexter[4] who derived the relationship (equation 1.12):-

$$k_{EN}(Exchange) = KJe^{-\left(\frac{2R_{DA}}{L}\right)} \qquad (1.12)$$

where k_{EN} is the rate constant for energy transfer, K is related to specific orbital interactions between donor and acceptor, J is a spectral overlap integral and R_{DA} is the donor/acceptor separation relative to the Van der Waals radii L. As can be seen in equation 1.12, the rate of exchange energy transfer falls off exponentially with distance and reflects the fact that electron cloud interaction is required for this mechanism to proceed efficiently (electron charge density as a function of distance from the nuclei can approximate to an exponential type function).

(c) Coulombic (Induced Dipole) Mechanism:- This mechanism does not require the spatial overlap between electron clouds of the donor and acceptor molecules in order to proceed. Coulombic energy transfer can be described in terms of long range coulombic forces experienced by an electron cloud of the donor and acceptor molecules analogous to the interaction of the electric field of a light wave with an electron cloud. For example, the oscillation of an electron in the LUMO of D^* may cause and electron in the HOMO of A to become more energetic. The resulting dipole-dipole interaction may cause the electron in the HOMO of A to be promoted to a LUMO with a corresponding relaxation of the electron in the LUMO of D^* to the HOMO yielding D. This is shown pictorially in figure 1.6:-

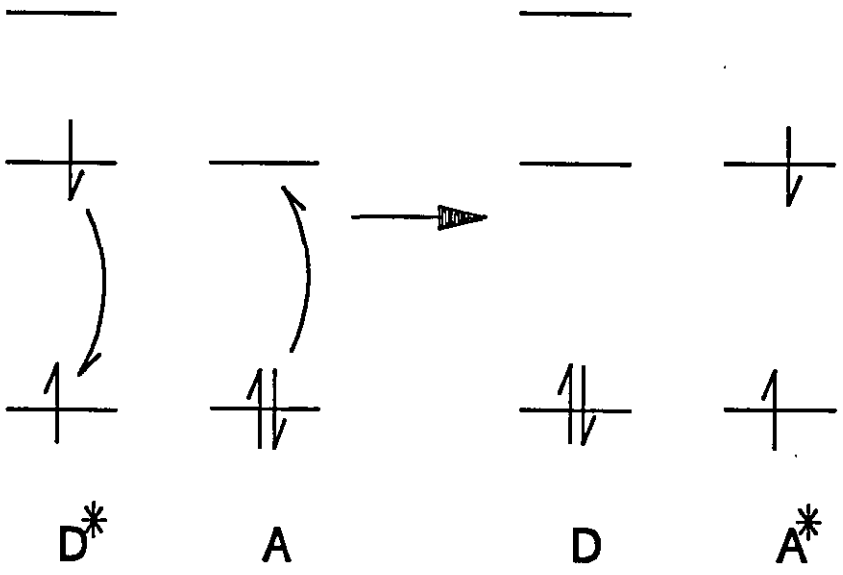

Figure 1.6:- Schematic Representation of Coulombic Energy Transfer

Dipole-dipole energy transfer can therefore occur at distances far greater than the sum of the Van der Waals radii of the respective donor and acceptor molecules. Quantitatively, the rate of energy transfer via a coulombic mechanism (k_{ET}) can be described according to the Forster[5] equation:-

$$k_{EN}(Coulombic) = K\frac{\kappa^2 K_D^0}{R_{DA}^6} J(\epsilon_A) \qquad (1.13)$$

where K is a constant accounting for the refractive index of the medium between D^* and A, κ^2 is an orientation factor for the two dipoles (equal to $(2/3)^{1/2}$ for a random distribution of D^* and A), K_D^0 is the radiative rate constant for the decay of the donor, R_{DA} is the molecular separation and $J(\epsilon_A)$ is the spectral overlap integral.

1.2 Light Sources For Laser Flash Photolysis

1.2.1 Xenon Arc Lamps

Xenon arc lamps are frequently used as analysing sources in photochemical experiments[6]. At low pressures, discrete wavelength transitions occur corresponding to emissive transitions of excited atoms. At high pressures (ca. 20 atmos.), a continuum light source is produced which has some line transitions superimposed upon it. Typical output powers in the range 150 W. To 1000 W. are used for photochemical investigations.

1.2.2 Lasers

The term LASER is an acronym for Light Amplification by the Stimulated Emission of Radiation. Presented below is a brief description of the processes involved in laser action together with a summary of the properties of laser light which make it suitable as both an excitation and analysing source in photochemical investigations. The main properties of laser light sources are as follows:-

(a) **Coherence:-** Coherence is the property which separates most clearly laser light from other light sources and is a result of the stimulated emission process (see later) which occurs in laser action as opposed to the spontaneous emission processes responsible for other light sources. Coherence essentially means that the phase of the light wave is correlated in both time and space.

(b) **Directionality:-** Lasers are highly directional light sources with low divergence properties.

(c) **Monochromaticity:-** Laser light sources are essentially monochromatic light sources since all photons are emitted as a result of an induced transition between the same two atomic or molecular energy levels and hence have almost exactly the same frequency (energy). In some cases, more than one lasing transition is possible, the desired wavelength transition can be selected by placing gratings within the laser cavity to only allow amplification of the desired output wavelength.

A commonly adopted approach in the understanding of laser dynamics is to consider a simple atomic two level system with lower and upper energy levels E_L and E_U with populations N_L and N_U respectively. Absorption of a photon can occur if the photon energy is equivalent to the energy gap E_{UL} (see also equation 1.1) between E_L and E_U, ie.,

$$E_{UL} = E_U - E_L \qquad (1.14)$$

We can define the power absorbed from a beam of photons with energy E_{UL} as:-

$$P_{Absorbed} = h\nu_{LU} B_{LU} N_L \rho(\nu_{LU}) \qquad (1.15)$$

where $\rho(\nu_{LU})$ is the power density of the incident photons and B_{LU} is the Einstein "B" coefficient of the transition for the upward transition (Einstein coefficients are essentially a measure of the strength of an electronic transition). Before proceeding further, it is necessary to define the three possible radiative processes for a non-degenerate two level system, ie., absorption, stimulated emission and spontaneous emission as shown in figure 1.7:-

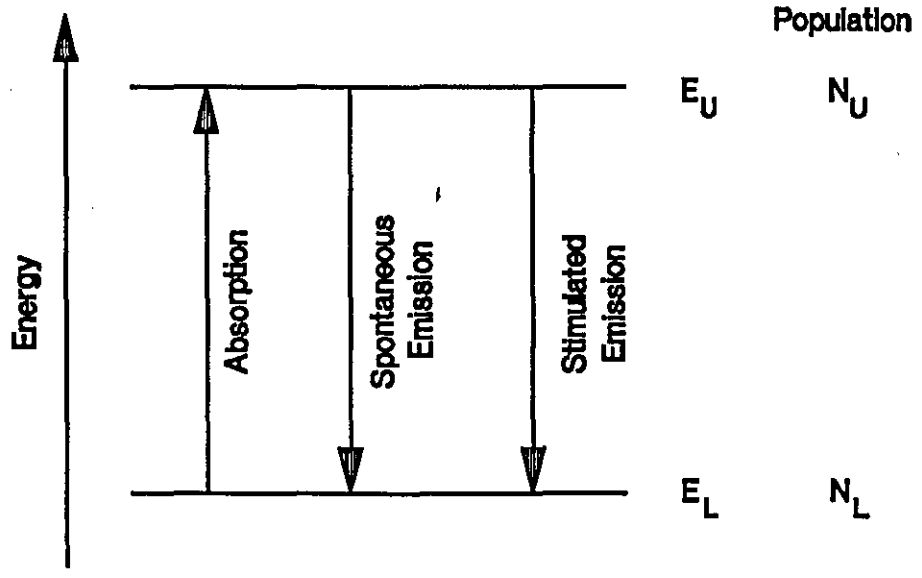

Figure 1.7:- Schematic Representation of Absorption, Stimulated Emission and Spontaneous Emission for a Non-degenerate Two Level Energy System

Einstein "B" coefficients refer to absorption (B_{LU}) and stimulated emission (B_{UL}) respectively where it can be shown that $B_{LU} = B_{UL}$. The Einstein "A" coefficient describes the intensity of spontaneous emission and is termed A_{UL} (it is possible to calculate A_{UL} from a known value of B_{UL}). Thus, the power radiated as a result of spontaneous emission can be defined according to equation 1.16:-

$$P_{Spontaneous} = h\nu_{LU} A_{UL} N_U \qquad (1.16)$$

Spontaneous emission is a random process, photons are emitted in all directions by excited state species in order to reach a lower energy state. Kinetically, the rate or loss of species from E_U to E_L is first order for a statistically large population of excited species. Stimulated emission is a process whereby an atom in E_U is stimulated to emit a photon of energy equivalent to the energy gap E_{UL}. The process can therefore be written (equation 1.17):-

$$A^* + h\nu \rightarrow A + 2h\nu \qquad (1.17)$$

The isoenergetic stimulated photon emitted is in the same direction as, and in phase with, the stimulating photon giving rise to the coherence property of a laser beam. The power radiated by stimulated emission can therefore be defined as:-

$$P_{Stimulated} = h\nu_{LU} B_{LU} N_U \rho(\nu_{LU}) \qquad (1.18)$$

If we divide equation 1.18 by equation 1.15 we obtain equation 1.19:-

$$\frac{P_{Stimulated}}{P_{Absorbed}} = \frac{h\nu_{LU} B_{UL} N_U \rho(\nu_{LU})}{h\nu_{LU} B_{LU} N_L \rho(\nu_{LU})} = \frac{N_U}{N_L} \qquad (1.19)$$

Thus, in order for emitted power to dominate over losses by absorption and spontaneous emission, we require that:-

$$\frac{N_U}{N_L} > 1 \qquad (1.20)$$

Under normal conditions, the ratio $N_U/N_L << 1$ as a direct result of the Boltzmann distribution. Therefore, in order to obtain the conditions required for laser action, ie., the creation of a "population inversion", energy must be supplied to the system. The process of "pumping" a laser medium can occur by one of two main methods:-

(a) Optical Pumping:- A flash tube discharge emitting at the appropriate frequency such that the laser material can become excited.
(b) Electrical Discharge:- This method results in the ionisation of particles which, following acceleration in an electric field, collide with particles of the laser medium which subsequently becomes excited.

Optical pumping is generally used for solid state lasers such as Nd:YAG lasers (neodymium doped yttrium aluminium garnet) while electrical discharge is generally used in gas phase laser (eg. Helium-neon lasers) systems.

A drawback of the two level laser system so far discussed is that both the absorption and stimulated emission processes can be evoked by the same photon. Consequently, to avoid such problems, three and four level laser systems are used in which a population inversion is more easily achieved. Such systems are presented in figure 1.8 for the ruby and Nd:YAG lasers respectively. The design of a laser cavity must ensure that the gain due to stimulated emission is greater than all other losses from the cavity such as absorption, scattering and spontaneous emission. This is achieved by arranging concave mirrors at either

end of the laser cavity (the output mirror is partially transparent) thus allowing many passes of the light through the laser medium.

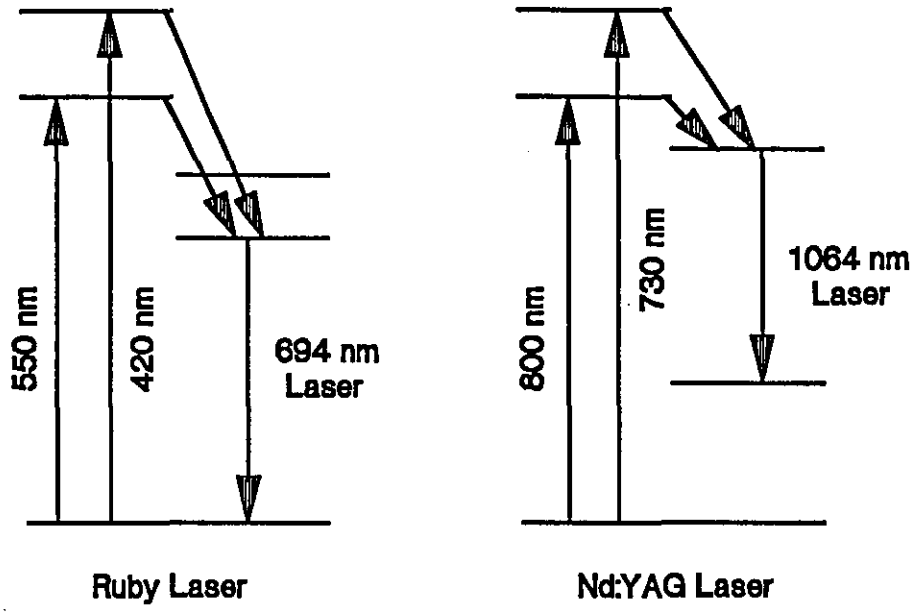

Figure 1.8:- Energy Levels Present in a Three Level Ruby Laser and Four Level Nd:YAG Laser

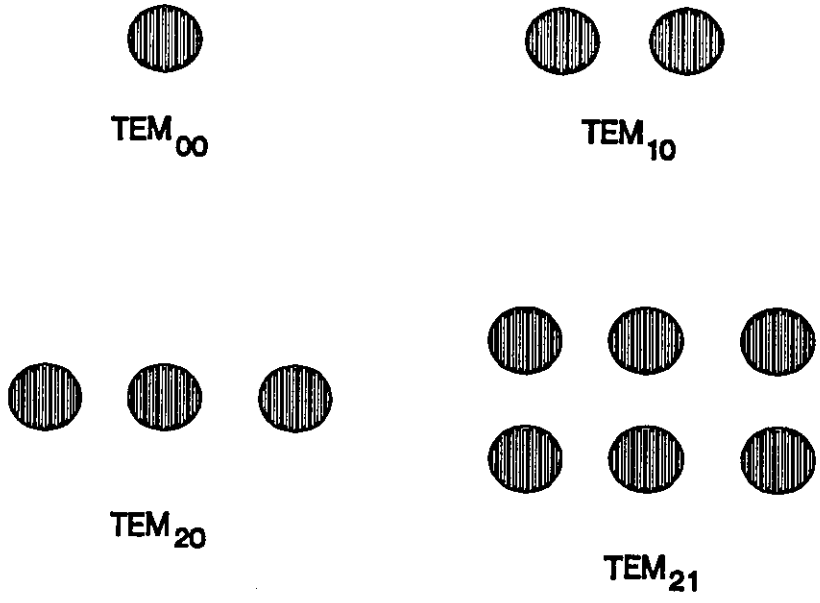

Figure 1.9:- Examples of Frequently Encountered Transverse Laser Modes

At this point, it is necessary to define the modes of oscillation (standing wave patterns) in an optical cavity:-

(a) Transverse Modes:- These reflect the light intensity profile across the output mirror of the laser cavity. The use of slightly concave end mirrors allows the oscillation of slightly off-axis light propagation along the length of the laser cavity. Such modes are described in terms of TEM_{PQ} where TEM stands for Transverse Electric and Magnetic Fields and the subscripts P and Q describe the number of intensity minima across the laser beam in two perpendicular directions as shown in figure 1.9. Ideally, operation of the laser in the TEM_{00} mode is desirable as it results in a gaussian intensity profile across the beam. This mode can be preferentially selected (and all other modes subsequently destroyed) by placing an iris concentric with the optical axis of the laser cavity.

(b) Axial Modes:- The length of the laser cavity L is such that a standing wave condition (ie. a series of points of zero amplitude within the laser cavity) is achieved where an integral number of half wavelengths of light fit into the laser cavity, ie:-

$$L = \frac{m\lambda}{2} \tag{1.21}$$

where M is an integer and λ is wavelength. The mode of oscillation for each standing wave pattern has associated with it a frequency distribution (figure 1.10).

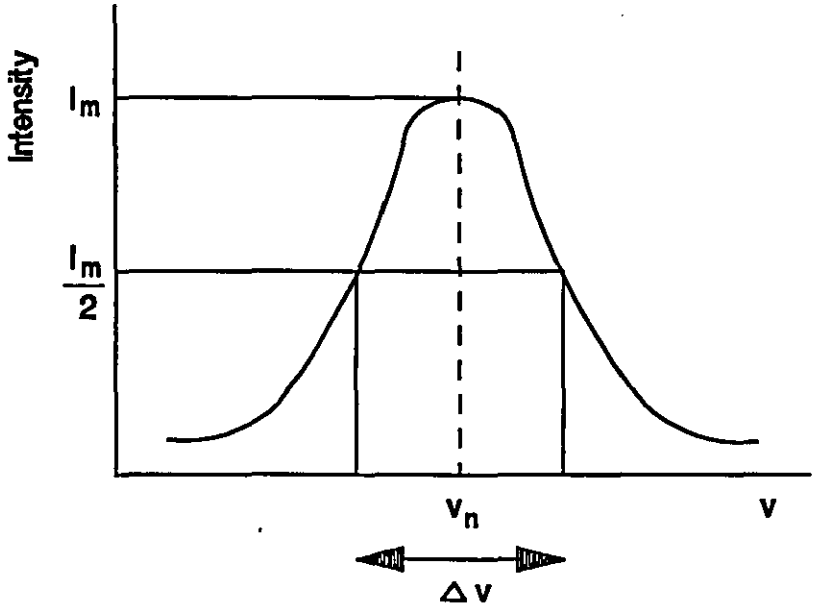

Figure 1.10:- Laser Intensity Profile as a Function of Laser Light Frequency

Such distributions, or line width result from a variety of line broadening processes[7]. The parameter $\Delta\nu$ is defined as the line width of the laser and is equal to the full width half maximum (FWHM) of the frequency distribution. From this distribution, the quality factor (or Q factor) for the laser cavity can be defined as:-

$$Q = \frac{\nu_n}{\Delta\nu} \tag{1.22}$$

where ν_n is the most intense emission frequency. Quality factors may be as high as 10^8 and may be achieved as a result of the narrow output bandwidth.

Lasers can be divided into two main categories, namely continuous wave (CW) and pulsed lasers. Time resolved laser flash photolysis techniques rely on the rapid population of a high concentration of excited state molecules and thus employ pulsed lasers as excitation sources. The process of Q-switching is frequently used to generate a high intensity short time duration laser pulse for such purposes. An alternative definition of the quality factor Q is given by:-

$$Q = 2\pi\nu_n \times \frac{energy\,stored\,by\,mode}{energy\,lost\,per\,second\,from\,mode} \tag{1.23}$$

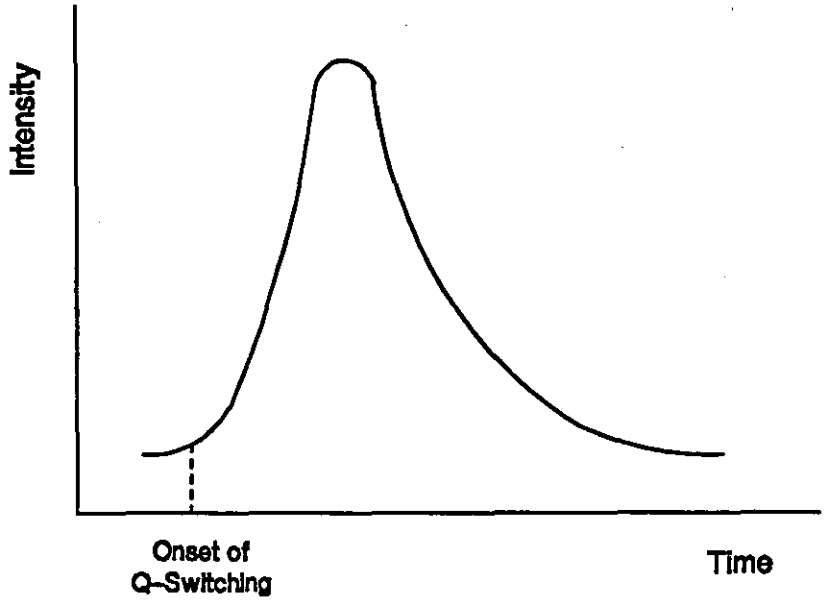

Figure 1.11:- Typical Temporal Profile for a Q-Switched Laser Pulse

The process of Q-switching therefore involves moving from a high loss, low Q situation to a low loss, high Q situation in the laser cavity. This is achieved in modern lasers with the use of electro-optic shutter placed within the cavity which generally takes the form of a Pockels cell. Briefly this optical shutter prevents laser action when an electric field is applied to the material and there exists a low Q-factor in the laser cavity. At this point the laser material is pumped to produce a good population inversion. When the voltage across the crystal is briefly turned off, the gain in the cavity rapidly increases and laser action can occur resulting in a high Q-factor and rapid depopulation of the upper lasing level of the laser material in the form of a single high intensity laser pulse of time duration generally of the order of 10^{-9} to 10^{-8} s. A typical temporal profile for a Q-switched laser pulse is shown in figure 1.11, laser pulse-widths are quoted as the FWHM of this temporal profile.

1.3 Singlet Oxygen

Oxygen is unlike any other homonuclear diatomic molecule. It possesses an even number of electrons resulting in it being paramagnetic in its ground state. A simple molecular orbital diagram of ground state molecular oxygen is shown in figure 1.12.

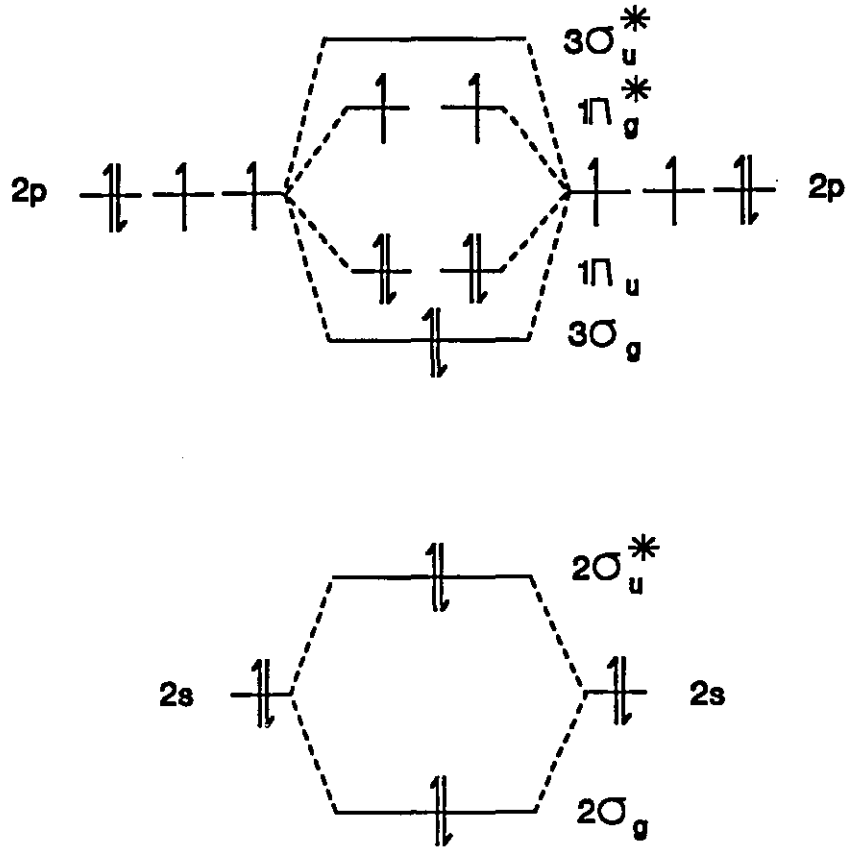

Figure 1.12:- Molecular Orbital Diagram for Ground State Molecular Oxygen

As can be seen from the singly occupied $1\pi_g^*$ orbitals, the ground state of molecular oxygen is triply degenerate and is given the term symbol $^3\Sigma_g^-$. There are two possible arrangements of the two electrons in the $1\pi_g^*$ orbitals.

(a) The electrons are spin paired in the same orbital leading to a double degenerate state.
(b) The electrons are spin paired in separate orbitals with the state being singly degenerate.

These two states are known as the $^1\Delta_g$ and $^1\Sigma_g^+$ excited singlet states of molecular oxygen and lie 95 kJ.mol.$^{-1}$ and 158 kJ.mol.$^{-1}$ above the ground state. Excitation into the $^1\Sigma_g^+$ excited state is followed by rapid relaxation to the $^1\Delta_g$ excited singlet state. It is the $^1\Delta_g$ state which is referred to as "singlet oxygen" and the state from which, due to its appreciable natural radiative lifetime (ca. 0.93 h.[8]), reaction may take place. Although singlet oxygen can be generated via chemical means with the use of the hyperchlorite/peroxide[9] reaction or via the electrical discharge in the gas phase[10], by far the frequent method of generation is via organic dye sensitised energy transfer to ground state molecular oxygen.

The triplet-singlet energy gap for molecular oxygen results in ground state molecular oxygen quenching the lifetime of almost all lowest lying triplet states of organic dyes as shown in equations 1.24 and 1.25:-

$$^3D^* + O_2(^3\Sigma_g^-) \rightarrow {}^1D + O_2(^1\Delta_g) + heat \qquad (1.24)$$

$$^3D^* + O_2(^3\Sigma_g^-) \rightarrow {}^1D + O_2(^3\Sigma_g^-) + heat \qquad (1.25)$$

where $^3D^*$ is the excited triplet state of an organic energy donor molecule. As can be seen, not all quenching leads to singlet oxygen formation. The quantum yield of singlet oxygen production (ϕ_Δ) can be determined via a technique known as thermal lensing which utilises the heat generated from the non-radiative deactivation pathways of excited states in solution[11]. The quenching of the lifetime of an excited state together with the formation of singlet oxygen are strong evidence in favour of the excited states being that of the triplet state of the molecule under examination. It must however be noted that, if the singlet state lifetime of the molecule under investigation is long or high oxygen concentrations are present, processes such as oxygen enhanced intersystem crossing (equations 1.26 and 1.27) or donor excited singlet state sensitization of singlet oxygen (equation 1.28) may also occur which and may confuse the initial assignment.

$$^1D^* + O_2(^3\Sigma_g^-) \rightarrow {}^3D^* + O_2(^3\Sigma_g^-) \qquad (1.26)$$

$$^1D^* + O_2(^3\Sigma_g^-) \rightarrow {}^3D^* + O_2(^1\Delta_g) \qquad (1.27)$$

$$^1D^* + O_2(^3\Sigma_g^-) \rightarrow {}^1D + O_2(^1\Delta_g) \qquad (1.28)$$

Reaction 1.27 can only occur if the singlet-triplet energy gap of the donor molecule is greater than 7880 cm.$^{-1}$ (ca. 95 kJ.mol.$^{-1}$), the (0,0) excitation energy of singlet molecular oxygen. A practical demonstration of the assignment of the first nanosecond timescale observed excited state of milled wood lignin (MWL) using singlet oxygen as a diagnostic tool can be found in section 5.4.4 of this thesis.

Although the radiative deactivation of singlet oxygen shown by equation 1.29 is an inefficient process with a phosphorescence quantum yield (ϕ_P) of ca. 10^{-6}, the development of infra-red sensitive germanium photodiodes has allowed detection of this process directly under many experimental conditions.

$$O_2(^1\Delta_g) \overset{k_{rad}}{\rightarrow} O_2(^3\Sigma_g^-) + h\nu(1270nm) \qquad (1.29)$$

Details of such apparatus can be found in section 3.7 of this thesis. Not only can the lifetime of singlet oxygen (τ_Δ) in a variety of environments be directly determined via this method, the singlet oxygen phosphorescence emission intensity (in pulsed laser experiments) extrapolated to zero time following the laser pulse (I_Δ^0) as a function of laser intensity can be used with an appropriate standard compound to determine singlet-triplet intersystem crossing quantum yields of unknown compounds (see sections 4.3.2 and 5.4.5).

There exist both physical and chemical deactivation pathways for singlet oxygen in fluid solution. Physical quenching processes can be divided into three broad deactivation mechanisms.

(a) Solvent quenching:- The lifetime (τ_Δ) of singlet molecular oxygen is severely shortened in certain solvents such as water, hydrocarbons and alcohols. This appears to be directly related to the absorption of the solvent at 7880 cm.$^{-1}$ (see above), the singlet oxygen itself deactivating via an electronic-vibrational energy transfer mechanism. This has been clearly demonstrated by deuteration of solvents reducing the absorption of such solvents in the 7880 cm.$^{-1}$ region of the spectrum. A comprehensive list of singlet oxygen lifetimes in a variety of solvents can be found in the literature[12].

(b) Charge Transfer Quenching:- Certain groups of compounds have been suggested to quench singlet oxygen via a charge transfer or partial charge transfer exiplex as shown by equation 1.30:-

$$O_2(^1\Delta_g) + {}^1A \leftrightarrow [O_2^{\delta^-} \cdots A^{\delta^+}] \rightarrow O_2(^3\Sigma_g^-) + {}^1A \qquad (1.30)$$

where A is a suitable quencher. Such groups of quenchers include phenols[13], amines[14], and sulphides[15], although some of these compounds may also quench via chemical reaction (see later).

(c) Energy Transfer:- Quenching via energy transfer mechanisms as shown in equation 1.31:-

$$O_2(^1\Delta_g) + {}^1A \leftrightarrow O_2(^3\Sigma_g^-) + {}^3A^* \qquad (1.31)$$

where A is an acceptor with a triplet energy of less than or close to 95 kJ.mol.$^{-1}$. The most widely known and studied compound with such properties is β-carotene[16], the sensitised production of triplet β-carotene (λ_{max}^{TT} at ca. 515 nm[17]) being clearly demonstrated to occur via an energy transfer mechanism with singlet oxygen acting as the energy donor molecule.

Singlet oxygen is known to undergo chemical reaction with a variety of substrates (see above). Probably the best known example of such a reaction is that with 1,3-diphenylisobenzofuran (DPBF) as detailed by figure 1.13:-

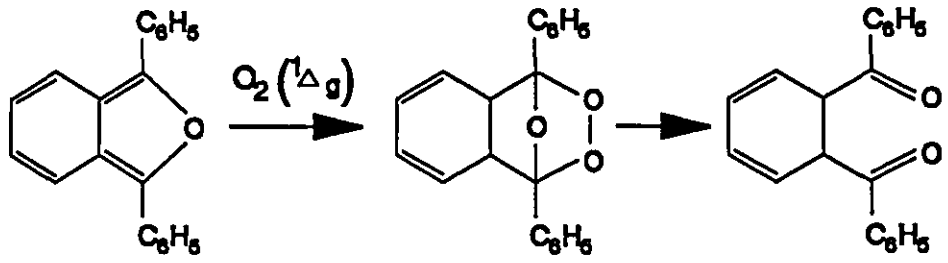

Figure 1.13:- The Reaction of Singlet Molecular Oxygen with 1,3-Diphenylisobenzofuran (DPBF) in Fluid Solution

Since, under suitable conditions, this reaction is quantitative, the bleaching of the absorption by DPBF (monitored at 420 nm[18]) has been used to study singlet oxygen in a variety of systems. Also, and of direct relevance to the theme of this thesis, is the chemical reaction between singlet oxygen and phenols to yield the phenoxy/ hydroperoxy ($HO_2\cdot$) free radical pair (see section 5.4.5 for details).

1.4 The Nature of Reflection From Diffusing Media

The reflection of light from any surface can be split into two discreet components namely specular (regular or mirror-like) reflection and diffuse reflection. Specular reflection can be regarded as taking place at the boundary of condensed phases where the equations to describe specular reflection derived by Fresnel[19] have been shown to apply. Many discussions of these equations can be found in the literature[20,21,22] and thus will not be discussed here. Diffuse reflection of light is observed from any matt surface and arises from light penetration into the interior of the sample whereupon it undergoes partial absorption and multiple scattering at the boundaries of the individual particles making up the sample. Various theoretical studies have attempted to predict the intensity of diffusely scattered light as a function of penetration depth

into the sample with some success. The attenuation of the diffusely reflected light (I) due to absorption within the sample, as a function of penetration depth can be predicted by the Bouguer-Lambert equation (equation 1.32) which states:-

$$I = I(0)\exp(-Kx) \tag{1.32}$$

where K is the absorption coefficient and x is the mean penetrated layer thickness. From the form of this equation the intensity of the diffuse light is shown to decrease exponentially with penetration depth into the sample. This is an important observation when one is considering excited state populations as a function of penetration depth for samples subjected to diffuse reflectance laser flash photolysis experiments (see later).

The Lambert cosine law[22] (equation 1.33), where α is the angle of incidence and Θ is the angle of observation, predicts that the intensity of diffusely reflected light B emerging from a diffuse scatterer should be of equal intensity at all angles with respect to the surface normal.

$$B = \left(\frac{I(0)}{\pi}\right)\cos\alpha\cos\Theta \tag{1.33}$$

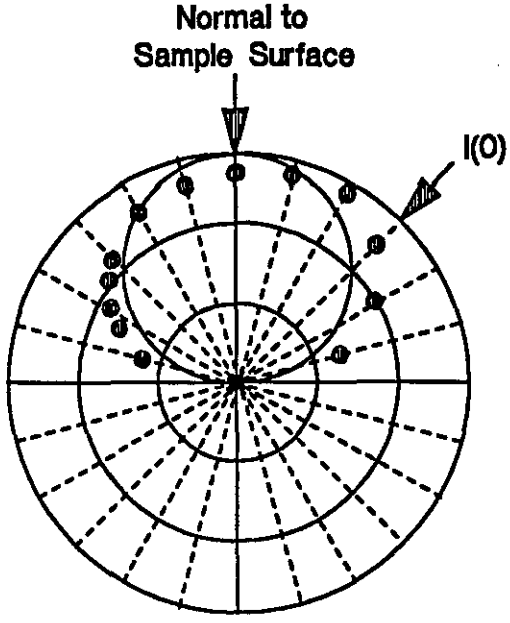

Figure 1.14:- Spherical Indicatrix of Diffusely Reflected Radiation from a Non-Absorbing Matt Surface According to Equation 1.33. (Experimental Points are for Sulphur in the Infra-Red[23])

The predicted "indicatrix" is thus a sphere with the diffusely reflected light being unpolarised irrespective of the polarisation of the incident light. Equations 1.33 has been shown experimentally to hold reasonably well for highly scattering samples[24,23] when α and Θ are small.

Deviation from the Lambert cosine law does occur when α and Θ are large, the indicatrix of intensity as a function of angle to the surface normal becoming more of an oblate ellipsoid than a sphere (see figure 1.14).

This observation can be explained in one of two ways:-

a) A matt surface consisting of small crystallites orientated at all possible angles with respect to the macroscopic surface, the combined specular reflection from all such surfaces being responsible for the scattering of the incident radiation.

b) Diffusion of light occurs by multiple scattering by individual particles within the sample interior.

Of the two postulates, the latter seems to be the more favoured explanation[25]. However, Jentzsch[26] suggested that a contribution from both specular and diffusely reflected light does occur, the exact contribution of each being a function of the nature of the sample under investigation.

When an opaque sample selectively absorbs some incident radiation, the situation in terms of the relative contributions from diffuse and specular reflected light to the overall reflectance from such a sample are further complicated. As has been discussed above (see equation 1.32), the regular reflection component approaches unity for strongly absorbing samples. Thus, for an absorption band, the two components of the reflected light can be regarded as opposing one another and both must be considered when the spectral intensity distribution from a sample is being studied.

A generally observed rule for weakly absorbing diffusely reflecting samples is that the smaller the particle size of the sample the lighter the material appears. This can be explained by a decrease in the penetration depth of incident light thus reducing the apparent absorption of the sample. Kortum and Vogel[27] confirmed this observation experimentally with weakly absorbing crystals of hydrated copper sulphate ($CuSO_4.5H_2O$), the observed absorption relative to a white reflectance standard from $CuSO_4.5H_2O$ decreasing with decreasing particle size. For weakly absorbing samples, the contribution to the observed reflectance spectrum by regular reflection is small. However, when one considers strongly absorbing samples such as potassium permanganate crystals ($KMnO_4$), where light penetration into the sample interior is extremely small due to strong absorption, a different effect is observed. Firstly, the observed absorption spectrum is less affected by particle size compared with $CuSO_4.5H_2O$ and the increased proportion of regular reflection in such a strong absorber makes the observed absorbance less than would be expected on the basis of diffuse reflection alone. Also, the absorption increases with decreasing particle size indicating that the amount of regular reflection is also decreasing, this effect outweighing the decrease in penetration depth. By removing the contribution due to regular reflection completely by cross polarising the analyser relative to the incident radiation two observations for a sample of $KMnO_4$ can be measured. The absorption of the sample is increased relative to the unpolarised absorption indicating that there is considerable contribution from the regular reflectance component for this sample and the absorption also becomes independent of particle size in keeping with the fact that the penetration depth of incident radiation for strongly absorbing samples is extremely small.

1.5 Kubelka-Munk Theory

The Beer-Lambert law (section 1.1) defines the relationship between the absorbance (A) and the concentration of a ground state absorber (C_A) for transparent media. As mentioned previously, opaque "optically thick" samples do not transmit light and therefore the Beer-Lambert law cannot be applied to such samples. The most widely applied theory which relates "absorption" and concentration for such samples is the theory derived by Kubelka and Munk[28,29], a brief description of which is presented below.

The Kubelka-Munk theory assumes that the sample in question contains randomly distributed absorbing and scattering particles whose dimensions are far less than the layer thickness and that the sample is illuminated with a monochromatic light source. A suitable starting point for the derivation of the Kubelka-Munk equation is the two differential equations 1.34 and 1.35[28,30] which describes a light flux in a thin slice of thickness dx at a distance below the irradiated surface of the sample.

$$dI(x) = -(K+S)I(x)dx + SJ(x)dx \tag{1.34}$$

$$dJ(x) = (K+S)J(x)dx - SI(x)dx \tag{1.35}$$

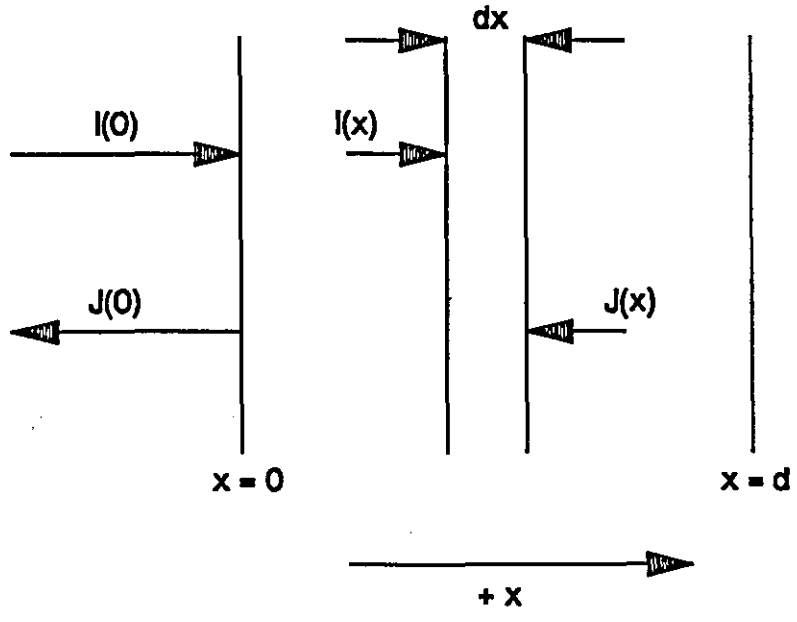

Figure 1.15:- Schematic Representation of a Layer of Absorbing and Light Scattering Particles

By convention, the two perpendicular light fluxes I(x) and J(x) describe the light flux into (the +x direction) and out (-x) of the sample. Hence, at the surface of the sample x = 0 and at an unirradiated depth into the sample x = d. The initial intensity of the light source entering the sample (x = 0) is defined as I(0) and the intensity of light emerging from the sample is defined as J(0). These definitions are shown diagrammatically in figure 1.15.

The parameters K and S refer to the absorption coefficient and scattering coefficient respectively both of which take the units of reciprocal distance (usually $cm.^{-1}$). The absorption coefficient K_A of an absorber A with concentration C_A and naperian extinction coefficient ϵ_A is defined as in equation 1.36:-

$$K_A = \omega \epsilon_A C_A \tag{1.36}$$

where ϵ_A and C_A have the units $l.mol.^{-1}cm.^{-1}$ and $mol.l.^{-1}$ respectively. The parameter ω is a geometry factor which accounts for the angular distribution of diffusely reflected light. For ideal diffusers $\omega = 2$[31]. Note from equation 1.34 that when S = 0 then:-

$$dI(x) = -KI(x)dx \tag{1.37}$$

which is the familiar Lambert law for transparent media.

Equations 1.34 and 1.35 can be solved for a layer so thick that any further increase in the layer thickness does not affect the reflectance from the sample which yield:-

$$I(x) = I(0)\exp(-bSx) \tag{1.38}$$

and

$$J(x) = RI(0)\exp(-bSx) \tag{1.39}$$

where

$$b = \frac{(K^2 + 2KS)^{0.5}}{S} = \left(\frac{1}{2R} - R\right) \tag{1.40}$$

and R is the reflectance from surface of the sample (x = 0). Thus, dividing equation 1.39 by equation 1.38 for when x = 0 gives:-

$$R = \frac{J(0)}{I(0)} \tag{1.41}$$

When the transmittance of the sample (T) is equal to zero then the reflectance R is defined as R_∞, the reflectance of an optically thick sample.

Further manipulation of equations 1.38 and 1.39 give the familiar form of the Kubelka-Munk equation (equation 1.42):-

$$F(R_\infty) = \frac{(1-R_\infty)^2}{2R_\infty} = \frac{K}{S} = \frac{2\epsilon_A C_A}{S} \qquad (1.42)$$

The parameter $F(R_\infty)$ is referred to as the Remission Function, a unitless quantity which is directly proportional to the concentration C_A of an absorbing species A. If we take logarithms of equation 1.42 we obtain:-

$$\log_{10} F(R_\infty) = \log_{10} K - \log_{10} S \qquad (1.43)$$

The validity of equation 1.42 was tested by Kortum *et al*[32] who recorded the transmission spectrum of a didymium glass filter relative to clear glass filter and compared the observed spectrum with the reflectance spectrum obtained by grinding the didymium filter to a fine powder and measuring the reflectance spectrum relative to a ground-up clear glass filter. Using $\log_{10} F(R_\infty)$ as the ordinate scale for the reflectance spectrum, the two spectra were almost superimposible (displaced from each other by $\log_{10}S$ on the ordinate scale) demonstrating that the assumptions made in order to derive equation 1.42 are small and in most cases can be neglected.

The Kubelka-Munk theory thus provides a parameter ($F(R_\infty)$) which is directly proportional to C_A for opaque samples in a similar manner to the Beer-Lambert law where the absorbance (A) is proportional to C_A for transparent non-diffusing samples.

The scattering coefficient defined in the Kubelka-Munk equation (equation 1.42) has no equivalent coefficient in the Beer-Lambert law for transparent media and thus merits a brief discussion here. The Kubelka-Munk equation provides no information concerning the variation of S as a function of wavelength (λ) since it assumed a monochromatic light source for its derivation. Experiments performed by Kortum *et al*[32] demonstrated that the scattering coefficient was inversely proportional to the root mean square particle diameter $(\bar{d}^2)^{0.5}$ for a BG36 glass filter ground to different particle sizes and that the scattering coefficient increased as the wavelength of the incident light decreased. Further experiments by Kortum and Oelkrug[33] using a variety of materials showed that for samples where $(\bar{d}^2)^{0.5} < \lambda$ then S is proportional to $\lambda^{-2.6}$ to $\lambda^{-3.6}$. Also, when $(\bar{d}^2)^{0.5} \sim \lambda$ then S is proportional to λ^{-1} and for $(\bar{d}^2)^{0.5} > \lambda$ then S is proportional to λ^{-1} to λ^{0}. These observations approach the predicted theory for light scattering from samples where $(\bar{d}^2)^{0.5} << \lambda$ where the scattering is known as Rayleigh scattering and S is proportional to λ^{-4}.

1.6 Diffuse Reflectance Laser Flash Photolysis

Laser flash photolysis experiments involve the photochemical generation of transient species which absorb light in a different wavelength region to the ground state. If we consider a ground state absorber (A) with concentration C_A which, following pulsed laser excitation, produces a population of excited states (T) with concentration C_T with a quantum yield ϕ_T for the conversion then from equations 1.38, 1.39 and 1.40 it can be shown that:-

$$\frac{dC_T}{dt}(x) = K^e \phi^T (1 + R^e) I^e(0) \exp(-b^e S x) \qquad (1.44)$$

where the superscript e indicates the excitation wavelength, K_e is the naperian absorption coefficient at the excitation wavelength, R^e is the ground state reflectance at the excitation wavelength and $I^e(0)$ is the laser intensity. As can be seen from equation 1.44, when the percentage of ground state molecules converted to the excited state (T) is low, the concentration of transient species immediately following the laser pulse falls off exponentially as a function of penetration depth x into the sample.

The observable parameter in diffuse reflectance laser flash photolysis experiments is the fractional reflectance change at an analysing wavelength (a) as a function of time ($\Delta R(t)$) defined according to equation 1.45:-

$$\Delta R(t) = \frac{\Delta J(t)}{J(0)} = \frac{R_B^a - R_C^a(t)}{R_B^a} \qquad (1.45)$$

where R_B^a is the sample reflectance at the analysing wavelength before excitation and $R_C^a(t)$ is the reflectance corrected for emission at time t after excitation. In keeping with the convention of the Kubelka-Munk theory (see section 1.5) where J represents the intensity of diffusely reflected light emerging out of a scattering sample, we can define the intensity of diffusely reflected light before laser excitation as J(0) and the change in diffuse reflected light intensity at time t following the laser pulse as $\Delta J(t)$. In some cases, the percentage reflectance change is used instead of the fractional reflectance change and is defined as $100\Delta R(t)$.

The analysis of data obtained from diffuse reflectance is not as straight forward as that for transmission laser flash photolysis experiments. A knowledge of the concentration of excited states (C_T) as a function of penetration depth into the sample must be known so that the correct analytical model can be applied to the data. This distribution is dependent upon many sample parameters including the concentration of ground state molecules before laser excitation ($C_A(0)$), the molar extinction coefficient of the ground state molecules at the laser excitation wavelength (ϵ_A), the reflectance (R_s^a) and scattering coefficient (S_s) of the support material, and the excitation pulse intensity ($I^e(0)$). Detailed below is a brief description of these effects, a full discussion of which can be found in the literature[34,35].

There exists two limiting cases for the concentration profiles of excited states as a function of depth into the sample together with an intermediate type profile shown diagrammatically in figure 1.16.

Case A:- The transient concentration C_T falls off exponentially with increasing penetration depth into the sample. This applies to samples with low conversion of ground state molecules to the excited state and is also more likely when $I^e(0)$ is low and ϵ_A is high resulting in the laser pulse being significantly attenuated upon penetration into the sample. The Kubelka-Munk equation (equation 1.42) cannot be applied to such a system as a prerequisite of its use for

absorption measurements from diffuse media is that the concentration of the absorber be randomly distributed as a function of penetration depth into the sample. What is needed in this case is a solution to equations 1.38 and 1.39 at the analysing wavelength (superscripted a) where the absorption coefficient K^a varies exponentially with x. The equations have been solved by Lin and Kan[36] who give (equation 1.46):-

$$R = R_B^a \frac{1 + \frac{\gamma}{\delta}u + \frac{\gamma(\gamma+1)u^2}{\delta(\delta+1)2!}\cdots}{1 + \frac{\gamma+1}{\delta}u + \frac{(\gamma+1)(\gamma+2)u^2}{\delta(\delta+1)2!}\cdots} \tag{1.46}$$

where

$$\gamma = (b^e R_B^a)^{-1} \tag{1.47}$$

$$\delta = \gamma + 1 - \frac{R_B^a}{b^e} \tag{1.48}$$

and

$$u = \frac{2K^a(0)}{b^e S} \tag{1.49}$$

This series converges for all values of u and thus, for diffusely reflecting/absorbing samples which exhibit low percentage conversion of C_A to C_T or small reflectance changes following pulsed laser excitation, equation 1.46 can be used for analysis of data obtained from such samples.

It has been shown that, from the solution to equations 1.38, 1.39 and 1.40 given by Lin and Kan (equation 1.46), $\Delta R(t)$ is proportional to C_T provided that $\Delta R(t) < 0.1$. For $\Delta R(t)$ values up to 0.3 deviation from linearity is small but becomes significant as $\Delta R(t) \rightarrow 1$[37]. Thus, for a given decay function for the transient (f(t)) defined as in equation 1.50, f(t) can be obtained directly from the experimental values of $\Delta R(t)/\Delta R(0)$ where $\Delta R(0)$ is the reflectance change at zero time following the laser pulse providing that the proportionality between C_T and $\Delta R(t)$ (equation 1.45) has been established.

$$f(t) = \frac{C_T(t)}{C_T(0)} \tag{1.50}$$

Under certain experimental conditions, the fall-off in C_T as a function of x is not described by equation 1.44, an alternative analytical method for the data obtained from such samples being required as discussed below.

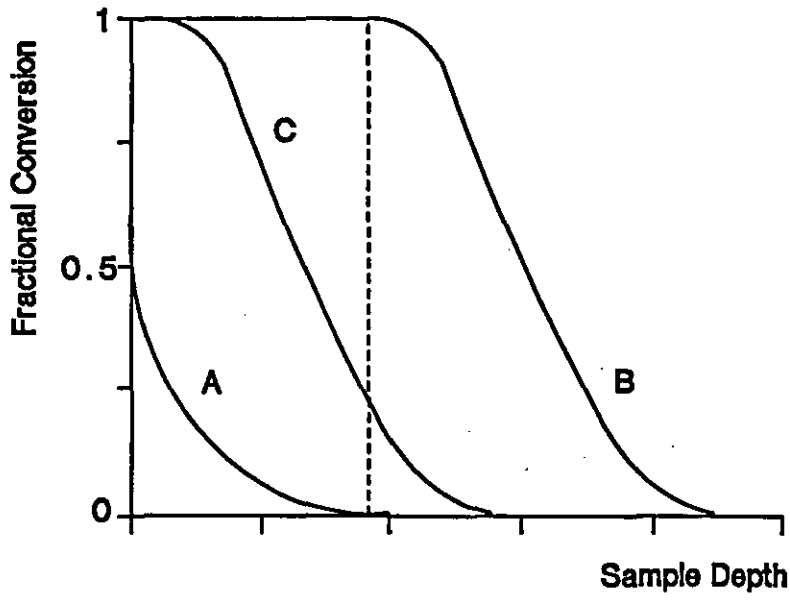

Figure 1.16:- Schematic Representation Of The Two Limiting Types Of Transient Concentration Profile And An Intermediate Between The Two Formed By Laser Excitation Of Solid Samples
Case A:- Exponential Profile, Case B:- Plug Profile, Case C:- Intermediate Profile. The Dashed Line Represents The Penetration Depth Of The Analysing Light

Case B:- A combination of low ground state concentration of absorbing species ($C_A(0)$) which possess a low extinction coefficient (ϵ_A) at the laser excitation wavelength coupled with high laser fluences lead to the formation of a "plug" of excited states close to the sample surface (see figure 1.16) which extends deeper into the sample depth than is probed by the analysing light source (dashed line in figure 1.16). Upon reaching a certain depth into the sample, C_T rapidly falls off in a sharp sigmoid type behaviour, this narrow depth transitional phase separating the plug of excited states from totally photochemically unconverted molecules.
For a homogeneous distribution of excited state species, the Kubelka-Munk theory[28,29] can be applied to such experimental data where C_T is proportional to $F(R_\infty)_i - F(R_\infty)_b$. Details of the analytical procedure applied to such data can be found in section 3.8.2.

Case C:- In such intermediate cases, the excited state concentration profile as a function of penetration depth into the sample is a combination of a plug type behaviour and also that of an exponential fall-off. That is to say, close to the surface of the sample there exists a total conversion of the ground state which rapidly falls off deeper into the sample eventually with an exponential type behaviour. However, the analysing light is of sufficient intensity to probe both regions of the concentration profile (dashed line in figure 1.16) and therefore neither of the analytical method described above can be applied to such data. In such a case, the transient concentration profile is calculated via computer simulation following input of parameters such as laser intensity ($I^e(0)$), scattering coefficient of the support material (S_S), concentration and naperian extinction

coefficient of the absorbing species A (C_A and ϵ_A respectively). From the transient concentration profile, the reflectance change as a function of time ($\Delta R(t)$) after the laser pulse observed from the sample is calculated using estimated values for the naperian absorption coefficients of the ground and excited states at the analysing (α) wavelength (ϵ_A^a and ϵ_T^a respectively). Kinetic analysis is performed by assuming the form of the decay function f(t) and calculating the decay of $\Delta R(t)$ from the transient concentration profile. The decay constants are then varied until a match between the calculated and observed decay curves is obtained. Further details of this procedure can be found elsewhere[37].

Chapter 2

Wood and Lignin Chemistry

2 Wood and Lignin Chemistry

2.1 Introduction

A knowledge of the chemical composition of wood is essential in understanding the chemical and photochemical behaviour of such a complex natural material. It is beyond the scope of this thesis to give detailed anatomical and morphological descriptions of woody tissue. However, it is felt that some information relevant particularly to the photochemical behaviour of lignin as a result of its chemical structure is required to explain fully some of the aspects of the results presented in chapters 5 and 6 of this thesis.

2.2 Gross Structure of Wood

2.2.1 Chemical Composition

The chemical constituents of wood have been well documented in many articles to which the reader is referred for further details[38,39]. The major cell wall constituents of wood are found to consist of cellulose, hemicellulose and lignin. Although the cellulose content is approximately equal between softwood and hardwood species (ca. 41 % to 45 %), it is observed that hardwoods contain less lignin than their softwood counterparts, typical lignin content for softwoods being approximately between 25 % and 35 % and for hardwoods between 18 % and 25 %[40]. The occurrence of all three major chemical components in the cell walls of woody tissues are not confined to discreet morphological regions, rather that intimate cross-linkages occur between the lignin and the carbohydrate fractions of the material which structurally benefit the tree in terms of strength and stability (see section 2.3). Although the precise nature of such intimate cross-linking is not fully understood or quantified, articles detailing experiments and key lignin-carbohydrate linkages can be found in the literature[41,42].

As is well known, the chemical structure of cellulose is based upon a regular repeating unit with chemical formula $(C_6H_{10}O_5)_n$ arranged in a structural conformation known as a (4-O-β-D-glucopyranosyl-D-glucose) sub-unit as shown in figure 2.1.

As can be seen for the linkage of two glucose units to form a cellobiose unit, each sugar unit is linked between the 1 and 4 position by a β linkage. Unlike hemicellulose and lignin, cellulose is a linear chain crystalline polymer, each repeating unit adopting a chair conformation (for energetic reasons) with all three hydroxyl moieties and the primary alcohol functionality occupying the equatorial positions in the ring system.

Hemicellulose is a complex mixture of polysaccharides which closely interpenetrates between the lignin and cellulose fractions of the wood tissue. Unlike cellulose, hemicellulose does not contain a single repeating unit in a linear chain-like fashion but is characterised by being considerably branched and also by having a lower molecular weight than cellulose itself. Many reviews of the structure and biosynthesis of hemicellulose exist in the literature to which the reader is referred to for further detail[43].

The third major wood component, and by far the most significant in terms of photodegradation of wood and paper products, is lignin. Lignin is a three dimensional cross linked heterogeneous "polymer" intimately cross linked with the cellulose and hemicellulose components of the wood material.

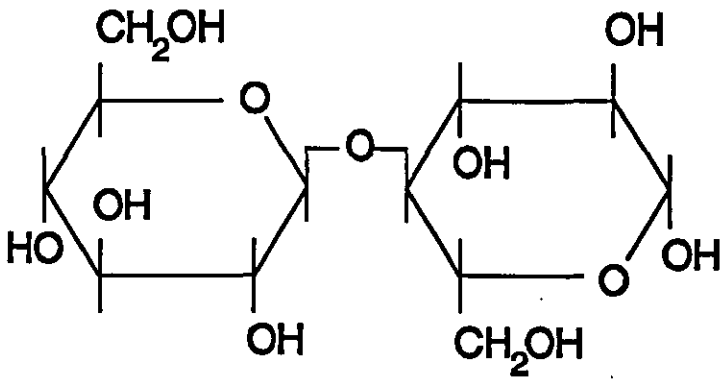

Figure 2.1:- Repeating Sub-Unit of Cellulose Based on the Cellobiose Repeating Structural Unit

Unlike cellulose, lignin is essentially confined to vascular plants which develop specialised tissue for aqueous solution transportation and mechanical support; for example, fungi, algae and mosses do not contain lignin[44]. The roles of lignin within the tree are mainly of a reinforcement and strengthening variety, it is lignin which gives wood its unique elastic and strength properties and its ability to also withstand the large compressive forces enabling trees to grow to such considerable sizes. Unlike cellulose, lignin has no single repeating sub-unit in its structure rather comprising of a structure with an empirical formula based upon a C_9 phenylpropane sub-unit. Extraction of lignin from the carbohydrate matrix involves a certain degree of chemical modification to the structure (see section 5.1). Analysis of chemically extracted lignin known as milled wood lignin (MWL) yield empirical formulae of $C_9H_{8.83}O_{2.37}(OMe)_{0.96}$ and $C_9H_{7.92}O_{2.40}(OMe)_{0.92}$ from two different sources of spruce MWL[45,46].

2.2.2 General Features of Wood Cell Structure

A brief overview of the main cell structure type found in softwood species (known as tracheid cells) is presented below in order to describe the chemical relationship between lignin, cellulose and hemicelluloses found in such cells. Tracheid cells (or fibres) are long hollow tubular structures which are tapered and sealed off at each end. The length of such cells in softwoods species such as Black Spruce (Picea mariana) are, on average, around 3.5 mm long and extend in the direction of the tree length. Typical length to width ratios are of the order of 100:1. The first tracheids formed in the growing season have the greatest fibre width and thinnest cell walls, a region known as the earlywood or springwood growing zone. A growth zone follows, known as summerwood or latewood, where cell wall thickness is greatly increased corresponding to a more strength orientating role for such tracheid cells relative to earlywood which is more suited to the conduction of water and nutrients through

the tree from the roots to developing shoots. Figure 2.2 shows the cell wall organisation of a typical softwood tracheid.

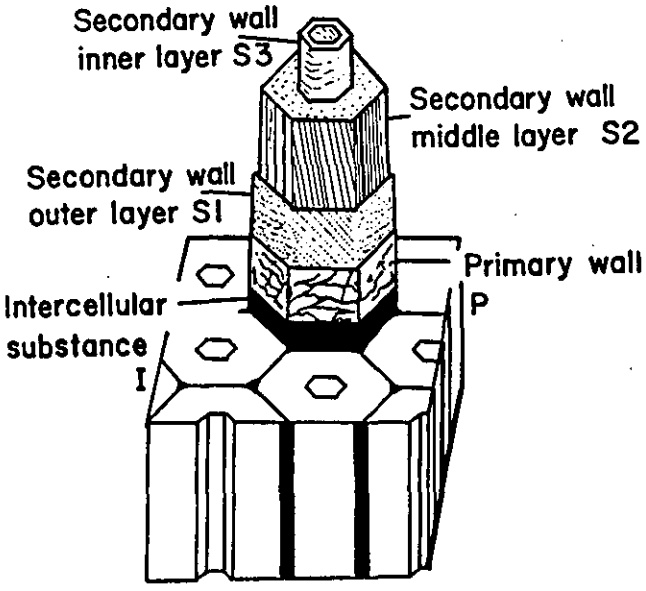

Figure 2.2:- Schematic Diagram representing the Gross Structure of a Softwood Tracheid

As can be seen, the cell wall is split into morphological regions and consists of the primary (P) and secondary (S) wall layers. The primary cell wall is formed during the initial stages of the differentiation of the woody cell, the secondary cell wall layer being formed on the inside of the primary cell resulting in the thickening of the woody cell wall. That is to say, P grows in area but not in thickness whereas S grows in thickness and not area. The secondary wall (S) is further divided into three well defined sub-regions known as the S_1, S_2 and S_3 layers. Typical thicknesses of the P, S_1, S_2 and S_3 are found to be 0.015μm, 0.2μm, 2.5μm and 0.1μm respectively. Differences in the distribution of cellulose, hemicellulose and lignin have been shown to occur between these discreet cell wall layers[47]. The primary cell wall is found to be rich in lignin and hemicellulose and can be regarded as the transition zone between the intercellular substances and the secondary cell wall. The intercellular substance is more commonly known as the middle lamella region (ML) and is essentially made up of lignin and hemicellulose with no cellulose present. Since differentiation between the P and ML layers is often difficult, the term compound middle lamella (CML) is often used to describe this region.

As has been stated earlier, cellulose in woody cells is primarily a polymeric crystalline substance with a fixed repeating unit. In the tracheid cell walls, the polymer orientates itself in the form of cellulose microfibrils. The relationship between these cellulose microfibrils, hemicellulose and lignin can be envisaged as the hemicellulose forming a matrix between the

cellulose microfibrils and lignins being an encrusting substance solidifying the cell wall structure. The differentiation of the secondary cell wall is based upon the orientation of the cellulose microfibrils relative to the longitudinal axis of the tracheid itself.

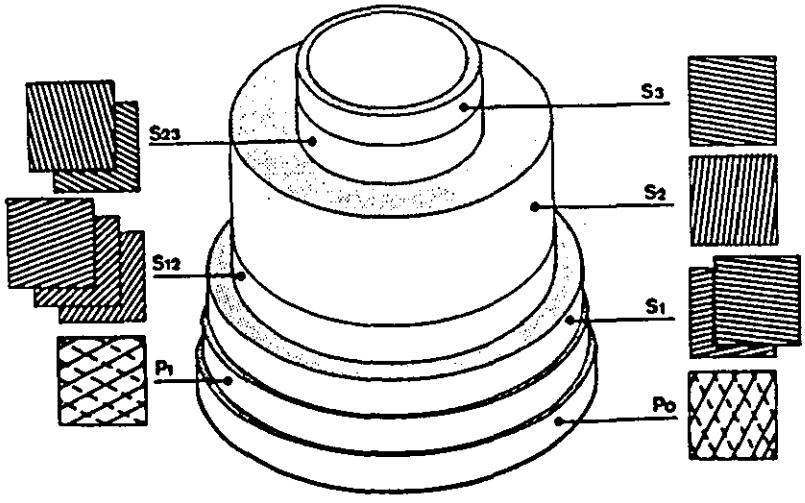

Figure 2.3:- Schematic Diagram of the Microfibril Orientation in the Primary Cell Wall and the Different Layers of the Secondary Cell Wall[48]
P_0 and P_1 are the outer and inner part of the primary wall respectively; S_{12} and S_{23} are intermediate layers between S_1 and S_2 and between S_2 an S_3 respectively

As can be seen in figure 2.3, the orientation of such fibrils in the S_1 and S_3 layers of the secondary cell wall are at a large angle to the longitudinal axis whereas the S_2 layer contains microfibrils at only a small angle to such an axis thus giving added strength to the cell wall. The distribution of lignin within P and S layers also varies considerably. Numerous studies have been conducted which demonstrate not only that the concentration but also the type of lignin present in such regions is variable. The differences in lignin structure between morphological regions of the wood tracheid are discussed fully in section 6.3.2. Shown in figure 2.4 is the concentration of lignin across two cell walls and one middle lamella region of earlywood Black Spruce tracheids measured by UV microscopy at 240 nm[49].

As can be seen, the middle lamella region shows a peak in the concentration of lignin, the distribution of lignin across the secondary cell walls being uniform throughout. However, given that the secondary cell wall region constitutes 87 % of the cell volume, most of the lignin is contained within this region.

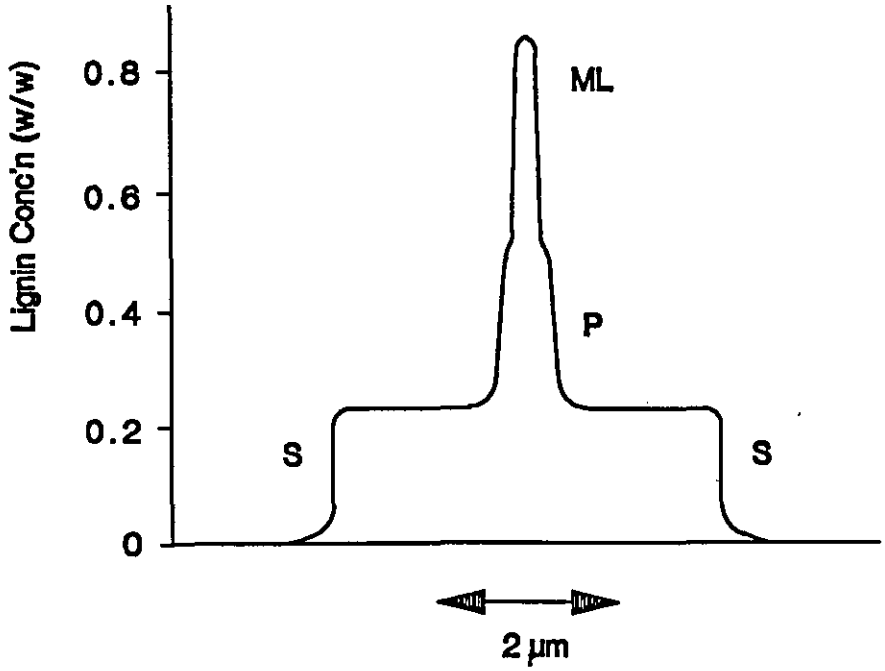

Figure 2.4:- Concentration of Lignin Across Two Cell Walls and One Middle Lamella Region of Earlywood Black Spruce Tracheids Measured by UV Microscopy at 240 nm

2.3 Bio-Genesis and Chemical Composition of Lignin

In spite of extensive research into the lignification process taking place in woody tissues, a full understanding of the processes involved is still incomplete. It was Freudenberg[50] who first clearly demonstrated that the initial precursor to softwood lignin was based upon a C_9 phenylpropane glycosidic molecule (and analogues for hardwood species) known trivially as coniferin, the structure of which is shown in figure 2.5.

Coniferin is characterised by increased solubility in aqueous media and also is reasonably stable to oxidation since the phenolic moiety is protected by the glucosidic linkage. It is these properties which allow easy storage (without premature polymerisation) and transport (when required) of coniferin through the water conducting systems of the tree to the site of lignification.

An enzymatic decoupling of the glycosidic linkage by β-glucosidase leads to the commonly known C_9 precursor unit coniferyl alcohol, first established as a precursor to the lignification process by Klason[51].

The processes leading to such a precursor molecule can be traced back to the absorption by the tree of gaseous carbon dioxide from the atmosphere, the bio-synthetic pathways of which have been detailed in many reviews in the literature[52,53]. Also shown in figure 2.5 is the nomenclature first proposed by Sarkanen and Ludwig[54] in order to describe the random coupling reactions occurring between the canonical forms of the phenoxy radical of the C_9 phenylpropane lignin precursor which ultimately lead to the lignin macromolecule. Thus, following liberation of coniferyl alcohol from coniferin by the enzyme β-glucosidase, the coniferyl alcohol precursor

undergos an enzymatic dehydrogenation reaction to generate the corresponding phenoxy radical as shown in figure 2.5 which sets in motion the formation of the entire lignin generating polymerisation process. The random coupling reactions leading to the heterogeneous lignin structure arises from the existence of five canonical forms of the phenoxy radical. From these species, a total of 25 theoretical inter-unit linkages between C_9 monomer units are possible. Due to steric or thermodynamic constraints, only 15 combinations form stable couplings, some of which being more favourable than others. The couplings which form stable products are shown in table 2.1 according to the nomenclature of Sarkenen and Ludwig[17].

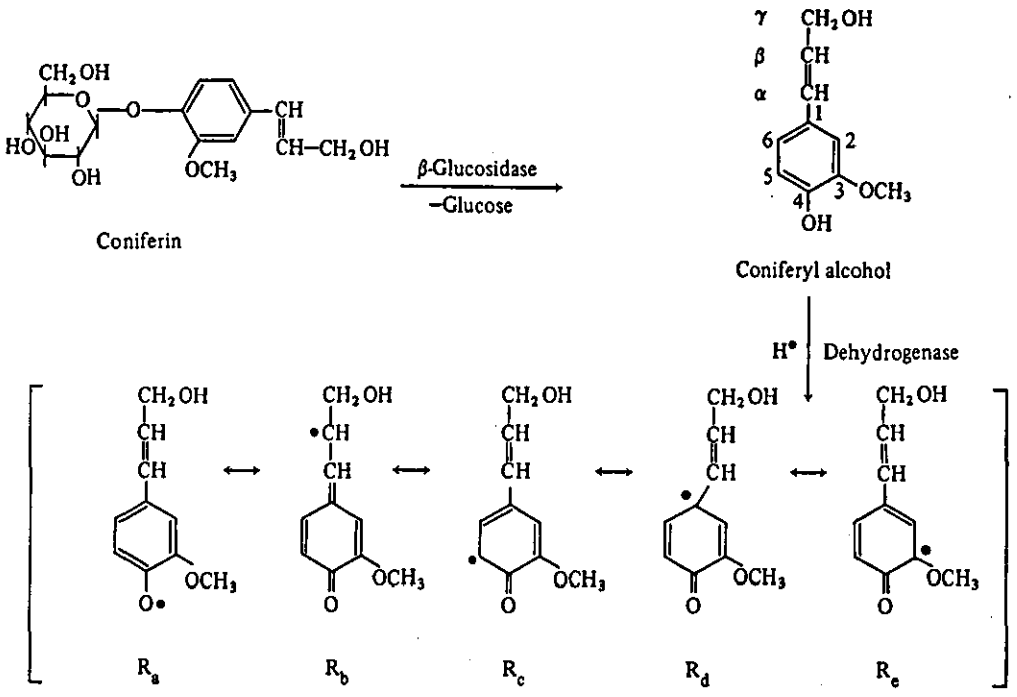

Figure 2.5:- Chemical Structure of Coniferin and the Enzymatic Dehydrogenation of Coniferyl Alcohol to Yield Phenoxy Radical Species

The initial step in the formation of the lignin macromolecule is the formation of dimeric structures known a "dilignols" via coupling of the form indicated in table 2.1. Following this, so called "end wise" polymerisation occurs where either a C_9 "monolignol" unit couples with the phenolic end group of a di- or oligolignol structure or, two end-group radicals couple to form a stable linkage. Such mechanisms have been shown to occur (rather than coupling of monolignols with each other to form dimeric structures) by the limited number of coniferyl alcohol and coniferaldehyde end group present in Bjorkmann lignin obtained from spruce and is probably the result of a restricted supply of monomers in the lignifying cell[53]. The net result of these processes is a three dimensional crosslinked "heterogeneous" polymer. The probability, and therefore the frequency of a coupling reaction occurring between C_9 monomer units is primarily governed by the electron spin density of the delocalised unpaired electron at one of the five positions shown in figure 2.5.

	R_a	R_b	R_c	R_d	R_e
R_a	Unstable	β-O-4	4-O-5	1-O-4	Sterically Hindered or Thermo-dynamic ally Disfavoured
R_b	β-O-4	β-β	β-5	β-1	
R_c	4-O-5	β-5	5-5	1-5	
R_d	1-O-4	β-1	1-5	1-1	
R_e	Sterically Hindered or Thermodynamically Disfavoured				

Table 2.1:- Coniferyl Alcohol Phenoxy Radical Coupling Modes

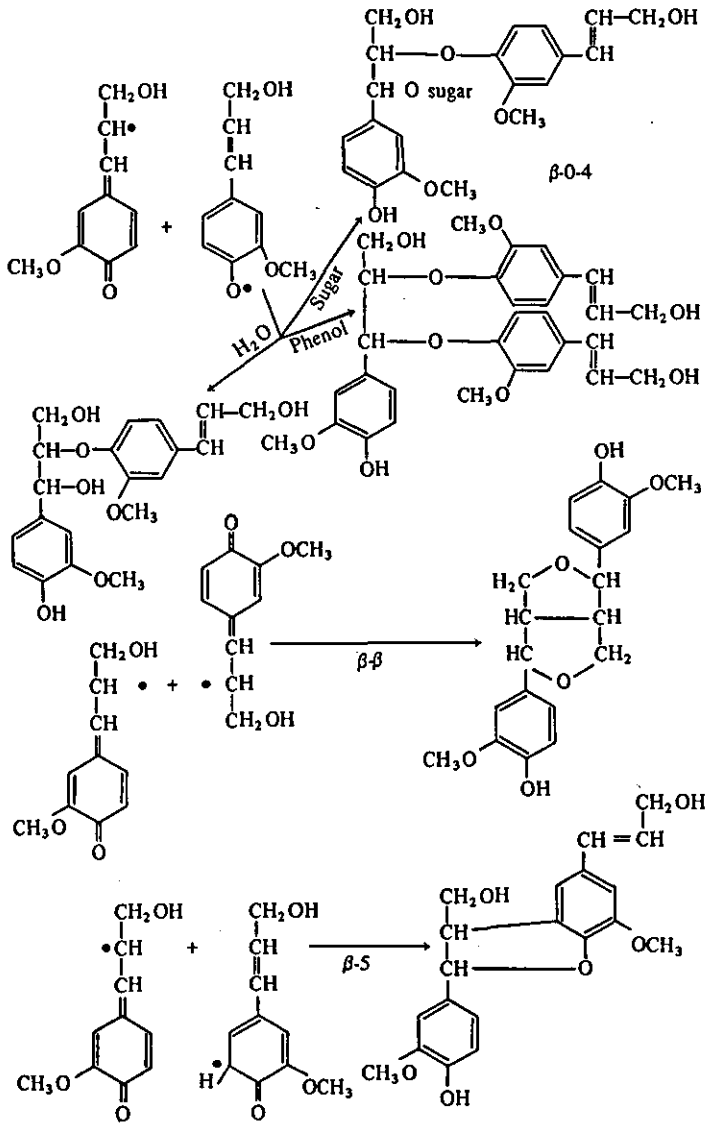

Figure 2.6:- Coupling of Phenoxy Radicals Leading to Prominent Inter-unit Linkages in Lignin

Theoretical calculations together with experimental observations with 4-hydroxycinnamyl alcohol[55] have demonstrated that the highest electron spin density is located at the phenolic oxygen atom resulting in the highest probability of forming an aryl-ether linkage (ie. a β-O-4 linkage) between two C_9 precursor radicals greater than any other inter-unit linkage. Of the other linkages, coupling reactions between two R_b radicals and R_b and R_c radicals (figure 2.5) to produce stable dimeric structures known as β-β and β-5 linkages are the most likely (figure 2.6). As can be seen, the precise nature of the β-O-4 linkage is determined by the availability of phenolic, sugar or water in the vicinity of the reaction.

In all three linkages, there exists a quinomethide intermediate which may stabilise through intramolecular or external addition of hydroxy containing moieties. The mechanisms involved in the addition to the quinomethide intermediates do not require the radicalisation of a phenolic moiety therefore allowing addition of non-phenolic hydroxy moieties as seen in figure 2.6 for β-O-4 linkages to yield ether or ester type linkages. The frequency of addition is dependent upon the nucleophilicity of the hydroxy carrying compound. Thus, it is found that phenolic hydroxyl groups add at a higher rate than aliphatic hydroxyl groups or water. The intimate contact between quinonoid intermediates with cellulose and hemicellulose in the cell wall of the wood tracheid therefore make possible the formation of lignin-carbohydrate linkages in the form of ether or ester type linkages. The linkages which lead to β-5 structures are almost entirely internal, intramolecular addition to the phenolic hydroxy group of the reaction partner to the quinomethide leading to the coumaran-type structure as shown in figure 2.6. A similar reaction also occurs in the case of β-β combinations which lead to pinoresinol-type structures also shown in figure 2.6. As seen in table 2.1, other linkages between C_9 phenylpropane sub-units are also possible including the 5-5 biphenyl type linkages. However, it has been shown that β-O-4 linkages are by far the most frequent inter-unit linkage present in the lignin macromolecule. For example, a study by Erickson *et al*[56] demonstrated that β-O-4 linkages contribute up to 50 % of linkages in the lignin macromolecule. Full classification of Spruce MWL have been summarised in the literature[57]. Computer simulated models for the structure of lignin based upon the phenyl-propane sub-unit 4-hydroxycinnamyl alcohol have been reported in the literature[58], the most extensive of which involved 94 phenylpropane sub-units with a molecular weight in excess of 17000[59]. Cross correlation with classical analytical techniques applied to lignin structure determination have resulted in a simulated structure which closely resembles the structure of lignin isolated from a single tree species, Loplolly Pine (Pinus taeda)[60]. In nature, the net result of such radical linkages is a macromolecule with a molecular weight greater than 10^6, that is intimately linked to the cellulose and hemicellulose fractions of the wood tracheid cell wall. It must be noted that the structural description given above is based upon a coniferyl alcohol precursor unit. Large differences exist between softwood lignins based on such a guaiacyl (4-hydroxy-3-methoxycinnamyl alcohol) unit and that of hardwood lignins which are based on both guaiacyl and syringyl (4-hydroxy 3,5-dimethoxycinnamyl alcohol) sub-units thus making linkage frequencies different in hardwood lignins than those observed for softwood lignins.

2.4 Pulping and Bleaching of Wood Fibres

There exists a wealth of information concerning the pulping and bleaching processes applied to wood to produce paper products. It is beyond the scope of this thesis to attempt to cover all aspects of the various processes involved in producing the various grades of commercially available paper. The author therefore refers the reader to the review book edited by Casey for further detail[61,62]. However, it is felt that a brief description of the three major categories of paper widely available will be of use to the reader.

(a) Chemical Pulp:- To the pulp and paper manufacturer, lignin is regarded in many ways as the unwanted ingredient of wood which requires removal from the cellulosic matrix in order to produce high brightness, photostable white papers. This process of lignin removal begins at the pulping stage of paper making and continues into the bleaching stages of the manufacturing process. The Kraft or sulphate pulping process was the last classical chemical pulping process to be developed around 1879 and has since come to dominate pulp production methods throughout the world. The pulp process involves the cooking of wood chips under alkali conditions with a sodium sulphide/sodium hydroxide mixture which dissolves the lignin from the cellulose and hemicellulose fractions of the woody tissue. The result of such a process is an initially highly coloured wood pulp with a lignin content of approximately 3 %. The production of high brightness papers therefore requires the removal of residual lignin during bleaching. Single stage bleaching processes are seldom used today, multistage processes being the standard practice. Many bleaching stages involve the use of chlorine based chemicals (such as chlorine/water, hypochlorite and chlorine dioxide together with alkali extraction stages) to remove the residual lignin.

Given the aromatic nature of a lignin macromolecule, it is not surprising that analysis of waste water outflows from chemical pulp producing paper mills contains a mixture of chlorinated organics which have been shown to have carcinogenic and mutagenic effects upon fish and other river dwelling creatures[63]. Among the most toxic found were 3,4,5-trichloroguaiacol, 3,4,5,6-tetrachlorguaiacol and dioxin (2,3,7,8-tetrachlorodibenzo-p-dioxin)[64], all of which are produced in high levels via the bleaching process.

The net result of full chemical removal of lignin is a Kraft paper with an ISO[65] brightness of greater than 80 % which has good strength properties. However, the price to pay in terms of paper yield is high; yields ranging between 40 % and 55 % being typical for such paper grades. It is both economic and environmental pressure which has led to the development of other pulping and bleaching methods which utilise the wood raw material more efficiently and release less potentially toxic by-products into paper mill waste water outflows.

(b) Semi-chemical and Chemi-mechanical Pulps:- Such pulping processes where developed with the objective of producing pulps in yields higher than those obtained in full chemical pulping methods where raw material and production cost savings can be achieved. Typical yields for these processes are between 65 % and 90 %. Although all fibrous materials can be pulped by the semi-chemical pulping process, the majority of species used in this process are hardwood species. Semi-chemical and chemi-mechanical pulping processes are essentially two stage processes:-

(i) Mild chemical treatment (with or without heat).
(ii) Mechanical refining to complete separation of pulp into fibrous material.

Such pulping methods occupy an intermediate region between classical chemical pulping processes and pulping process leading to the production of so called "high yield pulps" via mechanical pulping processes. The most widely known and used semi-chemical pulping process is the so called NSSC process (Neutral Sulphide Semi-Chemical Process). The two stages (as mentioned above) of this pulping process involve firstly the cooking of wood chips in a mixture of sodium sulphite (Na_2SO_3), sodium carbonate (Na_2CO_3) and sodium bicarbonate ($NaHCO_3$) giving partial dissolution of the lignin fraction from the pulp matrix. Following this, mechanical action has the effect of breaking down the pulp into fibres which can be used for paper making. The net result is a pulp which resembles a chemical pulp in terms of fibre composition when examined under a light microscope. Semi-chemical and chemi-mechanical pulps are generally used in paper products which do not put a large emphasis on brightness properties although it is possible to bleach such pulps to ISO brightnesses of 80 % by conventional bleaching methods. This however is expensive and, given that such pulps contain a high percentage of lignin (ca. 10 % to 14 %), is also depends heavily upon the source of the raw material itself. Thus, semi-chemical pulps are used for low grade paper products such as corrugated cardboard and together with other pulp grades in the production of newsprint and telephone directories etc.

(c) **Mechanical Pulps:-** The principal grade of mechanical pulp discussed here is known as thermomechanical pulp (TMP), the photochemistry of which is discussed in chapter 6 of this thesis. As the name suggests, TMP is produced by the steaming of raw wood chips for a short period at an elevated temperature. The precise conditions of this processing stage are dependent upon the source of the raw material and also the size of the wood chips involved but typically two minutes of steaming at 120°C is sufficient to soften the wood chips prior to mechanical fibre separation. Mechanical production of wood fibres is achieved by a process known as disk refining, details of which can be found elsewhere[66]. Briefly, rotating disk refiner plates containing different sizes of breaking bars grade the pulp fibre depending upon its size. Crude fibres enter into the centre of the disk refiner (breaking zone) and leave via the periphery following size grading by one or two refining zones towards the outer of the plates. The result of these processes are TMP fibres which can then be bleached to acceptable brightness levels for use as paper making material. The TMP fibres have not been significantly altered chemically during the pulping process which means that pulp yields of between 91 % and 95 % can easily be achieved. Clearly, the presence of lignin in the fibres gives undesirable optical properties to such papers which can be improved by multistage bleaching processes. The only commercially used bleaching system for mechanical pulps is that based upon a hydrogen peroxide/sodium hydroxide bleaching mixture. Addition of sodium silicate (Na_4SiO_4) has the effect of buffering the hydrogen peroxide at a pH where it is most effective and is often added to the bleaching mixture. Two stage bleaching with alkaline hydrogen peroxide and sodium silicate under certain conditions can yield pulps with an ISO brightness of greater than 85 %. Care must be taken that the pulp is chelated with, for example, ethylenediamine tetra-acetic acid (EDTA) prior to the addition of the peroxide since metal ions (especially manganese (IV), copper (II) and iron (III))[67,68] present in the pulp and water catalyse the degradation of hydrogen peroxide and therefore reduce the efficiency of the

bleaching process. Much work has been documented upon the optimum conditions for peroxide bleaching[69,70]. Important factors include temperature, pH, pulp consistency and reaction time, all of which determine the efficiency of the bleaching process. For example, the bleaching of TMP samples used for photochemical investigations in chapter 6 were bleached with 4 % alkaline hydrogen peroxide at 60°C for two hours at 20 % consistency to yield an ISO brightness of 75 %.

Under alkaline conditions, the reactive species responsible for initiating the bleaching processes for TMP has been shown to be the hydroperoxy anion, HO_2^-. The removal of coloured chromophoric moieties believed to be present in the lignin fraction of TMP, such as coniferaldehyde end groups and ortho and para quinones have been demonstrated with the use of appropriate lignin model compounds[71,72,73,74,75]. The resulting destruction of conjugation in the lignin macromolecule therefore decreasing absorption of light by the TMP sample in the visible part of the electromagnetic spectrum (wavelengths greater than 400 nm). Coniferaldehyde end groups are believed to undergo side change cleavage between the α - and β-carbon atoms as shown in figure 2.7[76] whereas destruction of quinones is believed to take place via rupturing of the ring system present in the quinone chromophore leading to the formation of series of carboxylic acids[73,77]. As mentioned previously, brightness levels close to those obtained for chemical pulps are obtainable for TMP under the correct bleaching conditions. However, their share of the high quality writing and printing paper market cannot be realised until the problem of photoreversion or photoyellowing as a result of their high lignin content (see later) is overcome.

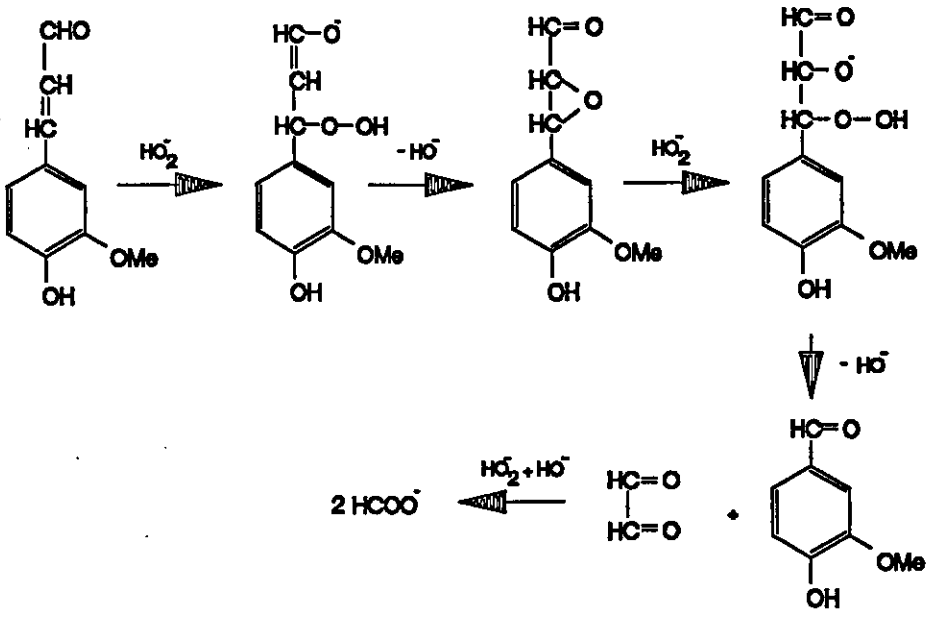

Figure 2.7:- Reaction of Hydroperoxy Anions with 4-Hydroxy-3-methoxycinnamaldehyde Demonstrating the Cleavage of Coniferaldehyde Type Side Chains Present in Unbleached TMP

Thus TMP and other high yield pulps are principally used in the short life-span paper product markets such as newsprint, telephone directories and advertising hoardings where optical brightness is not a primary consideration in the choice of paper grade required.

2.5 Market and Environmental Trends in the Pulp and Paper Industry

In recent years, two distinct trends in the development and application of pulping and bleaching techniques have occurred:-

(a) A decrease in the use of sulphur containing species in the pulping and chlorine containing species in the bleaching of chemical pulps.
(b) Increase demands for high yield mechanical pulps with acceptable optical and mechanical properties.

The former is the direct result of environmental considerations and new legislation to control the waste output into river outflows, the second attributable to the diminishing supply of raw material available to the industry. Shown in figure 2.8 is the projected worldwide demand for paper in the early 21st century.

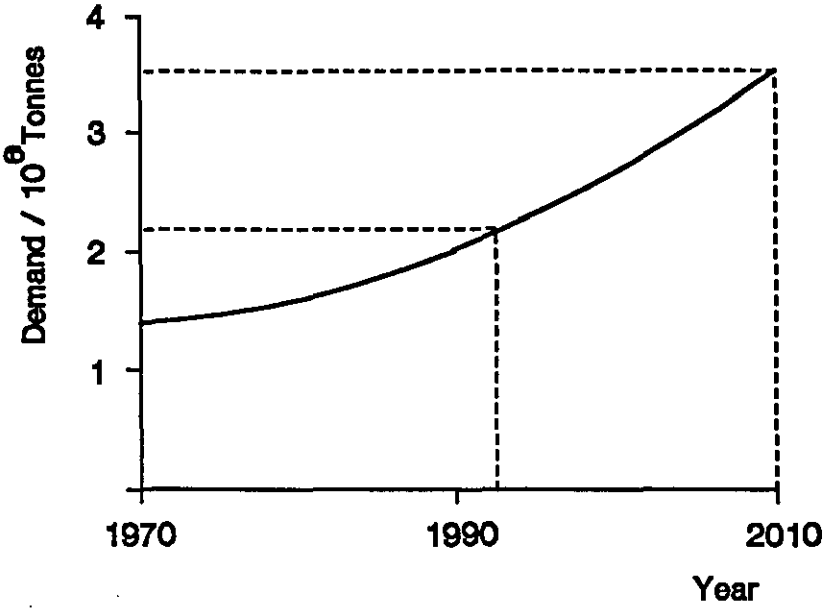

Figure 2.8:- Projected World-wide Demand For Paper Products into the 21st Century

As can be seen, demand for paper and paper board is seen to increase steadily from approximately 220 million tonnes per year at present to approximately 350 million tonnes in 17 years time. Under closer examination, when such a projected increase is split into the major categories of commercially available paper grades (table 2.2) it is seen that the highest (compound annual) average percentage increase in demand will be for high quality letter and printing papers.

	1985	2010	% Annual Growth(1)
Newsprint	28.1	45.4	1.9
Printing and Writing	51.4	118	3.4
Other Paper and Paperboard	113.1	178.6	1.8
Total	192.6	342.4	2.3

Table 2.2:- World Paper and Paperboard Consumption and Growth Rate by Product 1985 to 2010 (millions of tonnes)[78]

(1) Compound Annual Average

This market share has been traditionally filled by chemical pulps (section 2.4). However, due to environmental regulations and raw material availability, coupled with the low percentage paper yield (ca. 50 %) obtained from chemical pulping and bleaching processes, high yield semi-chemical, chemi-mechanical and mechanical pulp grades will become increasingly important in meeting the demands of the consumer while making optimum utilisation of available raw materials. The fundamental problems associated with such grades of paper is their tendency to turn yellow upon exposure to sunlight (wavelengths greater than 300 nm) by a process known as photoreversion or brightness reversion. Until this problem has been overcome or the consumer attitude towards preferring white photostable papers can be changed, expansion of high yield pulps into the long life paper product market will not be achieved.

2.6 Photoreversion of High Yield Thermomechanical Pulps

Detailed below is a brief overview of the initial research directed towards the light stabilisation of high yield thermomechanical pulps. Reviews of the published literature relevant to the photochemistry of lignin model compounds and MWL can be found later in sections 4.1 and 5.4.1 respectively.

Research into the mechanisms by which high yield thermomechanical pulps degrade under irradiation with near ultraviolet light has been extensive over the past 50 or so years. It is only in the last 20 years that a dramatic intensification of research into the photoreversion of high yield pulps has taken place, driven on by the environmental and economic pressures exerted upon the pulp and paper industry worldwide. In that time, the application of photochemical techniques to an area of research initially dominated by the wood scientists interested in the yellowing of paper has become ever more prevalent, culminating in a symposium at the 203rd American Chemical Society meeting in San Francisco[79] devoted entirely to the photochemistry of high yield pulps.

Much of the early literature was of the form of empirical observations upon the effect of sunlight on lignin rich paper products (and also wood chips) such as newsprint. This initial research established the importance of light, oxygen, humidity and temperature in the yellowing mechanisms, and demonstrated that the degree of yellowing was related to lignin content of the wood[80,81,82,83,84]. It was Leary who linked the loss of methoxyl content in wood during irradiation with colour formation, and was the first to propose the formation of ortho-quinone type moieties as one of the colour contributing species[85], an observation recently confirmed by Lebo *et al* with the aid of ^{31}P n.m.r. Spectroscopy[86]. More recently, much research has been directed

towards the carbonyl groups present in lignin. These consist of conjugated aromatic, aliphatic and quinone type moieties. Experiments have demonstrated that, when these groups are totally reduced using sodium borohydride, light induced yellowing is reduced, but not stopped. Leary continued his work to demonstrate the interaction between the α-carbonyl and the phenolic hydroxyl groups present in the lignin. By fully reducing the carbonyl groups with sodium borohydride, and then fully methylating all phenolic hydrogens, colour formation was reduced to levels just above those observed with Kraft type pulps. The fact that pulps which have been fully reduced and methoxylated still undergo photoinduced yellowing suggests the existence of at least one more reaction mechanism leading to photoyellowing (see section 4.1 for details).

The aim of this thesis was to investigate more closely the photochemical behaviour of α-carbonyl and phenolic hydroxyl groups present in the lignin macromolecule, and also to consider the other modes of photochemical reactivity of lignin which lead to the yellowing process. One must bear in mind that much of the evidence substantiating the phenolic hydrogen abstraction mechanism was largely based upon model compound studies in fluid solution. The molecular dynamics which exist in the solid phase are likely to be much removed from such solution phase systems which allow easy molecular diffusion of yellow photoproduct forming intermediates (such as free radical species) in order that they may react. In the actual pulp environment itself, chromophoric groups are held fairly rigidly by the 3-dimensional polymer matrix thus making material diffusion almost impossible. Therefore, although model studies play an important role in the elucidation of the photoyellowing mechanisms involved, experiments conducted with the pulp material itself are essential if the ultimate aim of photostabilising such pulps is to be achieved.

The results presented in this thesis cover both approaches to the problem of the photoyellowing of lignin rich paper samples together with an intermediate photochemical system involving chemically extracted soluble lignin (milled wood lignin or MWL). Therefore, the results presented in this thesis have been divided into three chapters, namely experiments with α-carbonyl lignin model compounds, milled wood lignin (MWL) and high yield thermomechanical pulp (TMP) itself. The technique of time resolved transmission laser flash photolysis has been applied to both lignin model systems and MWL. It is the development of diffuse reflectance laser flash photolysis (DRLFP) (sections 1.6 and 3.8.2) which has enabled the photochemical generation and study of the short lived transient species of lignin chromophores within the TMP matrix itself to be studied for the first time in detail. The results of DRLFP studies are presented partly in section 5.5 for samples of MWL adsorbed onto a microcrystalline cellulose substrate and in chapter 6 for samples of TMP itself.

Chapter 3

Experimental

3 Experimental

3.1 Ground State Absorbance And Ground State Diffuse Reflectance Spectra

All ground state absorbance and ground state diffuse reflectance spectra were recorded using a Phillips PU-8800 dual beam UV-Visible spectrophotometer. All solution phase spectra, unless otherwise stated, were obtained by placing samples in 1 cm x 1 cm quartz cuvettes.

Ground state diffuse reflectance spectra were recorded using a 12" integrating sphere attachment (Pye Unicam). All internal surfaces of the integrating sphere (with the exception of the specular reflection beam dumps) were coated using an aerosol of white reflectance coating (Eastman Kodak Ltd.). At least three coats of the reflectance coating were applied to all internal surfaces ensuring an optically thick layer (ie. any increase in the number of coats of white reflectance standard will not increase the intensity of the diffusely reflected observed from the integrating sphere) of the material throughout. Samples were placed in . 2 cm diameter, 1 cm pathlength quartz cuvettes and mounted in the integrating sphere with the aid of a purpose made circular metal plate which had a circular recess the same diameter as the sample cells. The metal surface closest to the spectrophotometer beam was covered with a matt black card to prevent stray specular reflected light from reaching the photomultiplier. An aperture approximately 1 cm in diameter was cut in the card to allow light to the sample. Sufficient packing densities were used to ensure that all samples were optically thick at all wavelengths investigated (typically 300 to 700 nm).

Ground state diffuse reflectance spectra were recorded relative to a barium sulphate white reflectance standard (Eastman Kodak Ltd.) which was given a reflectance value of 100 %.

3.2 Steady State Emission Spectra

All steady state emission spectra were recorded using a Perkin Elmer series 3000 fluorescence spectrometer. Solution phase emission spectra were recorded using right angle emission collection geometry while solid sample emission spectra were recorded using front face geometry. Appropriate interference and cut-off filters were used to prevent sample excitation light from reaching the photomultiplier detector.

3.3 Preparation of Thermomechanical Pulp Samples

All thermomechanical pulp samples were prepared in the laboratories of the Pulp And Paper Research Institute Of Canada (PAPRICAN), Pointe Claire, Quebec, Canada.

These samples were of thermomechanical pulp (TMP) obtained from black spruce (Picea mariana). Following milling and chipping of the wood, pulp fibres of 20 % consistency were bleached to an ISO brightness (the reflectance at 457 nm relative to a white reflectance standard[65]) of approximately 75 % by treatment with a 4 % v/v solution of hydrogen peroxide at 60°C for 2 hours. Pulp samples were studied in one of two forms, either as pulp handsheets or as a fine powder and were prepared by the following methods:-

a) TMP handsheets with a diameter of approximately 15 cm were prepared by taking the appropriate mass of bleached pulp fibres suspended in approximately 20 l. of de-ionised water. The suspension was then placed in a stainless steel British Sheet machine and stirred to give a "homogeneous" distribution of fibres in the vessel. A valve at the base of the vessel was then

opened allowing rapid removal of the water from the vessel. The pulp fibres become trapped on a 74 μm teflon mesh to yield a hand sheet of even fibre density and thickness across the whole area of the sheet. The hand sheets were then air dried at room temperature. Depending upon the amount of pulp fibres initially used, handsheets of variable thickness and density can be easily made. Samples typically used were a thickness of 5.5×10^{-2} cm with a fibre density of 0.44 g.cm.$^{-3}$. Due to the compressible nature of pulp handsheets, samples are often described in terms of their basis weight (mass per unit area). Typical sample basis weights were of the order of 2.4×10^{-2} g.cm.$^{-2}$.

b) Powdered samples were prepared by grinding bleached TMP fibres to approximately a 40 mesh powder in a Wiley Mill. Samples of this type were packed into quartz cuvettes at a sufficient packing density to ensure optical thickness at all wavelengths of study. Under these conditions, the optical properties of this form of pulp sample were the same as those for an optically thick handsheet.

3.3.1 Methoxylation Of Thermomechanical Pulp

The methoxylation of TMP to produce pulp samples of varying lignin phenolic hydroxyl content was achieved according to the method of Erickson *et al*[87] as follows; 10 g of peroxide bleached TMP (see section 3.3) was suspended in 600 ml of a nitrogen purged equivolume solvent of water, ethanol and dimethoxyethane. The pH of the solvent was adjusted to 11 by addition of 10 % w/v potassium hydroxide solution. To the suspension was added the appropriate volume of dimethyl sulphate to give the required methoxyl content. Under the conditions of the treatment, 90 ml and 125 ml of dimethyl sulphate giving methoxyl contents of 7.23 % and 8.13 % by mass respectively. The pulp suspension was stirred for 7 1/2 hours maintaining throughout a constant pH of 11 by further dropwise addition of potassium hydroxide. The pH was then adjusted to 3 by addition of 0.5 M phosphoric acid and stirred for a further hour after which the pH was adjusted to 6.5 with potassium hydroxide. The pulp was then filtered, triply washed with distilled water and air dried. The determination of lignin phenolic hydroxyl content was according to the method of Gellerstedt *et al*[88]. Analysis of pulp samples for methoxyl content were performed at the Schwarzkopf Micro-analytical Laboratories, Woodside, New York.

3.4 Preparation Of Milled Wood Lignin

Milled wood lignin samples were prepared and analysed in the laboratories of the Pulp And Paper Research Institute Of Canada (PAPRICAN), Pointe Claire, Quebec, Canada.

Black Spruce wood chips were ground to between 20 and 40 mesh in a Wiley mill. To the ground wood was added acetone (analytical grade), the slurry being allowed to stand for two days before a further solvent extraction using 10 % v/v water/acetone. The extracted wood in the solvent phase was then air dried and ground to a fine powder in a ball mill[89]. The wood meal was then dispersed in a cosolvent of 4 % v/v water/ 1,4-dioxane (analytical grade) and stirred under oxygen and light free conditions for approximately three weeks. The resulting solution phase was decanted off from the remaining solid material. The solvent from the solution phase was then removed by rotary evaporation, the lignin residue remaining being dried under vacuum at between 50 and 60°C. At this stage, the extracted lignin was still in a fairly crude form and therefore required further purification. This was achieved by successive precipitations firstly

in an aqueous based solvent system followed by an organic based solvent system as follows[90,91]; the lignin was dissolved in a co-solvent of 10 % v/v water/ ethanoic acid (analytical reagent). This solution was then added dropwise to water (ca. 250 ml of water per gram of lignin) to precipitate the lignin. The precipitate/solvent suspension was then centrifuged to separate the precipitate from the solvent, residual solvent being removed by freeze drying. The residue remaining was then redissolved in a co-solvent of 66 % v/v 1,2 dichloroethane/ ethanol (both analytical reagents). Approximately 20 ml of solvent per gram of lignin was required for this phase of purification. Lignin was then precipitated by dropwise addition of the solution to freshly distilled dry diethyl ether (250 ml per gram of lignin). Completion of the purification process was achieved with two further washings with diethyl ether (analytical reagent). The lignin was then thoroughly dried initially using a stream of dry air and finally under vacuum over phosphorus pentoxide. The lignin remaining was faintly cream coloured and free from ash. It is this material that is known as milled wood lignin (MWL). Analysis of the MWL showed it to have a mean molecular weight of approximately 25,000. All experiments with this material were performed without further purification.

3.5 Model Compounds Adsorbed on Microcrystalline Cellulose Powder

Cellulose powder (20 μm mean particle size, Aldrich Ltd.) was dried under vacuum (65 mBar) at 70°C overnight prior to use. A known mass of the cellulose was weighed into a 100 ml beaker and immediately covered with the appropriate solvent being used in the sample preparation to avoid moisture uptake. To the resultant slurry was added a solution of the molecule to be adsorbed to give a known surface concentration in the range 5×10^{-6} to 1×10^{-4} mol.g.$^{-1}$ of cellulose powder. Samples were then magnetically stirred, the solvent being allowed to slowly evaporate until only residual solvent remained. Samples were then dried under vacuum (65 mBar) at 30°C for at least 12 hours. All samples were stored in a vacuum dessicator prior to experimental investigation.

3.6 Nanosecond Laser Flash Photolysis

3.6.1 Apparatus

There are two nanosecond laser flash photolysis apparatus in use in Loughborough. Both sets of apparatus are built around pulsed Q-switched Neodymium doped Yttrium Aluminium Garnet (Nd:YAG) lasers whose fundamental wavelength is located in the infra-red at 1064 nm. This wavelength is not the most useful for photochemical investigations involving paper pulp samples and therefore it was necessary to generate harmonics of the fundamental wavelength by passing it through appropriate frequency doubling/mixing crystals. For convenience, and to reduce equipment set-up time, one set of apparatus has become dedicated to transmission laser flash photolysis investigations, the other set-up being used for diffuse reflectance laser flash photolysis and time resolved singlet oxygen luminescence studies (section 3.7). With the exception of a few subtle differences, the two sets of apparatus are identical in their construction and the method by which the data acquired from laser flash photolysis experiments is collected and stored for further analysis. Outlined below

are the sequence of events which facilitate data collection (section 3.6.2). The transmission laser flash photolysis apparatus is constructed around a JK Lasers (now Lumonics) JK2000

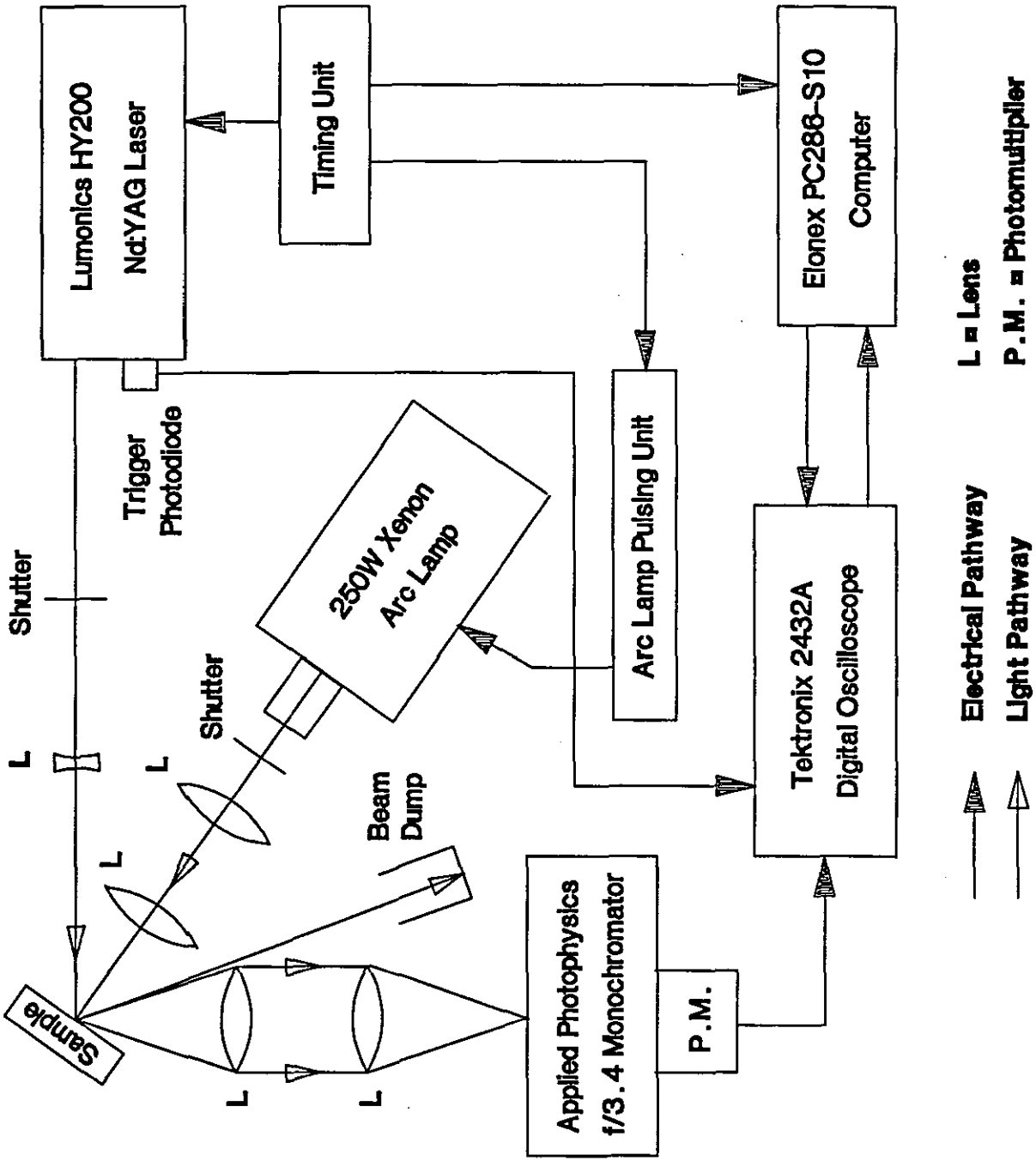

Figure 3.1:- Schematic Diagram of The Apparatus Used For Diffuse Reflectance Laser Flash Photolysis Experiments

Q-switched Nd:YAG laser with a two stage (oscillator/amplifier) dye laser associated with it.

The diffuse reflectance laser flash photolysis apparatus is built around a Lumonics HyperYAG HY200 Q-switched Nd:YAG laser. A schematic diagram of the apparatus used for diffuse reflectance laser flash photolysis is shown in figure 3.1.

The laser pulses generated by these instruments are gaussian with respect to time and have full width half maxima (FWHM) of approximately 20 and 8 ns respectively. Second harmonic generation to give 532 nm can be achieved by passing the fundamental through a deuterated caesium dihydrogen arsenate crystal (DCDA), frequency mixing of the 532 nm light with the remaining undoubled 1064 nm in a potassium dihydrogen phosphate (KDP) crystal resulting in the generation of the third harmonic at 354.7 nm. The fourth harmonic, located at 266 nm, is obtained by frequency doubling the second harmonic in an ammonium dihydrogen phosphate (ADP) crystal.

The excitation wavelength used almost exclusively for the photochemical studies described in this thesis was 354.7 nm with occasional use of the 266 nm harmonic (see section 4.4).

The analysing source used on both systems is a 300 W xenon arc lamp (Optical Radiation Corporation). Appropriate filters were placed between the arc lamp and the sample to cut off unwanted wavelengths. The use of an arc lamp pulsing unit (Applied Photophysics Ltd.), provides the lamp with an extra pulse of voltage resulting in an increase in the intensity of the analysing source approximately 1 ms in duration. The pulse profile has a region, approximately 500 μs long, where the lamp output intensity is flat with respect to time. This region provides approximately a tenfold increase in the intensity of the analysing source.

The detection systems comprise of an f/3.4 grating monochromator (Applied Photophysics Ltd) which has fully variable (0 to 8 mm) 21 mm height bilateral slits front and back and an R928 side window photomultiplier tube (Hammamatsu Ltd.). The accelerating voltage applied to the photomultiplier tube was supplied by a 412B high voltage supply (Fluke). Spectral resolution is related to the monochromator slit width[92] as defined in equation 3.1:-

$$SpectralResolution/(nm) = SlitWidth/(mm) \times 4.65 \qquad (3.1)$$

In all cases, both the front and rear slit widths were set to 1 mm giving a spectral resolution of 4.65 nm (FWHM). The signal from the photomultiplier tube is directed into the input of one of two digitising devices; a 2432A digital oscilloscope (Tektronix Ltd) which has a maximum single shot digitising rate of 4 ns per point or a 7612D transient digitiser (Tektronix Ltd.) with a 7A13 differential comparator plug-in (Tektronix Ltd.) which has a maximum single shot digitising rate of 5 ns per point. Both devices have the facility of a programmable number of pre-trigger points which were set as 28 and 24 points respectively out of a total data record length of 512 points. Communication of these devices with an IBM compatible personal computer is achieved via a PC2A general purpose interface bus (GPIB) (National Instruments) running communication software provided by National Instruments and Tektronix.

Both sets of apparatus have shutters placed between the laser and the sample and the analysing source and the sample. Opening and closing of shutters is controlled by the computer via a DT2808 digital/analogue analogue/digital (D/A A/D) card (Data Translation Ltd).

3.6.2 Data Collection

The software used to control and operate both sets of apparatus and to acquire and store data records has been written in Loughborough by Dr. D.R. Worrall, Dr. G.P. Kelly and Mr. P.A. Leicester.

The timing of the events leading to data collection for both flash photolysis apparatus is controlled by one central timing unit built in Loughborough consisting of a quartz oscillator and a series of analogue delay modules.

The initial step in the data collection sequence is the triggering of the computer. Once triggered, the computer then instructs the digitiser, over the GPIB board to arm its timebase and trigger upon receipt of its next signal. The next event is the opening of the shutters located between the laser and the sample and the analysing source and the sample. This depends upon which data set is to be collected. The baseline is collected with only the analysing source shutter opened, transient absorption (analysing source and laser shutters opened), emission trace (laser shutter only opened) and top line (no shutters opened). The correct opening of the shutters is achieved by the computer setting the correct bit pattern over the DT2808 board which either enables or disables the shutter opening depending upon which data set is being collected. For digitising sweeps of less than 500 μs, the arc lamp can be pulsed to give extra light intensity (see above). The timing box triggers the pulsing unit to pulse after the shutters have been opened, the "plateau" region coincides with the next event in the collection sequence, the firing of the laser. The two digitising devices operate in slightly different ways. Taking the example of the 7612D, the digitiser initially records a full data record of pre-laser trigger points in a time gate of 2 ns for each data record point to give a total record length of 512 pre-trigger points. The laser firing results in the triggering of the digitiser to digitise the photomultiplier signal and overwriting the pre-trigger data record excluding the pre-programmed number of pre-trigger points, the result of which is a data record comprising of both pre and post laser data points.

The triggering of the digitiser by the laser is achieved in one of two ways; the JK2000 laser triggers the digitiser by reflecting some of the laser pulse off a glass slide into a fibre optic cable which in turn is incident upon a photodiode, the HY200 laser triggering the digitiser via a photodiode triggered itself by residual 1064 nm light leakage from the end mirror of the laser cavity. Following the completion of the digitisation of the signal obtained from the photomultiplier, the data is transferred to the computer over the GPIB, displayed on the screen and then stored for later analysis. This is the complete data collection cycle. The computer then waits for the next signal from the timing unit for the sequence to begin again. During routine data collection, a single collection loop takes approximately 1.6 s.

3.7 Singlet Oxygen Luminescence Detection

The detection of the phosphorescence emission at 1270 nm resulting from the radiative relaxation of the lowest lying excited singlet state of molecular oxygen ($^1\Delta_g$) was achieved using a singlet oxygen luminescence detector similar to the one described by Keene *et al*[93]. The detector consists of a reverse biased germanium photodiode (Judson J16-8SP-1205M) coupled to a 55 dB gain pre-amplifier (Judson PA100). The rise time of the diode detector (the time taken for the signal to go from 10 % to 90 % of its peak amplitude) was of the order of 500 ns. Samples were placed in quartz cuvettes and excited with the 354.7 nm harmonic of the Nd:YAG laser. A filtering system was required in order to prevent light of unwanted wavelengths from reaching the detector. This consisted of a 2" square BG38 (Oriel Scientific Ltd.) placed after the laser harmonic separator to filter out residual 1064 nm from the laser and a long pass infra-red silicon filter (Oriel Scientific Ltd. filter 57900) placed in front of the photodiode preventing all wavelengths below 1100 nm from reaching the detector. The detector was placed close to the face of the sample cuvette, the luminescence being detected perpendicular to the exciting source. The signal from the detector is digitised and stored by the computer for future analysis.

For these experiments, typical laser pulse energies of less than 2 mJ.cm.$^{-2}$ were used, the laser energy being attenuated by a solution of sodium nitrite in deionised water with the required absorbance at the laser excitation wavelength (354.7 nm).

3.8 Analysis of Data Obtained From Flash Photolysis Experiments

As stated in section 3.6.2, four data traces are recorded during flash photolysis experiments. Further data manipulation is then required to obtain the desired parameters of absorbance change as a function of time ($\Delta A(t)$) for transmission flash photolysis experiments and reflectance change as a function of time ($\Delta R(t)$) in the case of diffuse reflectance experiments.

3.8.1 Transmission Laser Flash Photolysis

The data manipulation required for transmission laser flash photolysis is as follows; a data array corresponding to the signal intensity following the laser pulse, corrected for emission, is generated by subtracting the emission trace (E) from the transient absorption trace (TA). Reliable emission corrected data can only be obtained if the emission trace does not overload the photomultiplier (ie. the emission trace remains on screen or after the photomultiplier has recovered from the overload). The dynamic range of the screen is calculated by subtracting the top line (TL) from the baseline (BL) ensuring that the change in transmission is independent of the position of these two traces on the screen. The transmission change at time t after the laser flash ($\Delta T(t)$) is then defined as in equation 3.2:-

$$\Delta T(t) = 1 - \frac{(TA - E)}{(BL - TL)} \qquad (3.2)$$

$$\Delta A(t) = \log_{10}\left(\frac{1}{1-\Delta T(t)}\right) = \log_{10}\left(\frac{(BL-TL)}{(TA-E)}\right) \qquad (3.3)$$

The parameter required from transmission laser flash photolysis experiments is the change in absorbance as a function of time, $\Delta A(t)$, which from the Beer-Lambert Law (equation 1.2), $\Delta A(t)$ is given by equation 3.3.

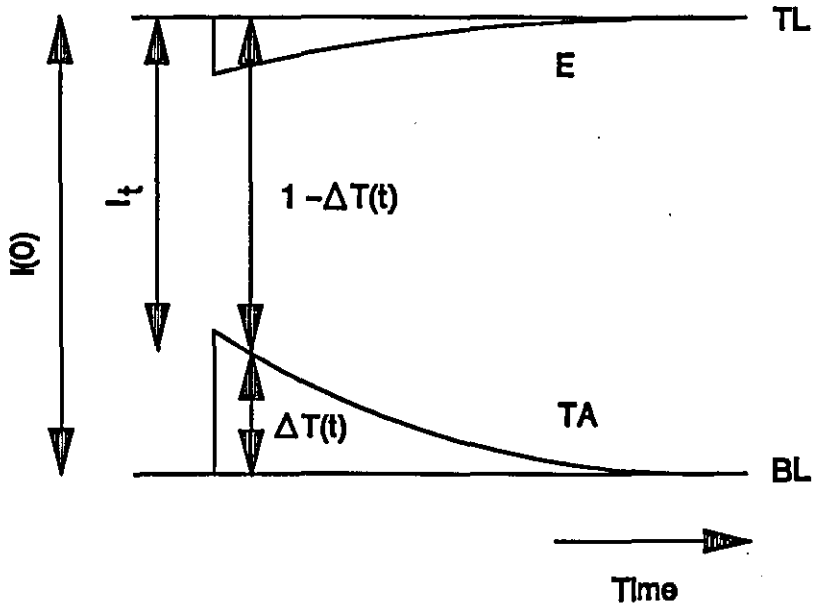

Figure 3.2:- Schematic Diagram Of The Experimental Data Traces Recorded For Transmission Laser Flash Photolysis Experiments Showing The Relationship Between $\Delta T(t)$, I(0) and $I_C(t)$

3.8.2 Diffuse Reflectance Laser Flash Photolysis

The Beer-Lambert Law can only be applied to non-scattering systems which allow transmission of the analysing light through the sample. Highly scattering/absorbing samples require a flash photolysis apparatus geometry optimised for the detection of changes in the intensity of diffusely reflected analysing light emerging from the sample. This intensity change can then be used to probe the excited state absorption, emission and kinetic properties of molecules found in such non-homogeneous non-transparent media. The geometry required for such studies is shown diagramatically in figure 3.1; details of which can be found in section 1.6.

As with transmission laser flash photolysis experiments, four data traces are recorded for diffuse reflectance laser flash photolysis namely baseline (BL), top line (TL), transient absorption (TA) and emission (E). In this case the transient absorption corresponds to a

change in the intensity of diffusely reflected analysing light from the sample following pulsed laser excitation. As previously, the dynamic range of the screen (BL-TL) and emission corrected absorption as a function of time (TA-E) are both calculated (see figure 3.3).

The observable parameter in diffuse reflectance laser flash photolysis experiments is the fractional reflectance change as a function of time ($\Delta R(t)$) defined according to equation 3.4:-

$$\Delta R(t) = \frac{\Delta J(t)}{J(0)} = \frac{R_b - R_C(t)}{R_b} = 1 - \left(\frac{(TA-E)}{(BL-TL)} \right) \qquad (3.4)$$

where R_b is the sample reflectance before excitation and $R_C(t)$ is the reflectance corrected for emission at time t after excitation.

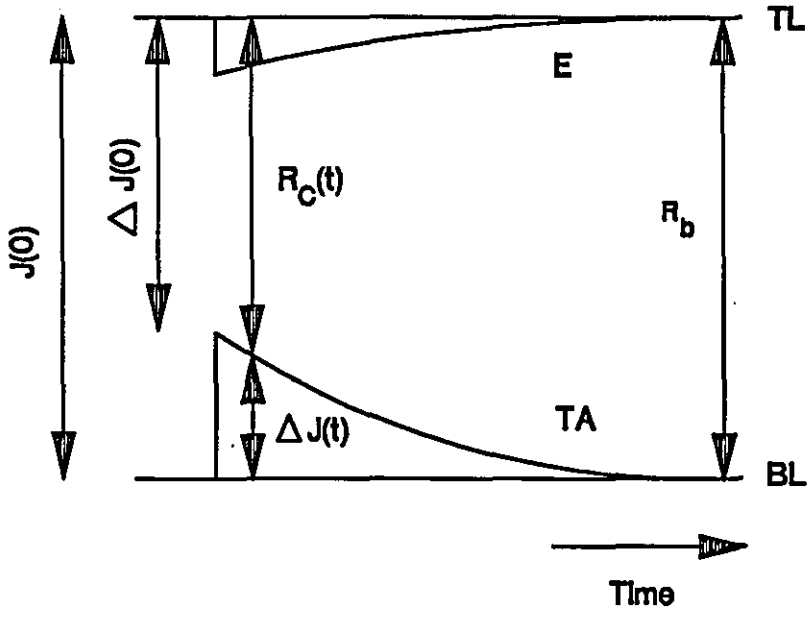

Figure 3.3:- Schematic Diagram Of The Experimental Data Traces Recorded For Diffuse Reflectance Laser Flash Photolysis Experiments Showing The Relationship Between R_b, $R_C(t)$, J(0) and $\Delta J(t)$

The intensity of diffusely reflected light before laser excitation (J(0)) is proportional to (BL-TL) and the change in diffuse reflected light intensity at time t following the laser pulse $\Delta J(t)$ is equal to (BL-TL)-(TA-E). In some cases, the percentage reflectance change is used instead of the fractional reflectance change and is defined as $100\Delta R(t)$.

As has been seen in section 1.3, the analysis of data obtained from diffuse reflectance is not as straight forward as that for transmission laser flash photolysis experiments, a knowledge of the concentration of excited states (C_T) as a function of penetration depth into the sample being required so that the correct analytical model can be applied to the data.

The distribution of C_T is dependant upon many sample parameters including the concentration of ground state molecules before laser excitation ($C_A(0)$), the molar absorption coefficient of the ground state molecules at the laser excitation wavelength (ϵ_λ), the reflectance (R_S^∞) and scattering coefficient (S_s) of the support material, and the excitation pulse intensity (I_e). As a consequence, there exists two limiting cases for the concentration profile of excited states as a function of penetration depth into the sample which require different data treatment methods. The shape of the concentration profiles for these two limiting cases are shown diagramatically in figure 1.3. Details of the derivation of the analytical methods applied to the data and of the Kubelka-Munk equation can be found in sections 1.5 and 1.6 of this thesis.

When the transient concentration C_T falls off exponentially with increasing penetration depth into the sample (Case A in figure 1.3), $\Delta R(t)$ is directly proportional to C_T provided that $\Delta R(t) < 0.1$. For $\Delta R(t)$ values up to 0.3 deviation from linearity is small but becomes significant as $\Delta R(t) \rightarrow 1$[37]. Thus, for a given decay function for the transient (f(t)) defined as in equation 3.5, f(t) can be obtained directly from the experimental values of $\Delta J(t)/\Delta J(0)$ providing that $C_T \propto \Delta R(t)$ has been established.

$$f(t) = \frac{C_T(t)}{C_T(0)} \tag{3.5}$$

For a sample where a homogeneous "plug" of excited states close to the sample surface (case B in figure 1.3) which extends deeper into the sample depth than is probed by the analysing light source (dashed line in figure 1.3) data analysis is achieved by applying the Kubelka-Munk theory (section 1.2). The Kubelka-Munk equation[28,29] relates the diffuse reflectance of an optically thick sample R_∞ to the absorption coefficient K and scattering coefficient S according to equation 3.6:-

$$F(R_\infty) = \frac{(1-R_\infty)^2}{2R_\infty} = \frac{K}{S} \tag{3.6}$$

The unitless quantity $F(R_\infty)$ is often referred to as the remission function[94].

Therefore, according to the Kubelka-Munk theory, $C_T \propto F(R_\infty)_t - F(R_\infty)_0$ as defined in equations 3.7 and 3.8 (see also figure 3.3):-

$$F(R_\infty)_t = \frac{(1-R_C(t))^2}{2R_C(t)} \tag{3.7}$$

$$F(R_\infty)_b = \frac{(1-R_b)^2}{2R_b} \qquad (3.8)$$

where $F(R_\infty)_t$ is the remission value at time t after the laser pulse and $F(R_\infty)_b$ is the remission value before the firing of the laser.

The arrangement of experimental conditions such that excited state profiles intermediate to the exponential and "plug" type profiles discussed above are generally adopted. In such a case where an intermediate excited state concentration profile does occur, the iterative method of obtaining excited state parameters detailed in section 1.3 (case C) is applied.

3.8.3 Extraction of Transient Absorption Spectra From Flash Photolysis Data

The change in the absorption for solution phase studies or reflectance for solid state samples ($\Delta A(t)$ and $\Delta R(t)$) respectively are collected at each analysing wavelength required giving a series of kinetic traces at all digitised times following the laser pulse. In order to obtain transient absorption spectra, points are selected at desired time delays following the firing of the laser. The analysis program then reads each kinetic trace sequentially in the flash photolysis file and extracts a value of $\Delta A(t)$ or $\Delta R(t)$ at the selected delay point in the kinetic trace. Following completion, a display of the observed spectrum at each selected delay is produced which can then be stored as a file for future inspection.

3.9 Materials

All solvents (benzene, cyclohexane, n-hexane, methanol, ethanol, acetonitrile and N,N-dimethylformamide) were of spectrophotometric grade (Aldrich Ltd.) and were used as received. For milled wood lignin studies, 1,4-dioxane was distilled with calcium hydride to remove water prior to use.

Benzophenone (Aldrich Ltd. Gold Label), naphthalene (Aldrich Ltd. Scintillation Grade), perylene (Aldrich Ltd. Gold Label), phenol (Aldrich Ltd. Gold Label), methoxybenzene (Aldrich Ltd. Gold Label), para-methylphenol (Aldrich Ltd. > 99 %), 4-methoxyacetophenone (Aldrich Ltd. > 99 %), 3,4,5-trimethoxyacetophenone (Aldrich Ltd. > 99 %) were all used as received. The lignin model compounds 3,4-dimethoxyacetophenone (Aldrich Ltd. 98 %) and 4-hydroxy-3-methoxyacetophenone (Aldrich Ltd. 98 %) were purified by vacuum sublimation at a pressure of ca. 1 x 10^{-5} mBar. The lignin model dimer molecule 3,4-dimethoxy-α-(2-methoxyphenoxy)-acetophenone was kindly prepared by Mr. N. Muradali at PAPRICAN according to the method of Alder *et al*[95] and triply recrystallised from ethanol (Aldrich Ltd. Spectrophotometric Grade). The phenolic lignin model compound *tert*-butylguaiacylcarbinol was synthesized by Dr. H. Tylli (University of Helsinki) according to the method of Roberti *et al*[96] and was purified according to Forsskahl[97] by column chromatography and recrystallisation.

Milled wood lignin (MWL) and thermomechanical pulp (TMP) samples were prepared as detailed in sections 3.4 and 3.3 respectively.

Oxygen and nitrogen were supplied by B.O.C. Ltd and were water-free.

Microcrystalline cellulose powder (Aldrich Ltd. 20 μm mean particle size) was used as received.

Chapter 4

Experiments With Lignin Model Compounds

4 Experiments With Lignin Model Compounds

4.1 Introduction

As has been discussed in section 2.6, early work relating to the photoyellowing of lignin rich high yield mechanical pulps demonstrated the role of lignin, oxygen and moisture in the light induced processes leading to brightness loss with time. In order to prevent such undesirable processes, chemists and wood scientists began to address the complex photochemical reactions present in such a chemically intricate molecule as lignin. Many empirical studies involving steady-state irradiation of potential yellow product forming chromophores followed by product analysis have been documented and postulates formed as to the relevance of such studies to the photochemistry of lignin present in its natural form[84,98,99]. It was Kringstad[84] who first proposed that ortho-quinones were one of the chromophores responsible for the yellow colour of mechanical pulps following exposure to near UV light (300 nm to 400 nm). This has recently been confirmed by Lebo *et al* using phosphorus (^{31}P) NMR spectroscopy[86]. Throughout the lignin macromolecule, many diverse chromophoric structures exist which play no direct part in the photoyellowing processes since they do not absorb light at wavelengths greater than 300 nm (cut-off wavelength of natural solar irradiation[100]). The chromophores present in the lignin structure which absorb at wavelengths greater than 300 nm that have been most widely studied are ring conjugated carbonyl moieties and ring conjugated carbon-carbon double bonds. Since we are interested in **bleached** TMP where all ring conjugated double bonds (coniferaldehyde type structures) have been removed from the lignin structure (section 2.4), the remainder of the discussion here will be concerned with the photochemical behaviour of the α-carbonyl moieties. Model studies involving the photochemical behaviour of coniferaldehyde lignin model compounds can be found in the literature[101,102].

The photochemical interaction between α-carbonyl lignin model compounds with phenolic hydroxyl moieties also present in the lignin macromolecule have demonstrated that the hydrogen atom abstraction of phenolic hydroxyl hydrogens by excited states of α-carbonyl moieties is an efficient process and leads to a phenoxy-ketyl free radical pair. The fate of such species is dependent upon both substitution patterns on the aromatic ring system and also the availability of ground state molecular oxygen[103,104]. The reaction pathways leading to yellow photoproducts in the form of ortho and para quinones and other coloured oligomeric materials are still not fully understood. Many of the studies involving α-carbonyl and phenolic lignin model compounds were performed in fluid solution[105,106,107] where free diffusional mobility of reactive species and dissolved oxygen are considerably enhanced relative to diffusional processes in TMP fibres where oxygen diffusion is considerably slower[108]. Consequently, direct photochemical comparisons between the behaviour of lignin model compounds and chromophores present in TMP can only be made with this observation in mind.

The role of singlet molecular oxygen ($^1\Delta_g(O_2)$), sensitized by excited triplet states of α-carbonyl moieties has also been studied[109,110]. The ability of singlet oxygen to abstract hydrogen atoms from phenolic hydroxyl moieties has been demonstrated in fluid solution[111,112] leading to the formation of a phenoxy free radical and a hydro-peroxy radical($HO_2\cdot$), the phenoxy radical possibly going on to form yellow photoproducts. The observation that high yield pulp samples actually photobleach upon exposure to singlet oxygen[113] serves to highlight the

problem of extrapolating results obtained in fluid solution with those of lignin in its native environment. A summary of the photochemical interaction between α-carbonyl triplet states and phenolic hydroxyls known to be present in the lignin matrix which ultimately lead to the formation of ortho and para quinones is shown in figure 4.1:-

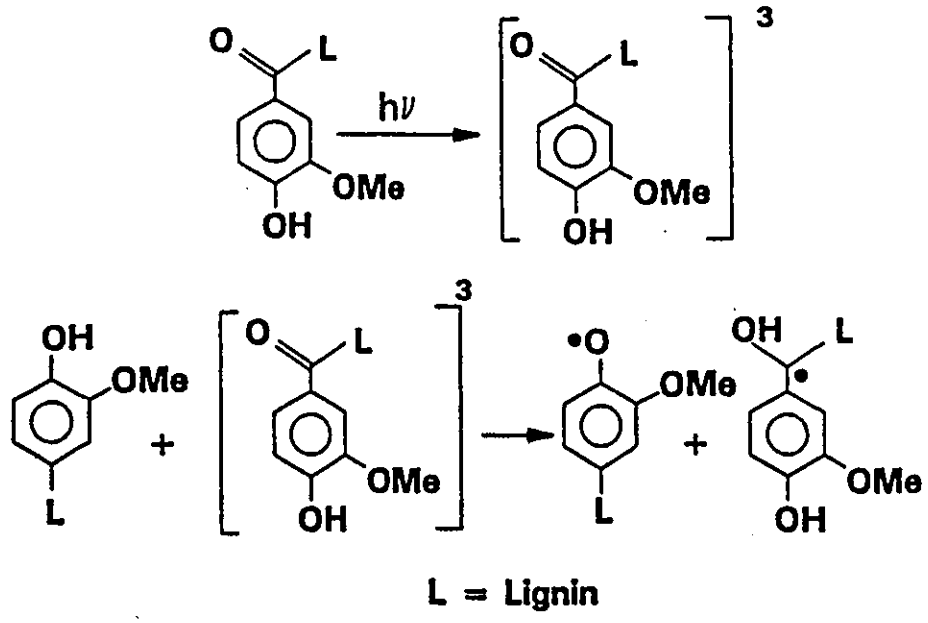

Figure 4.1:- A Summary of the Photochemical Interaction Between α-carbonyl Triplet States and Phenolic Hydroxyls Present in the Lignin Matrix

More detailed reaction schemes can also be found in the literature[103]. The observation that treatment of milled wood lignin (MWL) with sodium borohydride (ie. removing all α-carbonyls) reduces the extent of photoyellowing clearly implicates the α-carbonyl moieties as a photo-sensitiser in the lignin degradation mechanism[114]. The observation by many workers that, following chemical replacement of all lignin phenolic hydroxyls with methyl or acetyl groups (ie. removal of a primary source of phenoxy free radicals), high yield pulps still undergo photoyellowing suggest the presence of at least one more colour reversion mechanism[83,115]. When TMP is both reduced and alkylated, decrease in the extent of brightness loss to levels just above those observed for Kraft pulps is observed[116]. It was Gierer and Lin who first demonstrated that non-phenolic α-carbonyl phenacyl-aryl-ether type lignin model compounds (section 2.3) under air equilibrated conditions yellowed upon exposure to simulated solar irradiation[115]. Many subsequent studies[117,118,119,120] into the photochemical behaviour of such β-O-4 aryl-ether linkages both in solution and adsorbed onto lignin free paper[121,122,123] have since been documented in the literature[124,125,126]. In solution, the photochemistry of this type of molecule is dominated by efficient inter-molecular β-phenyl quenching of the excited α-carbonyl triplet state yielding extremely short triplet lifetimes of the order of a few hundred picoseconds to a few hundred nanoseconds depending upon substitution patterns upon the aromatic rings, electron

donating groups on the ring systems having the effect of extending the triplet lifetime. In addition to the efficient quenching mechanism, a degradation mechanism involving the photochemical cleavage of the C-O bond to yield a phenoxy-phenacyl free radical pair is also observed, a phenomenon enhanced by electron donating groups on the aromatic ring systems. Studies involving the quenching of all photochemically generated triplet states suggest that such a cleavage reaction may occur from both excited singlet and triplet manifolds[124], a result which has been recently confirmed by chemically induced dynamic nuclear polarisation (CIDNP) spectroscopy[127]. A summary of the proposed photochemical behaviour of β-O-4 lignin model dimers is presented in figure 4.2:-

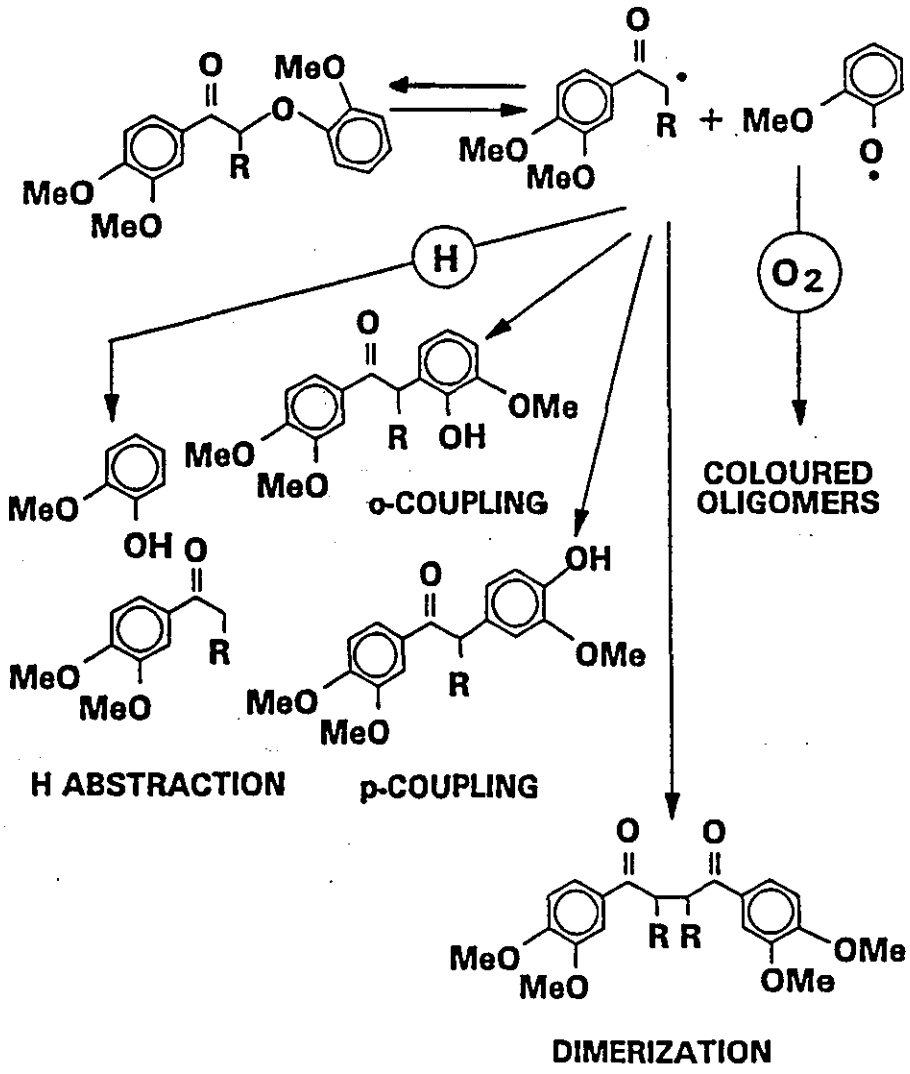

Figure 4.2:- Proposed Photochemical Behaviour of β-O-4 Lignin Model Dimers in Fluid Solution[120]

Product analysis following the photochemical degradation of α-(2-methoxyphenoxy) -3,4-dimethoxyacetophenone are consistent with the following mechanisms:-

(a) Scavenging of phenacyl and guaiacoxyl radicals by hydrogen donors
(b) Ortho and para couplings leading to phenacyl-guaiacols isomeric to the starting material
(c) Dimerisation of phenacyl radicals
(d) Formation of yellow oligomeric materials
(e) Radical recombination to regenerate the starting material

As can be seen from both figures 4.1 and 4.2, substituted phenoxy type radicals are formed by at least three mechanisms in solution. The fate of such a radical species is dependent upon the availability of oxygen or a good hydrogen donor to deactivate. Also, photodegradation product distribution shows some solvent dependency indicating that the environment in which the phenoxy radical is formed plays a role in determining which deactivation process will dominate.

Other model compounds systems have been studied in solution under steady state irradiation conditions. Irradiation of α-O-4 lignin model dimer molecules have also been shown to photodegrade via a cleavage reaction involving the α-carbon to oxygen bond, again yielding a phenoxy free radical species[128]. In all of the above mechanisms, a vast array of identified products are recovered as a result of random couplings between free radical species, some of which give the irradiated solutions a yellowish colour.

Many of the studies involving lignin model compounds have been performed in solution under steady-state irradiation conditions. It was the aim of the currently described section of work to investigate the time resolved transient photochemistry of a simple α-carbonyl lignin model compound in an attempt to gain insight into the behaviour of such a chromophore when present as part of the lignin macromolecule itself. The model compound chosen for this purpose was acetoveratrone (3,4-dimethoxyacetophenone). Although transient data concerning this compound can be found in the literature[120], little is specifically known as to the effect of solvent upon its transient behaviour in terms of triplet-triplet absorption maxima, absorption coefficient and triplet state lifetime. Such studies may serve as useful indicators in the assignment of the short lived transient species observed following pulsed laser excitation of MWL (in solution and adsorbed onto microcrystalline cellulose) and also from TMP itself.

4.2 Excited State Photochemistry Of 3,4-Dimethoxyacetophenone in Fluid Solution

4.2.1 Triplet-Triplet Absorption Spectra and Triplet Lifetimes

The molar absorption coefficient of 3,4-dimethoxyacetophenone in all the solvents used in the following studies at the laser excitation wavelength (354.7 nm) is extremely small (< 30 $l.mol.^{-1}cm.^{-1}$) and therefore it was required that a ground state concentration of approximately 10^{-2} $mol.l.^{-1}$ was required in order to gain sufficient absorbance at this wavelength to perform flash photolysis experiments. The transient absorption spectrum of

3,4-dimethoxyacetophenone in degassed benzene solution is shown in figure 4.3 at four time delays following the laser pulse.

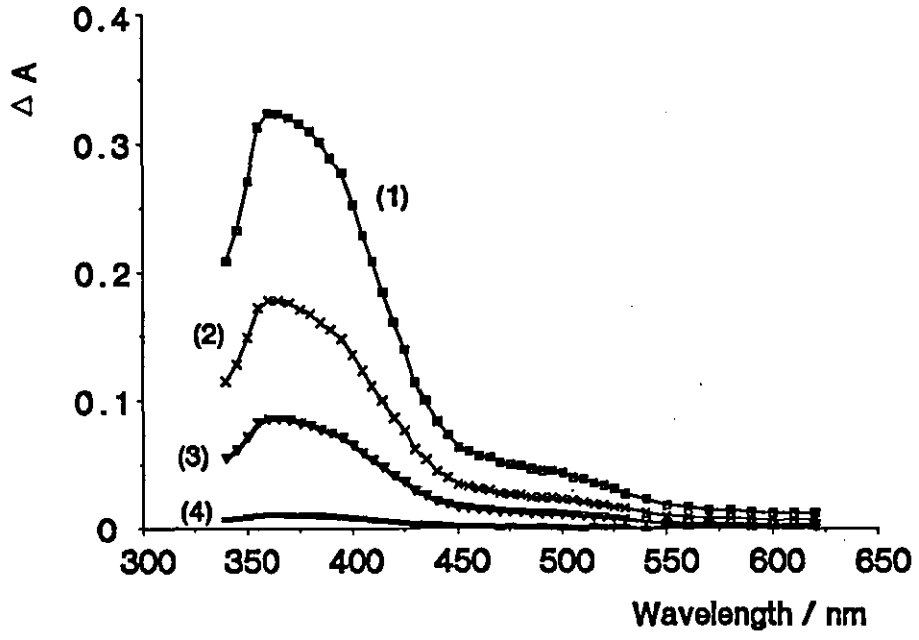

Figure 4.3:- Transient Absorption Spectrum of 3,4-Dimethoxyacetophenone in Degassed Benzene Solution at Four Time Delays Following the Laser Pulse
Delay Times are (1) 0.6 μs, (2) 3.5 μs, (3) 8.6 μs and (4) 46.6 μs

The spectra are characterised by a single λ_{max} located at ca. 365 nm which does not change with time delay following the laser pulse, and a broad structureless absorption extending to beyond 600 nm. By attenuating the laser energy to ca. 1 mJ.cm.$^{-2}$ per pulse, a clean first order fit (global fit of 4 individual traces) to the transient decay (analysing at 370 nm) is observed (figure 4.3) yielding a lifetime for the transient of 40 μs $\pm$ 0.5 μs. The transient decays with the same kinetics at all analysing wavelengths indicating that the absorption spectrum is due to a single transient species. The lack of long lived transient species following decay of the initial transient signal demonstrates the inertness of this excited state to photochemical reaction, a point further demonstrated by the superimposition of the ground state absorption spectrum following exposure of a sample of 3,4-dimethoxyacetophenone (in degassed benzene) to approximately 400 laser pulses (ca. 25 mJ.cm.$^{-2}$ per pulse). The spectrum is assigned as absorption from the lowest lying triplet state of 3,4-dimethoxyacetophenone. The lowest lying triplet state is assigned as the $^3(\pi,\pi^*)$ state based on the following evidence:-

(a) The triplet-triplet absorption spectrum and λ_{max} position are similar to those observed for 4-methoxyacetophenone in cyclohexane solution[129]. Also, 4-methoxyacetophenone has been shown to have a $^3(\pi,\pi^*)$ lowest lying triplet state[130,131] in all solvents.

(b) No room temperature phosphorescence is observed for this molecule in benzene solution indicating that the natural radiative lifetime is long.

The triplet-triplet absorption spectrum of 3,4-dimethoxyacetophenone was also obtained in acetonitrile and N,N-dimethylformamide. As with benzene, a single transient species at short time delays after the laser pulse was observed (figures 4.4 and 4.5). However, a small residual absorption following decay of the triplet state observed at long time delays following the laser pulse was observed which reflect a small degree of photochemical reactivity of 3,4-dimethoxyacetophenone in these solvents.

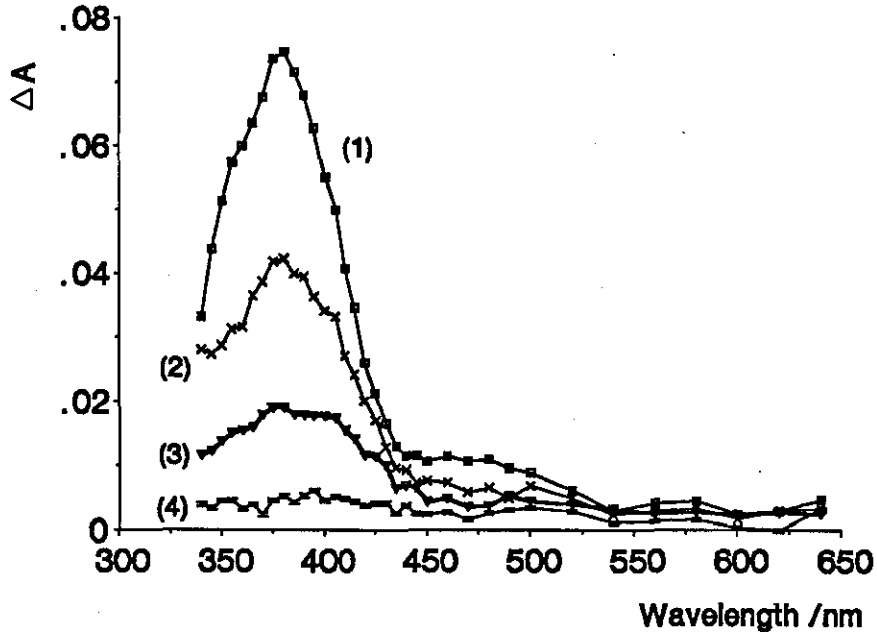

Figure 4.4:- Transient Absorption Spectrum of 3,4-Dimethoxyacetophenone in Degassed Acetonitrile Solution at Four Time Delays Following the Laser Pulse
Delay Times are (1) 1.7μs, (2) 9.5μs, (3) 24.3μs and (4) 140μs

The position of the triplet absorption λ_{max} is observed to be red shifted relative to its position in benzene by ca. 15 nm to 20 nm to ca. 380 nm. First order fits to the kinetic traces (using low laser intensities) at the absorption λ_{max} yield triplet lifetimes of 16 μs ± 0.5 μs in acetonitrile and 20 μs ± 0.5 μs in N,N-dimethylformamide respectively.

Relative to solvent effects, electron donating groups (such as methoxyl or methyl moieties) present on the aromatic ring of acetophenone derivatives have a considerable influence in determining the nature of the lowest lying triplet state of such compounds. Acetophenone itself is well known to have a lowest lying triplet state that is $^3(n,\pi^*)$ in nature whereas 4-methoxyacetophenone has a lowest lying $^3(\pi,\pi^*)$ state[129]. For methoxy substituted acetophenone derivatives, electron donating moieties also determine the energy

separation between the lowest lying triplet $^3(\pi,\pi^*)$ state and the T_2 state which has $^3(n,\pi^*)$ character.

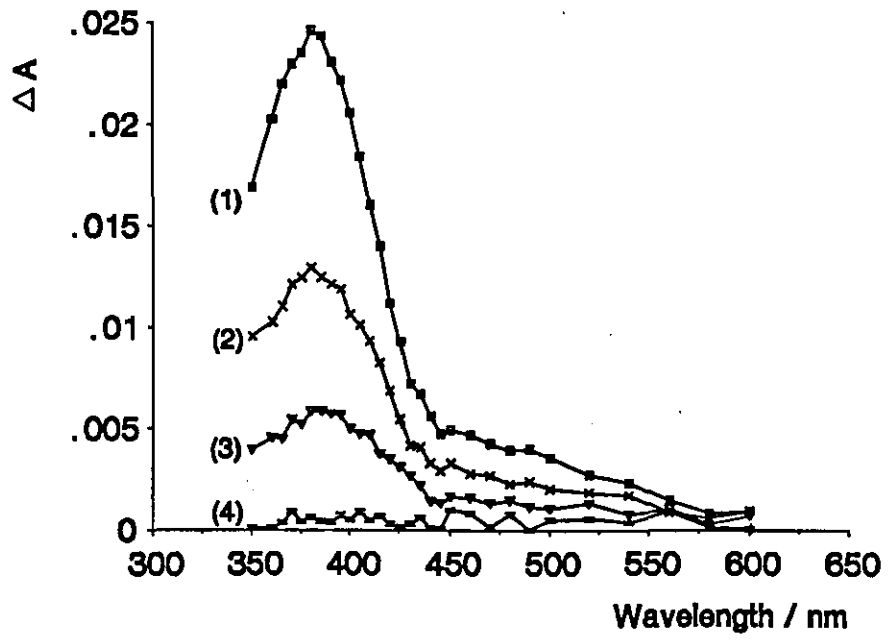

Figure 4.5:- Transient Absorption Spectrum of 3,4-Dimethoxyacetophenone in Degassed N,N-Dimethylformamide Solution at Four Time Delays Following the Laser Pulse
Delay Times are (1) 2.6 μs, (2) 16.4 μs, (3) 36.1 μs and (4) 117 μs

For example, the triplet lifetime of 4-methoxyacetophenone in N,N-dimethylformamide was observed to be approximately 6.5 μs. This may be explained in one of two ways:-

(a) The removal of the methoxy moiety in the three position on the aromatic has the effect of reducing the energy gap (ΔE_T) between the two almost iso-energetic $^3(\pi,\pi^*)$ and $^3(n,\pi^*)$ triplet states.
(b) Increased coupling between the two triplet states as a result of changing the mixing coefficients of the two triplet states (section 1.1.3) will have the effect of shortening the triplet lifetime (τ_T) due to an equilibrium population of upper $^3(n,\pi^*)$ states being present as ΔE_T decreases.

Unequivocal assignment of transient absorption spectra shown above as that of the triplet state of 3,4-dimethoxyacetophenone was obtained by sensitization experiments with perylene and naphthalene as triplet energy acceptors. Shown in figure 4.6 is the transient absorption spectrum for triplet naphthalene in de-oxygenated benzene sensitized by 3,4-dimethoxyacetophenone.

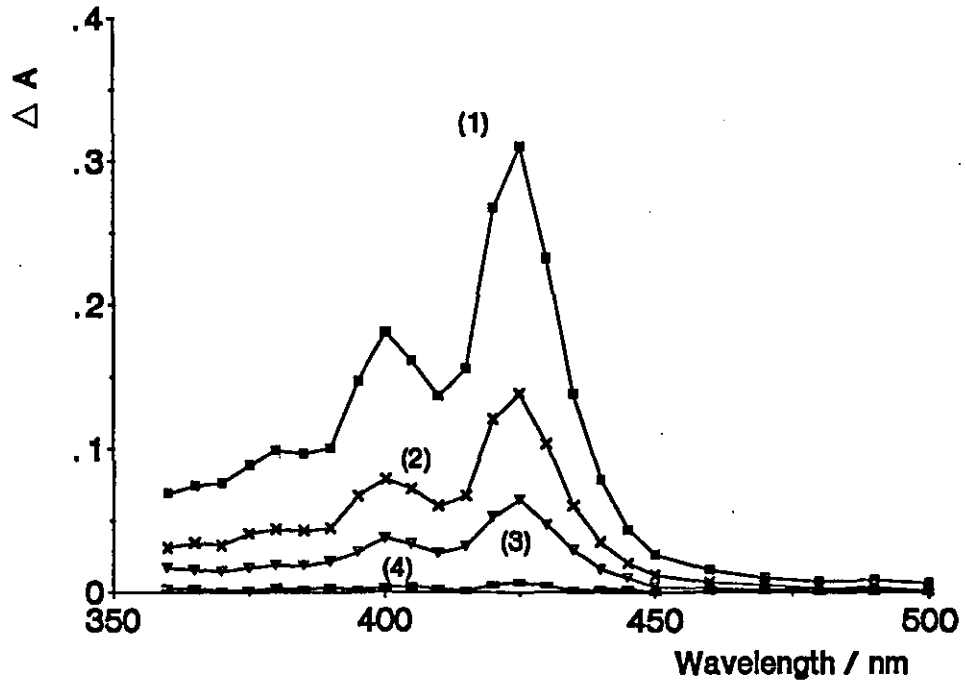

Figure 4.6:- Triplet-Triplet Absorption Spectrum of Naphthalene Sensitised By 3,4-Dimethoxyacetophenone in Degassed Benzene Solution
Time Delays are (1) 1.83 μs, (2) 10.0 μs, (3) 26.4 μs and (4) 160 μs

The concentration of naphthalene (0.1 mol.l.$^{-1}$) was such that all the photoinduced triplet states of the lignin model compound are quenched instantaneously on the timescales of these experiments. The characteristic sharp absorption bands of the naphthalene triplet state (λ^{TT}_{max} = 400 nm and 425 nm) are observed and are in good agreement with the literature[132]. In the following section, the quenching of laser induced triplet states with a high concentration of naphthalene (0.1 mol.l.$^{-1}$) has been used to determine the singlet-triplet intersystem crossing quantum yields (ϕ_T) of the lignin model compounds under investigation in the present study. All acetophenone derivatives have a triplet energy close to or slightly above 300 kJ.mol.$^{-1}$[133] therefore quenching by naphthalene whose triplet energy is located at 255 kJ.mol.$^{-1}$[134] is a process which takes place with unit efficiency[135].

4.2.2 Singlet-Triplet Intersystem Crossing Quantum Yields

The intersystem crossing quantum yields (ϕ_T) were measured for a series of acetophenone derivatives that are structurally similar to the α-carbonyl chromophoric moieties found in native lignin. Benzophenone is well documented to have a intersystem crossing quantum yield of 1 in benzene solution[136] and therefore was used as a standard for these experiments.

The triplet quantum yields were measured by two methods, a reaction scheme applicable to both techniques being detailed below where K is the ketone (or benzophenone) and

N is naphthalene present at a concentration (0.1 mol.l.$^{-1}$) sufficient to quench all photo-induced ketone triplet states.

$$^1K \xrightarrow[354.7\,nm]{h\nu} {}^1K^* \tag{4.1}$$

$$^1K^* \xrightarrow{\phi_{ISC}} {}^3K^* \tag{4.2}$$

$$^3K^* + {}^1N \xrightarrow{100\%} {}^1K + {}^3N^* \tag{4.3}$$

$$^3N^* \xrightarrow{k_d} {}^1N \tag{4.4}$$

$$^3N^* + {}^3\Sigma_g^-(O_2) \rightarrow {}^1N + {}^1\Delta_g(O_2) \tag{4.5}$$

$$^1\Delta_g(O_2) \xrightarrow{k_{rad}} {}^3\Sigma_g^-(O_2) + h\nu(1270nm) \tag{4.6}$$

In the absence of oxygen, the change of absorbance at 425 nm (ΔA^{425nm}) due to the formation of triplet naphthalene (equations 4.1 to 4.4) as a function of laser intensity (the laser intensity was attenuated by means of sodium nitrate filters of known absorbance at the laser excitation wavelength) is monitored for a benzophenone/naphthalene sample and also the ketone/naphthalene sample under identical conditions. Each of the samples was optically matched at the laser excitation wavelength to ensure an equal number of photons absorbed by each sample, typical absorbances being approximately 0.5 at 354.7 nm. From equations 4.1 to 4.4, the triplet quantum yield (ϕ_T) for the unknown ketone (K) is obtained according to equation 4.7:-

$$\phi_T^K = \frac{slope K}{slope Bzp} \times \frac{(1-10^{-A})_{Bzp}}{(1-10^{-A})_K} \tag{4.7}$$

where the first term is the ratio of the slopes of ΔA^{425nm} (extrapolated to zero time after the laser pulse) as a function of laser intensity for the unknown ketone (K) and benzophenone (Bzp) respectively. The second term in equation 4.7 accounts for small differences in absorbance (A) between samples at the excitation wavelength (354.7 nm). In all cases, correction factors no greater than 1 ± 0.05 were required.

In the presence of oxygen (all samples were air equilibrated), equations 4.5 and 4.6 also apply whereupon the singlet oxygen luminescence intensity (I_Δ^0), extrapolated to zero

time following the laser pulse, as a function of laser intensity are plotted and equation 4.7 applied to the resultant data. For the luminescence data collection, the samples were contained in 1 cm x 1 cm quartz cuvettes, the singlet oxygen luminescence being detected at right angles to the direction of the laser (see section 3.7 for details of the singlet oxygen luminescence detection system).

The samples studied were benzophenone, 4-methoxyacetophenone, 3,4-dimethoxyacetophenone, 4-hydroxy-3-methoxyacetophenone, 3,4,5-trimethoxyacetophenone and α-(2-methoxyphenoxy)-3,4-dimethoxyacetophenone. Representative plots of I_{Δ}^{0} as a function of laser intensity for the sensitizers benzophenone, 3,4-dimethoxyacetophenone and α-(2-methoxyphenoxy)-3,4-dimethoxyacetophenone are shown in figures 4.7, 4.8 and 4.9 together with the best least squares straight line fit to the data.

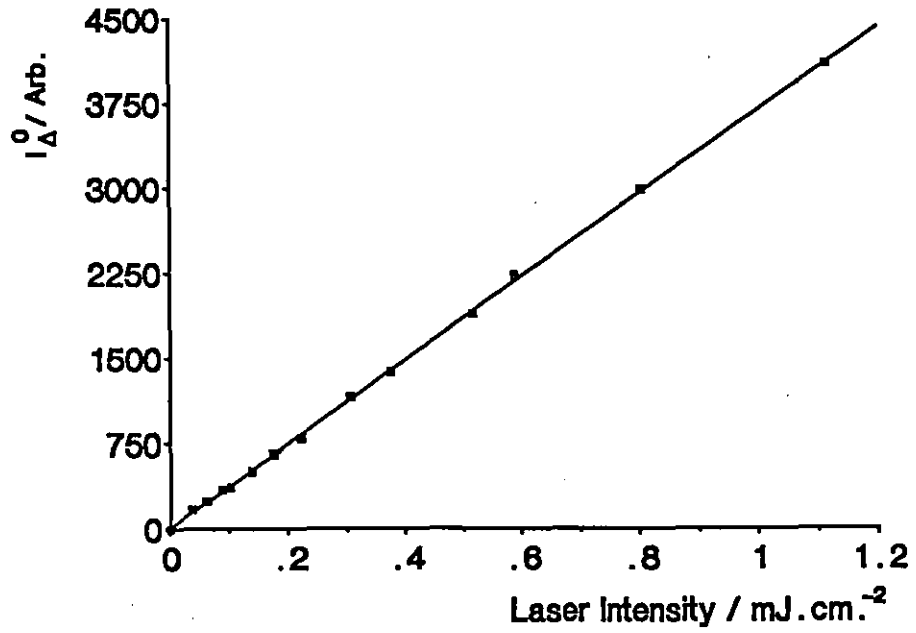

Figure 4.7:- A Plot of I_{Δ}^{0} as a Function of Laser Intensity with Benzophenone as Sensitizer together with the Best Straight Line Fit to the Data

Linear regression analysis was only performed at sufficiently low laser intensities to ensure that the plots of I_{Δ}^{0} as a function of laser intensity were linear which were found to be up to 4 % of the full laser intensity of ca. 28 mJ.cm.$^{-2}$. At high laser intensities, deviation from linearity was observed for such plots (figure 4.10) due to absorption of the laser pulse by the naphthalene triplet state resulting in a less than predicted yield of singlet molecular oxygen, an observation also noted by other workers[137].

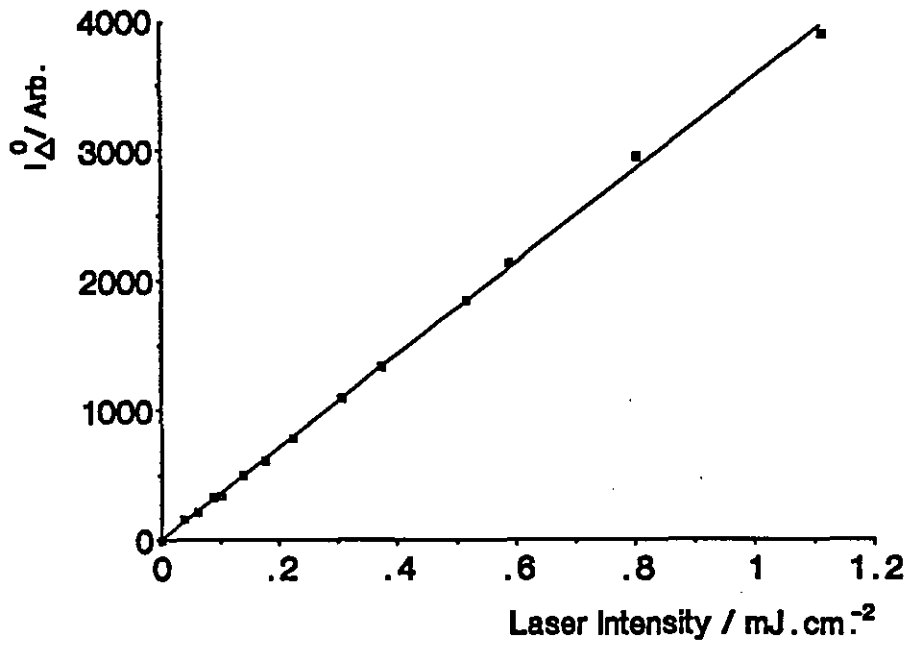

Figure 4.8:- A Plot of I^0_Δ as a Function of Laser Intensity with 3,4-Dimethoxyacetophenone as Sensitizer together with the Best Straight Line Fit to the Data

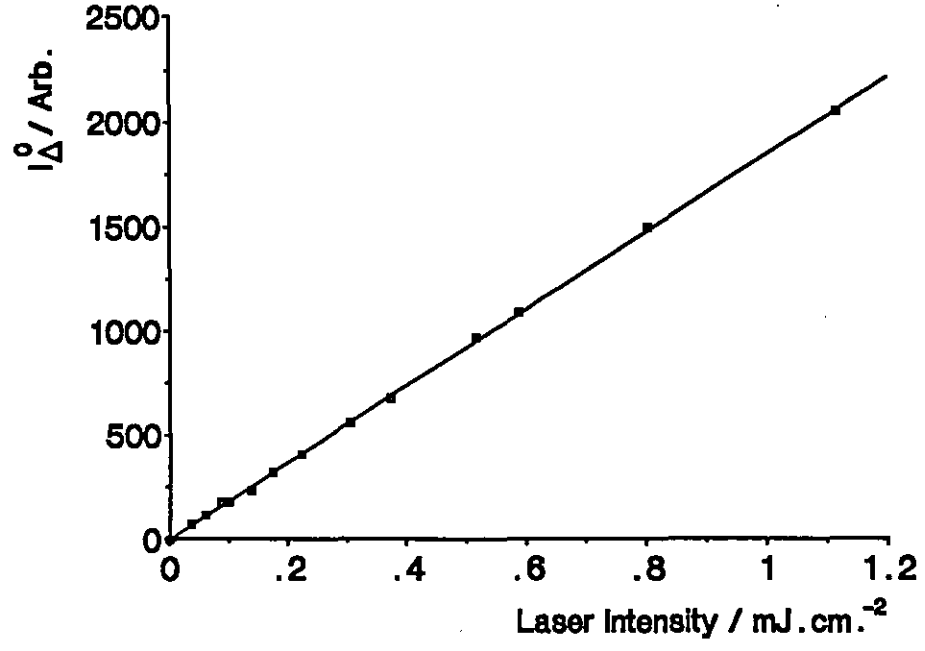

Figure 4.9:- A Plot of I^0_Δ as a Function of Laser Intensity with α-(2-methoxyphenoxy) -3,4-dimethoxyacetophenone as Sensitizer together with the Best Straight Line Fit to the Data

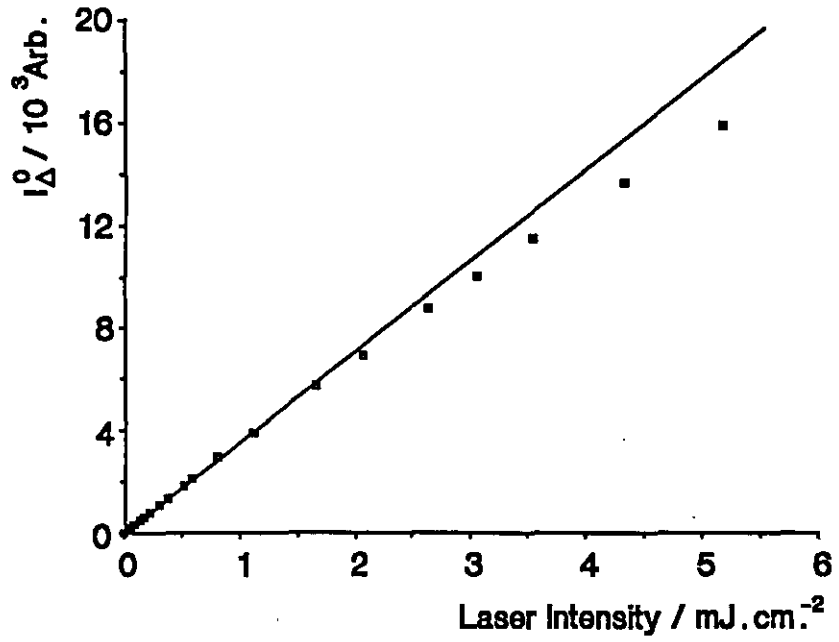

Figure 4.10:- A Plot of I_Δ^0 as a Function of Laser Intensity with 3,4-Dimethoxyacetophenone as Sensitizer together with the Best Straight Line Fit to the Data from figure 4.7

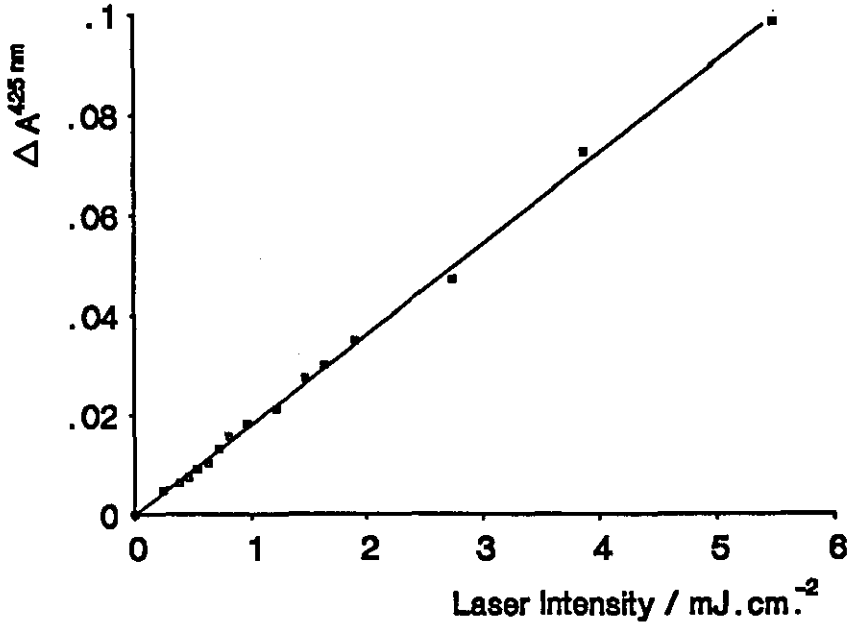

Figure 4.11:- A Plot of $\Delta A^{425\,nm}$ as a Function of Laser Intensity with Benzophenone as Sensitizer together with the Best Straight Line Fit to the Data

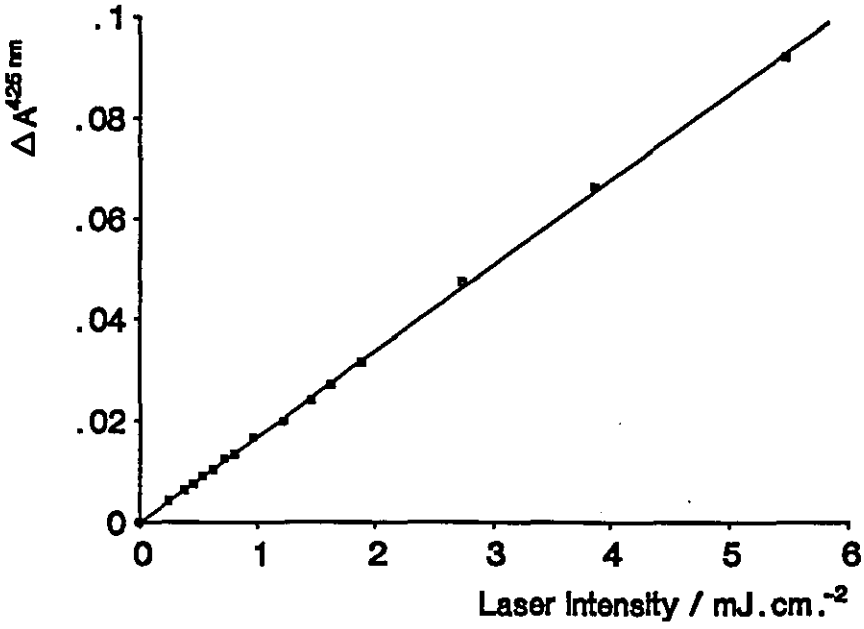

Figure 4.12:- A Plot of $\Delta A^{425\,nm}$ as a Function of Laser Intensity with 3,4-Dimethoxyacetophenone as Sensitizer together with the Best Straight Line Fit to the Data

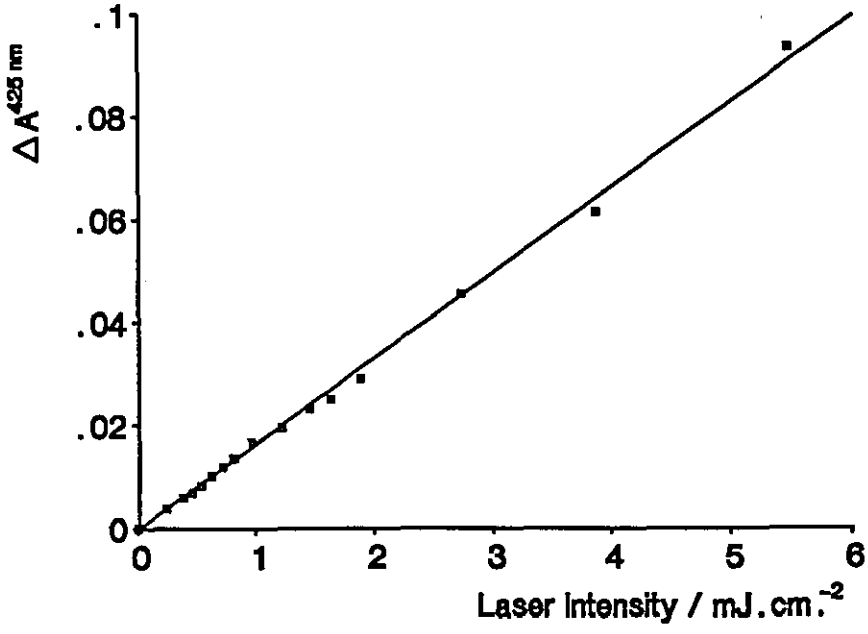

Figure 4.13:- A Plot of $\Delta A^{425\,nm}$ as a Function of Laser Intensity with 4-Hydroxy-3-methoxyacetophenone as Sensitiser Together with the Best Straight Line Fit to the Data

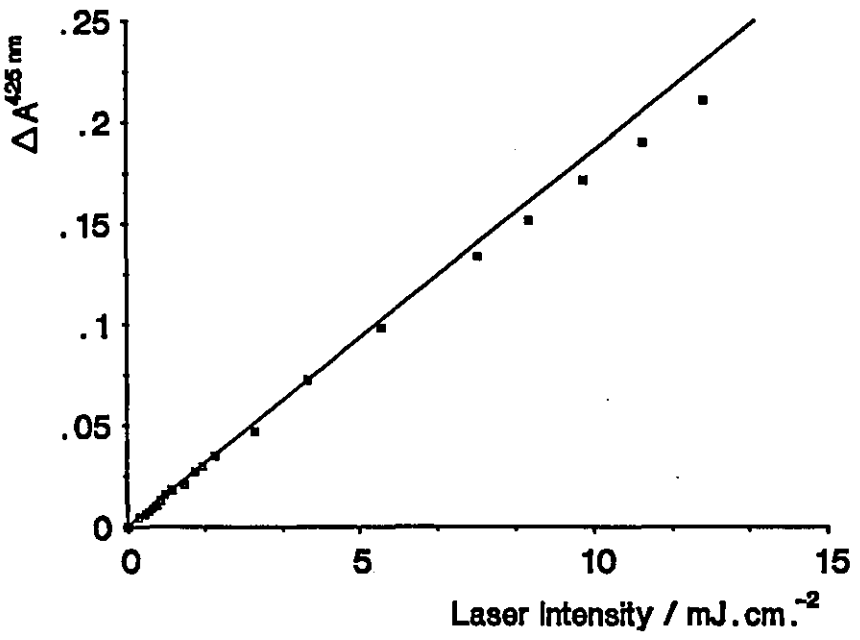

Figure 4.14:- A Plot of $\Delta A^{425\,nm}$ as a Function of Laser Intensity with Benzophenone as Sensitiser together with the Best Straight Line Fit to the Data from figure 4.11

Corresponding representative plots of $\Delta A^{425\,nm}$ as a function of laser intensity are shown in figures 4.11, 4.12 and 4.13 for the sensitizers benzophenone, 3,4-dimethoxyacetophenone and 4-hydroxy-3-methoxyacetophenone together with a higher laser intensity plot for benzophenone sensitization (figure 4.14).

A similar curvature of such plots is observed when analysing by the $\Delta A^{425\,nm}$ method. Unfortunately, direct comparison of the extent of curvature at high laser intensities between I^0_Δ and $\Delta A^{425\,nm}$ is not possible due to the data sets being recorded on two different flash photolysis systems. The results of the studies are shown in table 4.2 (P.T.O.).

As can be seen, all acetophenone derivatives have triplet quantum yields which approach unity with the exception of the β-O-4 lignin model dimer molecule which has a triplet quantum yield of approximately 0.5, an observation in agreement with other workers[138]. This observation supports the evidence of Palm *et al* who proposed that photodegradation of this molecule occurred via the singlet and triplet excited states[127], and also those of Schmidt *et al*[124] based on the fact that the addition of sufficient triplet state quencher (1,3-butadiene) to quench 99 % of photoinduced triplet states failed to prevent photodegradation of this molecule.

Ketone	ϕ_T^K(1)	
	I_Δ^0	ΔA^{425nm}
Benzophenone	1.00(2)	1.00(2)
4-methoxyacetophenone	0.98	0.98
3,4-dimethoxyacetophenone	0.96	0.94
3,4,5-trimethoxyacetophenone	0.91	0.94
4-hydroxy-3-methoxyacetophenone	0.94	0.92
α-(2-methoxyphenoxy)-3,4-dimethoxyacetophenone	0.50	0.55

Table 4.2:- Summary of Results Determining ϕ_T^K for a Series of Lignin Model Compounds in Benzene Solution by Two Different Methods

(1) An error of ± 10 % is estimated for these measurements
(2) ϕ_T^K = 1 as standard[136]

It must be noted that, the triplet quantum yield upon successive methoxylation does show a decreasing trend, an observation in agreement with Wagner *et al*[139] who obtained a triplet quantum yields for 4-methoxyacetophenone in benzene of 0.98 relative to acetophenone (ϕ_T = 1[136]). However, it must be borne in mind that, given that the estimated error in these measurements is ± 10 %, this observation may simply be experimental error.

4.2.3 Triplet State Molar Absorption Coefficients

The molar absorption coefficient of triplet 3,4-dimethoxyacetophenone and the lignin model dimer α-(2-methoxyphenoxy)-3,4-dimethoxyacetophenone were measured in degassed benzene solution relative to that of the benzophenone (Bzp) triplet at 525 nm (ϵ = 7220 l.mol.$^{-1}$cm.$^{-1}$)[140]. In all cases, a fast digitising time base was employed such that the change of absorbance (ΔA) at zero time after the laser pulse could be read directly from the data trace. The change in absorbance at the λ_{max} of the transient absorption (λ_{max}^{TT}) for each optically matched sample (absorbance approximately 0.2 at the laser excitation wavelength) was recorded three times at a series of laser intensities (100 % laser intensity = ca. 25 mJ.cm.$^{-2}$). The results were average and plotted as shown in figure 4.15 for benzophenone and 3,4-dimethoxyacetophenone.

Each data set was fitted with a linear least squares fitting routine to obtain the best straight line fit to the data, the molar absorption coefficient for the unknown ketones (K) being calculated according to equation 4.8. As previously (equation 4.7), the second term on the right hand side of the equation accounts for the small differences in absorbance at the laser excitation wavelength (354.7 nm), the third term accounting for the less than unity value of the triplet quantum yield for the dimer molecule. For calculation of the molar absorption coefficient of the dimer molecule, a triplet quantum yield of 0.53 (ie. an average of the values obtained from table 4.2) was used. A summary of the results is presented in table 4.3.

$$\epsilon_K^{\lambda_{max}} = \frac{slope K}{slope Bzp} \times \frac{(1-10^{-A})_{Bzp}}{(1-10^{-A})_K} \times \frac{\phi_T^{Bzp}}{\phi_T^K} \times 7220 \qquad (4.8)$$

Ketone	ϕ_T	λ_{max}^{TT}/nm	$\frac{\epsilon_K^{\lambda_{max}}}{l.mol.^{-1}cm.^{-1}}$ (3)
Benzophenone	1(1)	530	7220(4)
3,4-dimethoxyacetophenone	1	365	12500
α-(2-methoxyphenoxy)-3,4-dimethoxyacetophenone	0.53(2)	395	8900

Table 4.3:- Triplet Molar absorption Coefficients of the Lignin Model Compounds 3,4-dimethoxyacetophenone and α-(2-methoxyphenoxy)-3,4-dimethoxyacetophenone in Benzene Solution

(1) ϕ_T = 1[136] as standard

(2) Average of the Values Obtained in table 4.2

(3) An error of ≈ 10 % is estimated for these measurements

(4) ϵ = 7220 l.mol.$^{-1}$cm.$^{-1}$[140] as standard

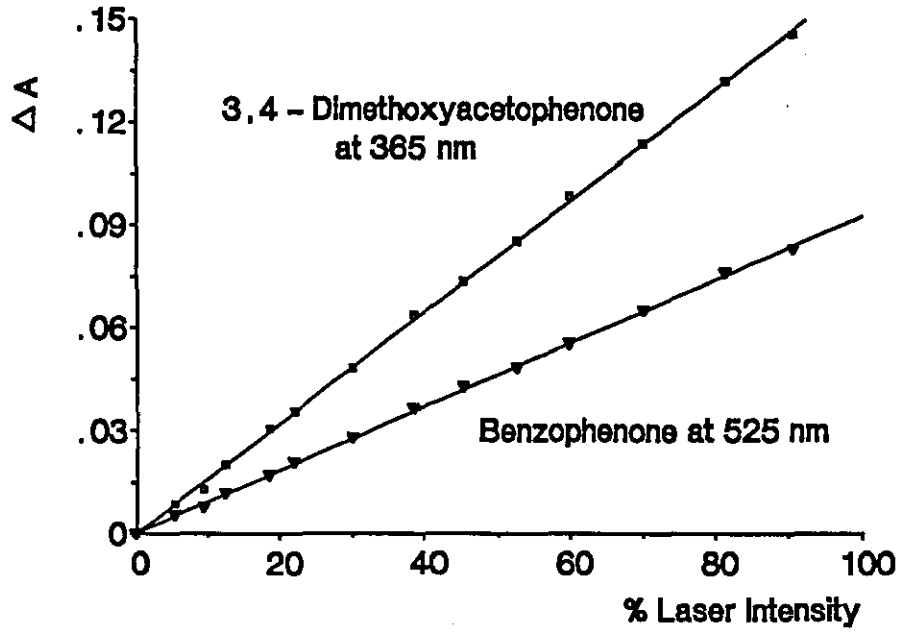

Figure 4.15:- Plots of ΔA at the Transient Absorption Maxima (λ_{max}^{TT}) as a Function of Laser Intensity for Benzophenone and 3,4-Dimethoxyacetophenone Together With the Best Straight Line Fit to the Data.

A similar value for the molar absorption coefficient of triplet 3,4-dimethoxyacetophenone in N,N-dimethylformamide was also observed. Typical error in the values quoted in table 4.3 are ca. ± 10 %. The values for the molar absorption coefficient of acetophenone derivatives are in good agreement with the literature[129]. It is interesting to note also that the absorption maximum of the triplet state of the dimer molecule is bathochromically shifted by some 30 nm relative to that of 3,4-dimethoxyacetophenone in benzene solution, a point which will be discussed later in this chapter (section 4.4).

4.2.4 Triplet State Quenching by Phenol and Methoxybenzene

The photochemically induced phenolic hydroxyl hydrogen atom extraction by excited triplet states of aromatic ketones has been demonstrated to be an efficient process for both $^3(\pi,\pi^*)$ states and $^3(n,\pi^*)$ states[141]. The quenching rate constant for a predominantly $^3(\pi,\pi^*)$ carbonyl triplet 4-methoxypropiophenone was found to be greater than those observed for benzophenone itself. This may be attributed partly to the existence of an equilibrium population of $^3(n,\pi^*)$ and $^3(\pi,\pi^*)$ states (ΔE_T = 12 to 17 kJ.mol.$^{-1}$) and also to the fact that the lowest lying $^3(\pi,\pi^*)$ state possesses some $^3(n,\pi^*)$ character[139].

In the lignin macromolecule, substitution effects and the polarity of environment are conducive to the lowest lying α-carbonyl triplet state being predominantly of $^3(\pi,\pi^*)$ character resulting in greatly reduced reactivity towards alcoholic or hydrocarbon hydrogens within the lignocellulosic matrix[142,143,144,145,146]. The rate constant (k') for the decay of the triplet state of 3,4-dimethoxyacetophenone in the presence of the quencher (Q) is related to the rate constant for triplet state decay in the absence of a quencher (k_d), the quenching rate constant k_q and the quencher concentration ([Q]) according to equation 4.9:-

$$k' = k_d + k_q[Q] \qquad (4.9)$$

Thus, a plot of k' as a function of [Q] should be linear with slope equal to k_q and intercept k_d. The triplet state decays were obtained by simultaneously fitting four kinetic traces with a first order function of the form (equation 4.10):-

$$A(t) = A(0)e^{-(k_{exp}t)} + B \qquad (4.10)$$

where A(t) is the change in absorbance (analysing at 365 nm) at time t after the laser pulse and A(0) is the absorbance at zero time following the laser pulse. The term B accounts for a small amount of residual absorption due to the formation of the ketyl radical of 3,4-dimethoxyacetophenone which decays on a timescale at least two orders of magnitude longer than that of the triplet state and can therefore be regarded as a baseline offset on the timescale of the experiment. In the case of phenol, B also has a contribution from absorption by the corresponding phenoxy radical. The results of the data analysis are shown in tables 4.4 and 4.5 and are shown graphically in figures 4.16 and 4.17.

$[phenol]/10^{-5}mol.l.^{-1}$	$k'/10^{5}s.^{-1}$
4.34	2.56
8.67	5.21
13.01	8.15
17.34	11.09
21.68	14.73

Table 4.4:- Experimental Rate Constants (k') as a Function of Phenol Concentration for the Quenching of Triplet 3,4-Dimethoxyacetophenone in Benzene Solution

$[Methoxybenzene]/10^{-2}mol.l.^{-1}$	$k'/10^{5}s.^{-1}$
2.61	0.73
5.23	1.60
7.85	1.96
10.46	2.91
13.08	3.58

Table 4.5:- Experimental Rate Constants (k') as a Function of Methoxybenzene Concentration for the Quenching of Triplet 3,4-Dimethoxyacetophenone in Benzene Solution

The quenching rate constant for 3,4-dimethoxyacetophenone (absorbance at 354.7 nm $\approx$ 0.1) by phenol or methoxybenzene in benzene solution were determined to be 6.3 x 10^9 and 2.6 x 10^6 l.mol.$^{-1}$s.$^{-1}$ respectively. The data demonstrates that the triplet states of 3,4-dimethoxyactophenone is efficiently quenched by phenol even though it has been demonstrated that it is predominantly of a $^3(\pi,\pi^*)$ nature. Quenching by methoxybenzene proceeds at a considerably slower rate than phenol via a mechanism not involving the triplet state of methoxybenzene given that the triplet energy of methoxybenzene (340 kJ.mol.$^{-1}$[134]) relative to the acetophenone derivatives (approximately 300 kJ.mol.$^{-1}$) make efficient triplet-triplet energy transfer an energetically unfavourable process.

The above data demonstrates the efficiency of the quenching mechanism between aromatic α-carbonyl triplet states and phenolic functionalities. Given the considerable spectral overlap of the phenoxy-ketyl radical pair at 365 nm, it was not possible to determine the quantum yield of the free radical pair from these experiments. Estimates of such yields using a substituted phenol with a phenoxy radical whose absorption maxima is sufficiently red shifted to allow detection with only minor interference from the respective ketyl radical (eg. p-cyanophenol, λ_{max} = 443 nm[147]) have shown that the quantum yield of phenoxy-ketyl free radical pairs is of the order of 0.55 when determined for a p-methoxypropiophenone/ p-cyanophenol system in degassed benzene solution[141].

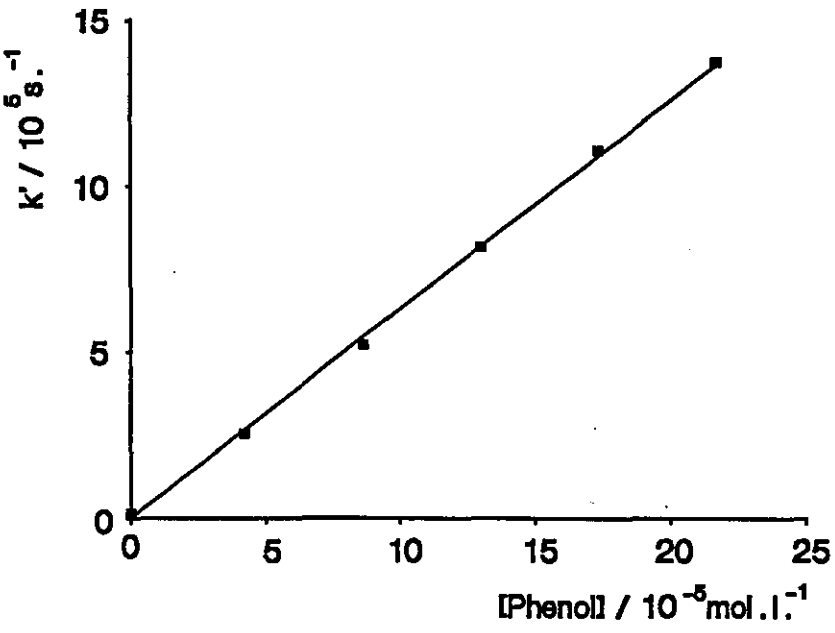

Figure 4.16:- A Plot of Experimental Rate Constant (k') as a Function of Phenol Concentration for the Quenching of Triplet 3,4-Dimethoxyacetophenone in Benzene Solution

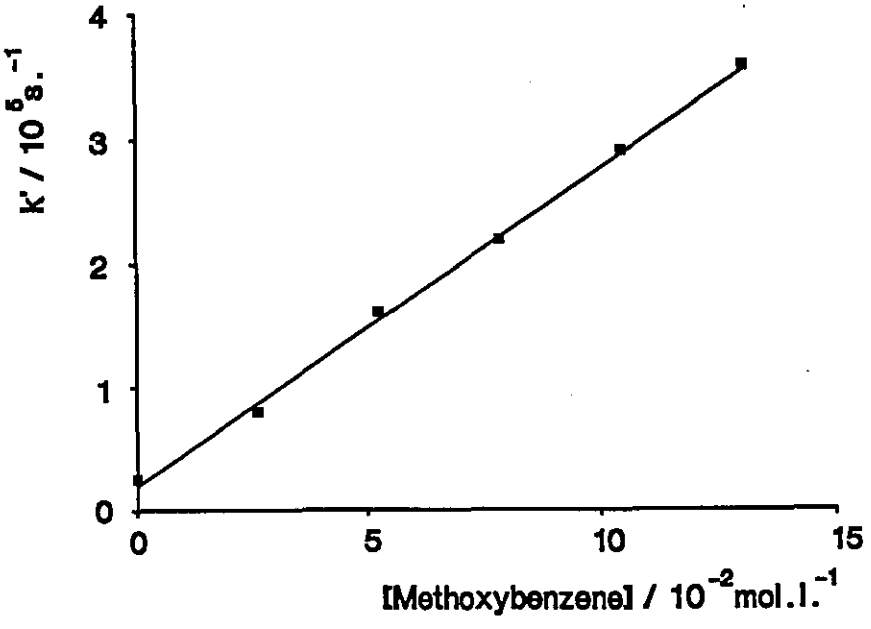

Figure 4.17:- A Plot of Experimental Rate Constant (k') as a Function of Methoxybenzene Concentration for the Quenching of Triplet 3,4-Dimethoxyacetophenone in Benzene Solution

This suggests that the quenching of the triplet state of 3,4-dimethoxyacetophenone by phenol in the above experiments to yield the corresponding phenoxy-ketyl free radical pair may be an efficient process.

4.3 Photochemistry of 3,4-Dimethoxyacetophenone Adsorbed Onto Microcrystalline Cellulose

A series of samples of varying concentration of 3,4-dimethoxyacetophenone adsorbed onto microcrystalline cellulose were prepared according to the method detailed in section 3.5. Shown in figure 4.18 are the ground state diffuse reflectance spectra for these samples together with the ground state diffuse reflectance spectrum of blank cellulose itself. Shown in figure 4.19 are the respective uncorrected (see later) Kubelka-Munk spectra (see equation 3.6) for this series of samples.

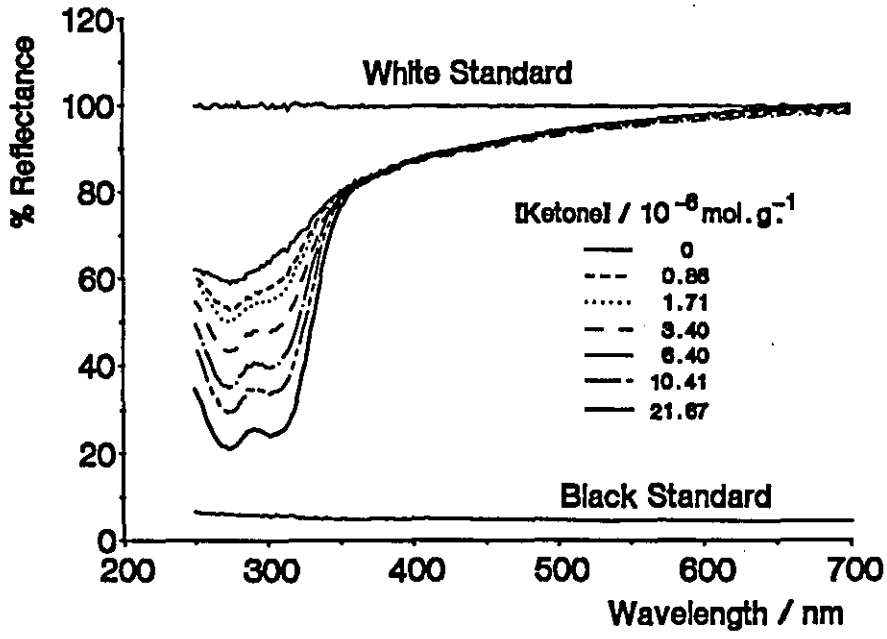

Figure 4.18:- Ground State Diffuse Reflectance Spectra of a Series of Samples of 3,4-Dimethoxyacetophenone Adsorbed onto Microcrystalline Cellulose

From these spectra the following points can be noted:-

(a) The absorption lambda maxima for 3,4-dimethoxyacetophenone adsorbed onto microcrystalline cellulose are located at 274 nm and 307 nm and are located at wavelengths almost identical to those observed in polar solvents (λ_{max} in ethanol are 274 nm and 304 nm respectively[148]).
(b) A similar ratio of molar absorption coefficients ($\epsilon^{274nm}/\epsilon^{307nm}$) for 3,4-dimethoxyacetophenone both in solution and when adsorbed onto microcrystalline cellulose is observed.
(c) At the loadings of 3,4-dimethoxyacetophenone studied, there is little or no ground state absorption at the usual laser excitation wavelength of 354.7 nm. Consequently, following pulse

laser excitation at this wavelength, no easily detectable reflectance changes using diffuse reflectance laser flash photolysis were observed for this series of samples.

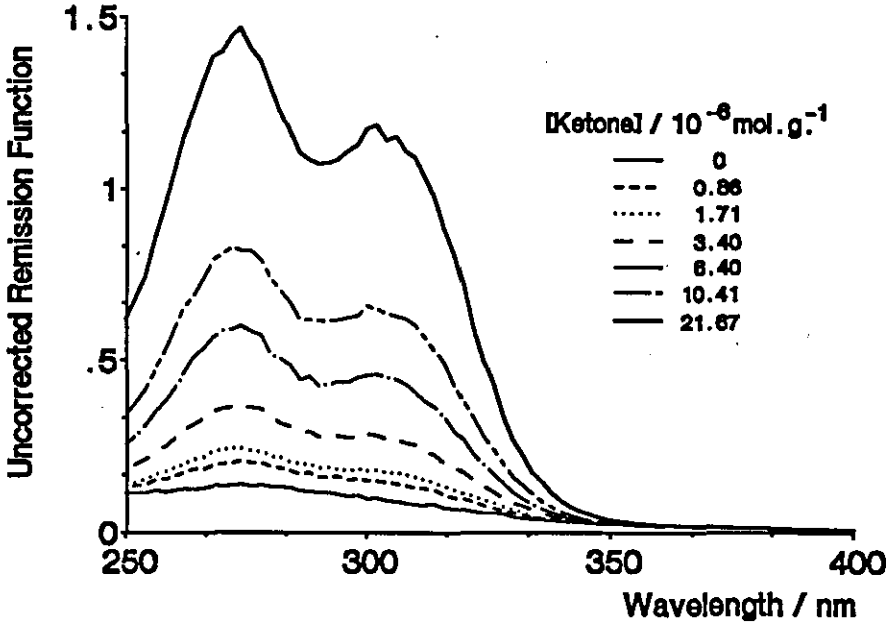

Figure 4.19:- Corresponding Kubelka-Munk Spectra for a Series of Samples of 3,4-Dimethoxyacetophenone Adsorbed onto Microcrystalline Cellulose

As mentioned in section 3.1, all ground state diffuse reflectance spectra were measured relative to a barium sulphate white reflectance standard. The reflectance of the white standard is set to 100 % prior to the recording of sample reflectance spectra. However, when quantitative values for the Kubelka-Munk Remission Function ($F(R_\infty)$) (see section 1.5) are required, such an assignment is not valid given that the absolute reflectance of barium sulphate is less than 100 % at all wavelengths of interest to the physical photochemist. At wavelengths between 400 nm and 800 nm, an absolute percentage reflectance value of 97.5 % as given by Middleton and Sanders[149] is typically used for such quantitative studies (under ideal contaminant free conditions, absolute reflectance measurements of greater than 99 % have been observed for highly purified samples of barium sulphate[150,151]).

The dynamic range of the spectrophotometer is determined by assigning the white standard as having a percentage reflectance value of 100 at all wavelengths of study and then measuring the reflectance of a matt black sample of carbon black. In practice, a reflectance of between 4 % and 7 % for such a sample is observed relative to the barium sulphate standard. Across the whole visible region of the electromagnetic spectrum, a reflectance of 5 % is observed for the carbon black sample (see figure 4.18). What is required therefore, is a reflectance correction method which accounts for the non-ideal behaviour of both the white and black standards in order to obtain quantitative values of $F(R_\infty)$ for the series of samples under study here. Given that for the wavelength region 400 nm to 800 nm, the reflectance of both the white and black

standards do not change relative to each other, the correction procedure is therefore relatively simple and is summarised as follows:-

For a sample of measured percentage reflectance R^{obs}, the reflectance corrected for the white standard (R_W^C) is given by:-

$$R_W^C = R^{obs} x \frac{100}{R_W^{abs}} \tag{4.11}$$

where R_W^{abs} is the absolute percentage reflectance of the barium sulphate at a given wavelength. By a similar argument, the percentage reflectance of the black standard corrected for the white (R_B^C) is given by:-

$$R_B^C = R_B^{obs} x \frac{100}{R_W^{abs}} \tag{4.12}$$

It therefore follows that the percentage reflectance of a sample corrected for both the white and black standards (R_{WB}^C) is given by:-

$$R_{WB}^C = \frac{R_W^C - R_B^C}{\left(1 - \frac{R_B^C}{100}\right)} \tag{4.13}$$

The correction of ground state diffuse reflectance spectra at wavelengths below 400 nm is however complicated by the fact that the absolute reflectance of barium sulphate does not remain constant but gradually falls to a value of ca. 93 % at 250 nm. The absorption maximum located at 274 nm (figure 4.19) observed for the series of samples of 3,4-dimethoxyacetophenone adsorbed onto microcrystalline cellulose was used to test this correction procedure, the results of which are shown in table 4.6 and graphically in figure 4.20. The values for the percentage reflectance of the white reflectance standard at 274 nm was estimated to be 93.0 %. The measured reflectance of the black standard at this wavelength was observed to be ca. 6.2 %, the corrected reflectance data detailed in table 4.6 being based upon these values.

As can be seen in figure 4.20, the application of the correction technique detailed in equations 4.11 to 4.13 produces a linear behaviour between ketone concentration and $F(R_\infty)$ and serves to emphasise the necessity to correct reflectance spectra for the non-ideal behaviour of reflectance standards. As we will see later in this section, the intensity of laser induced reflectance changes as a function of ketone loading (figure 4.22) are therefore less likely to be explained simply by errors in the determination of ketone concentration on the surface of the cellulose. Also, the fact that a linear behaviour is observed is indicative of the fact that the highest loading of ketone has not produced a surface coverage of a full monolayer[152].

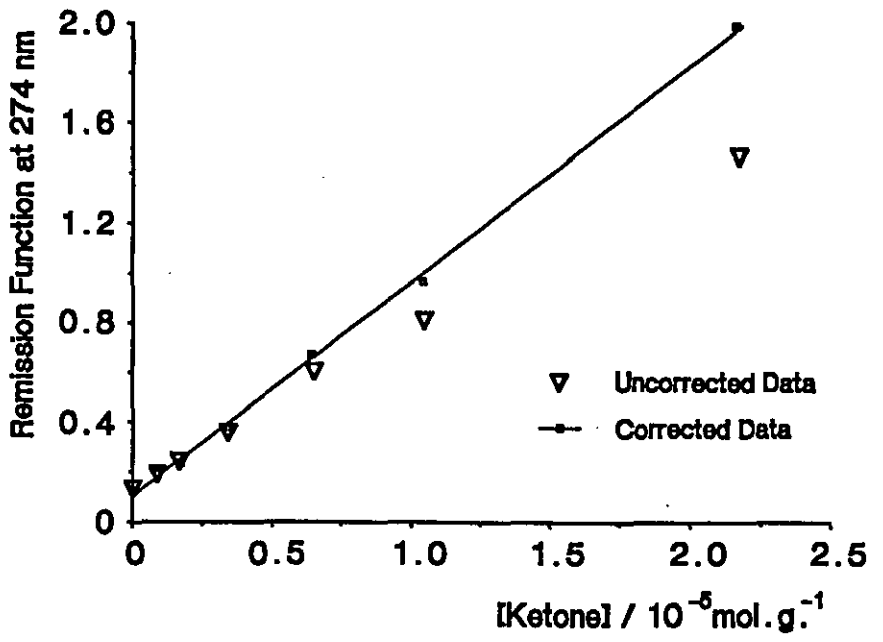

Figure 4.20:- Plots of Corrected and Uncorrected Kubelka-Munk Remission Function ($F(R_\infty)$) Values (measured at 274 nm) as a Function of the Concentration of 3,4-Dimethoxyacetophenone Adsorbed onto Microcrystalline Cellulose

[Ketone] / 10^{-6} mol.g.$^{-1}$	$R^{274\ nm}$	$F(R_\infty)^{UC}$	R_W^C	R_{WB}^C	$F(R_\infty)^C$
0	59.05	0.142	63.49	60.88	0.126
0.86	53.02	0.208	57.01	53.94	0.197
1.71	50.34	0.245	54.13	50.85	0.238
3.40	43.40	0.369	46.67	42.86	0.381
6.40	35.09	0.600	37.73	33.28	0.669
10.41	29.89	0.822	32.14	27.29	0.969
21.67	21.17	1.468	22.76	17.69	1.986

Table 4.6:- Data Relating to the Correction of the Values of the Kubelka-Munk Remission Function ($F(R_\infty)$) at 274 nm for a Series of Samples of 3,4-Dimethoxyacetophenone Adsorbed onto Microcrystalline Cellulose

$R^{274\ nm}$ = Observed Reflectance at 274 nm
$F(R_\infty)^{UC}$ = Uncorrected Kubelka-Munk Remission Value
R_W^C = Reflectance Value Corrected for the White Reflectance Standard
R_{WB}^C = Reflectance Value Corrected for the White and Black Reflectance Standards
$F(R_\infty)^C$ = Corrected Kubelka-Munk Remission Value

As had been mentioned, the lower molar absorption coefficient of 3,4-dimethoxyacetophenone at the laser excitation wavelength typically used in these studies did not yield a transient absorption which could easily be studied by diffuse reflectance laser flash photolysis. It was therefore necessary to make use of the fourth harmonic of the Nd:YAG laser (266 nm) as an excitation source. Diffuse reflectance laser flash photolysis using 266 nm laser excitation has scarcely been reported in the literature. Wilkinson *et al* obtained the transient difference spectrum for a series of ketones adsorbed onto the hydrophobic zeolite silicalite[153]. However, no reference can be found reporting the direct excitation of adsorbed molecules on a microcrystalline cellulose support material using 266 nm laser excitation. The transient difference spectrum observed following 266 nm (ca. 9 mJ.cm.$^{-2}$) pulse laser excitation of 3,4-dimethoxyacetophenone (1.04 x 10^{-5} mol.g.$^{-1}$) adsorbed onto microcrystalline cellulose is shown in figure 4.21 together with the transient difference spectrum of blank cellulose sample recorded under identical conditions.

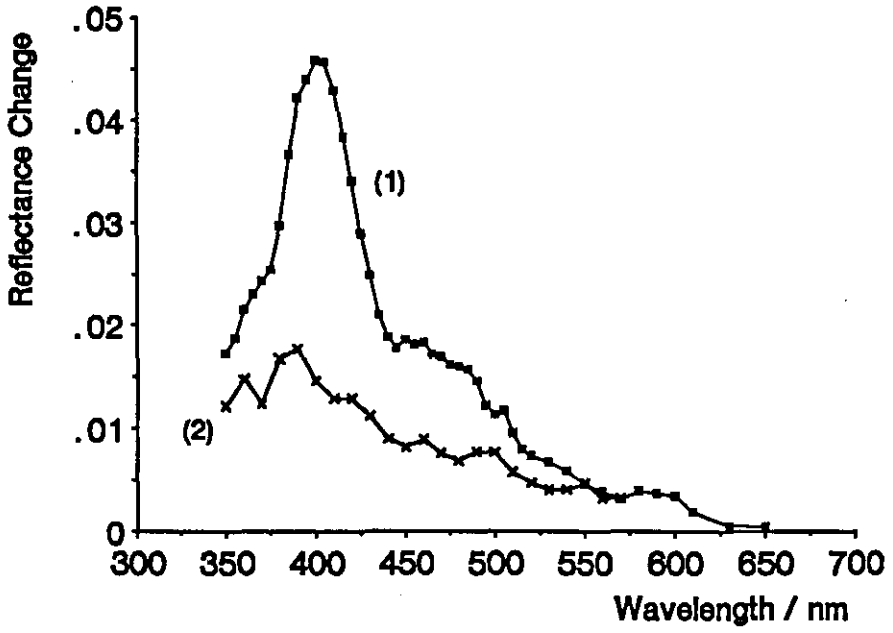

Figure 4.21:- Transient Difference Spectrum of 3,4-Dimethoxyacetophenone (1.04 x 10^{-5} mol.g.$^{-1}$) Adsorbed onto Microcrystalline Cellulose and the Transient Difference Spectrum for a Blank Cellulose Sample Recorded Under Identical Conditions
Spectra Were Obtained at a Time Delay of 3 μs After the Laser Pulse

As can be seen, the transient absorption λ_{max} for the ketone sample is located at 400 nm and is assigned as the triplet-triplet absorption spectrum of 3,4-dimethoxyacetophenone on the grounds of its similarity to the triplet-triplet absorption spectrum of this compound found in solution[120]. The transient observed for blank cellulose shows a broad structureless absorption with no easily identifiable absorption λ_{max}. Assign. ment of the transient species responsible for this absorption is difficult but possibly may be attributed to one (or both) of the following species:-

(a) Microcrystalline cellulose, during its formation may result in the formation of residual carbonyl moieties which, following laser excitation form excited states (or excited state photo-products) which absorb in the visible region of the spectrum[154].
(b) Direct photolysis at 266 nm leads to the formation of free radical species via cleavage of the oxygen bridge between two linked monomer units[155].

For a sample of 3,4-dimethoxyacetophenone adsorbed onto cellulose, the percentage of the total laser excitation pulse absorbed by the cellulose support material itself can be calculated according to equation 4.14:-

$$\%Absorbed = \frac{F(R_\infty)^{cel}}{F(R_\infty)^{tot}} x\,(1 - R_\infty)^{tot} \qquad (4.14)$$

where $F(R_\infty)^{cel}$ and $F(R_\infty)^{tot}$ are the Kubelka-Munk Remission values (calculated according to equation 3.6) for the blank cellulose and the cellulose/ketone samples respectively and $(1 - R_\infty)^{tot}$ is the total percentage of light absorbed by the sample at the laser excitation wavelength (266 nm). It is therefore calculated that for sample whose transient difference spectrum is shown in figure 4.21, the cellulose itself is only absorbing approximately 7.5 % of the laser pulse directly whereas for the blank cellulose sample (see figure 4.19), approximately 38 % of the laser pulse is directly absorbed. It can therefore be concluded that the transient difference spectrum shown in figure 4.21 for 3,4-dimethoxyacetophenone adsorbed onto microcrystalline cellulose is due almost entirely to the excited state of the ketone itself with very little interference from the directly photogenerated cellulose transient species.

The λ_{max} of the triplet-triplet absorption spectrum is independent of time following the laser pulse and is located at 400 nm, red shifted relative to its position in polar solvents (section 4.3.1). Given that the ground state diffusion reflectance spectra demonstrated absorption λ_{max} almost identical to those observed in polar solvents, it can be concluded that the cellulose surfaces has further lowered the transition energy between T_1 and T_N relative to non-polar and polar solvents. It has not been established whether T_1 or T_N has been affected most.

The transient decays via complex kinetics which reflect the heterogeneity of the adsorption sites on the surface of the cellulose. The first empirical half-life of transient signal is approximately 2 ms. Subsequent second and third empirical half-lives of 15 ms and 32 ms are observed. Even though the samples were not deoxygenated prior to the experiment, it is observed that the lifetime of the triplet state is greatly extended (by approximately a factor of 100) when adsorbed onto microcrystalline cellulose. This is the direct result of the ability of cellulose through its rigidity and large capacity for hydrogen bonding to protect excited states of molecules from quenchers such as molecular oxygen[156]. This property is further enhanced when the cellulose support material has been thoroughly dried (as is the case here) prior to use[157,158]. The intensity of the transient signal, extrapolated to zero time following the laser pulse (obtained by using a fast

digitiser time per point sweep and reading directly of the signal intensity), as a function of ketone loading is shown in figure 4.22:-

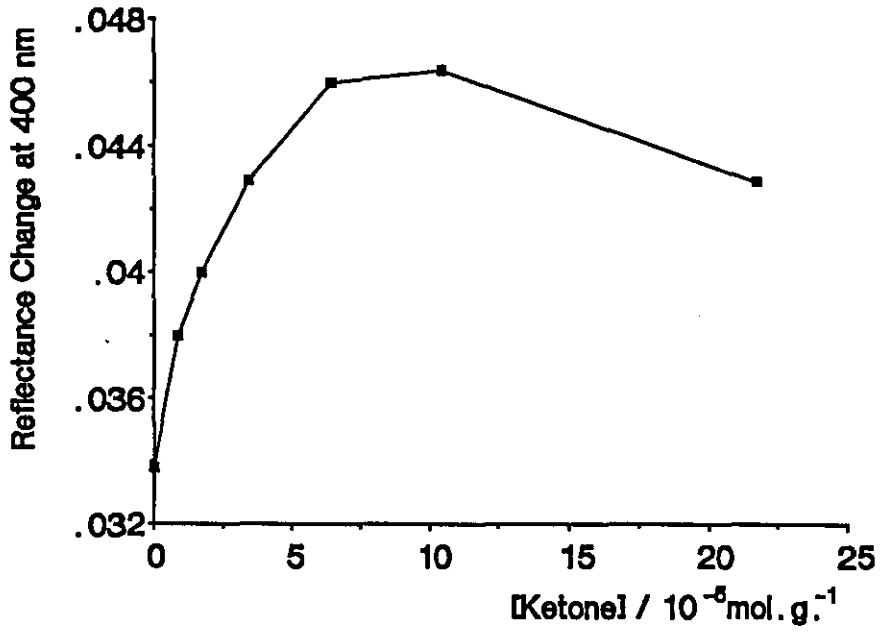

Figure 4.22:- Transient Signal Intensity as a Function of 3,4-Dimethoxyacetophenone Concentration Adsorbed onto Microcrystalline Cellulose

As can be seen, the relationship is non-linear and is accounted for by a triplet-triplet annihilation deactivation pathway for the ketone triplet at higher surface loadings. The observed kinetics of decay for this series of samples does not change with ketone loading and therefore it is concluded that the process is one primarily of a static nature where two excited triplets annihilate instantaneously on the timescales of these experiments (equations 4.15 to 4.17).

$$^3K^* + {}^3K^* \rightarrow {}^1K^* + {}^1K \qquad (4.15)$$

$$^1K^* \overset{ISC}{\rightarrow} {}^3K^* \qquad (4.16)$$

$$^3K^* \overset{k_d}{\rightarrow} {}^1K \qquad (4.17)$$

The resultant singlet excited state (equation 4.15) intersystem crosses for a second time to yield a triplet state detected in our experiments. Such a curvature as seen in figure 4.22 has been observed for other organic substrates adsorbed onto solid support materials[159]. It is interesting to note that curvature occurs at ketone surface coverages of approximately 5 % of a monolayer

for a concentration of 5 x 10^{-6} moles of ketone per gram of support material suggesting that adsorption on the cellulose surface is not homogeneous; some highly preferred sites on the surface being occupied by an aggregation of a few ketone molecules in intimate proximity to each other[160] thus promoting static triplet-triplet annihilation deactivation pathways at higher surface coverages.

Re-recording of the ground state diffuse reflectance spectra for samples of 3,4-dimethoxyactophenone adsorbed onto microcrystalline cellulose which had been exposed to many (approximately 400 pulses at ca. 9 mJ.cm.$^{-2}$ per pulse) laser pulses demonstrated that these samples had not degraded significantly, an observation consistent with the low reactivity of ($^3(\pi,\pi^*)$) states towards aliphatic alcoholic O-H bonds (see section 5.4.3)[161]. It may be concluded therefore that adsorption onto a cellulose support material has the effect of extending the triplet lifetime of 3,4-dimethoxyacetophenone but does not initiate photodegradation via a hydrogen atom abstraction from alcoholic or hydroxyl moieties abundant in the support matrix. It is therefore suggested that photoyellowing of TMP itself via this particular reaction pathway does not significantly contribute to the overall yellowing process.

4.4 Conclusions

Some fundamental photochemical parameters for simple lignin model compounds have been determined in a variety of solvent systems and when adsorbed onto a microcrystalline cellulose support material. It has been shown that methoxyl substitution upon the aromatic ring of acetophenone type model compounds has a marked effect upon the λ_{max} of the triplet-triplet absorption spectrum of such compounds and also upon the lifetime of the triplet excited state. The lowest lying triplet state for 3,4-dimethoxyacetophenone has been shown to be of a predominantly $^3(\pi,\pi^*)$ character in all solvents/environments which can account for its apparent lack of reactivity in solution and when adsorbed onto microcrystalline cellulose.

A quenching rate constant of 6.3 x 10^9 l.mol.$^{-1}$s.$^{-1}$ was observed for the quenching of triplet 3,4-dimethoxyactophenone by phenol demonstrating the high susceptibility towards phenolic hydroxyl moieties of $^3(\pi,\pi^*)$ states. This observation may be accounted for by the mixing of the almost iso-energetic $^3(n,\pi^*)$ states.

Pulsed laser excitation of 3,4-dimethoxyactophenone adsorbed onto microcrystalline cellulose yielded a transient assigned as the triplet state of the compound which had an absorption maximum at 400 nm. The transient decayed via complex kinetics reflecting the heterogeneity of adsorption sites on the cellulose surface.

The main implications of these studies to the photochemistry of milled wood lignin (MWL) and thermomechanical pulp (TMP) outlined in chapters 5 and 6 are:-

(a) Substitution patterns on aromatic rings of α-carbonyl moieties has the effect of producing triplet states with predominantly $^3(\pi,\pi^*)$ character.
(b) Such triplet states show extended lifetimes relative to $^3(n,\pi^*)$ in fluid solution.
(c) Triplet-triplet absorption maxima are bathochromically shifted in polar environments.
(d) Reactivity of $^3(\pi,\pi^*)$ states is greatly reduced towards alcoholic hydrogen atoms present in the cellulose fraction of TMP fibres. However, quenching rate constants for α-carbonyl $^3(\pi,\pi^*)$ states by phenolic hydroxyl hydrogens present in the lignin fraction of the TMP fibre are equal to or slightly greater than those observed for the corresponding $^3(n,\pi^*)$ states.

(e) Certain substitution patterns such as α-carbonyl β-O-4 lignin model dimers are able to undergo homolytic cleavage reactions from both the singlet and triplet manifolds to generate a free radical pair which may react further to produce yellow photoproducts.

In chapter 5, an intermediate photochemical system between lignin model compounds and TMP itself is studied in the form of milled wood lignin (soluble lignin) in both fluid solution and when adsorbed onto microcrystalline cellulose.

Chapter 5

Photochemistry of Milled Wood Lignin

5 Photochemistry of Milled Wood Lignin

5.1 Introduction

The extraction and chemical characterisation of lignin separated from the polysaccharide components which make up wood fibres has been extensively studied in a desire to quantify its chemical composition and understand its complex chemical and photochemical reactions. The lignin macromolecule can be described in terms of being a three dimensional "heterogeneous" polymer intimately cross-linked to the cellulose and hemi-cellulose components of the wood fibre. Because of this, and the fact that it is such a large molecule (molecular weights range between 2000 and 10^6 for lignin isolated from the other wood components[162]), any attempt to extract lignin in a non - chemically-modified form is, in practice, an impossibility.

Many methods of obtaining lignin in a form free from polysaccharides have been developed over the years. The methods of extraction fall into two main categories:-

(a) Insoluble lignins are obtained by treating the wood fibres with strong mineral acids such as 72 % sulphuric acid (to yield Klason lignin) or fuming hydrochloric acid (to yield Willstatter lignin). These acids have the effect of dissolving the polysaccharide components of the wood material and leaving the lignin fraction as an insoluble residue. Treatments such as 72 % sulphuric acid and fuming hydrochloric acid to yield Klason lignin[163] and Willstatter lignin[164] respectively come into this category. Such lignin preparations however tend to undergo extensive condensation reactions during their extraction and therefore are not representative of the lignin macromolecule in its native form.

(b) Soluble lignins are obtained by dissolving the lignin fraction of the wood fibre out of the carbohydrate matrix with the use of appropriate organic solvents. This method has the advantage over insoluble lignin isolation in that it suffers much less chemical modification upon extraction. As seen in section 3.4, the milled wood lignin (or Bjorkmann lignin) used in these studies was extracted by essentially a two stage process. Breaking of chemical bonds (lignin/lignin, lignin/carbohydrate and carbohydrate/carbohydrate) was achieved by mechanical means in a ball mill. This is followed by mild solvent extraction (with acetone or acetone/water mixtures) and further purification processes, details of which can be found in section 3.4. Finally, the purified MWL is bleached with 4 % v/v hydrogen peroxide at approximately 60°C for 2 hours. The resulting material is almost free from carbohydrate (< 0.05 %) and is free from ash.

It must be emphasised that there is always a trade-off between yield of lignin extracted and the degree of chemical modification which has occurred. The yield of MWL in this case is approximately 50 % but, more importantly for this research, it has undergone little chemical modification during the extraction and purification processes. MWL is regarded as being the most representative lignin preparation relative to the lignin found naturally in wood fibres[165].

5.2 Ground State Absorption Spectrum of Milled Wood Lignin

Milled wood lignin is soluble in some organic solvents such as 1,4-dioxane and N,N-dimethylformamide. It is also possible to maintain MWL in solution in a cosolvent of methanol/1,4-dioxane (90/10 v/v) provided that the lignin is first dissolved in the 1,4-dioxane and the methanol added after dissolution.

The ground state absorption spectrum of MWL (180 g.l.$^{-1}$) in 1,4-dioxane is shown in figure 5.1.

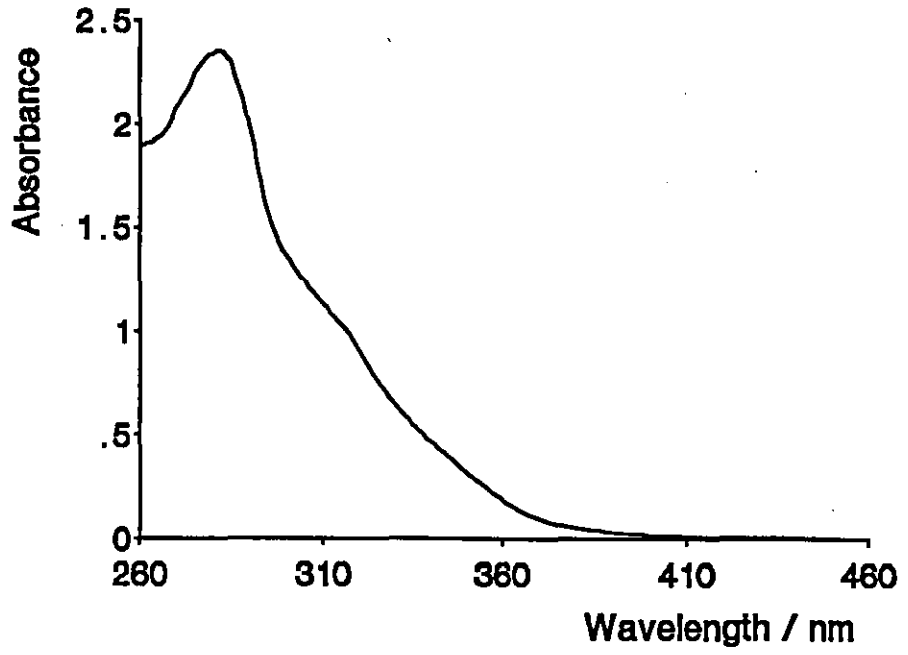

Figure 5.1:- Ground State Absorption Spectrum of MWL (180 g.l.$^{-1}$) in 1,4-Dioxane

The λ_{max} located at 278 nm is in a typical position for softwood MWL in 1,4-dioxane solution[166]. Strong absorption below 250 nm is observed for MWL, another absorption peak being observed at ca. 205 nm[167] not shown here due to strong absorption by the solvent at this wavelength. The absorption extends beyond 400 nm which, for concentrated solutions of MWL in 1,4-dioxane, gives the solution a slightly yellow appearance. By comparison with appropriate lignin model compounds, assignment of absorption bands to specific chromophores present in lignin have been documented in the literature[168]. The phenylpropane C_9 precursor to the lignin macromolecule in softwood species was first shown by Klason[51] to be predominantly the guaiacyl moiety trans-coniferyl alcohol (4-hydroxy-3-methoxycinnamyl alcohol) (see section 2.3). Proceeding along this line, Aulin-Erdtman and Sanden[168] studied the ground state absorption spectra of this type of phenylpropane unit and assigned the absorption bands below 300 nm in lignin as being due to such guaiacylpropane moieties.

The difference absorption spectrum ($\Delta\epsilon_i$) of lignin obtained by measuring the absorption spectrum under alkali and neutral conditions and subtracting one from the other has been used

in the past as a method of estimating the phenolic hydroxyl content of lignin[169]. Taking this procedure a stage further, Alder and Marton obtained difference absorption spectra ($\Delta\epsilon_r$) for lignin samples which had been ionised and reduced by treating the sample with alkaline sodium borohydride[170]. From the $\Delta\epsilon_r$ spectrum they assigned four different types of conjugated carbonyl groups present in lignin by their rate of reduction and their λ_{max} in the $\Delta\epsilon_r$ spectrum. These are summarised in table 5.1, a full description of the formation, structure and nomenclature of the lignin macromolecule is presented in section 2.3.

Carbonyl Type	Structure	λ_{max}/nm	Reduction Half-Life
(1)	*G-CH=CH-CHO*	418	Fast (20 min.)
(2)	*R-O-4-G-CH=CH-CHO*	ca. 300	Very Fast (1 min.)
(3)	*G-CO-R*	345-355	Slow (2-24 hours)
(4)	*R-O-4-G-CO-R*	303-314	Fast (2-28 mins.)
(4)	*G-CH_2-CO-R*	ca. 312	Fast (1-8 mins.)
(4)	*R-O-4-G-CH_2-CO-R*	290	Fast (2.5 mins.)

Table 5.1:- $\Delta\epsilon_r$ and Rates of Reduction of Conjugated Carbonyl Moieties Found in Unbleached Milled Wood Lignin (according to Alder and Marton[170])

G = guaiacyl unit

R = linkage to another phenylpropane unit in the lignin structure

R-O-4 = linkage to another phenylpropane unit through the oxygen in the 4 position of the guaiacyl ring

From this data, and the $\Delta\epsilon_i$ data, it was concluded that lignin absorption at wavelengths greater than 300 nm is in part due to conjugated carbonyl moieties in the propane side chain of the guaiacylpropane units of the lignin macromolecule together with other side chain groups including conjugated carbon-carbon double bonds, biphenyls[171] and stilbene type moieties[172]. These chromophoric assignments were based upon MWL preparations which had **not** been bleached with alkaline hydrogen peroxide as is the case for the sample under study here. Following such treatment, removal of the coniferaldehyde end groups is achieved with unit efficiency[72,74,173] leaving the α-carbonyl type moieties (structure 3 in table 5.1) as the primary photochemical absorber at the laser excitation wavelength of 354.7 nm.

5.3 Steady State Emission

The steady state emission spectra of milled wood lignin in 1,4-dioxane solution at three excitation wavelengths are shown in figure 5.2. In each case the absorbance at the excitation wavelength (due solely to the MWL- see figure 5.1) was approximately 0.05 to minimise self absorption effects. As can be seen, excitation into different parts of the absorption tail produces different emission lambda maxima and can be attributed to the fact that more than one absorbing

chromophore is present in the MWL sample; excitation at 300 nm, 350 nm and 400 nm producing emission maxima at 363 nm, 410 nm and 482 nm respectively. It is interesting to note that, even at wavelengths greater than 400 nm, easily detectable fluorescence spectra can be obtained. The nature of the chromophore responsible for such emission is, as yet, unknown although studies into the fluorescent nature of appropriate lignin model compounds have been documented in the literature[174,175].

From a practical standpoint, the detection of absorbing transient species in the 400 nm to 500 nm region of the spectrum following pulsed laser excitation of MWL in 1,4-dioxane solution (see section 5.4.1) are made more difficult as a result of this prompt emission due to it having the effect of overloading the photomultiplier detector at short timescales (0 to ca. 100 ns) following the laser pulse. Consequently, all transient measurements were made using a pulsed arc lamp analysing source (see section 3.6.1 for details) and, given that emission is non-directional, an iris was placed on the detector side of the sample cell which allowed the collimated analysing light source to enter the detector, at the same time removing a large proportion of this prompt emission.

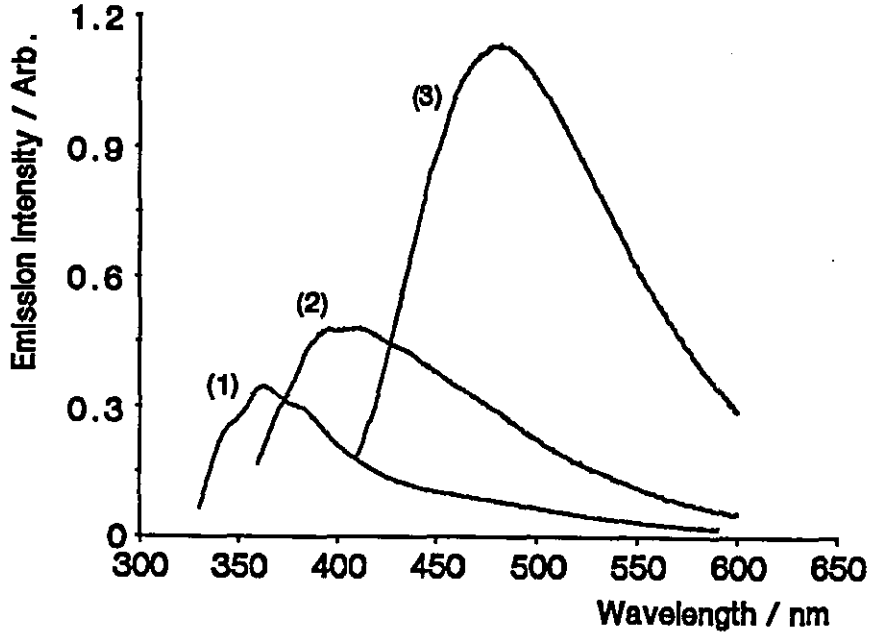

Figure 5.2:- Steady-State Emission Spectra for MWL in 1,4-Dioxane Solution Exciting at a Variety of Wavelengths
Excitation Wavelengths are (1) 300 nm; (2) 350 nm and (3) 400 nm

A similar prompt emission signal is observed from handsheets of bleached thermomechanical pulp, details of which can be found in section 6.2 of this thesis.

5.4 Transmission Laser Flash Photolysis Studies of Milled Wood Lignin

5.4.1 Summary of Previous Work

Attempts to understand the processes leading to the photoyellowing of high yield thermomechanical pulps and other wood products which contain high percentages of lignin have been complicated by the fact that the system under study is a natural material making full quantification of its chemical and photochemical behaviour in its native form extremely difficult. Photochemists and wood scientists have directed many of their research efforts towards studying appropriate lignin model compounds in fluid solution and then extrapolating these results to the behaviour of lignin in its natural form. This approach has its merits and much useful information has been obtained from such studies. However, the study of lignin itself is essential in order to fully understand the processes involved in the photoyellowing of lignin rich thermomechanical pulps. A useful intermediate between model compounds in solution (and adsorbed onto cellulose fibres) and lignin contained within wood fibres has been the study of MWL in fluid solution.

Lin and Kringstad studied the effects of steady state irradiation upon the lignin macromolecule in fluid solution. A variety of analytical methods were utilised including UV/visible spectroscopy[84], gas-liquid chromatography[176] and electron spin resonance (ESR)[177]. From these studies, the importance of ground state molecular oxygen upon the photoyellowing mechanisms was established. Under deoxygenated conditions, structural changes were observed in the lignin sample without the formation of yellow photoproducts. However, if the sample was then exposed to oxygen and irradiated further, yellowing to the same extent as from a sample exposed to oxygen without the degassing phase was observed. Comparison of the changes in the absorption spectra ($\Delta\epsilon$) observed before and after irradiation for MWL and lignin model compounds demonstrated that α-carbonyl moieties and carbon-carbon double bonds conjugated to an aromatic ring structure were the principle photoinitiators in the yellowing processes[114]. By fully reducing samples of MWL with sodium borohydride and then hydrogenating over a palladium catalyst, photoyellowing was prevented. In a separate experiment, it was shown that methoxylation of MWL (ie. removal of all phenolic hydroxyl groups present in the lignin) greatly reduced the rate of the photoyellowing process[115].

These experiments established the link between α-carbonyl moieties, carbon-carbon double bonds, phenolic hydroxyl groups and dissolved oxygen in the photoyellowing of MWL in solution. However, in the restricted environment of the pulp matrix, the relative efficiencies of the degradation pathways leading to photoyellowing may indeed be different to those in solution. For example, a residual ESR signal is observed from MWL in the solid phase attributed to the presence of a population of stable organic free radical species within the lignin structure which immediately disappear upon dissolution of the MWL in an organic solvent[178].

Theories proposed to explain the degradation of MWL in solution involving the excited state photochemistry of α-carbonyl moieties abstracting hydrogen atoms from phenolic hydroxyl moieties also present in the lignin molecule have been proposed by many authors[82,179,116] as the initial stage in the photoyellowing process and are now generally

accepted. However, no reference can be found in the literature identifying the transient absorption spectrum due to the triplet-triplet absorption of such α-carbonyls present in lignin. Neumann and co-workers studied the photochemistry of low molecular weight (M_r < 1000) lignin, extracted from rice husks, in 1,4-dioxane/water (50/50 v/v) solutions[180,181]. The excitation source was a 30 μs flashlamp, the time resolution of the apparatus being approximately 50 μs. A transient absorption with absorption maxima at 410 nm, 460 nm and 490 nm was observed. Similarities between this transient absorption and the transient absorption spectra obtained by flash excitation of suitable model compounds such as vanillin (4-hydroxy-3-methoxybenzaldehyde) and 4-hydroxybenzaldehyde led to the assignment of the transient absorption obtained from the lignin sample as being due to the phenoxy-ketyl free radical pair generated by hydrogen abstraction of phenolic hydroxyl hydrogen atoms by the triplet state of the α-carbonyls present in lignin. The intensity of the radical signal was decreased upon addition of oxygen, the oxygen providing a competing deactivation pathway for the carbonyl triplets via an energy transfer mechanism. The addition of ascorbic acid (a well known radical scavenger[182]) also decreased the transient signal intensity. However, the authors found no evidence for the formation of singlet molecular oxygen ($^1\Delta_g(O_2)$) via a triplet carbonyl energy transfer quenching mechanism[103].

5.4.2 Transient Difference Spectrum of Black Spruce Milled Wood Lignin

As was observed in section 5.4.1, MWL in solution is susceptible to photodegradation in the presence and absence of dissolved oxygen in the solvent. Thus, to avoid problems associated with degradation product build-up, the sample was changed between collection of each data point in the transient difference spectrum.

The intensity of the transient signal observed from MWL following laser excitation at 354.7 nm is extremely small and thus a high laser energy was required in order to detect the transient. The energy density used was approximately 15 mJ.cm.$^{-2}$.

The transient difference spectrum (ΔA^T) for MWL in 1,4-dioxane solution (absorbance = 0.75 at the laser excitation wavelength, approximate concentration = 330 mg.l.$^{-1}$) is shown in figure 5.3 at two time delays following the laser pulse.

The time resolved transient difference spectrum at short time delays (ca. 200 ns) following the laser pulse (trace 1, figure 5.3) shows two absorption maxima at 395 nm and 425 nm, an isobestic at approximately 370 nm, and ground state depletion which peaks at approximately 340 nm. The transient different spectrum recorded at long time delays after the laser pulse (ca. 2.3 μs) has a λ_{max} at approximately 385 nm, the absorption band at 425 nm having fully decayed on this timescale. This suggests that the transient different spectrum recorded at short time delays after the laser pulse in the 380 to 600 nm region of the spectrum comprises of at least two transient species, each decaying with a different rate constant. The shift in λ_{max} for the peak initially at 395 nm to 385 nm at delays after the fast transient has fully decayed is attributed to the short lived transient species absorbing more at 395 nm than at 385 nm, the superimposition of the transient absorption for both species giving the red shifted λ_{max} at 395 nm at short time delays after the laser pulse.

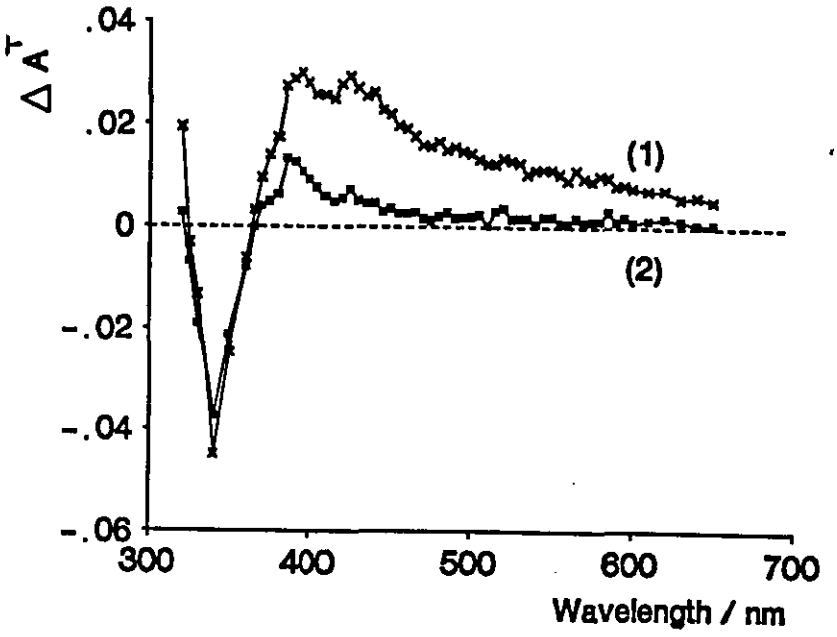

Figure 5.3:- Time Resolved Transient Difference Spectrum (ΔA^T) for MWL in 1,4-Dioxane Solution Under Aerated Conditions Recorded 200 ns (trace 1) and 2.3 μs (trace 2) After the Laser Pulse

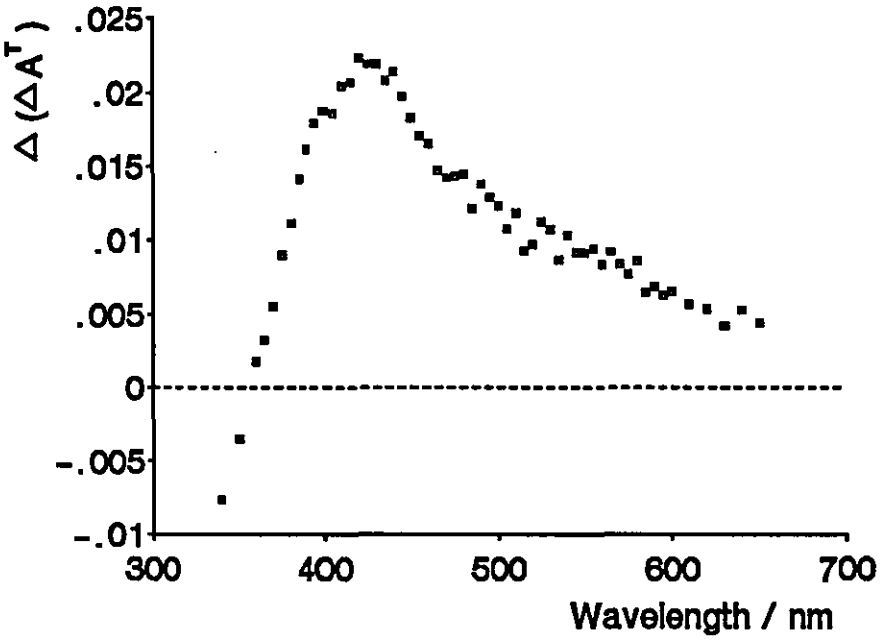

Figure 5.4:- Time Resolved Transient Difference Spectrum ($\Delta(\Delta A^T)$) for the Fast Transient Component of MWL in Aerated 1,4-Dioxane Solution

The transient decay trace recorded at 425 nm can be fitted to a biexponential decay model yielding rate constants for the decay of the two transient species of 2.85×10^6 s.$^{-1}$ and 4.71×10^5 s.$^{-1}$ for the fast and slow components respectively. As has been stated above, the transient difference spectrum for the slower component was recorded 2.3 μs after the laser pulse. This is approximately 6.5 times the lifetime of the fast transient and therefore is solely due to the time resolved difference spectrum of the slower component. From these two spectra, it is possible to deconvolute the transient absorption due to the fast component from that of the slow component by simply subtracting off the absorption due to the slow component. On the timescale of the experiment, the slow component of the transient decay can simply be regarded as a baseline offset to the absorption spectrum of the fast component. The result of this subtraction is shown in figure 5.4.

The transient difference spectrum for the fast component only shows a λ_{max} at ca. 425 nm and a broad structureless absorption which extends to wavelengths greater than 600 nm. It is interesting to note that the observed absorption band has a similar (but not identical) λ_{max} and spectral shape to the transient absorption observed from flash photolysis of thermomechanical pulp studied in diffuse reflectance mode (see section 6.3 later).

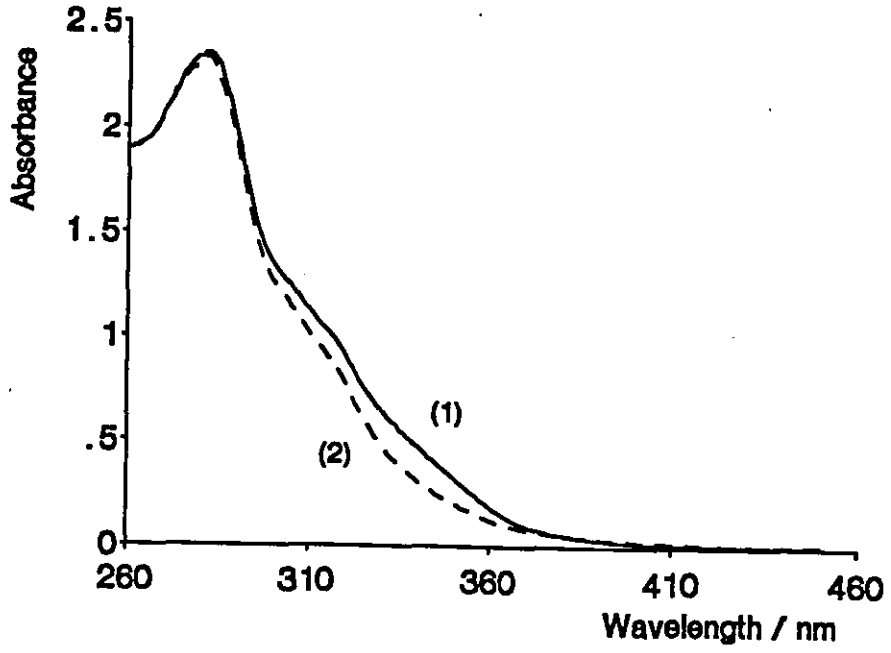

Figure 5.5:- Ground State Absorption Spectrum Of MWL in Aerated 1,4-Dioxane Solution Before (trace 1) and After (trace 2) Exposure to Approximately 300 Laser Pulses (ca. 15 mJ.cm.$^{-2}$ per pulse)

At wavelengths below 370 nm, the kinetics of the transient decay are different to those observed at longer wavelengths, only a small decay due to the fast component being observed. Following its decay, no change in absorption with time is observed suggesting that the absorption change induced by the laser at these wavelengths may be permanent and due to photodegradation of the lignin macromolecule in solution. Further evidence supporting this postulate is found from examination of the ground state absorption spectrum of a MWL sample before and after exposure to the laser as shown in figure 5.5.

The MWL sample was exposed to approximately 300 laser shots (with shaking every 10 shots) to obtain a change in the ground state absorption spectrum easily detectable on the spectrophotometer. By subtracting the ground state absorption spectrum of the MWL sample before exposure to the laser from the absorption spectrum after exposure to the laser, it is possible to produce a difference absorption spectrum due to permanent changes in the lignin sample (ΔA^P). This is shown in figure 5.6 and is similar to the ones obtained by other authors[84].

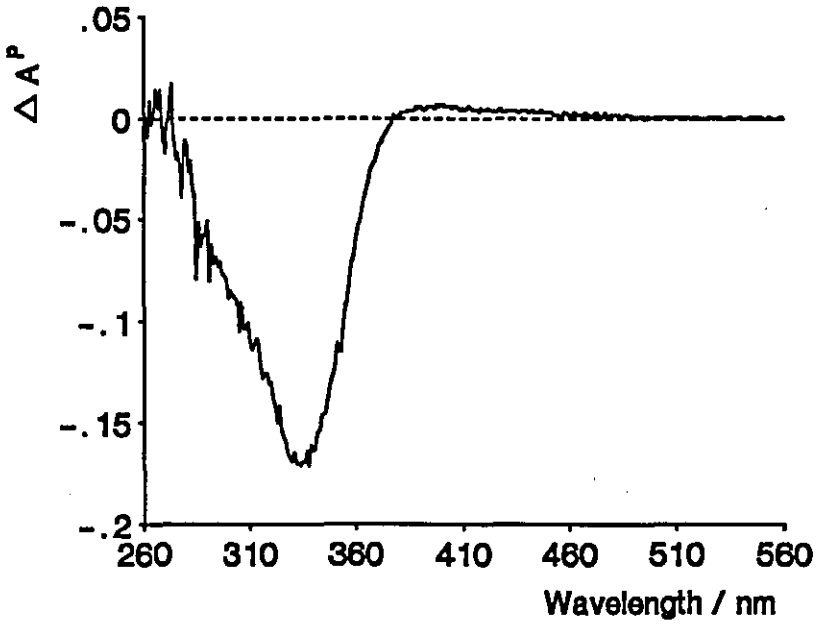

Figure 5.6:- ΔA^P Spectrum for a Sample of MWL in Aerated 1,4-Dioxane Solution Which had Been Exposed to Approximately 300 Laser Pulses (laser energy density = 15 mJ.cm.$^{-2}$ per pulse)

A maximum change in ground state absorbance is observed at approximately 340 nm and a small residual absorption at wavelengths greater than 400 nm due to lignin photoyellowing is also observed. The wavelength of maximum change in ground state absorbance is almost identical to the maximum change in absorbance (ΔA^T) observed in the single shot flash photolysis experiments suggesting that the two observations are indeed linked. However, inspection of the width of the depletion band observed in the time resolved experiments

shows that at wavelengths less than 340 nm the transient difference spectrum does not follow the change in absorbance measured by the spectrophotometer. This can be rationalised if the transient observed on slow timescales (trace 2 in figure 5.3) has more than one absorption band below 395 nm, the observed transient signal in this region of the spectrum being the difference between the change in the molar absorption coefficient of the ground state due to degradation and the molar absorption coefficient of the photoinduced transient species.

5.4.3 Time Resolved Transient Absorption Spectra Of Phenoxy Radicals in Benzene Solution

A relatively clean and simple method of obtaining the transient absorption spectra of phenoxy and other free radical species in solution has been developed by Scaiano and co-workers[147,161,183]. The method involves the photogeneration of *tert*-butoxy radicals ($^tBuO\cdot$) by direct photolysis of a solution of 50/50 v/v di-*tert*-butylperoxide ($^tBuOO^tBu$)/benzene at 354.7 nm. Under these conditions, the absorbance at the excitation wavelength (due solely to the $^tBuOO^tBu$) was approximately 0.31. The *tert*-butoxy radical then abstracts the phenolic hydrogen from the phenol (with rate constant k_3) to yield the corresponding phenoxy radical and *tert*-butanol. This process is in competition with the pseudo-first-order decay of the *tert*-butoxy radical with rate constant k_2^{tot} as summarised by equations 5.1 to 5.3:-

$$^tBuOO^tBu \xrightarrow{h\upsilon} 2t\text{-}BuO\cdot \qquad (5.1)$$

$$^tBuO\cdot \xrightarrow{k_2^{tot}} Products \qquad (5.2)$$

$$t\text{-}BuO\cdot + PhOH \xrightarrow{k_3} t\text{-}BuOH + PhO\cdot \qquad (5.3)$$

where equation 5.2 accounts for the decay of $^tBuO\cdot$ other than by reaction with the phenol and PhOH is the phenol (or substituted phenol) under study. The rate of build-up of the absorption, as a function of time, due to the phenoxy radical ($PhO\cdot$) follows pseudo first order kinetics according to equation 5.4:-

$$k_{exp} = k_2^{tot} + k_3[PhOH] \qquad (5.4)$$

where k_{exp} is the experimentally observed rate constant for the absorption build-up due to the phenoxy free radical. Thus, a plot of k_{exp} versus [PhOH] should be linear with slope k_3 and intercept k_2^{tot}.

From equations 5.1 to 5.3, it can be shown that the concentration of $^tBuO\cdot$ and $PhO\cdot$ as a function of time are according to equations 5.5 and 5.6 respectively:-

$$[^tBuO\cdot]_t = [^tBuO\cdot]_0 e^{-(k_2 + k_3[PhOH])t} \tag{5.5}$$

$$[PhO\cdot]_t = [PhO\cdot]_\infty (1 - e^{-(k_2 + k_3[PhOH])t}) \tag{5.6}$$

where $[PhO\cdot]_\infty$ is the concentration of phenoxy radicals at the plateau region of the kinetic trace. The kinetic analysis of the experimental data to determine k_{exp}, ie., the rate of growth of the phenoxy radical as a function of time, can be achieved by fitting the data with a mono-exponential with baseline kinetic function ($f(t)$) as shown in equation 5.7:-

$$f(t) = Ae^{-(k_{exp}t)} + B \tag{5.7}$$

where $A = -[PhO\cdot]_\infty$ and $B = [PhO\cdot]_\infty$ respectively. At t = 0, f(t) = 0; it therefore follows that, from equation 5.7, B = - A.

Experiments to determine k_{exp} were conducted at low laser energy densities such that the decay of the *tert*-butoxy radical followed a pseudo first order decay mode, the primary deactivation pathway (other than by reaction with the phenol) being detailed in equations 5.8 and 5.9:-

$$^tBuO\cdot + {}^tBuOO^tBu \rightarrow {}^tBuOH + \cdot CH_2(CH_3)_2COO^tBu \tag{5.8}$$

$$^tBuO\cdot \rightarrow CH_3CO\ CH_3 + \cdot CH_3 \tag{5.9}$$

According to Scaiano *et al*, the formation of propanone and the methyl free radical via a β-cleavage reaction (equation 5.9), is believed to be of little importance relative to the deactivation pathway shown in equation 5.8[147].

The time resolved absorption spectra observed for phenoxy radicals derived from substituted phenols are dependent upon both the nature and position of substituents on the aromatic ring of the phenol. As a general, though not strictly obeyed rule, substituents in the ortho position to the phenolic moiety give a blue shift in the observed λ_{max} relative to phenol itself (λ_{max} = 400 nm), whereas substitution in the meta or para positions tend to shift the λ_{max} to the red of that observed for phenol itself. The molar absorption coefficients observed for phenoxy radicals also depend upon substitution patterns on the aromatic ring. For a given substituent, the maximum observed molar absorption coefficients tend to follow

the order para > meta > ortho. Relative to the molar absorption coefficient of the phenoxy radical of phenol itself ($\epsilon_{max} \approx$ 2000 l.mol^{-1}.cm.$^{-1}$)[147], para substituents tend to give larger molar absorption coefficients whereas substituents in the meta or ortho positions tend to yield decreased molar absorption coefficients for their respective phenoxy radicals. The phenoxy radicals, generated in MWL by hydrogen atom abstraction of a lignin phenolic hydrogen by the excited triplet state of α-carbonyl moieties, are derived mainly from guaiacyl-phenylpropane type lignin sub-units which contain the phenolic hydroxyl group in the 4 position, a methoxy group in the 3 position and a C_3 propane side chain in the 1 position of the aromatic ring (see section 2.3).

The transient absorption spectrum of the phenoxy radical of the mono-substituted phenol, 4-methylphenol, is shown in figure 5.7. The phenoxy radical of this mono-substituted phenol is well documented in the literature[147] and was therefore initially studied as a reference compound.

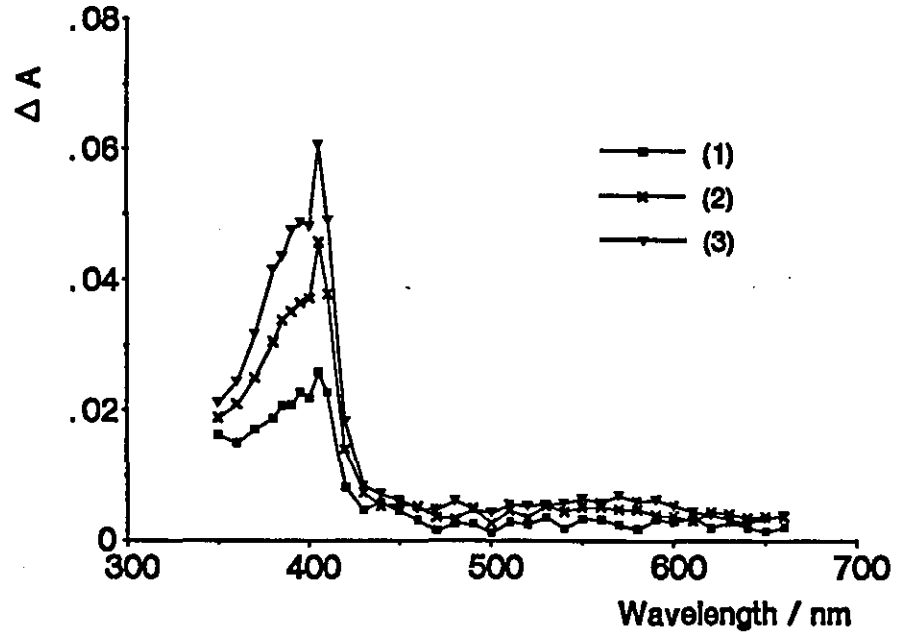

Figure 5.7:- Transient Absorption Spectrum of the Phenoxy Radical of 4-Methylphenol (4 x 10^{-3} mol.l.$^{-1}$) in 50/50 v/v di-tert-butylperoxide/benzene Recorded at Three Delays After the Laser Pulse
Time Delays After the Laser Pulse; (1) 310 ns, (2) 730 ns, (3) 1.5 μs (The Plateau Region of the Kinetic Trace)

The λ_{max}, located at 405 nm, is in good agreement with the literature[147]. Close inspection of the spectrum suggests that there is also another weak absorption band with a λ_{max} located at ca. 575 nm.

By varying the concentration of 4-methylphenol and fitting the data according to equation

5.7, k_2^{tot} and k_3 defined in equations 5.2 and 5.3 respectively were obtained for para-methylphenol by plotting k_{exp} as a function of $[PhOH]$ as shown in figure 5.8 and tabulated in table 5.2.

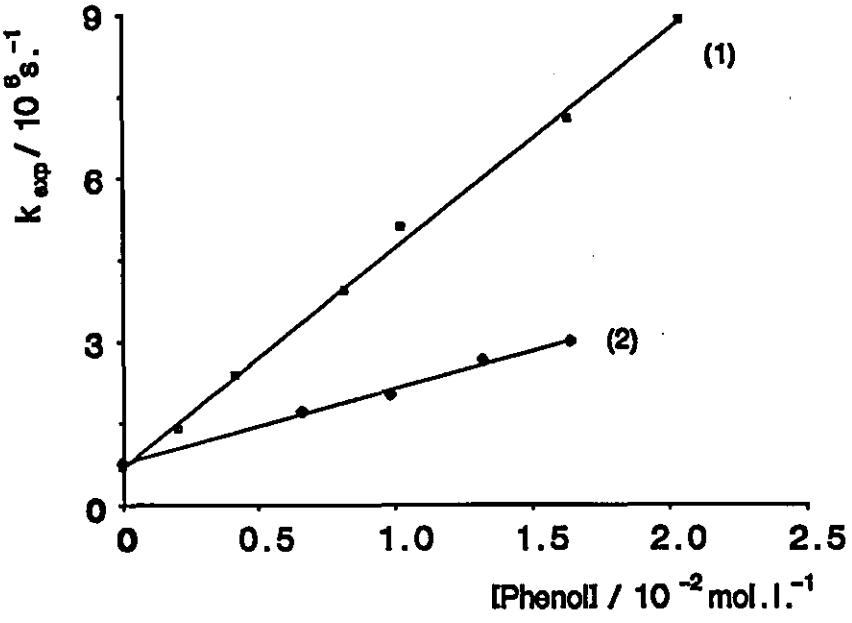

Figure 5.8:- Plots of k_{exp} as a function of $[PhOH]$ for (1) 4-Methylphenol and, (2) tert-Butylguaiacylcarbinol to Determine k_2^{tot} and k_3

$[PhOH]/10^{-3} mol.l.^{-1}$	$k_{exp}/10^6 s.^{-1}$
2.0	1.39
4.1	2.38
8.2	3.95
10.2	5.10
16.3	7.11
20.4	8.92

Table 5.2:- Experimentally Determined Rate Constant (k_{exp}) as a function of $[PhOH]$ for 4-Methylphenol in 50/50 v/v di-tert-butylperoxide/benzene analysing at 405 nm

From this data, k_2 and k_3 were determined to be 6.4 x 10^5 s.$^{-1}$ and 4.1 x 10^8 l.mol.$^{-1}$ s.$^{-1}$ respectively and are in good agreement with the literature[147,161] values of 5.7 x 10^5 s.$^{-1}$ and 5.5 x 10^8 l.mol.$^{-1}$ s.$^{-1}$.

The phenolic lignin model compound *tert*-butylguaiacylcarbinol (1-(4-hydroxy-3-methoxy)-2,2-dimethylpropan-1-ol) has been frequently used as a guaiacyl-phenylpropane

phenolic lignin model compound to simulate the interaction with photochemically excited triplet states of α-carbonyl moieties under steady state irradiation conditions[105,107,184]. The molecule contains a methoxyl group ortho to the phenolic moiety in the 3 position of the aromatic ring (ie. a guaiacyl type substitution pattern) together with a primary alcohol group on the α-carbon of the side chain attached to the ring system para to the phenolic hydroxyl group. The *tert*-butyl group attached to the β carbon of the side chain attempts to simulate a bond to the lignin macromolecule.

The quenching rate constant (k_q) for hydrogen atom abstraction of phenolic hydroxyl hydrogen atoms by aromatic carbonyl triplet states ((n,π^*) or (π,π^*)) are of the same order of magnitude as those observed for *tert*-butoxy radicals, both of which are considerably faster (by approximately two orders of magnitude[161]) than the rate constants observed for hydrogen atom abstraction by carbonyl triplet states and *tert*-butoxy radicals from alcohols or hydrocarbons (eg. k_q for the reaction *tert*-butoxy radicals with propan-2-ol and 1-phenylethanol have both been determined as 1.8×10^6 l.mol.$^{-1}$s.$^{-1}$)[161]. Thus, the rate constant for the hydrogen atom abstraction of the alcoholic hydrogen on the α-carbon of the side chain by $^tBuO\cdot$ relative to that of the phenolic hydroxyl hydrogen is kinetically unfavourable. Therefore, it is assumed that the reaction of $^tBuO\cdot$ with *tert*-butylguaiacylcarbinol will result in almost exclusive attack upon the phenolic hydroxyl hydrogen to yield the corresponding phenoxy radical species.

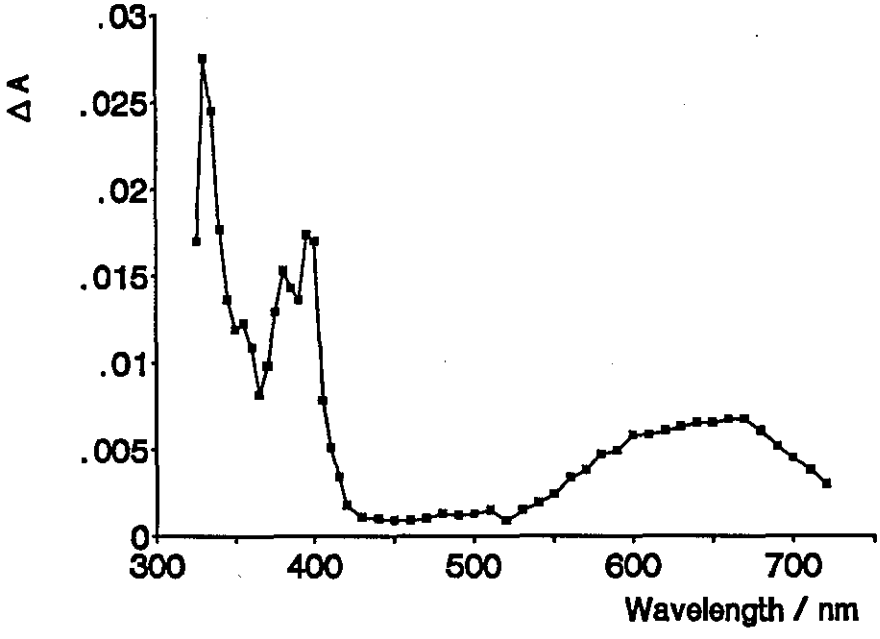

Figure 5.9:- Transient Absorption Spectrum of the Phenoxy Radical of tert-Butylguaiacylcarbinol (6.6×10^{-3} mol.l.$^{-1}$) in 50/50 v/v di-tert-butylperoxide/benzene Recorded 1.2μs After the Laser Pulse (The Plateau Region of the Kinetic Trace)

The transient absorption spectrum of the phenoxy radical of *tert*-butylguaiacylcarbinol in 50/50 v/v degassed di-*tert*-butylperoxide/benzene is shown in figure 5.9. As can be seen, much fine structure in the absorption spectrum is observed below 400 nm with λ_{max} located at 335, 380 and 395 nm together with a broad absorption band with λ_{max} at approximately 660 nm. This red shifted absorption band is due to absorption by the phenoxy radical and was assigned as such on the grounds that its rate of formation was identical to that of the formation of the absorption bands located below 400 nm as seen in figure 5.10:-

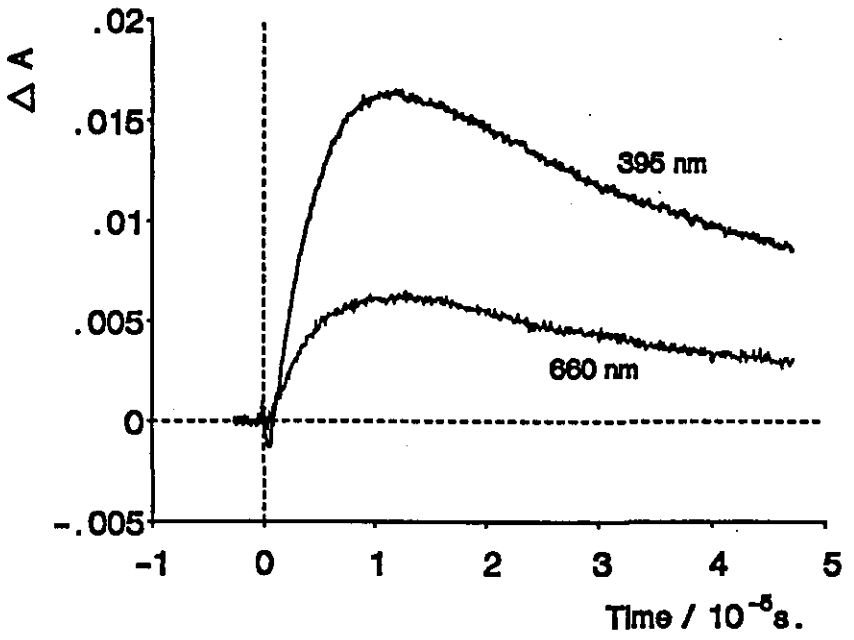

Figure 5.10:- Transient Absorption Traces Analysing at 395 nm and 660 nm for a Sample of tert-Butylguaiacylcarbinol (6.6×10^{-3} mol.l.$^{-1}$) in 50/50 v/v di-tert-butylperoxide/benzene

A similar absorption band has been observed for the phenoxy free radical of ortho-methoxyphenol obtained by a similar method to the one detailed above. A plot of the experimentally observed rate constant k_{exp} for the rise of the transient signal due to the phenoxy radical as a function of *tert*-butylguaiacylcarbinol concentration is shown in figure 5.8 and tabulated in table 5.3. The analysing wavelength used was 395 nm to avoid a small absorption due to $^tBuO\cdot$ observed at wavelengths less than 350 nm.

From this data, k_2 and k_3 were determined to be 7.6×10^5 s.$^{-1}$ and 1.38×10^8 l.mol.$^{-1}$s.$^{-1}$. The lower value of k_3 is consistent with those observed for ortho substituted phenols which generally have lower rate constants for hydrogen atom abstraction than for para substituted phenols, attributed mainly to some steric effects between $^tBuO\cdot$ and the phenol. For example, the rate constants for hydrogen atom abstraction (k_3) for 2-methoxyphenol and 4-methoxyphenol are 1.7×10^8 and 1.6×10^9 l. mol.$^{-1}$s.$^{-1}$ respectively[147].

$[PhOH]/10^{-3}mol.l.^{-1}$	$k_{exp}/10^{6}s.^{-1}$
6.6	1.72
9.8	2.04
13.2	2.67
16.4	3.02

Table 5.3:- Experimentally Determined Values of k_{exp} as a function of $[PhOH]$ for tert-Butylguaiacylcarbinol in 50/50 v/v di-tert-butylperoxide/benzene analysing at 395 nm

5.4.4 Assignment of the Transient Species Observed Following Laser Excitation of Milled Wood Lignin in 1,4-Dioxane Solution

As has been demonstrated in section 5.4.2, lignin undergoes photodegradation reactions upon exposure to UV light at 354.7 nm. This results in a loss of absorption in the wavelength region 280 nm to 370 nm (with a maximum ground state absorption at ca. 340 nm) and a corresponding increase in absorption following exposure to the laser at wavelengths greater than 370 nm, the maximum increase in absorption being observed at ca. 400 nm, the absorption band extending to approximately 550 nm giving even relatively weak solutions of MWL a yellowish tinge following exposure to the laser.

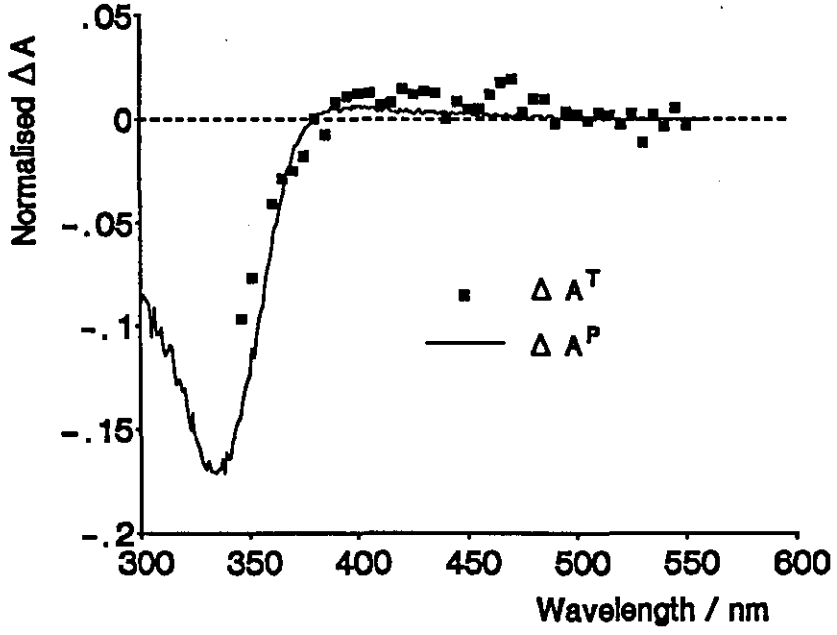

Figure 5.11:- Normalised Transient Difference Spectrum (ΔA^{r}) Recorded 31 μs After the Laser Pulse and Ground State ΔA^{r} Spectrum for a Sample of MWL in Aerated 1,4-Dioxane Solution

From the laser flash photolysis experiments, it has been established that at least two transient species are observed following pulsed laser excitation at 354.7 nm. The greatly differing rate constants for their decay enabled the transient difference spectra of the two species to be determined as seen in figures 5.2 and 5.3. The rate constant observed for the decay of the longer lived transient absorption was found to be unaffected by the presence of oxygen and was determined as 4.71×10^5 s.$^{-1}$. Therefore, at time delays greater than approximately 8 μs after the laser pulse, the observed transient difference spectrum should follow that of the laser induced changes in the ground state absorption spectra (see figure 5.6) measured before and after photolysis. The normalised transient difference spectrum, recorded 31 μs after the laser pulse for a sample of MWL in aerated 1,4-dioxane solution are shown in figure 5.11 together with the ground state ΔA^{r} spectrum as from figure 5.6 (section 5.4.2).

It can therefore be concluded that the ground state depletion observed under steady state irradiation conditions is similar to the time resolved transient difference spectrum observed at time delays greater than four lifetimes of that of the slowest observed transient species. A consequence of this observation however, is that the observed time resolved transient difference spectra also contains an absorption term due to the permanent changes in the lignin sample induced by the laser and, as such, may well be distorted by this extra absorption term. This will be most markedly observed in regions of the spectrum where large permanent absorption changes occur, ie., around 340 nm.

We have seen in section 5.4.3 that the transient absorption spectrum of the phenoxy radical of a non -carbonyl phenolic hydroxyl lignin model compound *tert*-butylguaiacyl-carbinol has many absorption features at wavelengths below 400 nm with λ_{max} located at 330 nm, 380 nm and 395 nm together with absorption minima located at 365 nm and 390 nm. That is to say, the absorption spectrum of the phenoxy radical of *tert*-butylguaiacylcarbinol at wavelengths below 400 nm is characterised by large changes in molar absorption coefficient over narrow wavelength ranges, the most marked example of this being the change in the molar absorption coefficient by almost a factor of 4 between 330 nm and 365 nm. The large changes in molar absorption coefficient for a transient species of this nature superimposed upon a permanent ground state depletion region similar to the one observed for MWL in 1,4-dioxane solution may explain the nature of the sharp transient feature observed for the slower transient species which has an absorption minimum at ca. 340 nm. At wavelengths below 340 nm, the molar absorption coefficient of the long lived transient species is increasing at a faster rate than the rate of the change in absorbance (as a function of wavelength) due to permanent changes in the lignin sample resulting in the sharp decrease in the laser induced absorbance change in this wavelength region. At wavelengths between 340 nm and 370 nm the change in absorbance due to permanent changes in the MWL sample (ΔA^{r}) is much greater than the absorption due to the laser induced transient (ΔA^{T}) whereas at wavelengths greater than 370 nm, $\Delta A^{T} >> \Delta A^{r}$. It is the balance between the molar absorption coefficient of the long lived transient species and that of the permanent change in the absorption spectrum of the lignin sample as a function of wavelength which, when combined, give the observed spectral features of the transient difference spectrum of the long lived species.

The photogeneration of phenoxy free radicals in samples of MWL has been demonstrated by comparison with the observed ESR signals and steady state product analysis data

obtained from phenolic lignin model compounds in the presence of α-carbonyl lignin model compound in solution[84,177]. One of the mechanisms proposed for the generation of the phenoxy radicals has been hydrogen atom abstraction of the phenolic hydroxyl hydrogen by the triplet excited state of α-carbonyl moieties present in the lignin macromolecule leading to the formation of a phenoxy-ketyl free radical pair. The absorption spectra of ketyl radicals obtained by a hydrogen atom abstraction reaction with cyclohexane by the triplet state of acetophenone derivatives have been documented in the literature[129]. Such spectra are characterised by weak absorption maxima at ca. 400 nm and 450 nm with a molar absorption coefficient of the order of 700 $l.mol.^{-1}cm.^{-1}$. At wavelengths below ca. 340 nm, strong absorption is observed with an absorption maximum located at a wavelength below 300 nm. The transient different spectrum for MWL observed at time delays greater than ca. 1 μs in the 400 nm to 500 nm wavelength range may be further complicated by weak absorption of ketyl free radical species which may explain the broadness of the observed absorption band. Due to the small changes in absorbance observed for MWL following laser excitation (figure 5.3), the kinetic data obtained at such wavelengths is not of sufficient quality to establish whether the decay in absorption in this wavelength region is due to more than one radical species, possibly further complicated if both the phenoxy and ketyl radical species have similar deactivation rate constants. However, the sharp increase in the transient absorption observed at wavelengths less than 340 nm, may be attributed to the sharp increase in the molar absorption coefficients of both the phenoxy and ketyl radicals in this spectral region.

By comparison of figures 5.3, 5.6 and 5.9, it can be seen that only a small wavelength shift and slight broadening of absorption bands in the transient absorption spectra of the phenoxy radical of phenolic lignin model compound *tert*-butylguaiacylcarbinol and the corresponding ketyl radical superimposed upon the permanent absorption changes observed for MWL following laser damage are required to assign the transient difference spectrum of the long lived species as being due to absorption by phenoxy (and possibly ketyl) radicals whose time resolved transient absorption spectrum are distorted by the permanent absorption changes observed for MWL following laser damage. The absorption band broadening may explain the apparent lack of an absorption band associated with the phenoxy radical at wavelengths greater than 600 nm as discussed in section 5.4.3. The fact that it is not observed for a sample of MWL can possibly be attributed to a combination of two effects, either the absorption band has, due to the nature of the lignin sample, been shifted to a longer wavelength or has been "smeared out" over a broader wavelength range to give an absorption band which was not detected in the flash photolysis experiments. Examination of time resolved transient absorption data at wavelengths greater than 650 nm for MWL suggests a hint of such an absorption band but reliability in the data obtained at such wavelengths, due to a combination of small absorbance changes coupled with small signal to noise ratios, does not afford confidence in stating the observation of such an absorption band.

It has been suggested by other authors that the lifetimes of the triplet states of photochemically generated α-carbonyl moieties present in MWL are extremely short (less than a few microseconds) in fluid solution[180,181]. There is no reference to the observation of the triplet-triplet absorption spectra of MWL in solution in the literature. The transient difference spectrum observed following laser excitation of MWL in 1,4-dioxane solution shows

a short lived transient species with lifetime under air equilibrated conditions of approximately 350 ns. A series of experiments involving laser excitation of MWL in the presence of varying concentrations of molecular oxygen in 1,4-dioxane were undertaken to assign the short lived transient species and are presented below.

Other authors have found no evidence for the triplet α-carbonyl sensitized formation of singlet oxygen following pulsed excitation of MWL in 50/50 v/v 1,4-dioxane/water solutions using DABCO (1,4-diazabicyclo-(2,2,2)-octane) as a chemical quencher of singlet oxygen[103]. Only small quantities of singlet oxygen are generated from MWL samples in aerated 1,4-dioxane solutions (see later). The radiative lifetime of singlet molecular oxygen in 1,4-dioxane solution measured by time resolved luminescence was determined to be ca. 26 μs$\pm$ 1 μs, in agreement with other authors[185,186]. The short singlet oxygen lifetime in the presence of water (ca. 4.4 μs in pure water[187] - an estimate of the lifetime of singlet oxygen in 50/50 v/v 1,4-dioxane/water is calculated to be ca. 8 μs assuming a mole fraction of 1,4-dioxane in 50/50 v/v 1,4-dioxane/water of 0.17 and a linear relationship between mole fraction of two miscible solvents and singlet oxygen lifetime[187]) coupled with the low singlet oxygen concentration generated by MWL and the relatively inefficient reaction of DABCO with singlet oxygen[188] may therefore explain the lack of chemical quenching observed by these researchers.

The quenching of excited triplet states of acetophenone and its derivatives by molecular oxygen in fluid solution has been demonstrated to be an efficient process[18,124,189] with quenching rate constants ($k_q^{O_2}$) in excess of 10^9 l.mol.$^{-1}$s.$^{-1}$. A simplified kinetic scheme to describe the quenching of such triplet states is shown in equations 5.10 to 5.14:-

$$^1K \xrightarrow{h\upsilon} {}^1K^* \tag{5.10}$$

$$^1K^* \xrightarrow[k_{ISC}]{\phi_T} {}^3K^* \tag{5.11}$$

$$^3K^* \xrightarrow{k_d} {}^1K \tag{5.12}$$

$$^3K^* + O_2(^3\Sigma_g^-) \xrightarrow{k_{q1}^{O_2}} {}^1K + O_2^*(^1\Delta_g) \tag{5.13}$$

$$^3K^* + O_2(^3\Sigma_g^-) \xrightarrow{k_{q2}^{O_2}} {}^1K + O_2(^3\Sigma_g^-) \tag{5.14}$$

where ϕ_T is the intersystem crossing quantum yield with rate constant k_{isc}, $k_{q1}^{O_2}$ and $k_{q2}^{O_2}$ are the oxygen quenching rate constants for the triplet ketone with and without production of singlet oxygen ($^1\Delta_g(O_2)$) and k_d is the decay of the triplet state in the absence of quencher. The singlet state lifetimes of α-carbonyl type compounds in solution are extremely short (of the order of a few picoseconds) and thus, quenching of the ketone singlet state by molecular oxygen was ignored given the range of oxygen concentrations used in the study (up to ca. 10^{-2} mol.l.$^{-1}$).

The efficiency of singlet oxygen production (ϕ_Δ) by energy transfer from the triplet state of the ketone is related to the quantum yield of triplet formation (ϕ_T) and the number of triplet ketone oxygen quenching events which lead to the formation of singlet oxygen (S_Δ) according to equation 5.15:-

$$\phi_\Delta = \phi_T \times S_\Delta \qquad (5.15)$$

where,

$$S_\Delta = \frac{k_{q1}^{O_2}}{k_{q1}^{O_2} + k_{q2}^{O_2}} \qquad (5.16)$$

The total triplet quenching rate constant (k_q^T) is therefore simply equal to the sum of $k_{q1}^{O_2}$ and $k_{q2}^{O_2}$ outlined in equations 5.13 and 5.14.

It has been established in section 4.3.2 that ϕ_T for α-carbonyl lignin model compounds such as 4-methoxyacetophenone[136], 3,4-dimethoxyacetophenone, 3,4,5-trimethoxyacetophenone and 4-hydroxy-3-methoxyacetophenone are unity within experimental error. Values of S_Δ for acetophenone derivatives in benzene and acetonitrile are dependent upon the electron donating/withdrawing properties of substituents on the aromatic ring. For such compounds, the presence of electron donating methoxy groups on the aromatic ring result in lower values for S_Δ (and therefore ϕ_Δ) relative to the unsubstituted acetophenone parent molecule. For example, S_Δ for acetophenone and 4-methoxyacetophenone have been measured as 0.35 and 0.27 in benzene and 0.52 and 0.42 in acetonitrile solution[18]. It is not unreasonable, therefore, to assume that the α-carbonyl triplet moieties proposed as being generated following 354.7 nm laser excitation of MWL will have S_Δ values of a similar magnitude.

The deactivation of singlet molecular oxygen (see section 1.3) ($^1\Delta_g$) to the ground state in fluid solution can be studied by monitoring the weak (0,0) vibronic band of the phosphorescence emission (λ_{max} centred at 1270 nm[185,190]) as a function of time for the process outlined in equation 5.17:-

$$O_2(^1\Delta_g) \xrightarrow{k_{rad}} O_2(^3\Sigma_g^-) + h\nu(1270nm) \qquad (5.17)$$

where k_{rad} is the radiative decay rate constant for the process. The apparatus and detection systems required for this purpose are described in section 3.7.

Under many circumstances, the rate constant for the decay of the triplet (k_d) is small relative to the quenching rate constant multiplied by the oxygen concentration for air equilibrated solvents ($k_q^T[O_2]$) and therefore the determination of singlet oxygen yields from triplet sensitizers usually does not require any greater concentration of oxygen in solution than present under air equilibrated conditions where, typically, greater than 95 % of the triplet sensitizer molecules are quenched by oxygen. Clearly, as k_d increases and approaches $k_q^T[O_2]$, a correction factor will need to be applied to the data to account for triplet decay processes (other than quenching by oxygen) competing with the quenching process.
Hence, for a photoinduced triplet state with decay constant k_d and quenching rate constant k_q^T, the rate of loss of triplet states ($^3K^*$) as a function of time is according to equation 5.18:-

$$\frac{-d[^3K^*]}{dt} = (k_d + k_q^T[O_2])[^3K^*] \qquad (5.18)$$

It therefore follows that the concentration of singlet oxygen extrapolated to zero time after the laser pulse ($[^1O_2]_0$) can therefore be defined as:-

$$[^1O_2]_0 = [^3K^*]_0 \phi_T S_\Delta \frac{k_q^T[O_2]}{k_d + k_q^T[O_2]} \qquad (5.19)$$

where, for a given laser energy $[^3K^*]_0 \phi_T S_\Delta$ is a constant C_1. The observed phosphorescence emission intensity extrapolated to zero time after the laser pulse (I_Δ^0) can therefore be expressed as:-

$$I_\Delta^0 = C_1 C_2 \frac{k_q^T[O_2]}{k_d + k_q^T[O_2]} \qquad (5.20)$$

where C_2 is a proportionality constant relating the observed signal intensity in digitiser pixels to $[^1O_2]_0$ formed by quenching energy transfer.
From equation 5.20, the predicted shape of plots of I_Δ^0 as a function of oxygen concentration are of a growth curve reaching a plateau region where $k_q^T[O_2] >> k_d$ due to k_d becoming insignificantly small. If we define $C_1C_2 = C_{TOT}$ then from equation 5.20, with suitable manipulation, it follows that:-

$$\frac{1}{I_{\Delta}^{0}} = \frac{k_d}{C_{TOT} k_q^T [O_2]} + \frac{1}{C_{TOT}} \qquad (5.21)$$

Therefore, plots of $1/I_{\Delta}^{0}$ versus $1/[O_2]$ should be linear with slope equal to $k_d/C_{TOT}k_q^T$ and intercept $1/C_{TOT}$. Such data therefore provides a measure of the ratio of k_d/k_q^T for triplet states with high values of k_d.

From flash photolysis experiments of MWL in 1,4-dioxane solution under variable oxygen concentrations, the fast transient (with lifetime equal to ca. 350 ns under air equilibrated conditions) is sensitive to the concentration of oxygen in the solution whereas the long lived transient species is insensitive to the presence of oxygen suggesting that the fast transient is indeed the triplet state of primarily α-carbonyl moieties present in MWL. However, for the unequivocal assignment, singlet molecular oxygen ($^1\Delta_g(O_2)$) must also be produced, the concentration of which is defined according to equation 5.19.

The variation of oxygen concentration in solution, except for the air equilibrated and oxygen saturated samples (achieved by bubbling the sample with a stream of oxygen for ca. 20 minutes), was achieved as follows; each sample was degassed using three freeze-pump-thaw cycles to a final pressure above the solution of no greater than 1×10^{-4} mBar. The degassed sample was then connected to a cylinder of pure, moisture free oxygen via a plastic tube which had itself been purged with oxygen from the cylinder for a minimum of 5 minutes. The sample was then exposed to the required pressure from the cylinder for a minimum of 5 minutes, during which the sample was shaken vigourously to allow equilibrium to be reached between the oxygen pressure above the solution and the oxygen concentration in the solvent.

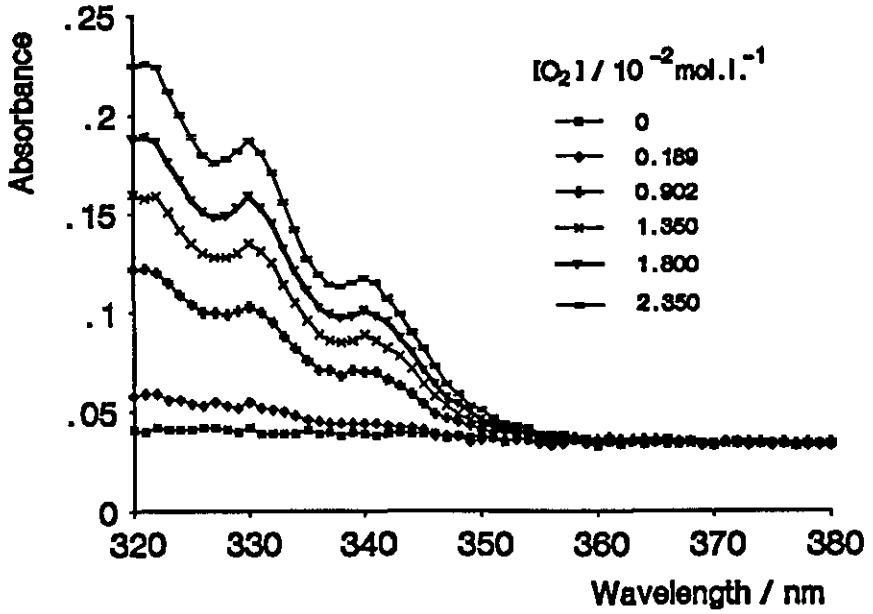

Figure 5.12:- Absorption Spectra of the Oxygen/Benzene Charge-Transfer Complex as a Function of Oxygen Concentration

The concentration of oxygen in oxygen saturated 1,4-dioxane solution was assumed to be 6.10 x 10^{-3} mol.l.$^{-1}$ at 20°C[191], oxygen concentrations for cylinder pressures greater than 1 Bar above the solution were calculated assuming that the partial pressure above the solution is proportional to the concentration of oxygen in solution. The linearity of the oxygen cylinder pressure gauge was established by measuring the absorption of the charge transfer bands of the oxygen/benzene charge-transfer complex at 321 nm, 330 nm and 340 nm. The absorption spectra (measured against air background) are shown in figure 5.12 assuming a concentration of oxygen in oxygen saturated benzene of 9.02 x 10^{-3} mol.l.$^{-1}$ at 20°C[191].

At all absorption maxima, good linear fit to plots of absorbance as a function of oxygen concentration were observed[192]. A representative plot is shown in figure 5.13 for the absorbance measured at 340 nm.

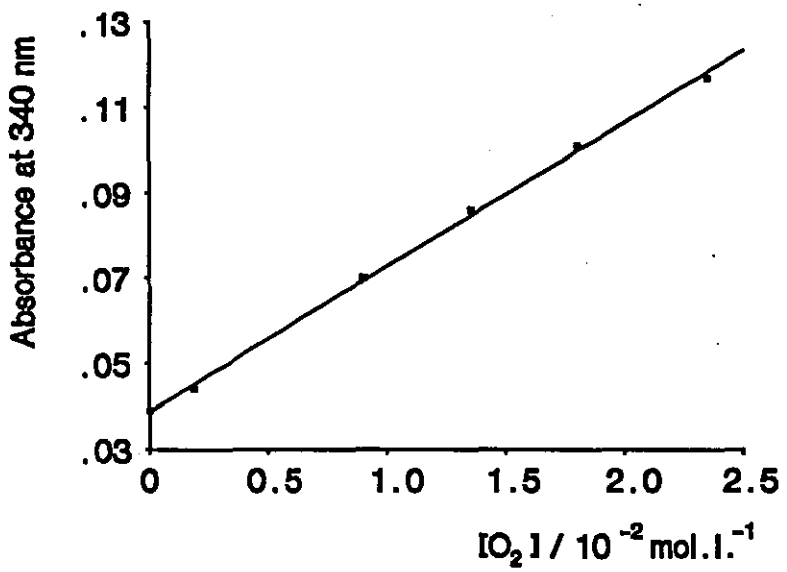

Figure 5.13:- A Plot of Absorbance at 340 nm as a Function of Oxygen Concentration for the Oxygen/Benzene Charge-Transfer Complex

The concentration of oxygen in an air equilibrated 1,4-dioxane solution (given that oxygen concentration in a oxygen saturated solution equals 6.10 x 10^{-3} mol.l.$^{-1}$) should be equal to 1.28 x 10^{-3} mol.l.$^{-1}$. As we will see later, anomalous behaviour of the singlet oxygen luminescence intensity (I_Δ^0) was observed for an air equilibrated MWL sample in 1,4-dioxane solution. A simple experiment to establish that the correct oxygen concentration in solution, calculated from above, in the presence of nitrogen was performed with the aid of a Stern-Volmer plot for the fluorescence quenching of perylene (1 x 10^{-5} mol.l.$^{-1}$) in 1,4-dioxane

solution. The excitation wavelength was 400 nm and the fluorescence intensity as a function of oxygen concentration in solution was monitored at 443 nm and 469 nm together with the integrated area under each emission curve, the variation of oxygen concentration being achieved according to the method detailed previously for the benzene/oxygen charge-transfer complex studies. From the ground state absorption spectra of the perylene it was shown that no charge transfer complex with oxygen was observed at the concentrations of oxygen used in these experiments. Perylene has a relatively long singlet state lifetime in the absence of a quencher ranging from 4.8 ns to 6.4 ns[193,194,195] and is thus sufficiently slow to be quenched by oxygen present in the solution. From the Stern-Volmer plot[196], the oxygen concentration in the air equilibrated solvent was shown to be as predicted from above. Thus, under air equilibrated conditions, the solubility of oxygen in 1,4-dioxane solution is not affected by the presence of nitrogen.

The lignin model compound α-(2-methoxyphenoxy)-3,4-dimethoxyacetophenone has been shown to have an extremely short triplet lifetime in 1,4-dioxane solution (ca. 183 ns[124]) with an oxygen quenching rate constant of ca. 3 x 10^9 l. mol.$^{-1}$s.$^{-1}$ in ethanol solution[124]. Thus, in 1,4-dioxane under air equilibrated conditions, only ca. 41 % of triplet states are quenched by oxygen since $k_d \gg k_q^T[O_2]$ This molecule was therefore chosen to test the relationship between $1/I_\Delta^0$ and $1/[O_2]$ defined in equation 5.21 for a range of oxygen concentrations.

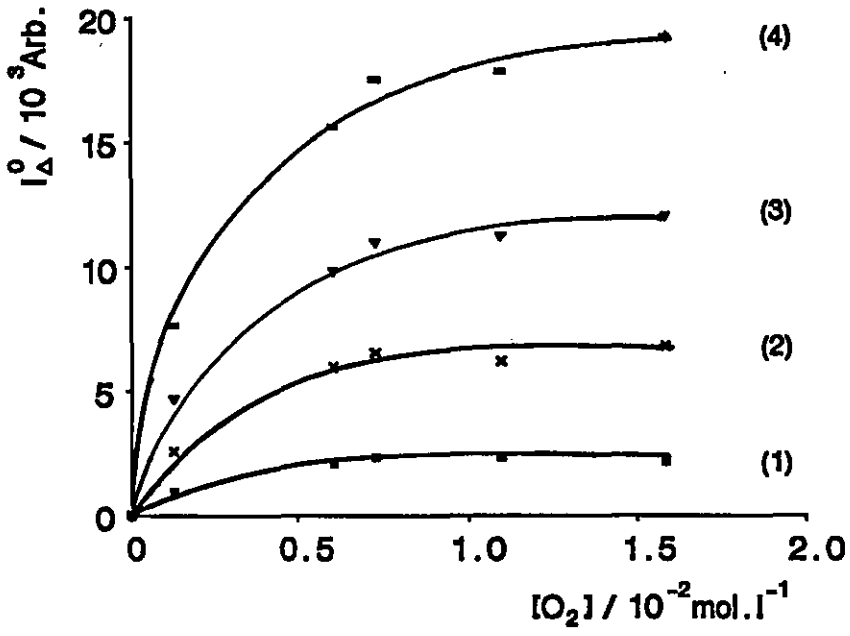

Figure 5.14:- Plots of I_Δ^0 as a Function of $[O_2]$ for α-(2-methoxyphenoxy)-3,4-dimethoxyacetophenone in 1,4-Dioxane Solution at Four Different Laser Intensities
Curves 1 to 4 represent 1.6, 5.0, 8.7 and 14.2 % of the Full Laser Intensity (100 % Laser Intensity = 12 mJ.cm.$^{-2}$)

Due to the sensitivity of the singlet oxygen luminescence detection system, very low laser intensities (< 3 mJ.cm.$^{-2}$) were required for the collection of the luminescence data ensuring absorption by the photogenerated triplet state at the laser excitation wavelength (354.7 nm) was sufficiently small so as not to produce a non-linear relationship between singlet oxygen luminescence intensity (extrapolated to zero time after the laser pulse), I_{Δ}^{o}, as a function of laser intensity (see also section 4.3.2). The laser energy was attenuated by means of a sodium nitrite filter with known absorbance at the laser excitation wavelength.

The singlet oxygen luminescence intensity data was collected with five randomly chosen laser intensities for each series of samples to monitor the extent to which the samples had degraded as a result of exposure to the laser. This was achieved by plotting I_{Δ}^{o} as a function of the laser intensity for each of the samples. Under the experimental conditions used here, degradation was found, in all cases, to be negligible. Plots of I_{Δ}^{o} as a function of [O_2] for α-(2-methoxyphenoxy)-3,4-dimethoxyacetophenone in 1,4-dioxane solution are shown in figure 5.14.

As can be seen, the intensity of the singlet oxygen luminescence signal (I_{Δ}^{o}) initially increases rapidly as a function of oxygen concentration and then flattens out at higher oxygen concentrations to give a plateau region where k_d becomes small relative to $k_q^T[O_2]$ as predicted by equation 5.20.

From this data, values of $1/I_{\Delta}^{o}$ as a function of 1/[O_2] were obtained and are tabulated in table 5.4:-

	$1/I_{\Delta}^{o}$ (2) as a Function of % Laser Intensity(3)						
$1/[O_2]$(1)	1.60	3.11	5.00	6.89	8.71	11.43	14.16
780.64	10.50	6.65	3.87	2.48	2.14	1.70	1.31
163.93	4.72	2.72	1.68	1.27	1.02	0.80	0.64
136.61	4.23	-	1.53	-	0.91	-	0.57
91.08	4.26	-	1.61	-	0.89	-	0.56
63.05	4.55	-	1.47	-	0.83	-	0.52

Table 5.4:- Data Relating $1/I_{\Delta}^{o}$ as a Function of 1/[O_2] for α-(2-methoxyphenoxy)-3,4-dimethoxyacetophenone in 1,4-Dioxane Solution

(1) l.mol.$^{-1}$

(2) Arbitrary Units / 10^{-4}

(3) 100 % laser intensity = 12 mJ.cm.$^{-2}$

The corresponding plots of $1/I_{\Delta}^{0}$ as a function of $1/[O_2]$ are shown for four laser intensities in figure 5.15 together with the best straight line fit to the data.

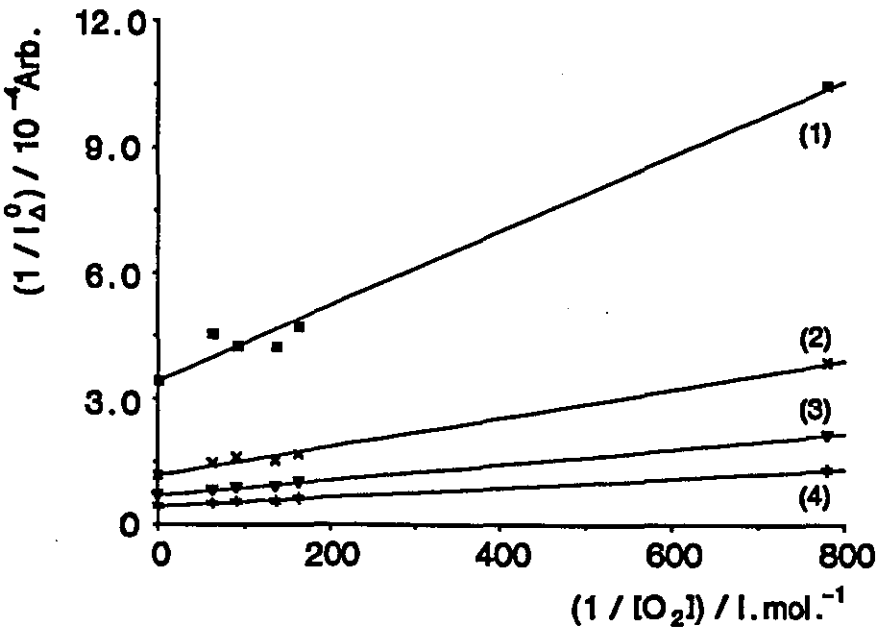

Figure 5.15:- Plots of $1/I_{\Delta}^{0}$ as a Function of $1/[O_2]$ for Four Laser Intensities for α-(2-methoxyphenoxy)-3,4-dimethoxyacetophenone in 1,4-Dioxane Solution
Curves 1 to 4 represent 1.6, 5.0, 8.7 and 14.2 % of the Full Laser Intensity (100 % Laser Intensity = 12 mJ.cm.$^{-2}$)

From these plots, the following values of k_d/k_q^T were obtained as presented in table 5.5:-

% Laser Intensity	Slope /10^{-7}	Intercept /10^{-4}	(1/Intercept) /10^{3}	$(k_d/k_q^T)^{(1)}$ /10^{-3} l.mol.$^{-1}$	$k_d^{(2)}$ /10^{6} s.$^{-1}$
1.60	8.95	3.44	2.91	2.60	9.08
5.00	3.41	1.18	8.47	2.89	10.00
8.71	1.84	0.70	14.25	2.62	9.15
14.16	1.10	0.45	22.47	2.47	8.63

Table 5.5:- Summary of the Fitted Data From Figure 5.15 For α-(2-methoxyphenoxy) -3,4-dimethoxyacetophenone in 1,4-Dioxane Solution

(1) From equation 5.21, k_d/k_q^T = Slope x (1/Intercept)

(2) Calculated assuming k_q^T = 3.5 x 10^9 l.mol.$^{-1}$s.$^{-1}$(see below)

An estimate of k_q^T equal to 3.5 x 10^9 l.mol^{-1}.s.$^{-1}$ was obtained by transmission laser flash photolysis experiments (monitoring at 395 nm) for a deoxygenated and air equilibrated sample of α-(2-methoxyphenoxy)-3,4-dimethoxyacetophenone in 1,4-dioxane solution. The values of k_d obtained from the singlet oxygen data are of the order of 30 % larger than observed for the direct measurement of k_d by laser flash photolysis experiments where k_d was observed to be 6.65 x 10^6 s.$^{-1}$. This may be attributed to the error in measuring k_q^T by the laser flash photolysis technique.

More importantly, from these experiments, it has been demonstrated that singlet oxygen luminescence intensity as a function of oxygen concentration does behave as predicted by equations 5.20 and 5.21 for a molecule whose triplet lifetime is less than 300 ns.

As seen in section 5.2, MWL in 1,4-dioxane solution undergoes permanent changes due to the photoreactivity of groups present within the macromolecule. Thus, for the corresponding set of singlet oxygen experiments with MWL, the lowest laser intensities required to observe singlet oxygen luminescence signals were used for data collection. As detailed above, a series of laser intensities were recorded in random order which demonstrated (via plots of I_Δ^0 verses % laser intensity being linear) that degradation during data collection was indeed minimal under these experimental conditions.

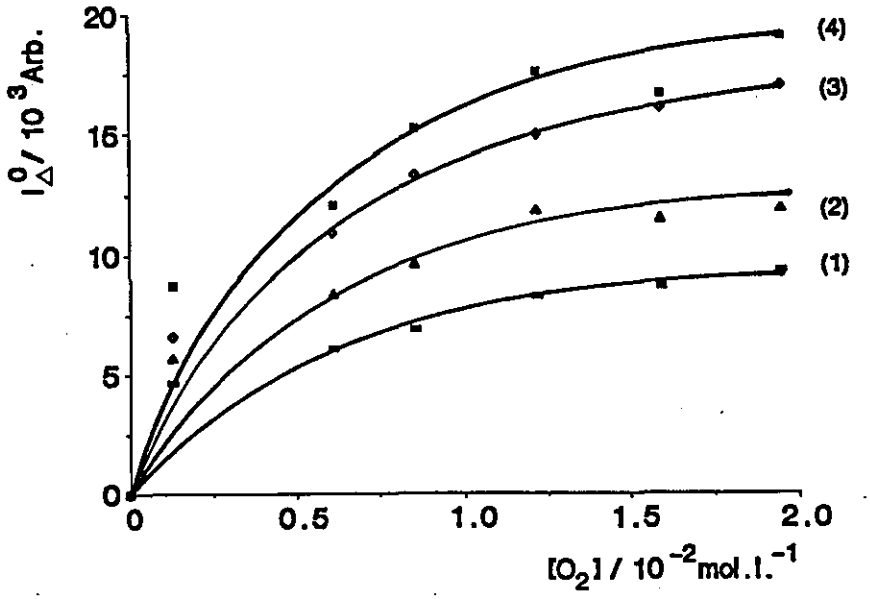

Figure 5.16:- Plots of I_Δ^0 as a Function of $[O_2]$ for MWL in 1,4-Dioxane Solution at Four Different Laser Intensities
Curves 1 to 4 represent 6.86, 10.30, 13.34 and 17.02 % of the Full Laser Intensity (100 % Laser Intensity = 12 mJ.cm.$^{-2}$)

Under similar conditions to those used for the lignin model compound, the intensity of the singlet oxygen luminescence signal following laser excitation of samples of MWL in 1,4-dioxane solution (absorbance at 354.7 nm = 0.6) as a function of oxygen concentration were obtained and are shown in figure 5.16.

	$1/I_{\Delta}^{0}$ (2) as a Function of % Laser Intensity(3)			
$1/[O_2]$(1)	6.86	10.30	13.34	17.02
780.64	2.15	1.76	1.51	1.15
163.93	1.65	1.20	0.92	0.83
117.10	1.45	1.04	0.75	0.66
81.97	1.21	0.85	0.67	0.57
63.05	1.15	0.87	0.62	0.60
51.23	1.07	0.84	0.59	0.52

Table 5.6:- Data Relating $1/I_{\Delta}^{0}$ as a function of $1/[O_2]$ for MWL in 1,4-Dioxane Solution

(1) l.mol.$^{-1}$

(2) Arbitrary Units / 10^{-4}

(3) 100 % laser intensity = 12 mJ.cm.$^{-2}$

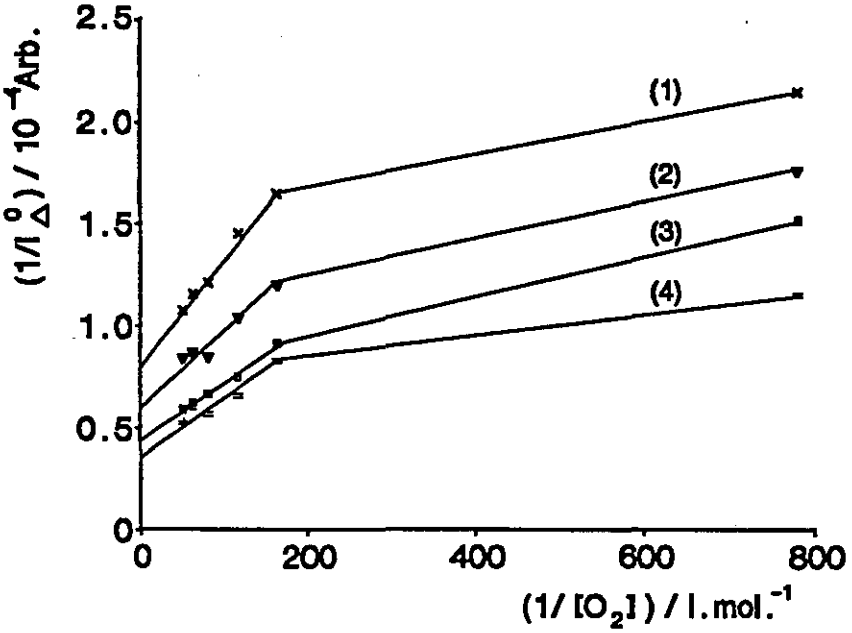

Figure 5.17:- Plots of $1/I_{\Delta}^{0}$ as a Function of $1/[O_2]$ for Four Laser Intensities for MWL in 1,4-Dioxane Solution
Curves 1 to 4 represent 6.86, 10.30, 13.34 and 17.02 %
of the Full Laser Intensity (100 % Laser Intensity = 12 mJ.cm.$^{-2}$)

Table 5.6 shows the luminescence data manipulated for application to equation 5.21 for the four different laser intensities used in the study. The corresponding plots of $1/I_{\Delta}^{0}$ as a function of $1/[O_2]$ for MWL obtained for a series of four laser intensities recorded in random order are shown in figure 5.17.

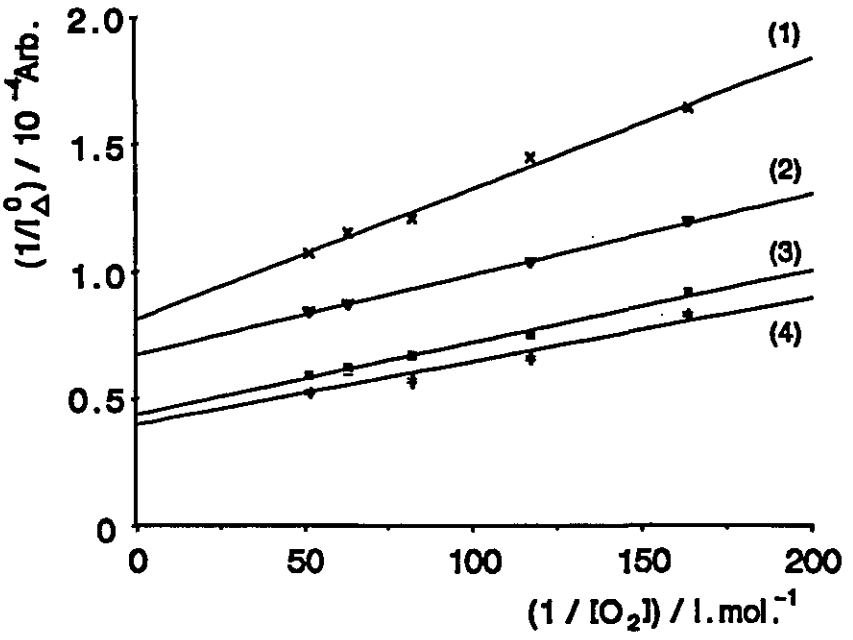

Figure 5.18:- Plots of $1/I_{\Delta}^{0}$ as a Function of $1/[O_2]$ for Four Laser Intensities for MWL in 1,4-Dioxane Solution Without the Data Points Equivalent to the air Equilibrated Sample

From the fitted data plots shown in figure 5.17 the following parameters were obtained and are tabulated in table 5.7:-

% Laser Intensity	Slope /10^{-7}	Intercept /10^{-5}	(1/Intercept) /10^{4}	(k_d/k_q^T) (1) /10^{-3} l.mol.$^{-1}$
6.86	5.16	8.12	1.23	6.36
10.30	3.18	6.71	1.49	4.74
13.36	2.84	4.37	2.29	6.50
17.02	2.48	3.99	2.51	6.22

Table 5.7:- Summary of the Fitted Data From Figure 5.14 For MWL in 1,4-Dioxane Solution Excluding the Air Equilibrated Data Points

(1) From equation 5.21, k_d/k_q^T = Slope x (1/Intercept)

As can be seen, a large deviation from linearity is observed for the MWL sample under air equilibrated conditions which was not observed for the corresponding model ketone under identical conditions. The same data, plotted without the air equilibrated sample is shown in figure 5.18 together with the best straight line fit to the data.

5.4.5 Estimation of Triplet Quantum Yield For Milled Wood Lignin

The singlet oxygen luminescence data obtained for MWL in 1,4-dioxane clearly demonstrates that as the concentration of oxygen in solution is increased a corresponding increase in the amount of singlet oxygen is produced consistent with the assignment of the short lived transient species with λ_{max} at 425 nm being due to absorption by photoinduced triplet state of MWL. Since the primary photochemical absorbers at 354.7 nm are the α-carbonyl moieties present in MWL, the triplet-triplet absorption spectrum is assigned as principally due to the absorption by such moieties.

An assumption in the derivation of equation 5.21 is that the triplet state decays with a single rate constant k_d. However, given the heterogeneous nature of MWL, many different absorbing chromophoric groups may lead to triplet states and as such this data treatment cannot be applied to MWL samples where triplet state decay is likely to follow a distribution of rate constants attributable to the heterogeneity of the sample. As the concentration of oxygen is increased, the width of this distribution becomes significantly smaller and approximates to a single decay rate constant when $k_q^T[O_2] \gg k_d$ which yields the straight line region of the $1/I_\Delta^0$ verses $1/[O_2]$ plots. From the linear fits to such data, an estimate of the quantum yield of triplet state production can be obtained, the intercept on the Y axis for such plots being equivalent to where all the photogenerated triplet states from MWL are quenched by oxygen, ie. the plateau region of the plots of I_Δ^0 as a function of $[O_2]$ extrapolated to infinitely high oxygen concentrations. The efficiency of singlet oxygen production, S_Δ, (and therefore ϕ_Δ since $\phi_T = 1$[136]) for benzophenone in benzene has been determined to be between 0.29 to 0.35[137,197]. The quantum yield of triplet formation for MWL can therefore be estimated according to equation 5.22 from the ratio of the slopes of plots of I_Δ^0 and $1/C_{TOT}$ versus $[O_2]$ for benzophenone and MWL respectively recorded under identical conditions.

$$\phi_T^{MWL} = \frac{SlopeMWL}{SlopeBzp} \times \frac{S_\Delta^{Bzp}}{S_\Delta^{MWL}} \qquad (5.22)$$

The slope of the benzophenone plot requires a minor correction to account for the fact that under aerated conditions, assuming that k_d^{Bzp} equals 1.64×10^5 s.$^{-1}$, k_q^{Bzp} equals 2.50×10^9 l.mol.$^{-1}$s.$^{-1}$ and $[O_2]$ equals 1.9×10^{-3} mol.l.$^{-1}$ for air equilibrated benzene[135,191,198], only approximately 96.5 % of triplet states are quenched by oxygen. The luminescence intensity as a function of percentage laser intensity are tabulated in table 5.8, plots of the data together with the best straight line fit are shown in figure 5.19.

	$I^{\circ}_{\Delta}/10^4$ Arb.	
% Laser Intensity(1)	MWL(2)	Bzp(3)
6.86	1.23	6.30
10.30	1.49	9.37
13.34	2.29	12.36
17.02	2.51	15.49

Table 5.8:- Data of I°_{Δ} and $1/C_{TOT}$ versus Laser Intensity for Benzophenone (in benzene) and MWL (in 1,4-dioxane)

(1) 100 % laser intensity = 12 mJ.cm.$^{-2}$

(2) Extrapolated to infinite oxygen concentration

(3) Air equilibrated sample

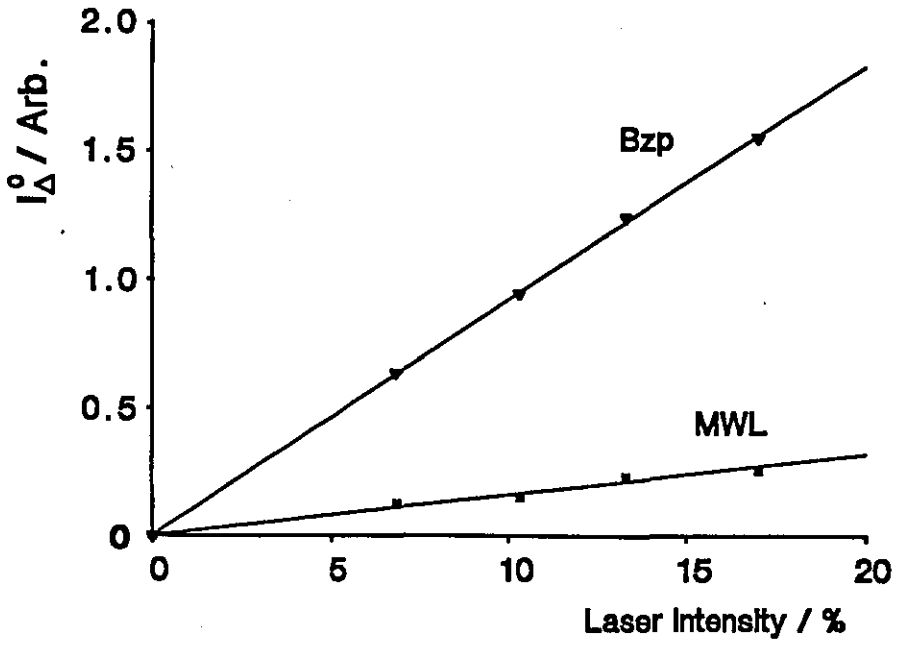

Figure 5.19:- Plots of I°_{Δ} and $1/C_{TOT}$ versus Laser Intensity for Benzophenone (Bzp) in benzene and MWL in 1,4-Dioxane Together With the Best Straight Line Fit to the Data

The value of S_{Δ} for MWL is assumed to be similar to the value obtained for substituted acetophenones; ie. 0.27 and 0.42 for 4-methoxyacetophenone in benzene and acetonitrile respectively[18]. If we assume that S_{Δ} for benzophenone in benzene is 0.32 (average of the values stated above) and assuming a lower S_{Δ} limit of 0.27 for MWL in 1,4-dioxane then, from the above data, the range of values obtained for ϕ_T^{MWL} are 0.19 when S_{Δ}^{MWL} equals 0.27 and 0.05 when S_{Δ}^{MWL} equals 1. This range of values does not appear unreasonable when one considers the nature of the MWL sample. MWL chromophores such as α-carbonyl moieties

absorb strongly at 354.7 nm and have high triplet quantum yield ranging between 0.5 and 1 depending upon substitution (see section 4.3.2). However, other chromophoric moieties present in MWL such as, amongst others, substituted biphenyls[199,200] and some phenolic hydroxyl moieties[201] absorb to an extent at 354.7 nm and have lower triplet state quantum yields (eg. ϕ_T = 0.32 and 0.39 for phenol[202] and biphenyl[203] respectively) than those observed for α-carbonyls.

At high oxygen concentrations, quenching processes leading to the deactivation of the triplet state dominate over other deactivation pathways such as phenolic hydroxyl hydrogen atom abstraction to generate a phenoxy-ketyl free radical pair which can then go on to produce yellow degradation products via a multi-step process. Even when a high percentage of triplet states are quenched by oxygen, permanent changes in the ground state absorption spectra of MWL samples are observed suggesting the possibility of another degradation mechanism not involving the triplet manifold. As was seen in section 4.1, photochemically induced bond cleavage of α-carbonyl β-O-4, and non-carbonyl α-O-4 linkages present in the lignin structure (leading to the production of phenoxy and other free radical species) can take place via the singlet state, the radicals may then deactivate to ultimately generate yellow photoproducts. Also, biphenyl strictures have been found to be susceptible to photodegradation as shown by Forsskahl[107] for 2,2' dihydroxy- 3,3'-dimethoxy-5,5'-dimethylbiphenyl in dimethoxyethane under steady state irradiation conditions and Castellan who studied a series of biphenyl derivatives adsorbed onto lignin free paper[204]. Phenolic groups which absorb above 300 nm (the cut-off wavelength of the suns radiation at ground level) may also be a source of phenoxy radicals via direct photolysis[205,206] which can then deactivate by, possibly, reaction with ground state oxygen to form yellow photoproducts.

The differing roles of singlet oxygen in the ultimate production of yellow photoproducts of MWL have been considered by many authors[107,109,207]. Quenching of singlet oxygen via a hydrogen atom abstraction reaction with phenolic hydroxyl hydrogen atoms to yield phenoxy radicals has been proposed as a deactivation pathway for singlet oxygen[111,112]. However, no evidence in support of this mechanism from the singlet oxygen luminescence data was obtained, the singlet oxygen radiative lifetime was unaffected by the nature of the sensitizer (MWL or α-(2-methoxyphenoxy)-3,4-dimethoxyacetophenone). This may simply be due to the low concentration of phenolic hydroxyl moieties in the solution, other deactivation pathways for singlet oxygen such as electronic-vibrational energy transfer into the vibrational energy levels of solvent molecules or other lignin bonds of appropriate energy (around 7880 $cm.^{-1}$)[208] competing favourably with radical formation.

5.5 Diffuse Reflectance Laser Flash Photolysis Studies Of Milled Wood Lignin Adsorbed Onto Microcrystalline Cellulose

The mobility of molecules and dissolved gasses within a solvent based sample can lead to high quenching rate constants for such processes as oxygen quenching (section 5.4.4) and hydrogen atom abstraction (section 5.4.3) ultimately leading to the degradation of the MWL sample. However, in the rigid cross-linked environment of the pulp fibre, the mobility of even small molecules such as oxygen is severely restricted and therefore, photochemical degradation is likely to take place more via static rather than diffusional quenching processes.

A logical progression from the work detailed above was to examine the effect upon the photochemistry of MWL when placed in an environment where diffusional processes become restricted due the nature of the support material. The ground state diffuse reflectance spectra of pure microcrystalline cellulose (section 3.5) and a sample of MWL (ca. 5.5 mg.g.$^{-1}$ of cellulose) adsorbed onto the microcrystalline cellulose are shown in figure 5.20:-

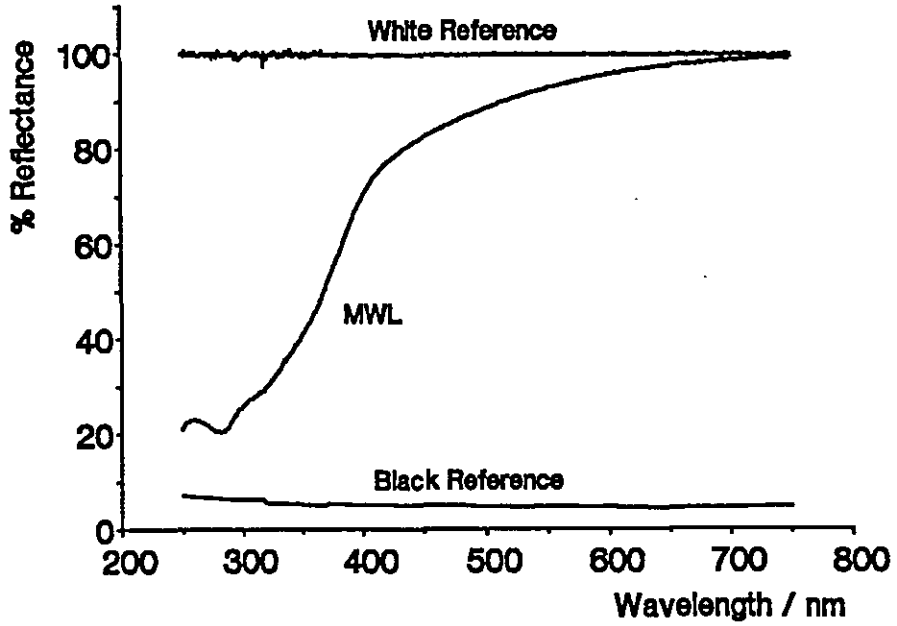

Figure 5.20:- Ground State Diffuse Reflectance Spectra of Microcrystalline Cellulose and MWL (ca. 5.5 mg.g.$^{-1}$ of cellulose) Adsorbed onto Microcrystalline Cellulose Support

The MWL sample was adsorbed onto the cellulose from a concentrated solution of MWL in 1,4-dioxane, the excess solvent/MWL being removed by filtration through a sintered glass filter. This method of adsorption was found to produce a more homogeneous sample relative to the method employed for lignin model compounds adsorbed on cellulose outlined in section 3.5. The corresponding Kubelka-Munk spectra are shown in figure 5.21.

As can be seen in figure 5.21, the Kubelka-Munk spectrum of MWL adsorbed on microcrystalline cellulose is almost identical to the absorption spectrum observed in 1,4-dioxane solution, a λ_{max} at ca. 280 nm and a broad absorption tail stretching to approximately 450 nm which gives the sample a pale yellow appearance.

The transient difference spectrum for a sample of MWL absorbed onto microcrystalline cellulose measured by diffuse reflectance laser flash photolysis (λ_{ex} = 354.7 nm) at three time delays following the laser pulse are shown in figure 5.22.

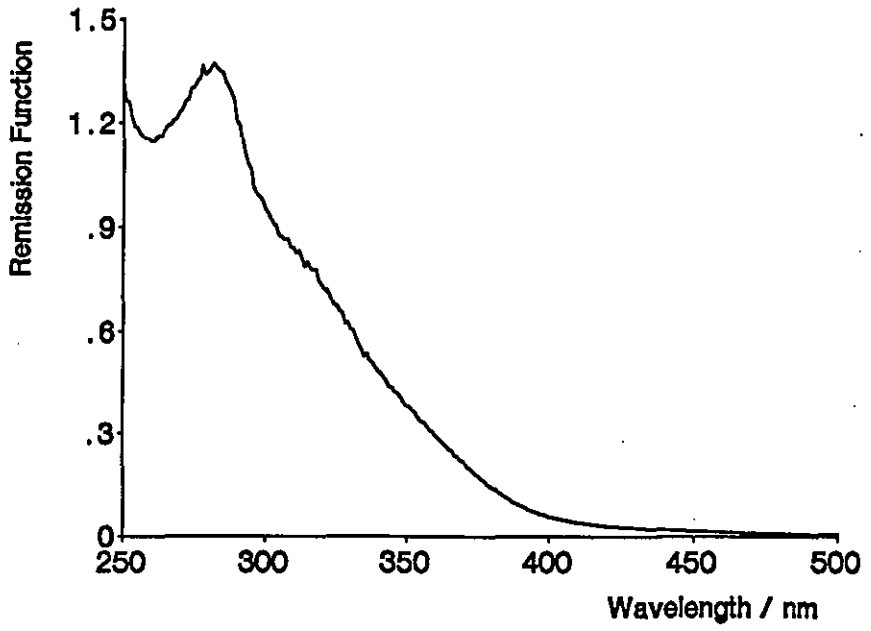

Figure 5.21:- Kubelka-Munk Spectra of Microcrystalline Cellulose and MWL (ca. 5.5 mg.g.$^{-1}$ of cellulose) Adsorbed onto Microcrystalline Cellulose

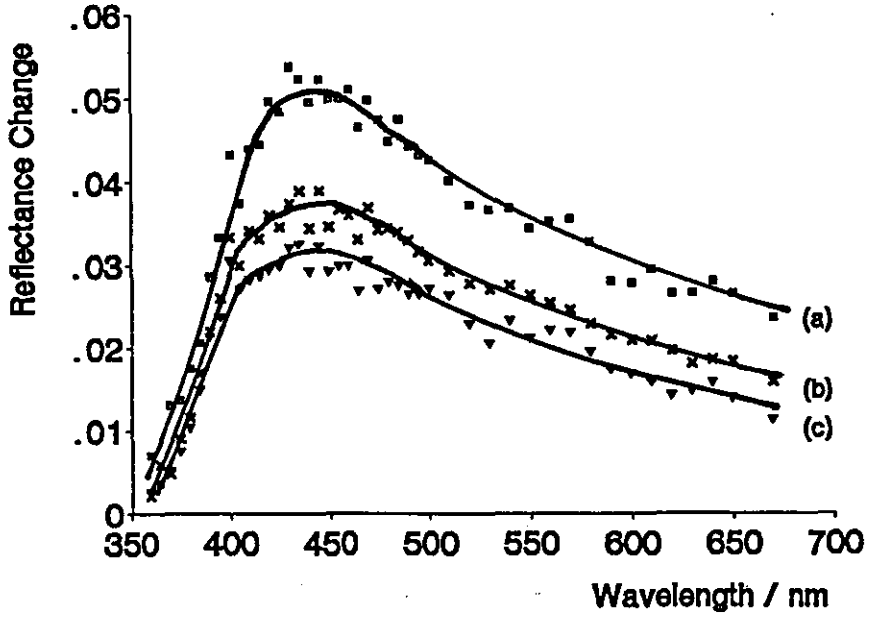

Figure 5.22:- Transient Different Spectrum of MWL Absorbed onto Microcrystalline Cellulose Spectra were recorded at time delays (a) 8.4 μs, (b) 87.5 μs and (c) 190 μs after the laser pulse

The λ_{max} of the transient absorption is located at ca. 440 nm and is independent of the time delay following the laser pulse. The spectrum is characterised by a broad structureless absorption band extending to wavelengths greater than 650 nm. The shape of the transient absorption spectrum is similar to that observed for the triplet-triplet absorption spectrum of MWL in 1,4-dioxane solution (section 5.4.2), the λ_{max} being bathochromically shifted by ca. 15 nm when adsorbed onto microcrystalline cellulose. The transient difference spectrum shows no dependence of λ_{max} with time following the laser pulse up to delays of ca. 200 μs suggesting that the transient absorption up to this time after the laser pulse (and on longer delays) is due to a single absorbing species. The decay of the transient follows complex kinetics reflecting the heterogeneity of both the absorption sites on the cellulose surface[209] and also the nature of the MWL sample itself.

A transient kinetic decay trace (analysing at 450 nm) built up by measuring the transient absorption on four digitiser timescales between 40 ns per point and 2 μs per point is shown in figure 5.23:-

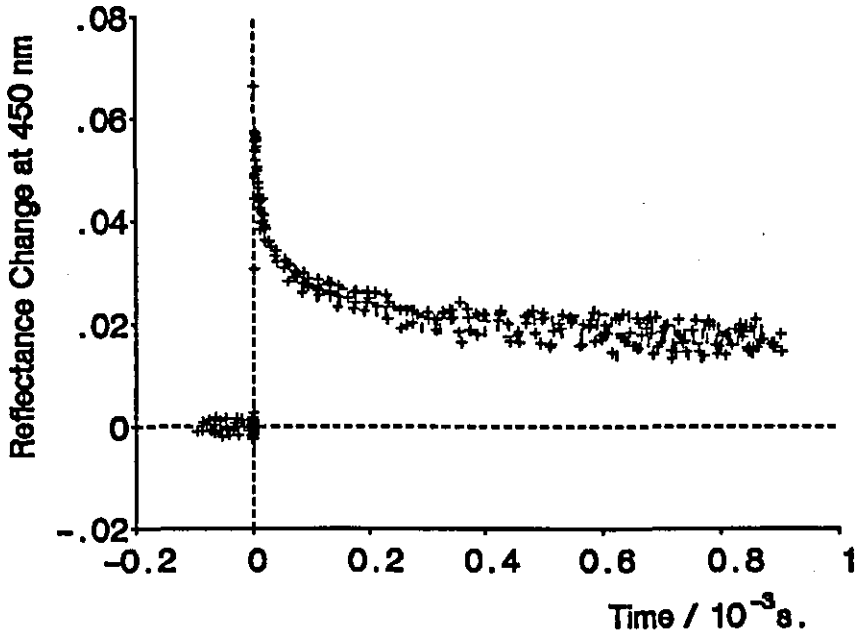

Figure 5.23:- Decay of the Transient (analysing at 450 nm) Observed Following Laser Excitation of MWL Adsorbed Onto Microcrystalline Cellulose

An estimate of the first, second and third empirical half-lives ($t_{1/2}$) for the transient were obtained by the following method; The reflectance change at zero time after the laser pulse (ie. $\Delta J(0)/J(0)$) (see section 3.8.2) was estimated from the fast kinetic traces, and the baseline offset (due to permanent absorption changes at 450 nm induced by laser damage to the sample) was estimated from the longest timescale measurements. The first, second and third empirical half-lives were found to be 11.6μs, 66.2μs and 93μs respectively emphasising the non-exponential

decay of the transient absorption signal.

From the shape and position of the λ_{max} of the transient spectrum relative to that in 1,4-dioxane solution, the transient is assigned as due to absorption by the lowest lying triplet state of MWL. The red shifted λ_{max} (relative to MWL triplet in 1,4-dioxane) is attributed to the adsorption of the MWL onto the cellulose surface. A similar phenomenon was also observed for the lignin model compound 3,4-dimethoxyacetophenone when absorbed onto microcrystalline cellulose as seen in section 4.4. The transient difference spectrum shows no change of λ_{max} with time except in intensity (in contrast to MWL in 1,4-dioxane solution) and may be attributed to the inability of reactive chromophores to diffuse together on the cellulose surface. The extended lifetime of the observed triplet states relative to the solution phase can, in part, be attributed to the properties of the support material which is able to protect (especially when moisture is removed) none chemically reactive triplet states from quenching by molecular oxygen[157,160]. The fact that the transient absorption does not return to the pre-trigger light level is indicative of the sample degrading following laser excitation. This suggests that some irreversible photodegradation of the sample is taking place either via triplet sensitization to generate radical species which form yellow photoproducts or, from other degradation pathways which do not proceed through the triplet state manifold such as direct photolysis of none α-carbonyl chromophores absorbing at 354.7 nm or singlet state α-carbonyl sensitized bond cleavage of β-O-4 aryl-ether bonds present in the lignin macromolecule.

5.6 Conclusions

The photochemistry of MWL in 1,4-dioxane has provided much useful information on the photodegradation processes involved in the photoyellowing of lignin. The transient difference spectrum assigned to absorption by the lowest lying triplet state(s) of α-carbonyl moieties present in MWL has been observed for the first time and identified on the strength of its ability to sensitize singlet molecular oxygen. An estimate of the triplet quantum yield (Φ_T^{MWL}) following laser excitation at 354.7 nm has also been obtained relative to that of benzophenone. Following decay of the triplet, a long lived transient species whose lifetime is unaffected by the presence of oxygen has been assigned as absorption due to free radical species produced by triplet α-carbonyl hydrogen atom abstraction of phenolic hydroxyl hydrogen atoms or via other mechanisms such as α-carbonyl excited singlet state homolytic cleavage of β-O-4 linkages present in the MWL sample. Other mechanisms such as direct photolysis of biphenyl, phenolic hydroxyl and α-O-4 linkages present in the MWL sample are also possible mechanisms which lead to photoyellowing since quenching of a high percentage of the MWL triplets by oxygen fails to prevent permanent chemical and structural changes in the lignin macromolecule in solution. Adsorption of MWL onto microcrystalline cellulose has demonstrated that a bathochromic shift in the transient absorption spectrum of MWL in a restricted environment is similar to the one observed for lignin model compounds adsorbed onto microcrystalline cellulose. A single transient species with λ_{max} at ca. 440 nm is observed which decays by complex kinetics. The spectral shape and λ_{max} of the transient absorption is similar to that of the triplet state of MWL in 1,4-dioxane solution, bathochromically shifted due to interactions (eg. hydrogen bonding[156]) with the support material. The bathochromic shift in λ_{max} and the lack of observation of transient species which can be assigned to the absorption by free radicals from MWL when absorbed onto cellulose serve

to emphasise the important role of the environment in which such as sample is studied, marked differences in the photochemical behaviour being observed between the solution and solid phase. As we will see in chapter 6, the significance of these observations will become apparent when attempting to interpret transient reflectance data observed from samples of thermomechanical pulp itself where lignin is present in its natural environment as part of the pulp fibre.

Chapter 6

Photochemistry of High Yield Thermomechanical Pulp

6 Photochemistry Of High Yield Thermomechanical Pulp

6.1 Introduction

As has been seen in chapters 4 and 5, much useful information concerning assignment and behaviour of chromophores believed to be involved in the photoyellowing processes of lignin can be obtained from lignin model compounds and MWL in both the solution and solid phases. However, it must be borne in mind that the behaviour of such chromophores within the three dimensional heterogeneous thermomechanical (TMP) fibre may be considerably modified due to the very nature of the material itself. Study of the photochemistry of such moieties actually within their native environment is therefore essential for understanding of the photodegradation processes involved. The development and application of time resolved diffuse reflectance laser flash photolysis has proved a powerful analytical tool in the study of such systems (see for example reference 210 and references therein). The first observation of short-lived transient species obtained following pulse laser excitation of bleached TMP at 354.7 nm have recently been observed in Loughborough and published in the literature[37,211]. Preliminary results concerning the effects of oxygen, phenolic hydroxyl content, sodium borohydride reduction and peroxide bleaching upon the photochemistry of TMP samples were obtained. Based upon this evidence, the assignment of the observed transient species was that of the triplet state of α-carbonyl moieties present in the lignin macromolecular component of the TMP fibre.

The aims of the work described here were to study these effects more closely and attempt to correlate the observed transient data with that observed for MWL and appropriate lignin model compounds studied in solution and adsorbed onto microcrystalline cellulose. The studies detailed below were performed on TMP samples in two forms; powdered, and optically thick hand sheets (see section 3.3). Direct comparison of TMP in these two forms demonstrated that there was no difference in optical properties provided that the powdered samples were packed

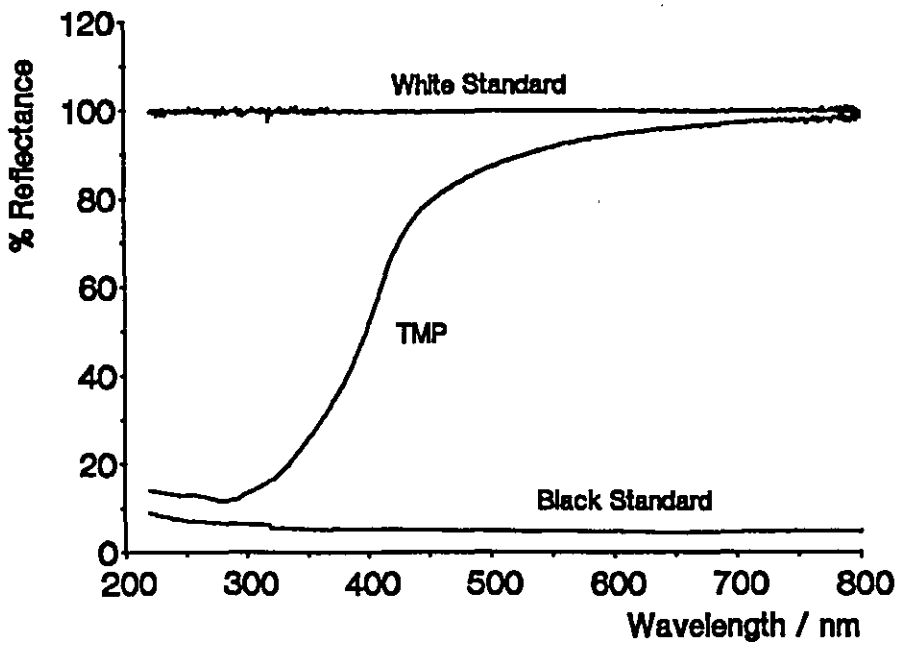

Figure 6.1:- Ground State Diffuse Reflectance Spectrum of Peroxide Bleached TMP

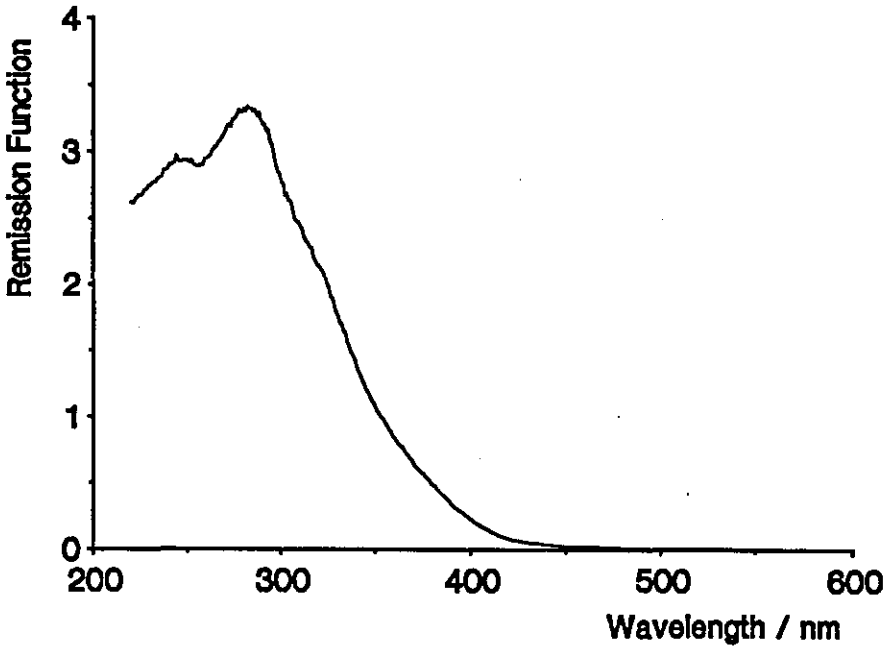

Figure 6.2:- Kubelka-Munk Spectrum of Peroxide Bleached TMP

into cuvettes at sufficient packing density to ensure optically thick samples at all wavelengths of study. The ground state diffuse reflectance spectrum of an optically thick peroxide bleached TMP hand sheet is shown in figure 6.1 measured relative to barium sulphate. The spectrum is characterised by a broad structureless decrease in reflectance upon going from 700 nm to 300 nm. Below 300 nm, strong absorption by the sample is observed reflecting the aromatic nature of the lignin component of the TMP sample. The corresponding Kubelka-Munk spectrum is shown in figure 6.2. The weak absorption above 400 nm for such samples give them their slightly yellow appearance. A Kubelka-Munk Remission Function value ($F(R_\infty)$) of ca. 3 at 300 nm is observed corresponding to absorption of approximately 88 % of the light at that wavelength. An absorption maximum located at ca. 280 nm is observed which is typical for lignocellulosic materials (see section 5.1 for details). Some of the problems associated with measuring ground state diffuse reflectance spectra at wavelengths below 300 nm have been discussed in section 4.3 of this thesis. In addition to the non-ideal behaviour of the white and black reflectance standard at these wavelengths, the fluorescent nature of the lignin fraction of the TMP sample (see section 5.3 and section 6.2 below), which is collected with equal efficiency to the diffusely reflected light by the integrating sphere may result in a small distortion effect upon the absolute shape of the reflectance spectrum. However, it is anticipated that this is not sufficient to significantly effect the position of the absorption maximum observed in Kubelka-Munk Remission spectrum shown in figure 6.2 (it is worthy of note that absorption maxima for MWL in 1,4-dioxane solution and when adsorbed onto microcrystalline cellulose are, within experimental error, identical as shown in figures 5.1 and 5.21).

6.2 Steady State Fluorescence Spectra of Bleached Thermomechanical Pulp

Other authors have investigated the effect of photoyellowing upon the fluorescence intensity and spectra observed from TMP[212,213].

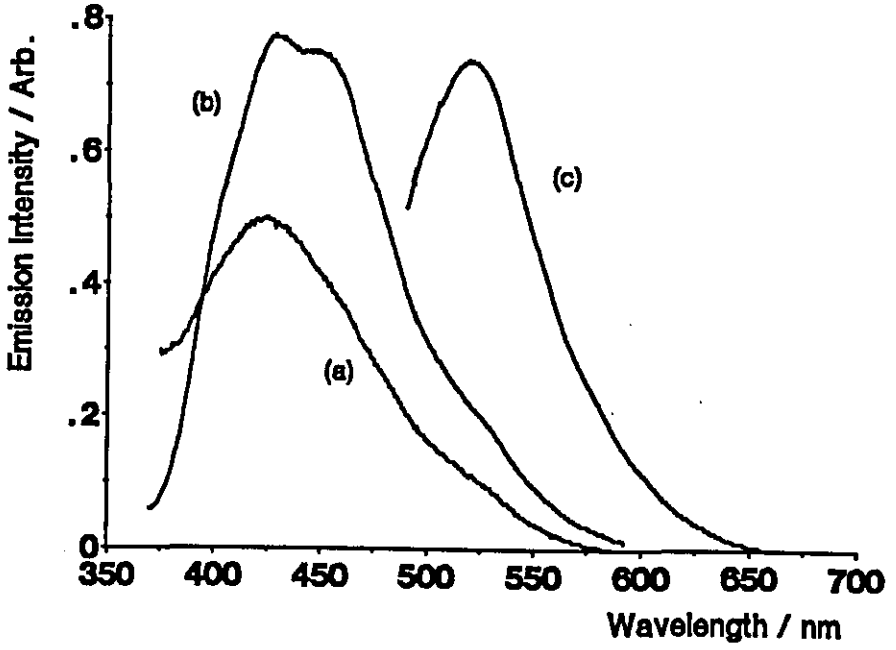

Figure 6.3:- Uncorrected Fluorescence Spectra Observed for Bleached TMP exciting at (a) 300 nm, (b) 350 nm and (c) 450 nm

It was found that, following peroxide bleaching, a large increase in the emission intensity is observed off-setting the yellowness of the bleached TMP samples. Uncorrected fluorescence spectra observed for the bleached TMP used in the present study exciting at 300 nm, 350 nm and 450 nm are shown in figure 6.3. As can be seen, excitation at 450 nm, where only weak ground state absorption is observed, yields an easily observable fluorescence emission spectrum with λ_{max} located at ca. 520 nm. Excitation at 300 nm yields a fluorescence maximum at 420 nm whereas, following excitation at 350 nm, two fluorescence peaks of almost equal intensity are observed at 435 nm and 445 nm. The variation of position of the fluorescence λ_{max} cannot be attributed to a Raman scattering effect but rather serves to reiterate the observations in section 5.3 for MWL in 1,4-dioxane solution; ie., that the fluorescence λ_{max} changes with excitation wavelength as a direct result of excitation of a number of fluorescence yielding chromophores all of which are present with differing environments within the lignin macromolecule. The chromophores responsible for the observed emission have, so far, not been clearly identified, although studies of the fluorescence spectra observed from lignin model compounds have been documented in the literature[174,175].

The prompt emission with λ_{max} at 425 nm and 445 nm obtained following 354.7 nm laser excitation of TMP samples has the undesired effect of preventing the determination of transient absorption spectra at time delays less that ca. 150 ns following the laser pulse due to the overload and recovery of the photomultiplier detector used in such experiments.

6.3 Diffuse Reflectance Laser Flash Photolysis Studies of Thermomechanical Pulp

Due to the susceptibility of TMP to undergo photoreversion following laser excitation at 354.7 nm, the transient difference spectra detailed below were recorded using a fresh sample of TMP for each transient absorption measurement. As we will see later, contrary to previous initial observations[211], the intensity of the laser induced reflectance change observed at 450 nm at given time t following the laser pulse ($\Delta J(t)/J(0)$) falls off initially at a fast rate and then levels off to a signal size of approximately 60 % of its original intensity following approximately 400 laser pulses (pulse energy = 18 mJ.cm.$^{-2}$ per pulse).

The transient different spectrum obtained following 354.7 nm pulsed laser excitation of TMP is shown in figure 6.4 at two time delays following the laser pulse. The spectra were recorded using a single laser shot for each point in the absorption spectrum to eliminate any accumulative effects due to product build-up/sample degradation. At all time delays following the laser, the spectrum has a λ_{max} located at ca. 450 nm with a broad structureless absorption extending to wavelengths beyond 700 nm. At wavelengths below 450 nm, the transient absorption signal decreases rapidly with wavelength as a consequence of increased TMP ground state absorption. As with MWL, the transient decays via complex non-exponential kinetics typical of a heterogeneous population of excited states[214]. Under air equilibrated conditions, the transient decay can be followed to time delays approximately 0.25 s after the laser pulse. Even at such long times, the transient signal fails to recover to the pre-laser absorption level at all analysing wavelengths due to build-up of photoproducts which absorb over a broad wavelength range between 350 nm and 700 nm. The ground state diffuse reflectance spectrum of a fresh TMP sample and a TMP sample which had been photoyellowed by exposure to 400 laser pulses is shown in figure 6.5.

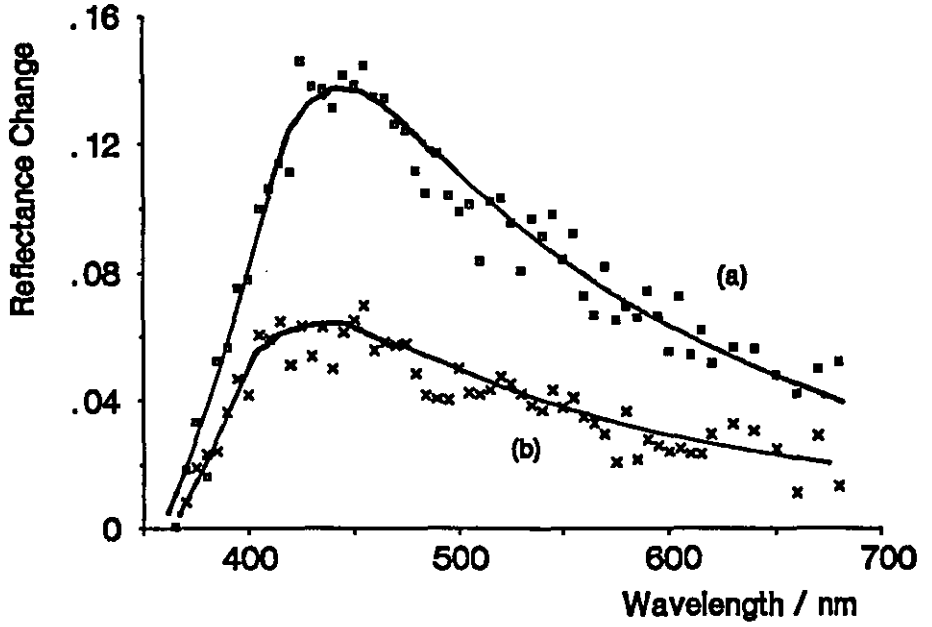

Figure 6.4:- Transient Different Spectrum of Bleached TMP at Two Time Delays Following the Laser Pulse. Time Delays are (a) 8 μs and (b) 100 μs

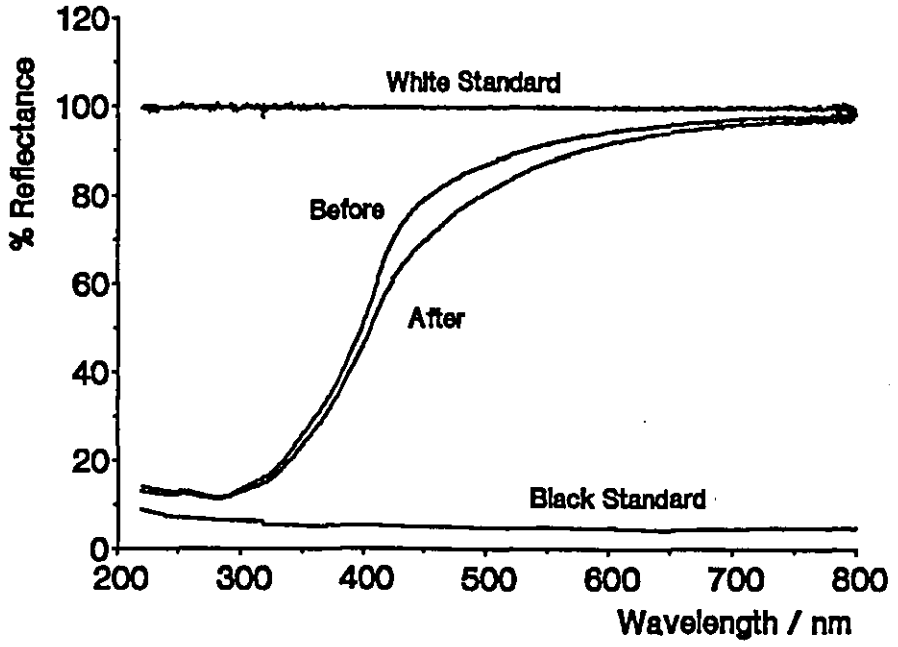

Figure 6.5:- Ground State Diffuse Reflectance Spectra of TMP Before and After Exposure of the Sample to 400 Laser Pulses

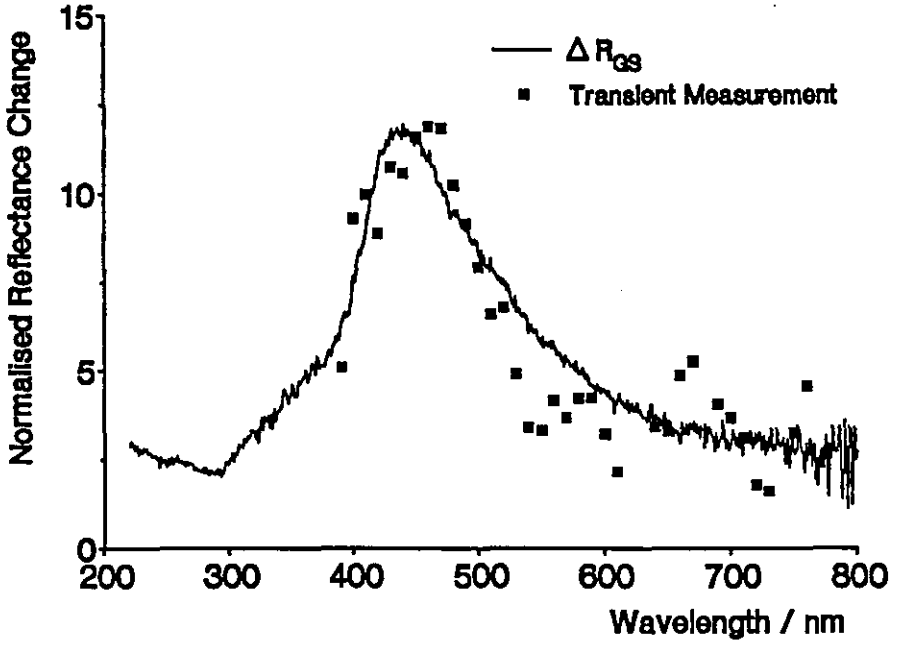

Figure 6.6:- Ground State Difference Reflectance Spectrum (ΔR_{GS}) and Residual Single Shot Transient Absorption Measurements Recorded ca. 0.25 s After the Laser Pulse.

The ground state difference reflectance spectrum (ΔR_{GS}), obtained by subtracting the reflectance spectrum of the damaged TMP sample from that of the unphotolysed sample, is shown in figure 6.6 together with the residual single shot transient absorption measurements recorded ca. 0.25 s. after the laser pulse. The relative intensities of the two spectra have been normalised for ease of comparison. As can be seen, the residual transient absorption follows that of the ΔR_{GS} spectrum inferring that they are one and the same absorption and not attributable to a very long lived transient species. The ΔR_{GS} spectrum has a λ_{max} at ca. 440 nm which gives the photodegraded TMP its characteristic yellow appearance.

The photoyellowing process leads to an absolute increase in absorption at the excitation wavelength of some 3 % to 4 % (see figure 6.6). The increased absorption at this wavelength does not, however, affect the observed transient difference spectrum observed from a thoroughly photoyellowed TMP sample, the observed spectrum simply being reduced in intensity relative (by ca. 40 %) to that observed from a fresh TMP sample. This decrease can be interpreted as due to both an inner filter effect of the yellow TMP degradation products and also by a consumption (by photochemical reaction) of the chromophores giving the transient absorption signal. Assuming that the yellow TMP degradation products are formed with the same distribution within the pulp fibre as the chromophores that are consumed, then the magnitude of the decrease in the transient absorption signal is too large to be explained simply by an inner filter effect. Even if the coloured moieties were formed preferentially at the surface of the TMP sample (perhaps as a result of oxygen accessibility), the decrease in the intensity of the transient signal is still too large to be accounted for by a inner filter phenomenon alone. Thus, it is concluded that some consumption of laser absorbing chromophores is taking place.

6.3.1 Effect of Oxygen on the Thermomechanical Pulp Transient Decay Kinetics

The quenching of aromatic α-carbonyl triplet states by molecular oxygen has been shown to be an efficient process in solution for both lignin model compounds and MWL. The mobility of oxygen and accessibility of triplet carbonyls to quenching processes involving oxygen within the TMP fibre is greatly reduced due to the densely packed three dimensional cross-linked nature of the lignin-cellulose macromolecule. In an earlier publication[211], an increase in the intensity of the transient reflectance change (observed at 450 nm) of some 20 % was observed following the removal of oxygen from a TMP sample relative to that observed for a TMP sample under atmospheric conditions. Under these conditions, no evidence of dynamic quenching of the transient signal was observed, the reduction in the intensity of the transient being attributed to static quenching processes requiring no diffusion of oxygen to the site of photochemical reaction. However, under enhanced oxygen atmospheres, dynamic quenching of the TMP transient by oxygen is observed. The samples used in the study were prepared in the following way; powdered TMP was packed into a quartz cuvette and then thoroughly degassed by evacuating the sample to a pressure of ca. 8×10^{-5} mBar. The sample remained exposed to the vacuum line for at least 3 hours to ensure that all moisture and oxygen was removed from the TMP fibres. Either pure oxygen or nitrogen were introduced

into the cuvettes in a similar fashion to that detailed in section 5.4.4, to a pressure above the TMP sample of approximately 2 Bar.

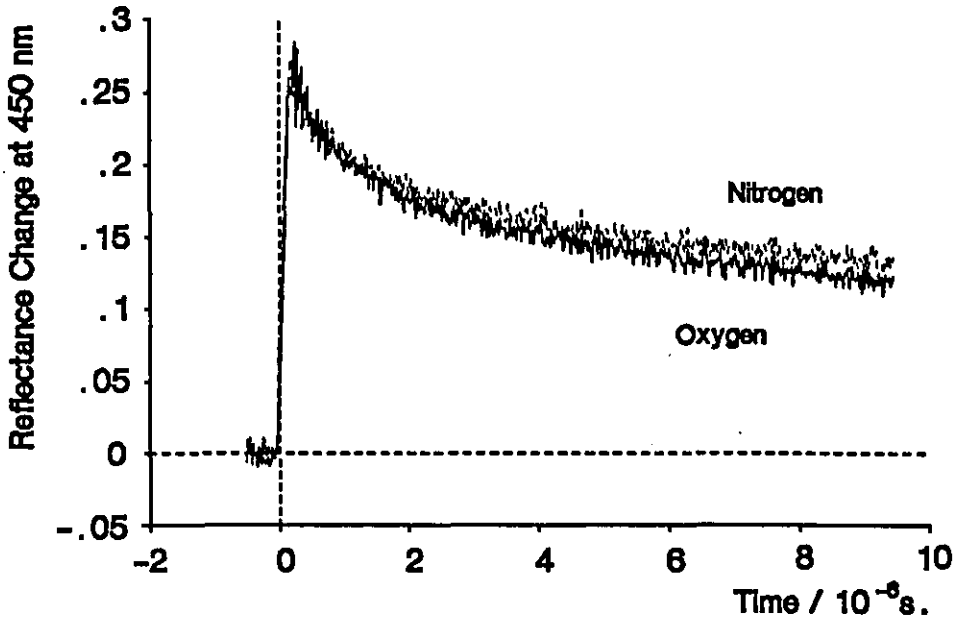

Figure 6.7:- Transient Kinetic Decay (Analysing at 450 nm) for a Sample of TMP under a 2 bar Atmosphere of Oxygen or Nitrogen on a Digitiser Setting of 20 ns per Point

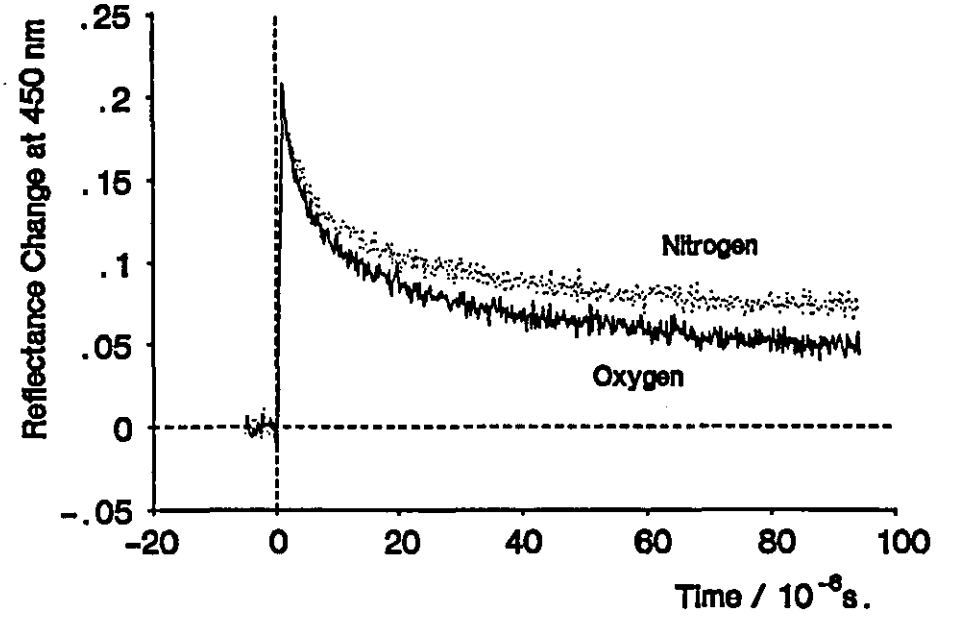

Figure 6.8:- Transient Kinetic Decay (Analysing at 450 nm) for a Sample of TMP under a 2 bar Atmosphere of Oxygen or Nitrogen on a Digitiser Setting of 200 ns per Point

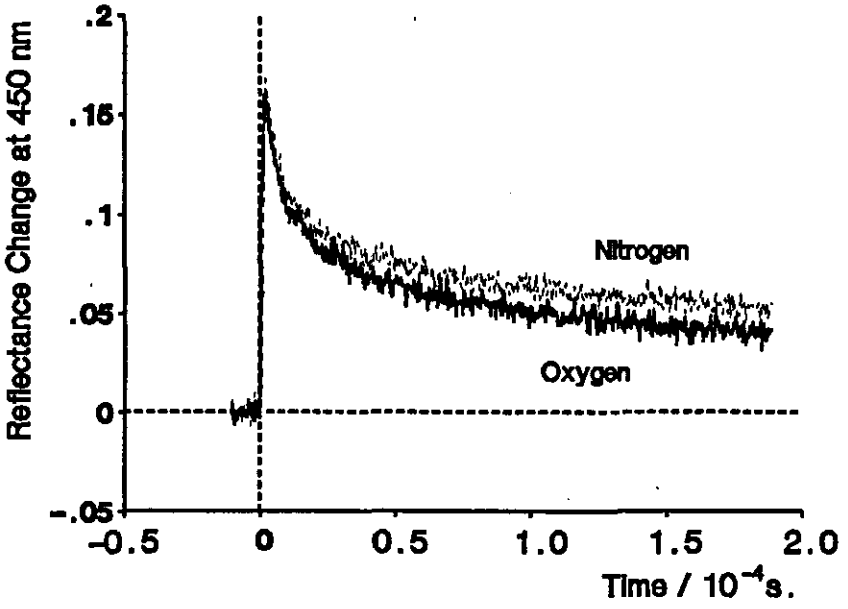

Figure 6.9:- Transient Kinetic Decay (Analysing at 450 nm) for a Sample of TMP under a 2 bar Atmosphere of Oxygen or Nitrogen on a Digitiser Setting of 400 ns per Point

The transient kinetic decay of samples of TMP under such oxygen and nitrogen atmospheres are shown in figures 6.7 to 6.9 on three different digitiser timescales. The data was obtained with a 450 nm interference filter over the entrance slit of the monochromator to minimise the prompt emission overload of the photomultiplier at short times after the laser pulse. As can be seen in figure 6.7, the transient signal intensity for both oxygen and nitrogen TMP samples at short timescales are, within experimental error, identical suggesting that static quenching of the transient (or its precursor) is not significant in this system. It must be noted however, that reliable transient kinetic data cannot be obtained on timescales less than approximately 150 ns after the laser pulse and it is on these timescales that fast static quenching processes are likely to be taking place. As can be seen, the kinetics of the decay of the transient in the presence of oxygen are slightly quicker than those for nitrogen equilibrated samples, suggesting the presence of dynamic quenching for this system under enhanced oxygen atmospheres. Whether this can be attributed to penetration of oxygen into the pulp fibre or simply due to more efficient quenching of excited states generated on or near the surface of the fibre has not been established. As has been mentioned previously, the transient decay for both samples is non-exponential but can be quantified according to their empirical half-lives, $t_{1/2}$. An estimate of the transient reflectance change at zero time after the laser pulse ($\Delta J(0)/J(0)$) was obtained from data recorded on a timescale of 4 ns per point. The intensity of the signal following decay of the transient at long time delays after the laser pulse (to obtain the residual permanent absorption due to photoyellowing) was obtained for the current set of samples by a similar method to that detailed in section

5.5. The first, second and third empirical half lives for DRY TMP under oxygen and nitrogen atmospheres are tabulated in table 6.1:-

	Transient Empirical Half Life / μs		
Sample	1st	2nd	3rd
TMP + Nitrogen	5.8	140	>1000
TMP + Oxygen	4.5	32.5	127.5

Table 6.1:- First, Second and Third Empirical Half-lives for Dry TMP Under Oxygen and Nitrogen Atmospheres

The accuracy of the half-lives quoted in table 6.1 are prone to some errors such as the estimation of the transient reflectance change at zero time after the laser pulse and also that of the residual absorption following total decay of the transient species. The data does however, together with figures 6.7 to 6.9, demonstrate clearly that dynamic quenching of the TMP transient species by molecular oxygen is indeed occurring when enhanced oxygen atmospheres are placed above the TMP sample.

In a separate experiment, TMP samples were saturated with water and then bubbled overnight with a stream of oxygen or nitrogen to investigate the effects of TMP fibre swelling on the empirical half-life of the transient species. The observed first empirical half-lives obtained for oxygen and nitrogen saturated WET TMP samples were found to be 0.65 μs and 0.9 μs respectively. Subsequent half-lives were also found to be susceptible to the presence of dissolved oxygen in the water. The large decrease in first empirical half-lives for such samples with or without the presence of oxygen may be attributed to the following:-

(a) The TMP readily absorbs water leading to swelling of the pulp fibre matrix. Dissolved oxygen will therefore be able to penetrate into the wet bulk fibre more easily thus enhancing quenching of the laser induced excited α-carbonyl triplet states.
(b) Swollen pulp fibres allow greater mobility of chromophoric moieties and therefore make deactivation (by photochemical reversible or non-reversible reaction pathways) more efficient. This postulate is applicable to pulps with and, especially without, the presence of dissolved oxygen in the water.

The overall net effect is a large decrease (by ca. a factor of 10) in the observed transient first empirical half-lives for both oxygen and nitrogen saturated wet TMP samples relative to those observed for TMP under dry conditions.

From previous studies, the intensity of the TMP transient signal was shown to decrease in proportion with the extent of sodium borohydride reduction of the TMP. This, coupled with the dynamic quenching of the transient signal by molecular oxygen[215] detailed here are consistent with assignment of the observed transient as due to absorption by the lowest lying triplet states of the aromatic α-carbonyl moieties present in the pulp fibre. The λ_{max} of the transient is red shifted by over 80 nm relative to the λ_{max} for triplet-triplet absorption

of a lignin model compound (3,4-dimethoxyacetophenone) in benzene solution. However, we have observed a progression of red shifted λ_{max} for 3,4-dimethoxyacetophenone when placed in polar solvents (λ_{max} in acetonitrile = 385 nm) and adsorbed onto microcrystalline cellulose (λ_{max} = 400 nm). Milled wood lignin also shows a similar trend, the λ_{max} for the α-carbonyl triplet state being located at 425 nm and 440 nm in 1,4-dioxane solution and when adsorbed onto microcrystalline cellulose respectively. The extra 10 nm red shift in the λ_{max} observed for lignin α-carbonyl triplet state moieties when part of the TMP fibre can therefore be attributed to the heterogeneous nature of the sample itself.

6.3.2 Effect Of Methoxylation Of Thermomechanical Pulp

In a previous study[211], the change in reflectance following pulsed laser excitation of an optically thick fully methoxylated TMP handsheet was shown to increase by approximately 30 % relative to an unmodified TMP sample. The increase in signal intensity was attributed as due to the removal of phenolic hydroxyls from the lignin structure effectively blocking one of the deactivation pathways for the α-carbonyl triplets formed by the laser pulse. Due to the rigid nature of the lignin matrix, such triplet state quenching processes are believed to occur purely via a static quenching mechanism, the rate of which is too fast to be observed by our nanosecond apparatus due to the fluorescent nature of the TMP samples preventing detection of transient species at times less than ca. 150 ns.

The present study was aimed at extending this initial observation to a series of TMP samples of varying methoxyl content and also to examine the effect of methoxylation upon the observed transient different spectrum and also the kinetics of transient decay observed from such samples. The methoxylation process and quantification of the TMP samples was achieved as detailed in section 3.3.1. The experiments were carried out using powdered TMP packed into quartz cuvettes to give an optically thick packing density. In all cases, the ground state diffuse reflectance spectra observed for these samples were identical within experimental error. Untreated TMP was found to have a phenolic hydroxyl content of 0.128 per C_9 phenylpropane lignin unit (see section 3.3.1), a value approximately 30 % larger than the one reported previously by Yang and Goring for Black Spruce wood[216] and was attributed by Heitner *et al*[217] as due to the formation of phenolic hydroxyl groups during the preparation of the bleached TMP. The methoxyl content of untreated TMP was determined to be 4.44 % by mass. If only phenolic hydroxyl groups were methoxylated then the total methoxyl content should rise to ca. 4.93 %. However, it was found that even with a methoxyl content of 8.13 % by mass, some phenolic hydroxyl moieties were still present in the pulp sample. This can be rationalised by the dimethyl sulphate methoxylation process being non-specific to phenolic hydroxyl groups, ie., methoxylation of acidic hydroxyl groups of the cellulose and lignin structure is also taking place. A plot of the TMP phenolic hydroxyl content as a function of methoxyl content for the series of samples studied is shown in figure 6.10, the data being tabulated in table 6.2.

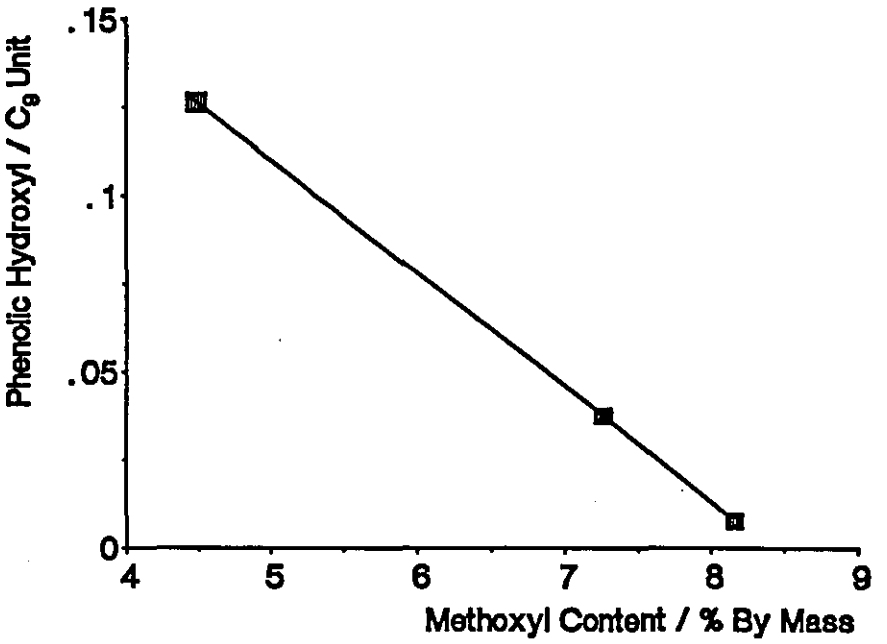

Figure 6.10:- A Plot of TMP Phenolic Hydroxyl Content as a Function of Methoxyl Content for a Series of TMP Samples

From the limited data available, a linear relationship between methoxyl content by mass and phenolic hydroxyl content per C_9 lignin unit is observed for the TMP samples studied in these experiments. From the intercept on the x-axis, a methoxyl content ca. 8.4 % by mass is predicted to be required to obtain total removal of phenolic hydroxyl moieties from the TMP sample. As mentioned previously, a TMP sample with a methoxyl content of 13.65 % by mass gave an increase in transient signal observed following laser excitation of some 30 %. As can be seen in figure 6.10, this methoxylated TMP (ie. some 5 % higher than the predicted point were all phenolic hydroxyl moieties had been chemically modified) was correctly assumed to be consistent with total removal of phenolic hydroxyl moieties from the pulp fibre.

	Bleached TMP	TMP Modified With Dimethyl Sulphate	
Methoxyl Content (% By Mass)	4.44 %	7.23 %	8.13 %
Phenolic Hydroxyl / C_9 Lignin Unit	0.128± 0.002	0.039± 0.004	0.0091± 0.0008

Table 6.2:- TMP Phenolic Hydroxyl Content as a Function of Methoxyl Content for a Series of TMP Samples

The transient different spectra for the three samples of TMP detailed in table 6.2 are shown in figure 6.11 at a delay of 3 μs following the laser pulse.

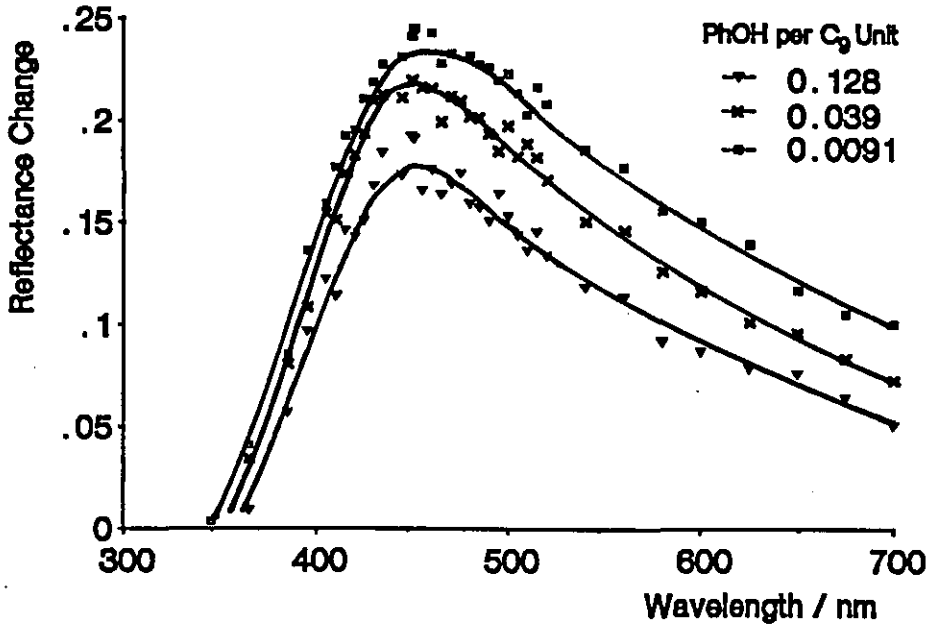

Figure 6.11:- Transient Difference Spectra for Three Samples of TMP with Differing Phenolic Hydroxyl Contents (as detailed in table 6.2) at a Delay of 3 μs Following the Laser Pulse.

Except for the intensity of the observed signal, the spectra are identical in both shape and λ_{max} (ca. 450 nm). Within experimental error, the kinetics of the decay of the transient species on the timescale required to obtain the transient spectra shown in figure 6.11 (ie. 3 μs) are identical irrespective of pulp methoxyl content. The relative intensities observed in figure 6.11 (analysing at 450 nm) of the laser induced transient reflectance change at zero time after the laser pulse ($\Delta J(0)/J(0)$) are shown in table 6.3:-

Phenolic Hydroxyl Content / C_9 Unit	Methoxyl Content (% by mass)	Relative $\Delta J(0)/J(0)$ (Analysing at 450 nm)
0.128	4.44	1.00
0.039	7.23	1.19
0.0091	8.13	1.29

Table 6.3:- Relative Intensities (analysing at 450 nm) of the Laser Induced Transient Reflectance Change ($\Delta J(0)/J(0)$) at Zero Time After the Laser Pulse for a Series of samples of TMP with Varying Degrees of Methoxylation

These results confirm those observed previously where a 30 % increase in size of the transient signal was observed for fully methoxylated TMP. The observation of such an increase may be explain in one of two ways:-

(a) Reduction in the number of phenolic hydroxyl moieties reduces the amount of quenching of the precursor to the α-carbonyl triplet state and therefore leads to a greater population of detected triplet states.
(b) Phenolic hydroxyl moieties statically quench the carbonyl triplets on timescales faster than those available in these experiments (ca. 150 ns due to the fluorescent nature of the TMP samples) resulting in less detected triplet states.

The first postulate would require an extremely high quenching rate constant to compete with rate constants for intersystem crossing of aromatic α-carbonyl moieties. For example, (although not directly comparable to α-carbonyl moieties in the lignin macromolecule) the intersystem crossing rate constant for benzophenone and 3,4-dimethoxyacetophenone in solution have been observed to be extremely fast processes with rate constants of the order of 10^{11} s.$^{-1}$[218]. Also, intersystem crossing rate constants of the same order have been measured for microcrystalline benzophenone[219] and xanthone adsorbed on silica gel[220] and therefore implies that rate constants for intersystem crossing to the triplet state for carbonyl chromophores are not significantly altered when the chromophore is in the solid phase.

Quenching of α-carbonyl triplet states by phenolic hydroxyl moieties have been demonstrated to proceed efficiently with quenching rate constants (k_q) of the order of 10^9 l.mol.$^{-1}$s.$^{-1}$ as seen in section 4.2.4 where the quenching rate constant for triplet 3,4-dimethoxyacetophenone by phenol was to determined to be 6.3×10^9 l.mol.$^{-1}$s.$^{-1}$. Further evidence of the high efficiency of such triplet state deactivation processes can be found in the literature for the self quenching of triplet 4-hydroxypropiophenone[141] and also for intramolecular remote hydrogen atom abstraction reactions by triplet carbonyls[221]. Such fast α-carbonyl triplet state deactivation processes will not be detected by the flash photolysis apparatus whose time resolution is increased from ca. 30 ns for non-fluorescent solid samples to approximately 150 ns by the fluorescent nature of the TMP samples under study. In the restricted environment of the pulp matrix, the photochemically generated phenoxy-ketyl radical pair formed as a result of postulate (b) above are also likely to decay on timescales faster than the time resolution of the flash photolysis apparatus. The intersystem crossing rate constants observed for triplet radical pairs in micelles[222,223] has been demonstrated to be of the order 2×10^6 to 5×10^6 s.$^{-1}$. Intersystem crossing rate constants for photoinduced radical pairs formed in the pulp matrix are expected to be even faster than those observed in micellar environments due to the rigidity of the pulp fibre matrix and thus will also elude detection by our apparatus.

Given that in unmodified TMP, the α-carbonyl and phenolic hydroxyl content have been determined to be 0.07[170] and 0.128 per C_9 lignin phenylpropane unit, the 30 % increase in the observed transient signal upon totally removing all phenolic hydroxyl moieties is too large to be explained simply by random distribution of α-carbonyl moieties relative to phenolic

hydroxyls in the lignin matrix. A few possible explanations of this larger than predicted signal increase are detailed overleaf:-

(a) The TMP used in these studies was manufactured from wood cells (and therefore lignin structure) at all stages of development from initial formation to full maturation (the completion of the lignification processes). Shown in table 6.4 is some data detailing the distribution and concentration of lignin in black spruce tracheids (Picea mariana) as determined by Fergus *et al*[49] for earlywood and latewood respectively (see section 2.2.2).

Wood Type	Morphological Region	Tissue Volume / %	Lignin / % of Total	Lignin Conc'n (g/g)	Phenolic Hydroxyl / C_9 Unit(1)
Earlywood	S	87	72	0.23	0.12
	ML	9	16	0.50	0.06(2)
	ML_{CC}	4	12	0.85	
Latewood	S	94	82	0.22	-
	ML	4	10	0.60	-
	ML_{CC}	2	8	1.00	-

Table 6.4:- A Table Detailing the Concentration and Distribution of Lignin Within Early and Latewood Black Spruce Tracheids (Picea mariana) according to Fergus et al[49]
S = secondary wall, M = middle lamella, CC = cell corner

(1) Data According to Yang and Goring[216]
(2) Total of ML and ML_{CC}

As can be seen, the concentration of lignin in the secondary wall (S) is much lower (see also figure 2.4) than that observed in the middle lamella region (ML or ML_{CC}). However, because the secondary wall constitutes 87 % of the wood cell tissue volume, most of the lignin is located in this region. The concentration of phenolic hydroxyl moieties per lignin C_9 unit in the secondary wall and middle lamella have been shown by Yang and Goring for early wood black spruce tracheids to be 0.12 and 0.06 respectively indicating differences in the lignin structure between these two components[224,225]. In the manufacture of TMP hand sheets, all components of the woody tissue are used which has the effect of averaging out such differences when analytical parameters such as phenolic hydroxyl content and α-carbonyl content are determined. Thus, the phenolic hydroxyl contents quoted here are average values assuming that (from table 6.4) the secondary wall and middle lamella contain 72 % and 28 % of the total lignin respectively. Less information concerning the distribution of conjugated α-carbonyl moieties exist in the literature. However, it has been shown that compression wood (wood which grows on the lower side of leaning wood stems, such wood has been shown to have different morphological structure to other woody tissues[226]) has more condensed aromatic structures, but more importantly, a higher proportion of unmethoxylated 4-hydroxyphenylpropane units[227,228] and less conjugated α-carbonyl moieties[229,230], a fact

which will be neglected in the overall analysis for such moieties. Thus, although lignin is regarded as being a completely heterogeneous macromolecule it is true to say that certain types of lignin may contain more or less of a particular functionality depending upon its origin. This may partly explain the large increase in the transient signal upon full methoxylation of TMP relative to unmethoxylated samples.

(b) Other factors (other than phenolic hydroxyl concentration) may also play a role in explaining the observed transient size increase. It has been shown that methoxylation with dimethyl sulphate also removes other sources of hydroxyl groups in the pulp structure such as α-carbon benzyl alcohol structures. A measure of the amount of such moieties present in the lignin structure was obtained by the analysis of spruce milled wood lignin where a total concentration of ca. 0.2 per C_9 lignin unit is observed[231].

(c) Cellulose itself contains high percentage of alcoholic type hydroxyl groups which may be in close proximity to the α-carbonyl triplet states due to the intimate cross linkages between the lignin and cellulose components of the pulp fibre. As mentioned previously, treatment with dimethyl sulphate is not specific to lignin phenolic hydroxyls and therefore methoxylation of such moieties in the cellulose fraction of the TMP may contribute to the observed increase in transient signal size following methoxylation.

It is not known which of the above postulates is the most important but it may be possible that each plays a role in the deactivation of photogenerated triplets state population in the pulp matrix.

6.4 Photoyellowing of Thermomechanical Pulp

It has been shown that under steady-state irradiation conditions, the initial rate of photoyellowing of TMP is decreased as the phenolic hydroxyl content of the pulp is decreased and also that the overall extent of photoyellowing decreases linearly with decreasing lignin phenolic hydroxyl content[217]. This clearly implicates the phenolic hydroxyl moiety as a participant in the photoyellowing processes. However, the extent of photoyellowing could not be accounted for solely via the formation of phenoxy radicals (via α-carbonyl triplet state hydrogen atom abstraction of phenolic hydroxyl hydrogens and the cleavage of β-O-4 phenacyl-aryl-ether bonds) alone.

In section 6.3, it was noted that a 40 % decrease in the size of the transient reflectance change (analysing at 450 nm) was observed for TMP following exposure to approximately 400 laser pulses (ca. 18 mJ.cm.$^{-2}$ per pulse) which was accounted for by a combination of inner filter effects and also destruction of the laser absorbing chromophore responsible for the transient absorption. A plot of the transient signal intensity (analysing at 450 nm) as a function of number of laser shots is shown in figure 6.12 for untreated TMP and TMP which has been methoxylated with dimethyl sulphate.

The signal intensities at the beginning of the traces reiterates the observation of a 29 % increase in transient signal for a sample containing 0.0091 phenolic hydroxyl moieties per C_9 lignin unit relative to a phenolic hydroxyl content of 0.128. As can be seen however, upon exposure to 400 laser shots, each of the three samples suffers approximately a 40 % loss in the transient absorption relative to the signal initially observed. The fact that, for all three sample, the same

percentage loss in transient absorption is observed suggests that α-carbonyls are being destroyed via a mechanism which does not involve the phenolic hydroxyls.

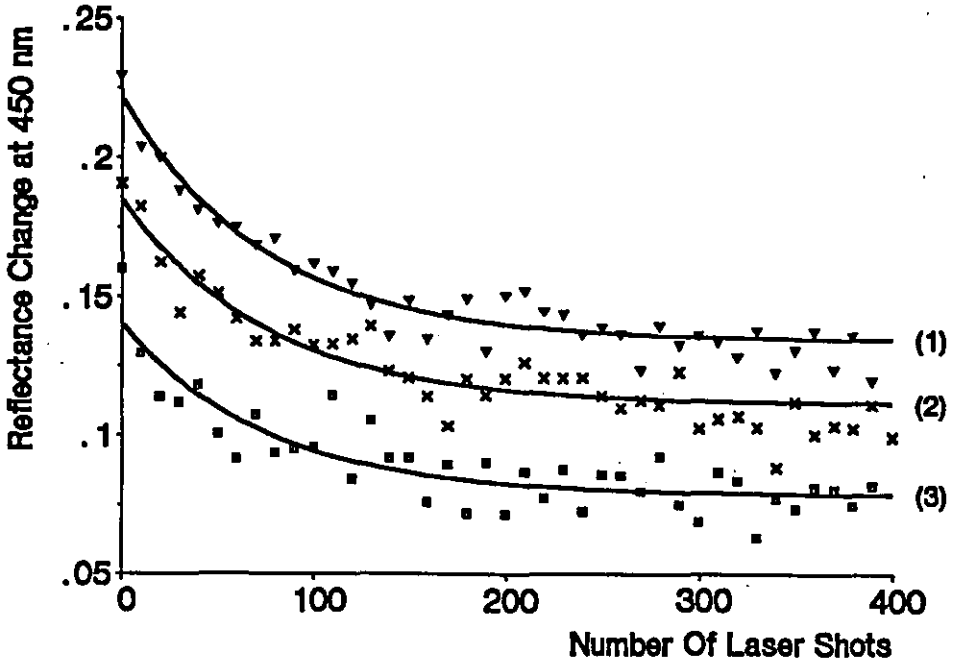

Figure 6.12:- A Plot of the Transient Reflectance Change ($\Delta J(t)/J(0)$) Analysing at 450 nm as a Function of Number of Laser Shots for Untreated TMP and TMP which has been Methoxylated with Dimethyl Sulphate. Phenolic Hydroxyl Content per C_9 Unit are (1) 0.0091, (2) 0.039 and (3) 0.128
Data was recorded ca. 3 μs after the laser pulse

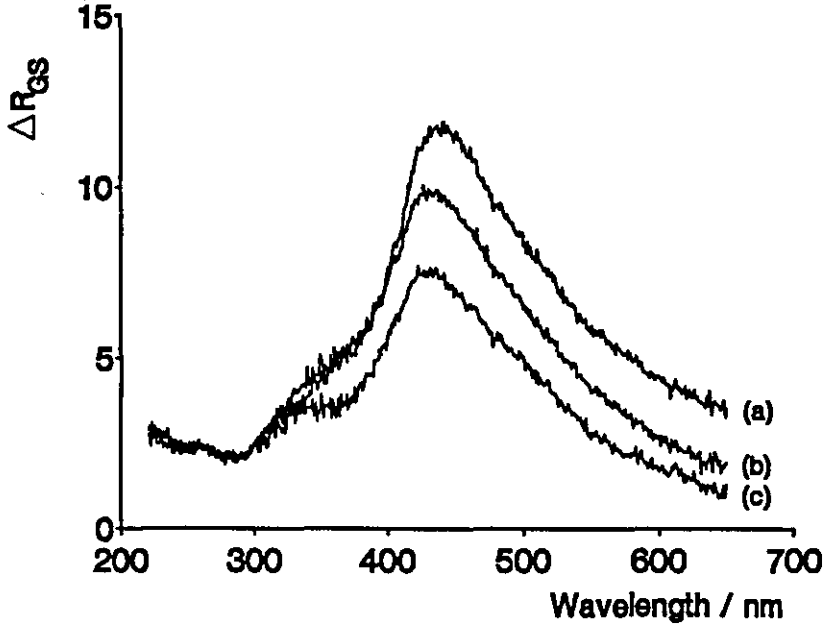

Figure 6.13:- Ground State Difference Reflectance Spectra (ΔR_{GS}) for TMP with (a) 0.128, (b) 0.039 and (c) 0.0091 Phenolic Hydroxyls per C_9 Lignin Unit

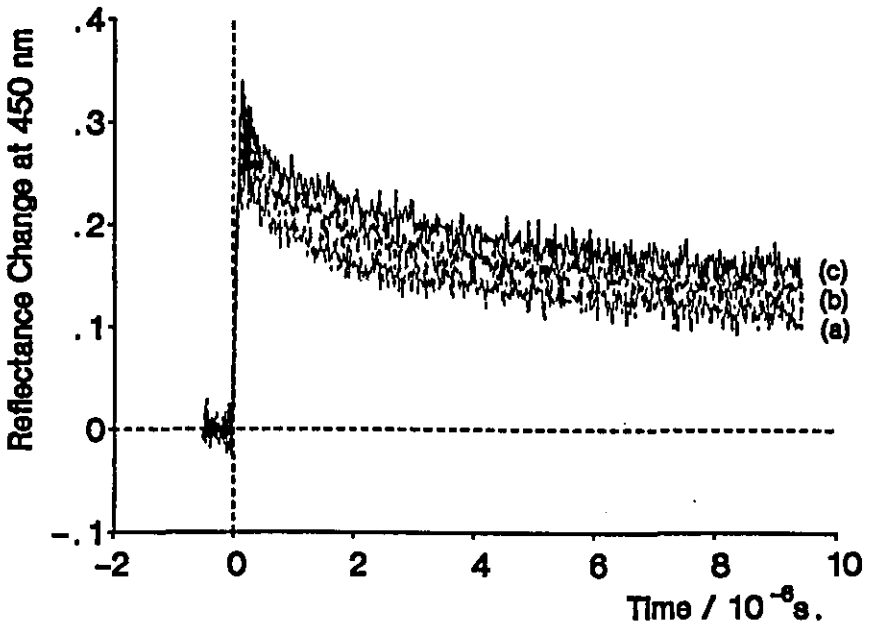

Figure 6.14:- Kinetics of Decay (analysing at 450 nm) of the Transient Reflectance Change for Samples of TMP with (a) 0.128, (b) 0.039, and (c) 0.0091 Phenolic Hydroxyls per C_9 Lignin Unit over a timescale of 10 μs

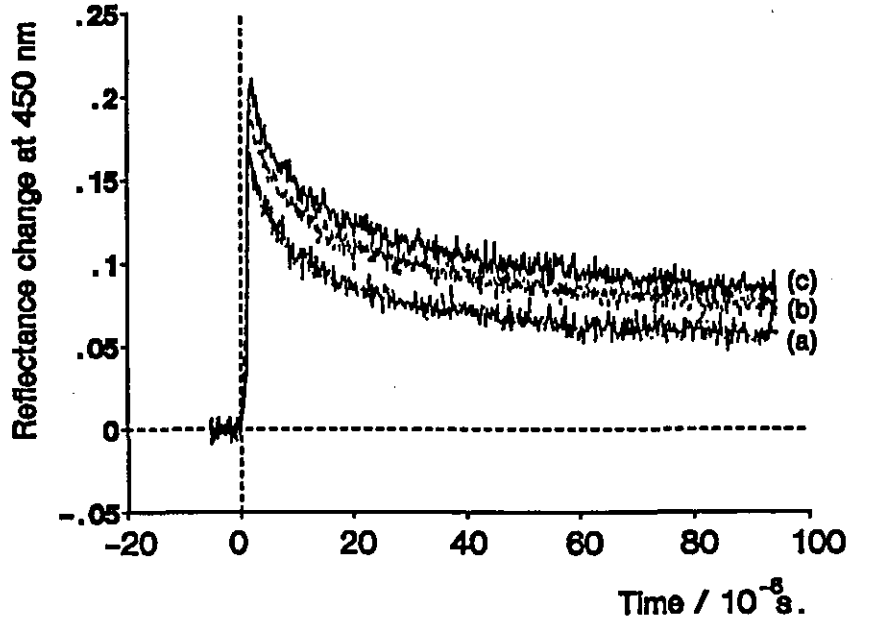

Figure 6.15:- Kinetics of Decay (analysing at 450 nm) of the Transient Reflectance Change for Samples of TMP with (a) 0.128, (b) 0.039, and (c) 0.0091 Phenolic Hydroxyls per C_9 Lignin Unit over a timescale of 100 μs

Also, from figure 6.12, the rate of loss of α-carbonyls does not depend upon the phenolic hydroxyl content of the pulp sample.

If we assume that the α-carbonyl concentration is 0.07 per lignin C_9 unit, then a "mass balance" of the fate of such chromophores in an unmethoxylated TMP sample following exposure to the laser can be compiled. From the methoxylation data, 0.3 x 0.07 = 0.02 α-carbonyls are assumed to be quenched by phenolic hydroxyl moieties, 0.4 x (0.07 - 0.02) = 0.02 are removed via another chemical deactivation mechanism leaving 0.03 α-carbonyls unreacted to give a transient absorption following photoyellowing with 400 laser pulses which does not decrease significantly upon further exposure to the laser. Measurement of the change in the ground state diffuse reflectance spectra (ΔR_{GS}) before and after photoyellowing demonstrates that methoxylation of TMP does provide some protection against brightness loss as seen in figure 6.13 and is in agreement with observations made by other authors[83,116].

Inspection of the kinetics of decay of the transient for the samples under study reveal, within experimental error, identical kinetics at short time delays (ca. 0 to 100 μs) following the laser pulse as shown in figures 6.14 and 6.15. However, over long timescales, a point is reached at approximately 2 ms following the laser pulse where the transient signal for each sample is of equal intensity (figure 6.16), after which the methoxylated sample transient signal becomes less intense than that of the non-treated TMP.

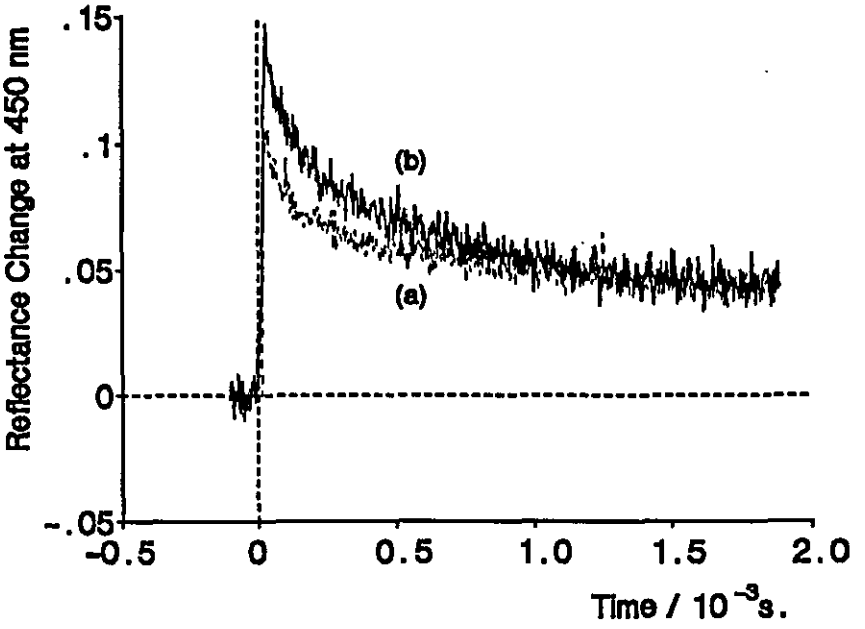

Figure 6.16:- Kinetics of Decay (analysing at 450 nm) of the Transient Reflectance Change for Samples of TMP with (a) 0.128 and (b) 0.0091 Phenolic Hydroxyls per C_9 Lignin Unit over a Timescale of 2 ms

Phenolic Hydroxyl Content / C_9 Unit	$\{\Delta J(0.1\,s.)/J(0)\}$ / 10^{-2}	ΔR_{CS} at 440 nm
0.128	1.192	11.90
0.039	0.924	9.81
0.0091	0.556	7.43

Table 6.5:- Single Shot Residual Reflectance Change at 450 nm ($\Delta J(t)/J(0)$) Recorded 0.1 s after the Laser Pulse and the Corresponding Values of ΔR^{cs} at 440 nm for Photoyellowed TMP Samples of Varying Phenolic Hydroxyl Content

The single shot residual absorption ($\Delta J(t)/J(0)$) observed at a delay of 0.1 s after the laser pulse together with the corresponding values of ΔR_{CS} at 440 nm for photoyellowed TMP samples are shown in table 6.5. The data in table 6.5 demonstrates that the observation of less residual single shot absorption for methoxylated pulp samples obtained from the flash photolysis experiments ($\Delta J(t)/J(0)$) follows a similar trend to that obtained from the accumulated photoyellowing (ΔR_{CS}) of a TMP sample. From the steady state data, an estimated decrease of ca. 50 % in the reflectance change due to yellowing for a fully methoxylated TMP sample relative to that of an untreated sample TMP is observed.

Due to the fully methoxylated TMP undergoing photoreversion, it is concluded that other photoyellowing mechanisms are involved in the degradation mechanism, Heitner and Schmidt reporting that under steady state irradiation conditions of a similar set of TMP samples that 75 % of yellow chromophores arise from chromophoric groups present in the TMP fibre other than the lignin phenolic hydroxyl moieties.

6.5 Discussion

From the experiments described above, the assignment of the transient absorption as that of the triplet state of α-carbonyl moieties present in the lignin fraction of the pulp fibre. The evidence in support of this assignment has been gathered in a series of experiments involving MWL and TMP samples and is presented below:-

(a) From quantification of the absorption in the 300 nm to 400 nm wavelength region of the spectrum, the α-carbonyl moieties are found to be a major photochemical absorber at the laser excitation wavelength (354.7 nm). Thorough reduction of TMP with sodium borohydride significantly reduces the absorption of the pulp sample in this region of the spectrum but does not eliminate it altogether suggesting that other chromophores are absorbing in this region.
(b) From the MWL adsorbed onto microcrystalline cellulose studies (section 5.5), the transient absorption with λ_{max} at 440 nm was assigned as that of the triplet state of MWL on the grounds of similarities to that of the solution phase triplet-triplet absorption spectrum, itself assigned as a triplet spectrum on the evidence of its sensitivity to molecular oxygen leading to the sensitization of singlet oxygen.
(c) Thorough reduction of TMP with sodium borohydride reduces the intensity of the observed

transient signal in proportion with the extent of reduction. Sodium borohydride reduces the α-carbonyl moieties to the corresponding alcohol which reduces the ground state absorption of the pulp fibre below 500 nm. The transient different spectrum decreases at all wavelengths to an equal extent as a function of the extent of reduction suggesting that the transient absorption is directly related to α-carbonyls in the lignin.

(d) Total removal of the lignin phenolic hydroxyl moieties in the pulp fibre results in a 30 % increase in the observed transient signal. This is consistent with the removal of a deactivation pathway for the carbonyl triplet resulting in more triplet α-carbonyl species being detected by our apparatus.

(e) The transient species is diffusionally quenched in the presence of high pressures of oxygen (ca. 2 Bar) relative to an identical sample under an atmosphere of pure nitrogen. Radical species are also known to be quenched by oxygen therefore making this observation equivocal on its own but does serve to add credence to the assignment of the transient species as that of the triplet state.

The involvement of α-carbonyls, phenolic hydroxyl moieties and the presence of oxygen and moisture in the photoyellowing of TMP have been exhaustively demonstrated. However, recent evidence suggests that chromophores first thought not to absorb at wavelengths greater than 300 nm (the cut-off point of solar radiation at sea level) such as the substituted phenols, biphenyl and stilbene type structures (formed by mechanical action) present in lignin do in fact have absorption bands above 300 nm possibly as a result of the matrix in which they are present. Even after thorough reduction with sodium borohydride for 18 hours (to remove all α-carbonyls), a small transient absorption signal following 354.7 nm excitation with a similar absorption spectrum and decay kinetics was still observed. This may be attributed to incomplete reduction of all carbonyl moieties present in the pulp; in section 5.2 it was shown that some α-carbonyls in MWL (in 1,4-dioxane) took up to 24 hours to be fully reduced by sodium borohydride. Heitner and Schmidt[217] found that sodium borohydride reduction times for TMP fibres under identical conditions to those employed by Schmidt *et al*[211] were of the order of ca. 45 hours before complete reduction was achieved. Alternatively, the transient may be attributed to that of a chromophoric moiety present in the lignin matrix which has similar λ_{max} and transient absorption spectrum to that of the triplet α-carbonyl moiety. For example, Lee *et al*[232] have proposed the formation of substituted stilbene type moieties (see structures A and B in figure 4.17) formed by mechanical action upon phenylcoumaran structures present in the lignin matrix (phenylcoumaran structures are formed by internal intramolecular addition following the β-5 linking of two phenylpropane lignin precursor units (see sections 2.2.2 and 2.3) as shown in figure 6.17. Structure A has been shown to absorb strongly below 400 nm with a λ_{max} in solution located at ca. 330 nm . Under steady state irradiation conditions, this functionality was shown to photodegrade to yield photoproducts which absorb strongly in the wavelength range 400 nm to 700 nm[204]. Light absorption at 354.7 nm has been attributed, to a large degree, to α-carbonyl moieties which have been shown unequivocally to act as photochemical sensitizers in the photoyellowing processes for TMP. Investigations into other mechanisms of photoyellowing involving biphenyl and stilbene chromophores has not received much attention so far and requires further investigation before comment is made as to their relative contribution to the overall

photoyellowing processes. Evidence that chromophores other than α-carbonyls which contain a phenolic moiety absorb light above 300 nm has recently been obtained by the action of Fremys salt upon peroxide bleached TMP[233]. Fremys salt (potassium nitrosodisulphonate) has been shown to selectively oxidise substituted phenols to ortho and para quinones depending upon substitution[234]. The action of alkaline hydrogen peroxide upon ortho and para quinones results in the formation of a colourless carboxyl ic acid (see section 2.4). Thus it was anticipated that treatment of bleached TMP with Fremys salt will yield an increase in absorption of the TMP sheet due to the formation of coloured chromophores. Subsequent treatment of this pulp sample with alkaline hydrogen peroxide (ie. rebleaching the pulp) should yield a zero difference spectrum at wavelengths greater than 300 nm if no phenolic moieties absorb in that wavelength region.

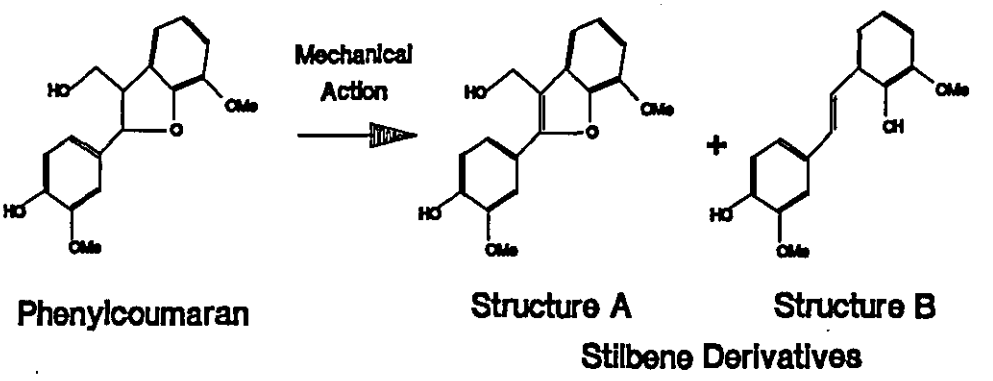

Figure 6.17:- Proposed Mechanism for the formation of Substituted Stilbene Derivatives From Phenylcoumaran Structures Present in the Lignin Matrix[232]

This was not however observed, a decrease in absorption relative to peroxide bleached TMP with λ_{max} at ca. 350 nm being observed. Figure 6.18 shows the difference specific absorption spectra ($-\Delta K^{Sp}$) for sodium borohydride treated TMP together with that of TMP treated with Fremys salt followed by further peroxide bleaching. As can be seen, the contribution to the absorption by phenolic moieties is significant at wavelengths greater than 350 nm. Isolated phenols do not typically absorb at wavelengths greater than 300 nm. This suggests that the phenolic moiety destroyed by the action of Fremys salt is conjugated with another chromophoric moiety within the lignin structure. As we have seen, conjugated α-carbonyls, and possibly substituted stilbene type structures (see figure 6.17) are present in the pulp fibre and absorb in the wavelength region in question (300 nm to 400 nm).

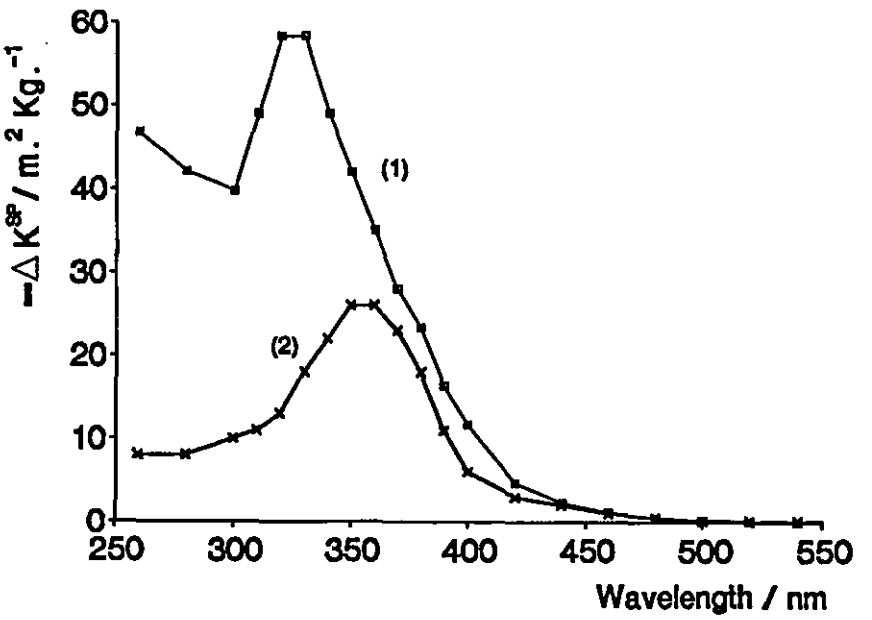

Figure 6.18:- Difference Specific Absorption Spectra (ΔK) for Sodium Borohydride Treated TMP (Curve 1) together with that of TMP Treated with Fremys Salt (Curve 2) Followed by Further Peroxide Bleaching.

Given that Fremys salt yields both ortho and para quinone structures, it is possible that some of the loss of absorption observed following this treatment may also be as a result of destruction of α-carbonyl moieties as well as the phenolic chromophore absorbing in this wavelength region. Consequently, the perceived absorption intensity attributed to phenolic functionalities may be exaggerated by the non-specific mode of action of Fremys salt.

It is worth considering the hypothesis that the observed transient signal following pulsed laser excitation of TMP may be attributed to chromophoric moieties other than triplet states of α-carbonyls. This has, however, been shown to be incorrect, fully sodium borohydride reduced TMP yielding little of no detectable transient reflectance signal[211].

It has been suggested that the removal of [illegible] of α-carbonyl moieties initially reduces the extent of TMP photoyellowing[235]. However, prolonged exposure to simulated solar irradiation results in the same extent of photoyellowing being observed eventually, removal of α-carbonyls therefore only slowing the rate of degradation[83]. The interpretation of the 40 % decrease in TMP transient absorption signal intensity following exposure to ca. 400 laser pulses (figure 6.12) was that α-carbonyl chromophores were undergoing irreversible photochemical reactions leading to photoyellowing. It has been suggested that α-carbonyls are also generated during the photoyellowing processes[236] possibly by the oxidation of α-carbon alcoholic moieties. Such behaviour has been demonstrated in the light induced degradation of woody material[237]. If this were the case, it would have the effect of offsetting the apparent decrease in transient signal upon exposure to a number of laser pulses until a photochemically stable concentration of

α-carbonyls present in the photoyellow TMP remain which are unable to photochemically deactivate by reaction giving the levelling off in the intensity of the observed transient signal. The formation of α-carbonyls would help to explain the observation that borohydride reduced TMP eventually photodegrades to the same extent as untreated TMP. It may be possible therefore to explain the observed transient signal from photoyellowed TMP as comprising of triplet α-carbonyls which were initially present in the lignin (but could not react to yield yellow photoproducts) and also some α-carbonyls formed during the photoyellowing process in new positions in the lignin matrix which also cannot react. Due to the structural similarities between such chromophores, no difference (except in intensity) is observed in the transient different spectrum of photoyellowed TMP relative to fresh unirradiated TMP. It therefore appears that α-carbonyls act as photosensitizers in the photoyellowing processes but do not produce photoproducts directly.

There exists two possibilities to explain the rate of formation of the baseline offset (due to photoyellowing) observed in the single shot transient intensity data:-

(a) The yellow photoproducts are formed instantaneously on the timescale of the nanosecond experiments.
(b) The α-carbonyl triplet decays with the same kinetics as the yellow photoproducts are formed.

It is difficult to distinguish between these two postulates, since at no analysing wavelength does the absorption by the yellow photoproducts outweigh the absorption by the α-carbonyl triplet states. It seems possible that (a) can occur as a result of the lack of diffusional quenching involved in the TMP fibre, ie. carbonyl triplets sensitize the production of radical species which statically react with other functional groups in the lignin macromolecule and oxygen which do not need to diffuse to the site of the free radical species. Given that the kinetics of decay of the transient species observed following excitation of a fresh TMP sample are, within experimental error, the same as that of the pre-photoyellowed TMP sample, it is suggested that in both cases, the observed transient decay may be due to α-carbonyls which do not, due to the lack of suitable quenching moiety, take part in the yellowing processes.

Addition of radical quenchers (such as ascorbic acid[238]) to TMP initially slows the rate of photoyellowing suggesting that the degradation processes proceed primarily via a radical chain reaction mechanism. The phenoxy radical has been shown to be a key precursor to the yellow photoproducts since removal of phenolic hydroxyl moieties leads to a decrease in the extent of photoyellowing of TMP samples. In addition to the triplet sensitized hydrogen atom abstraction reaction of α-carbonyls with phenolic hydroxyls, such radicals can be generated via other mechanisms within the pulp matrix such as:-

(a) Singlet state α-carbonyl mediated cleavage of β-O-4 aryl ether bonds.
(b) Photocleavage of α-O-4 ether linkages.
(c) Direct photolysis of the phenolic moiety shown to absorb at wavelengths greater than 300 nm (by the experiments with Fremys salt). The nature of such a moiety is presently unknown except that it contains a phenolic moiety. As was seen earlier, chemical modification of phenolic moieties with dimethyl sulphate produced no change in the absorption spectrum of the resultant TMP sample. This suggests that it is not the phenolic bond which gives the absorption at

wavelengths greater than 300 nm but rather a conjugated side chain in the 1 position on the phenylpropane ring, the action of Fremys salt upon such a chromophore resulting in the destruction of this conjugated side chain in the formation of a para quinone type structure. As was seen in figure 6.17, the stilbene derivative derived from phenylcoumaran structures contains both a phenolic hydroxyl moiety and also a ring conjugated side chain which adds weight to the proposal that such a chromophoric structure may be present in the TMP fibre.

The nature of the coloured materials formed following irradiation of such chromophores as biphenyls and stilbenes has not, as yet, been quantified. Clearly, the removal of all α-carbonyls and phenolic hydroxyl moieties is not sufficient to prevent yellowing of TMP. It is therefore essential that the photochemistry of other absorbing moieties are investigated to determine their relative contribution in the overall photoyellowing process.

Chapter 7

Conclusions and Recommendations For Further Work

7 Conclusions and Recommendations for Further Work

To fully achieve a complete, commercially viable, solution to the problem of photoyellowing of high yield thermomechanical pulps, it is of fundamental importance that the mechanisms by which these processes occur are clearly defined and understood. It is only when this knowledge is in place, and suitable modifications to the pulp fibre or fibre processing techniques made, that such materials can be used in higher added-value paper products. The work detailed in this thesis has gone part of the way to understanding the excited state photochemistry of lignin rich thermomechanical pulp fibres. As this work was progressing, there has been a general marked increase in the research field of lignin photochemistry from the angle of photoyellowing. This has been stimulated, in part, by both the current economic situation in the pulp and paper industry and new environmental legislation applied to the large pulp and paper producing countries in terms of waste effluent treatment and river discharge. The ever dwindling supply of forests has also encouraged paper manufacturers to optimise uses of available natural resources. For this reason, a steady growth in the production of TMP and CTMP has been observed over the past 10 years or so. At a recent conference[239], Cockram suggested that if the time taken for CTMP to photoyellow to an unacceptable level was increased from 3 months to 36 months, then an increase in the market demand for such papers would be from 0.6 million tonnes to ca. 2.2 million tonnes per annum, potentially giving a total market increased demand for TMP and CTMP of the order of 2.6 million tonnes per year.

The view that an intermediate point between current rates of TMP photoyellowing and total brightness stability (ie. extension of acceptable brightness levels to ca. 3 years) is also shared by this author. Indeed, much work has been directed towards this area of research[240]. Methods of slowing the rate of photoyellowing fall generally into four categories:-

(a) Chemical modification of the phenolic hydroxyl moieties present in the TMP pulp with dimethyl sulphate.
(b) Reduction of α-carbonyl moieties with sodium borohydride.
(c) Addition of UV absorbing chemical species to act as inner filters and,
(d) Addition of radical quenchers such as ascorbic acid or aromatic thiols which deactivate phenoxy and other free radical species present in the TMP sample following exposure to sunlight.

Each method has its advantages and disadvantages both in terms of the degree of protection offered to the TMP fibres and in relative cost.

Clearly, a considerable amount of work is still required to elucidate all the mechanisms by which high lignin content fibres degrade following exposure to UV light. From the work detailed in this thesis, it is clear that the triplet states of α-carbonyl moieties present in the lignin structure are a key chromophore in the photoyellowing processes. Based upon these observations, a few further continuation experiments which would prove useful in terms of our understanding of the excited state photochemistry of lignocellulosic materials are presented below.

(a) Experiments With Lignin Model Compounds:- As was seen in chapters 4 and 5 of this thesis, the use of simple lignin model compounds can be used effectively to obtain information which can be applied to the more complex photochemical systems such as MWL and TMP itself. Much research in this area has been directed towards studying the β-O-4 aryl ether type compounds both in solution

and when adsorbed onto filter paper (see section 4.1). As was seen in chapters 4 and 5 of this thesis, the environment in which a molecule is present can play a large part in determining its photochemical behaviour. It would be interesting to study these types of molecule placed in the restricted geometry of a zeolite cage or within a micellular environment with a view to determining the extent to which photodegradation of such lignin model compounds occurs relative to that observed in fluid solution.

Recently, it has been postulated that stilbene type moieties may be formed from phenylcoumaran type moieties (which are known to be present in the lignin macromolecule[241]) in the mechanical refining stage of TMP manufacture[232] (see figure 6.17). Again, a series of experiments to study the excited state photochemistry of such chromophores to establish their role in the photoyellowing processes would prove useful.

The observation that, following the reaction of Fremys salt with bleached TMP to produce ortho and para quinone moieties, and subsequent rebleaching of the TMP, did not produce a zero difference in the specific absorption spectrum of the TMP sample is extremely interesting. This led to the postulate that a phenolic moiety present in the lignin was absorbing at wavelengths greater than 300 nm. It is unlikely that an isolated phenol will absorb at wavelengths greater than 300 nm and therefore, it is assumed that the phenol is conjugated with another functionality probably on the propyl side chain (para to the phenolic hydroxyl) of the lignin C_9 unit (ie. α-carbonyls or stilbene type functionalities). It is not clear as to what (if any) effect Fremys salt has on the α-carbonyl moieties that are known to be present in the TMP. A similar experiment to the one above could be performed with a TMP sample which had been thoroughly reduced with sodium borohydride prior to treatment with Fremys salt. A comparison with the initial observation may determine whether, in the process of forming para quinone moieties, α-carbonyls are indeed being destroyed. Parallel experiments with simple softwood lignin model compounds such as 4-hydroxy-3-methoxyacetophenone (acetovanillone) could be performed to confirm the above postulates.

(b) Experiments with Thermomechanical Pulp:- The observation (detailed in this thesis - see section 6.3.1) that dynamic quenching of the photogenerated triplet states of α-carbonyls present in TMP by ground state molecular oxygen was first reported by us and is documented in the literature[215]. At that point, it was not established whether the effect of the addition of higher concentrations of oxygen than the one used previously would further enhance the dynamic quenching of the triplet state of TMP. Therefore, it is suggested that further investigation be conducted into this phenomenon.

The role of singlet oxygen in the photoyellowing mechanisms of TMP is, as yet, not fully understood. This thesis reported the first direct observation of the triplet-triplet absorption spectrum of the α-carbonyl moieties present in MWL (both in solution and adsorbed onto microcrystaline cellulose). Its identification was based upon its ability to sensitise singlet molecular oxygen in 1,4-dioxane solution. The characteristic lifetime for the decay of the singlet oxygen luminescence signal centred at 1270 nm was unequivocal evidence that triplet state quenching by molecular oxygen was taking place. Following along these lines, it would be an interesting experiment to attempt to detect singlet molecular oxygen sensitised during the quenching of the triplet state of TMP under enhanced oxygen atmospheres. Thermomechanical pulp is usually refined at 120°C at a pressure of ca. 2 atmospheres. If the refining pressure is increased to ca. 7 atmospheres, a fibre with a more lignin rich surface is obtained[242]. Such fibres are usually used for the production of medium density fibreboard (MDF) by combination with, typically, phenol-formaldehyde resin systems. Consequently, it may be anticipated that, there would be a greater chance of observing both enhanced

dynamic quenching of the α-carbonyl triplet state by molecular oxygen (relative to that observed for TMP fibres) and also the detection of singlet oxygen luminescence from the sample when studied using a diffuse reflectance apparatus geometry.

From the results presented in section 6.4 of this thesis, it is suggested that the observed photochemistry following 354.7 nm **nanosecond** pulsed laser excitation of bleached TMP samples is that of α-carbonyl triplet states which are unable to deactivate easily by photochemical reaction (to yield phenoxy-ketyl free radical pairs by phenolic hydroxyl hydrogen atom abstraction and ultimately yellow chromophores). It is likely that, given the close proximity of chrophoric moieties relative to each other in the lignin macromolecule, the excited states which are able to undergo such reactions do so on timescales too short to be monitored by the flash photolysis apparatus available in Loughborough. Consequently, the use of a picosecond laser flash photolysis system (in diffuse reflectance mode) would be required to detect and quantify the contribution that such fast photochemical processes have on the overall photoyellowing process. Initial experiments could concentrate on characterising the sub-nanosecond photochemistry of MWL in solution as it too is expected to undergo photochemical processes too fast to be detected by nanosecond flash photolysis techniques.

In conclusion, there remains much work in the research area of photoyellowing of lignocellulosic materials before a full understanding of photochemical processes involved is obtained. This goal, I believe, will be achieved at some point in the future provided that the rate of current progress in our understanding of the processes involved continues to gather momentum at its current level.

References

References

1 N.J. Turro, "Modern Molecular Photochemistry", Benjamin Cummings, (Menlo Park), p. 46, (1978)

2 M. Kasha, Discussions Faraday Soc., 9, 14, (1950)

3 R.P. Wayne, "Principles and Applications of Photochemistry", Oxford Science, (Oxford), p. 82, (1988)

4 D.L. Dexter, J. Chem. Phys., 21, 836, (1953)

5 T. Forster, Discuss. Faraday Soc., 27, 7, (1959)

6 I.R. Gould, "Xenon Arc Lamps", in J.C. Scaiano (ed.), "CRC Handbook of Organic Photochemistry", CRC Press, (Florida), Volume 1, p. 161, (1989)

7 D.L. Andrews, "Lasers in Chemistry", Springer-Verlag, (Berlin), p. 19, (1990)

8 E.A. Ogryzlo, in B. Ranby and J.F. Rabek (eds.), "Singlet Oxygen - Reaction With Organic Compounds and Polymers", Wiley, (Chichester), p. 8, (1978)

9 R.W. Murray, in H.H. Wasserman and R.W. Murray (eds.), "Singlet Oxygen", Academic Press, (New York), p. 59, (1979)

10 D.R. Kearns, Chem. Rev., 71, 395, (1971)

11 G. Rossbroich, N.A. Garcia and S.E. Braslavsky, J. Photochem., 31, 37, (1985)

12 A.A. Gorman and M.A.J. Rogers, "Singlet Oxygen", in J.C. Scaiano (ed.), "Handbook of Organic Photochemistry", CRC Press, (Florida), Volume 2, p. 233, (1987)

13 D. Bellus, in B. Ranby and J.F. Rabek (eds.), "Singlet Oxygen - Reaction With Organic Compounds and Polymers", Wiley, (Chichester), p. 90, (1978)

14 R.H. Young, D. Brewer, R. Kayser, R. Martin, D. Feriozi and R.A. Keller, Can. J. Chem., 52, 2889, (1974)

15 E.A. Ogryzlo and C.W. Tang, J. Am. Chem. Soc., 92, 5030, (1970)

16 A. Farmilo and F. Wilkinson, Photochem. Photobiol., 18, 447, (1973)

17 I. Carmichael, W.P. Helman and G.L. Hug, J. Phys. Chem. Ref. Data, 16, 239, (1987)

18 S.K. Chattopadhyey, C.V. Cumar, and P.K. Das, J. Photochem., 30, 81, (1985)

19 W.W. Wendlandt and H.G. Hecht, "Reflectance Spectroscopy", Chemical Analysis Monograph No. 21, Wiley Interscience, (New York), p. 16, (1966)

20 N.J. Harrick, Ann. N.Y. Acad. Sci., 101, 928, (1963)

21 F. Wilkinson and G.P. Kelly, "Diffuse Reflectance Laser Flash Photolysis" in J.C. Scaiano (ed.), "CRC Handbook of Organic Photochemistry", CRC Press, (Florida), Volume 1, p. 293, (1987)

22 W.W. Wendlandt and H.G. Hecht, "Reflectance Spectroscopy", Chemical Analysis Monograph No. 21, Wiley Interscience, (New York), p. 1, (1966)

23 G. Kortum, Rev. Universelle Mines, 15, 5, (1959)

24 H. Wright, Ann. Physik (4), 1, 17, (1900)

25 W.W. Wendlandt and W.G. Hecht, "Reflectance Spectroscopy", Chemical Analysis Monograph No. 21, Wiley Interscience, (New York), p. 49, (1966)

26 F. Jentzsch, Ann. Physik (4), 39, 997, (1912)

27 G. Kortum and J. Vogel, Z. Physik. Chem. (Frankfurt), 18, 230, (1958)

28 P. Kubelka and F. Munk, Z. Tech. Phys., 12, 593, (1931)

29 P. Kubelka, J. Opt. Soc. Am., 38, 448, (1948)

30 A. Schuster, Astrophys. J., 21, 1, (1905)

31 W.W. Wendlandt and H.G. Hecht, "Reflectance Spectroscopy", Chemical Analysis Monograph No. 21, Wiley Interscience, (New York), p. 58, (1966)

32 G. Kortum, W. Braun and G. Herzog, Angew. Chem. Intern. Edn., 2, 333, (1963)

33 G. Kortum and D. Oelkrug, Z. Naturforsch, 8a, 372, (1963)

34 R.W. Kessler, G. Krabichler, S. Uhl, D. Oelkrug, P. Hagan, J. Hyslop and F. Wilkinson, Optica Acta, 30(8), 1099, (1983)

35 D. Oelkrug, W. Honnen, F. Wilkinson, and C.J. Willsher, J. Chem. Soc. Faraday Trans. 2, 83(11), 2081, (1987)

36 T. Lin and H.K.A. Kan, J. Opt. Soc. Am., 60, 1252, (1970)

37 J.A. Schmidt, C. Heitner, G.P. Kelly, P.A. Leicester and F. Wilkinson, J. Photochem. Photobiol. A: Chemistry, 57, 111, (1991)

38 B.L. Browning, "The Chemistry of Wood", Wiley Interscience, (New York), p. 57, (1963)

39 H. Meier, in T. Higuchi (ed.), "Biosynthesis and Biodegradation of Wood Components", Academic Press, (New York), p. 43, (1985)

40 T.E. Timell, Wood Sci. Technol., 1, 45, (1967)

41 O.P. Grushnikov and N.N. Shorygina, Abstr. Bull. Inst. Paper Chem., 42, 11139, (1972)

42 D. Fengel and G. Wegener, "Wood - Chemistry, Ultrastructure, Reactions", Walter de Gruyter, (Berlin), p. 169, (1984) and references therein

43 G.D. McGinnis and F. Shafizaheh, "Cellulose and Hemicellulose", in J.P. Casey (ed.), "Pulp and Paper Chemistry and Technology", Wiley Interscience, (New York), p. 29, (1980) and references therein

44 M. Erickson and G.E. Miksche, Phytochem., 13, 2295, (1974)

45 A. Bjorkmann and B. Person, Svensk Papperstidning, 60, 158, (1957)

46 K. Freudenberg and A.C. Neish, "Molecular Biochemistry and Biophysics", Springer-Verlag, (Berlin), Volume 2, p. 113, (1968)

47 S. Saka, "Chemical Composition and Distribution", in D.N.-S. Hon and N. Shiraishi (eds.), "Wood and Cellulosic Chemistry", Marcel Dekker, (New York), p. 70, (1991)

48 M. Fujita and H. Harada, "Ultrastructure and Formation of Wood Cell Walls", in D.N.-S. Hon and N. Shiraishi (eds.), "Wood and Cellulosic Chemistry", Marcel Dekker, (New York), p. 21, (1991)

49 B.J. Fergus, A.R. Procter, J.A.N. Scott and D.A.I. Goring, Wood Sci. Technol., 3, 117, (1969)

50 K. Freudenberg and A.C. Neish, "Constitution and Bio-Synthesis of Lignin", Springer Verlag, (New York), (1968)

51 P. Klason, Svensk Kem. Tidskr., 9, 133, (1897)

52 K.V. Sarkenen, "Precursors and Their Formation", in K.V. Sarkenen and C.H. Ludwig (eds.), "Lignin - Occurrence, Formation, Structure and Reactions", Wiley Interscience, (New York), p. 95, (1971)

53 E. Alder, Wood Sci. Technol., 11, 169, (1977)

54 K.V. Sarkenen and C.H. Ludwig, "Definition and Nomenclature", in K.V. Sarkenen and C.H. Ludwig (eds.), "Lignin - Occurence, Formation, Structure and Reactions", Wiley Interscience, (New York), p. 2, (1971)

55 O. Martennson and G. Karlsson, Ark. Kemi, 31, 5, (1969)

56 M. Erickson, S. Larsson and G.E. Miksche, Acta Chem. Scand., 27, 903, (1973)

57 A. Sakakibara, "Chemistry of Lignin", in D.N.-S. Hon and N. Shiraishi (eds.), "Wood and Cellulosic Chemistry", Marcel Dekker, (New York), p. 156, (1991)

58 W.G. Glasser, in J.P. Casey (ed.), "Pulp and Paper - Chemistry and Chemical Technology", Wiley Interscience, (New York), p. 56, (1980)

59 W.G. Glasser and H.R. Glasser, Paperi jaa puu, 63, 71, (1981)

60 W.G. Glasser, H.R. Glasser and N. Morohoshi, Macromolecules, 14, 253, (1981)

61 J.N. McGovern, "Pulping", in J.P. Casey (ed.), "Pulp and Paper - Chemistry and Chemical Technology", Wiley Interscience, (New York), p. 161, (1980)

62 V. Loras, "Bleaching", in J.P. Casey (ed.), "Pulp and Paper - Chemistry and Chemical Technology", Wiley Interscience, (New York), p. 633, (1980)

63 K. Kringstad and K. Lindstrom, Envirom. Sci. Technol., 18, 236A, (1984)

64 G. Samdani, K. Gilges and K. Fouhy, Chemical Engineering, 98, 37, (1991)

65 International Standards Office No. 3688 (British Standard No. 4432: Part 4, (1980))

66 J.N. McGovern, "Pulping", in J.P. Casey (ed.), "Pulp and Paper - Chemistry and Chemical Technology", Wiley Interscience, (New York), p. 223, (1980)

67 D.W. Read, B.D. Eade and N.R. Slingsby, Pulp and Paper Mag. Can., 69, T296, (1968)

68 R. Agnemo and G. Gellerstedt, Acta Chem. Scand., B33, 337, (1979)

69 M.L. Slove, Tappi, 48, 535, (1965)

70 R.W. Pero and C.W. Dence, J. Wood Chem. Technol., 3, 195, (1983)

71 C. Heitner and T. Min, Cell. Chem. Technol., 21, 289, (1987)

72 R.H. Reeves and I.H. Pearl, Tappi, 48, 121, (1965)

73 G. Gellerstedt, H.L. Hardell and E.-L. Lindfors, Acta Chem. Scand., B34, 669, (1980)

74 G. Gellerstedt and R. Agnemo, Acta Chem. Scand., B34, 275, (1980)

75 C.W. Bailey and C.W. Dence, Tappi, 52, 491, (1969)

76 R.H. Reeves and I.H. Pearl, Tappi, 48, 121, (1965)

77 C.W. Bailey and C.W. Dence, Tappi, 52, 491, (1969)

78 B. Van Lierop, "Liason Report to the Canadian Pulp and Paper Association Bleaching Technology and Development Committee", (April 1990)

79 "Photochemical Processes in Lignocellulosic Materials", A Symposium of the Cellulose, Paper and Textile Division of the American Chemical Society, American Chemical Society 203rd Annual Meeting, San Francisco, April 5th to 10th 1992

80 L.V. Forman, Paper Trade Journal, 111, 34, (1940)

81 J.A. Van den Akker, H.F. Lewis, G.W. Jones, and M.A. Buchanan, Tappi, 32, 187, (1949)

82 G.J. Leary, Tappi, 50, 17, (1967)

83 G.J. Leary, Tappi, 51, 257, (1968)

84 S.Y. Lin and K.P. Kringstad, Norsk Skogindustri, 25, 252, (1971)

85 G.J. Leary, Nature, 217, 672, (1968)

86 S.E. Lebo, W.F.W. Lonsky, T.J. McDonough and P.J. Medvecz, Proc. Int. Pulping and Bleaching Conf., Orlando, (Florida), p. 247, (1988)

87 M. Erickson, S. Larsson and G.E. Miksche, Acta Chem. Scand., 27, 127, (1973)

88 G. Gellerstedt and E.-L. Lindfors, Svensk Papperstidning, 15, R115, (1984)

89 H.H. Brownell, Tappi, 48, 513, (1965)

90 A. Bjorkman, Svensk Papperstidning, 59(3), 477, (1956)

91 J.A. Schmidt, Personal Communication, (1992)

92 Applied Photophysics Ltd, "f/3.4 Grating Monochromator Reference Manual"

93 J.P. Keene, D. Kessel, E.J. Land, R.W. Redmond, and T.G. Truscott, Photochem. Photobiol., 43, 117, (1986)

94 W.W. Wendlandt and H.G. Hecht, "Reflectance Spectroscopy", Chemical Analysis Monograph No. 21, Wiley Interscience, (New York), p. 62, (1966)

95 E. Alder, B.O. Lindgren and U. Saeden, Svensk Papperstidning, 55, 245, (1952)

96 P.C. Roberti, R.F. York and W.S. MacGregor, J. Am. Chem. Soc., 72, 5760, (1950)

97 I. Forsskahl, Soc. Sci. Fenn. Commentat. Phys. Math., 61, 10, (1985)

98 G. Brunow and B. Eriksson, Acta Chem. Scand., 25, 2779, (1971)

99 G. Brunow and M. Sivonen, Paperi jaa puu, 57, 215, (1975)

100 J.S. Gratzl, Das Papier, 10A, V14, (1985)

101 G. Gellerstedt and E.-V. Pettersson, Acta Chem. Scand., B29, 1005, (1975)

102 K.P. Kringstad, Das Papier, 27, 462, (1973)

103 M.G. Neumann and A.E.H. Machado, J. Photochem. Photobiol. B: Biology, 3, 473, (1989)

104 M.G. Neumann, R.A.M.C. De Groote, A.E.H. Machado and R. Ruggiero, Proc. Int. Photochem. Symp., Lisbon, p. 514, (1976)

105 I. Forsskahl, J. Photochem., 27, 363, (1984)

106 I. Forsskahl, J. Photochem., 27, 85, (1984)

107 I. Forsskahl, J. Photochem., 25, 197, (1984)

108 C.L. Hsu and J.S. Hsieh, Tappi, 68, 92, (1985)

109 G. Gellerstedt, K.P. Kringstad and E.L. Lindfors, in B. Ranby and J.F. Rabek (eds.), "Singlet Oxygen - Reaction With Organic Compounds and Polymers", Wiley, (London), p. 302, (1978)

110 G. Brunow, I. Forsskahl, A.C. Gronlund, G. Lindstrom and K. Nyberg, in B. Ranby and J.F. Rabek (eds.), "Singlet Oxygen - Reaction With Organic Compounds and Polymers", Wiley, (London), p. 311, (1978)

111 T. Matsuura, N. Yoshimura, A. Nishinaga and I. Saito, Tetrahedron, 28, 4933, (1972)

112 A.A. Gorman, I.R. Gould, I. Hamblett and M.C. Standen, J. Am. Chem. Soc., 106, 6956, (1984)

113 I. Forsskahl, C. Olkkonen and H. Tylli, J. Photochem. Photobiol. A: Chemistry, 43, 337, (1988)

114 S.Y. Lin and K.P. Kringstad, Tappi, 53, 1675, (1970)

115 J. Gierer and S.Y. Lin, Svensk Papperstidning, 75, 233, (1972)

116 U. Tschirner and C.W. Dence, Paperi jaa puu, 70, 338, (1988)

117 A. Castellan, C. Vanucci, J.-P. Desvergre, H. Bouas-Laurent, M. Hawteville and M. Chandenson, C.R. Acad. Sci. Paris, 1, t301, (1985)

118 J.C. Scaiano and J.C. Netto-Ferreira, J. Photochem., 32, 253, (1986)

119 A. Castellan, P. Girard and C. Vanuccci, J. Wood Chem. Technol., 8, 73, (1988)

120 C. Vanucci, P. Fornier de Violet, H. Bouas-Laurent and A. Castellan, J. Photochem. Photobiol. A: Chemistry, 41, 251, (1988)

121 J.C. Netto-Ferreira and J.C. Scaiano, Tetrahedron Lett., 30, 443, (1989)

122 A. Castellan, N. Colombo, C. Cucuphat and P. Fornier de Violet, Holzforschung, 43, 179, (1989)

123 J.C. Netto-Ferreira, I.G.J. Avellar and J.C. Scaiano, J. Org. Chem., 55, 89, (1990)

124 J.A. Schmidt, A.B. Berinstain, F. de Rege, C. Heitner, L.J. Johnston and J.C. Scaiano, Can. J. Chem., 69, 104, (1991)

125 A. Castellan, J.H. Zhu, N. Colombo, A. Nourmamode, R.S. Davidson and L. Dunn, J. Photochem. Photobiol. A: Chemistry, 58, 263, (1991)

126 J.C. Scaiano, J.C. Netto-Ferreira and V. Wintgens, J. Photochem. Photobiol. A: Chemistry, 59, 265, (1991)

127 W.U. Palm and H. Dreeskamp, J. Photochem. Photobiol. A: Chemistry, 52, 439, (1990)

128 A. Castellan, C. Vanucci and H. Bouas-Laurent, Holzforschung, 41, 231, (1987)

129 H. Lutz, E. Breheret and L. Lindqvist, J. Phys. Chem., 77, 1758, (1973)

130 C.H. Nichols and P.A. Leermakers, in J.N. Pitts, G.S. Hammond and W.A. Noyes (eds.), "Advances in Photochemistry Series", Wiley, (New York), Volume 8, p. 315, (1971)

131 D.R. Kearns and W.A. Case, J. Am. Chem. Soc., 88, 5087, (1966)

132 R. Bensasson and E.J. Land, Trans. Faraday Soc., 67, 1904, (1971)

133 P.J. Wagner, R.J. Truman, A.E. Puchalski and R. Wake, J. Am. Chem. Soc., 108, 7727, (1986)

134 S.L. Murov, "Handbook of Photochemistry", Marcel Dekker, (New York), (1973)

135 D.J. McGarvey, P.G. Szekeres and F. Wilkinson, Chem. Phys. Lett., 199, 314, (1992)

136 A.A. Lamola and G.S. Hammond, J. Chem. Phys., 43, 2129, (1965)

137 A.A. Gorman, I. Hamblett, C. Lambert, A.L. Prescott, M.A.J. Rogers and H.M. Spence, J. Am. Chem. Soc., 109, 3091, (1987)

138 A.B. Berinstain, M.K. Whittlesey and J.C. Scaiano, "Laser Techniques in the Study of the Photochemistry of Carbonyl Compounds Containing Ligninlike Moieties", in C. Heitner and J.C. Scaiano (eds.), "Photochemistry of Lignocellulosic Materials", ACS Symposium Series No. 531, (Washington), p. 111, (1993)

139 P.J. Wagner, A.E. Kemppainen and H.N. Schott, J. Am. Chem. Soc., 95, 5604, (1973)

140 J.K. Hurley, N. Sinai and H. Linschitz, Photochem. Photobiol., 38, 9, (1983)

141 P.K. Das, M.V. Encinas and J.C. Scaiano, J. Am. Chem. Soc., 103, 4154, (1981)

142 N.C. Yang and R. Dusenbery, J. Am. Chem. Soc., 90, 5899, (1968)

143 E.J. Baum, J.K.S. Wan and J.N. Pitts, J. Am. Chem. Soc., 88, 2652, (1966)

144 N.C. Yang, D.S. McClure, S.L. Murov, J.J. Houser and R. Dusenberg, J. Am. Chem. Soc., 89, 5466, (1967)

145 F.D. Lewis and J.G. Magyar, J. Org. Chem., 37, 2102, (1972)

146 H. Lutz, M.C. Duval, E. Breheretand L. Lindquist, J. Phys. Chem., 76, 821, (1972)

147 P.K. Das, M.V. Encinas and J.C. Scaiano, J. Am. Chem. Soc., 103, 4162, (1981)

148 CRC Handbook of Physics and Chemistry, CRC Press, (Ohio), 52nd Edition, p. C94, (1971)

149 W.E.K. Middleton and C.L. Sanders, Illum. Eng., 48, 254, (1953)

150 J.B. Gillesbie, J.D. Lindberg and L.S. Laude, Applied Optics, 14(4), 807, (1975)

151 J.B. Gillesbie and J.D. Lindberg, Applied Optics, 31(7), 955, (1992)

152 M.M. Frodyma and V.T. Lieu, "Analysis By Means Of Spectral Reflectance of Substances Resolved on Thin Layers", in W.W. Wendlandt (ed.), "Modern Aspects of Reflectance Spectroscopy", Plenum Press, (New York), p. 88, (1968)

153 F. Wilkinson, C.J. Willsher, H.L. Casal, L.J. Johnston and J.C. Scaiano, Can. J. Chem., 64, 539, (1986)

154 G.O. Phillips and J.C. McArthur, "Photochemistry and Radiation Chemistry of Cellulose", in T.P. Nevell and S.H. Zeronian (eds.), "Cellulose Chemistry", Halsted Press, (New York), p. 292, (1985)

155 N. Duran, E. Gomez and M. Haun, J. Photochem. Photobiol. A: Chemistry, 51, 469, (1990)

156 E.M. Schulman and R.T. Parker, J. Phys. Chem., 81, 1932, (1977)

157 J. Murtagh and J.K. Thomas, Chem. Phys. Lett., 148, 445, (1988)

158 E.M. Schulman and C. Walling, J. Phys. Chem., 77, 902, (1977)

159 K.R. Gopidas and K.V. Prashant, J. Phys. Chem., 93, 6428, (1989)

160 F. Wilkinson, P.A. Leicester, L.F.V. Ferreira and V.M.M.R. Freire, Photochem. Photobiol., 53, 599, (1991)

161 H. Paul, R.D. Small and J.C. Scaiano, J. Am. Chem. Soc., 100, 4520, (1978)

162 D.A.I. Goring, "Polymer Properties of Lignin and Lignin Derivatives", in K.V. Sarkanen and C.H. Ludwig (eds.), "Lignin- Occurrence, Formation, Structure and Reactions", Wiley Interscience, (New York), p. 695, (1971)

163 E. Hagglund, in "Chemistry of Wood", Academic Press, (New York), p. 326, (1951)

164 R. Willstatter and L. Zechmeister, Chem. Ber., 46, 2401, (1913)

165 N. Morohoshi, in D.N.-S. Hon and N. Shiraishi (eds.), "Wood and Cellulose Chemistry", Marcel Dekker (New York), p. 367, (1991)

166 N. Duran, H. Mansilla and J.L. Reyes, J. Photochem., 35, 209, (1986)

167 N. Terashima, in J. Nakano (ed.), "Chemistry of Lignin", Unicohoo Co., (Tokyo), p. 170, (1979)

168 G. Aulin-Erdtman and R. Sanden, Acta. Chem. Scand., 22, 1187, (1968)

169 O. Goldschmid, Anal. Chem., 26, 1421, (1954)

170 E. Alder and J. Marton, Acta Chem. Scand., 13, 75, (1959)

171 J.C. Pew, J. Org. Chem., 28, 1048, (1963)

172 I. Falkenhag, J. Marton and E. Alder, Adv. Chem. Ser., 59, 75, (1966)

173 J. Gierer and F. Imsgard, Svensk Papperstidning, 16, 510, (1977)

174 H. Konschin, F. Sundholm and G. Sundholm, Acta Chem. Scand. Ser. B, 30, 262, (1976)

175 K. Lundquist, I. Egyed, B. Joseffson and G. Nyquist, Cell. Chem. Technol., 15, 669, (1981)

176 S.Y. Lin and K.P. Kringstad, TAPPI, 53(4), 658, (1970)

177 K.P. Kringstad and S.Y Lin, TAPPI, 53(12), 2296, (1970)

178 B. Ranby, K.P. Kringstad, E.B. Cowling and S.Y. Lin, Acta Chem. Scand., 23, 325, (1969)

179 S. Claesson, E. Olson and A. Wennerblom, Svensk Papperstidning, 71(8), 335, (1968)

180 M.G. Neumann, R.A.M.C. De Groote, and A.E.H. Machado, Polymer Photochem., 7, 401, (1986)

181 M.G. Neumann, R.A.M.C. De Groote, and A.E.H. Machado, Polymer Photochem., 7, 461, (1986)

182 P. Neta, R.E. Huie, S. Mosseri, L.V. Shastri, J.P. Mittal and P. Maruthamutha, J. Phys. Chem., 93, 4099, (1989)

183 R.D. Small, J.C. Scaiano and L.K. Patterson, Photochem. Photobiol., 29, 49, (1979)

184 I. Forsskahl, H. Tylli and C. Olkkonen, Proc. 5th Int. Conf. On Wood and Pulping Chemistry, (Orlando), p. 431, (1989)

185 J.R. Hurst, J.D. McDonald and G.B. Schuster, J. Am. Chem. Soc., 104, 2065, (1982)

186 M.A.J. Rogers, J. Am. Chem. Soc., 105, 6201, (1983)

187 M.A.J. Rogers and P.T. Snowden, J. Am. Chem. Soc., 104, 5541, (1982)

188 D. Bellus, "Quenchers of Singlet Oxygen- A Critical Review", in B. Ranby and J.F. Rabek (eds.), "Singlet Oxygen- Reactions with Organic Compounds and Polymers", Wiley, (Chichester), p. 61, (1978) and references therein

189 A. Garner and F. Wilkinson, Chem. Phys. Lett., 45, 432, (1977)

190 K.K. Iu and J.K. Thomas, J. Am. Chem. Soc. 112, 3319, (1990)

191 R. Battino, "Solubility Data Series, Volume 7: Oxygen and Ozone", Pergamon Press, (England), p. 519, (1981)

192 E.C. Lim and V.L. Kowalski, J. Chem. Phys., 36, 1729, (1962)

193 J.B. Birks and D.J. Dyson, Proc. Royal Soc. London Ser. A, 275, 135, (1963)

194 S.J. Strickler and R.A. Berg, J. Chem. Phys., 37, 814, (1962)

195 I.B. Berlmann, Handbook of Fluorescence Spectra, Academic Press, (New York), p. 176, (1971)

196 O. Stern and M. Volmer, Z. Physik, 20, 183, (1919)

197 R.W. Redmond and S.E. Braslavski, Chem. Phys. Lett., 148, 523, (1988)

198 D.R. Worrall, Ph.D. Thesis, Loughborough University of Technology, (1992)

199 G. Aulin-Erdtman and L. Haghom, Svensk Papperstidning, 61, 187, (1958)

200 J.C. Pew, Nature, 193, 250, (1962)

201 A. Sakakibara, in D.N.-S. Hon and N. Shiraishi (eds.), "Wood and Cellulosic Chemistry", Marcel Dekker, (New York), p. 113, (1991) and references therein

202 G. Koehler, G. Kittel and N. Getoff, J. Photochem., 18, 19, (1982)

203 T.F. Palmer and S.F. Parmar, J. Photochem., 31, 273, (1985)

204 A. Castellan, N. Colombo, A. Nourmamode, J.H. Zhu, D. Lachenal, R.S. Davidson and L. Dunn, J. Wood Chem. Technol., 10, 461, (1990)

205 E.J. Land and G. Porter, Faraday Trans. Soc., 59, 2016, (1963)

206 J. Feitelson, E. Hayon and A. Treinin, J. Am. Chem. Soc., 95, 1025, (1973)

207 H.H. Nimz and G. Turznik, Cell. Chem. Technol., 14, 727, (1980)

208 P.B. Merkel and D.R. Kearns, J. Am. Chem. Soc., 94, 7244, (1972)

209 B.H. Milosavljevic and J.K. Thomas, J. Rad. Chem. Phys., 23, 237, (1984)

210 F. Wilkinson and D.R. Worrall, Proc. Indian Acad. Sci. (Chem. Sci.), 104, 297, (1992)

211 J.A. Schmidt, C. Heitner, G.P. Kelly and F. Wilkinson, J. Pulp and Paper Sci., 16, J111, (1990)

212 R.S. Davidson, L.A. Dunn, A. Castellan and N. Nourmamode, J. Photochem. Photobiol. A: Chemistry, 58, 349, (1991)

213 H. Tylli, I. Forsskahl and C. Olkkonen, J. Photochem. Photobiol. A: Chemistry, 67, 117, (1992)

214 D. Oelkrug, S. Uhl, F. Wilkinson and C.J. Willsher, J. Phys. Chem., 93, 4551, (1989)

215 F. Wilkinson, A. Goodwin and D.R. Worrall, "Diffuse Reflectance Laser Flash Photolysis of Thermomechanical Pulp", in C. Heitner and J.C. Scaiano (eds.), "Photochemistry of Lignocellulosic Materials", ACS Symposium Series No. 531, (Washington), p. 86, (1993)

216 J-M. Yang and D.A.I. Goring, Can. J. Chem., 58, 2411, (1980)

217 C. Heitner and J.A. Schmidt, J. Wood Chem. Technol., In Press

218 R.W. Anderson, R.M. Hochstrasser, H. Lutz and G.W. Scott, J. Chem. Phys., 61, 2500, (1974)

219 N. Ikeda, K. Imagi, H. Masuhara, N. Nakashima and K. Yoshihara, Chem. Phys. Lett., 140, 281, (1987)

220 F. Wilkinson, C.J. Willsher, P.A. Leicester, J.R.M. Barr and M.J.C. Smith, J. Chem. Soc. Chem. Comm., 1216, (1986)

221 J.C. Scaiano, W.G. McGimpsey, W.J. Leighand S. Jakobs, J. Org. Chem., 52, 4540, (1987)

222 I.R. Gould, M.B. Zimmt, N.J. Turro, B.H. Baretz, and G.F. Lehr, J. Am. Chem. Soc., 107, 4607, (1985)

223 J.C. Scaiano, E.B. Abuinand L.C. Stewart, J. Am. Chem. Soc., 104, 5673, (1982)

224 B.J. Fergus and D.A.I. Goring, Holzforschung, 24, 113, (1970)

225 J.R. Wood and D.A.I. Goring, Pulp Paper Mag. Can., 72, T95, (1971)

226 A.J. Stamm, "Wood and Cellulose Science", Roland Press Company, (New York), p. 29, (1964)

227 K. Fukushima and T. Terashima, Wood Sci. Technol., 25, 371, (1991)

228 N. Terashima and K. Fukushima, Wood Sci. Technol., 22, 259, (1988)

229 M. Erickson, S. Larsson and G.E. Miksche, Acta Chem. Scand., 27, 1673, (1973)

230 S. Yasuda and A. Sakakibara, J. Jap. Wood Res. Soc., 21, 363, (1975)

231 E. Alder, H.D. Becker, T. Ishihara, and A. Stamvik, Holzforschung, 20, 3, (1966)

232 D.Y. Lee, M. Matsuoko and M. Sumimoto, Holzforschung, 44, 415, (1990)

233 J.A. Schmidt, Unpublished Data, (1992)

234 E. Alder and K. Lundquist, Acta Chem. Scand., 15, 223, (1961)

235 C. Heitner, "Light-Induced Yellowing of Wood-Containing Papers - An Evolution of the Mechanism", in C. Heitner and J.C. Scaiano (eds.), "Photochemistry of Lignocellulosic Materials", ACS Symposium Series No. 531, (Washington), p. 13, (1993)

236 C. Heitner, "Light-Induced Yellowing of Wood-Containing Papers - An Evolution of the Mechanism", in C. Heitner and J.C. Scaiano (eds.), "Photochemistry of Lignocellulosic Materials", ACS Symposium Series No. 531, (Washington), p. 19, (1993)

237 D.N.-S. Hon, in D.N.-S. Hon and N. Shiraishi (eds.), "Wood and Cellulosic Chemistry", Marcel Dekker, (New York), p. 552, (1991)

238 M. Ek, H. Lennholm, G. Lindblad, T. Iversen and D.G. Gray, "Photochromic Behaviour of UV-Irradiated Mechanical Pulps", in C. Heitner and J.C. Scaiano (eds.), "Photochemistry of Lignocellulosic Materials", ACS Symposium Series No. 531, (Washington), p. 152, (1993)

239 R.A. Cockram, "CTMP in Fine Papers", Proc. Int. Mechanical Pulping Conf., (Helsinki), (1989)

240 For a review of this research, see C. Heitner, "Inhibition of Light-Induced Yellowing of Lignin-Containing Papers", in C. Heitner and J.C. Scaiano (eds.), "Photochemistry of Lignocellulosic Materials", ACS Symposium Series No. 531, (Washington), p. 192, (1993)

241 E. Alder and K. Lundquist, Acta Chem. Scand., 17, 13, (1963)

242 J.M. Lawther, Private Communication, (1993)